MARIA S. MERIAN-Berichte

MSM67

SEGMENT

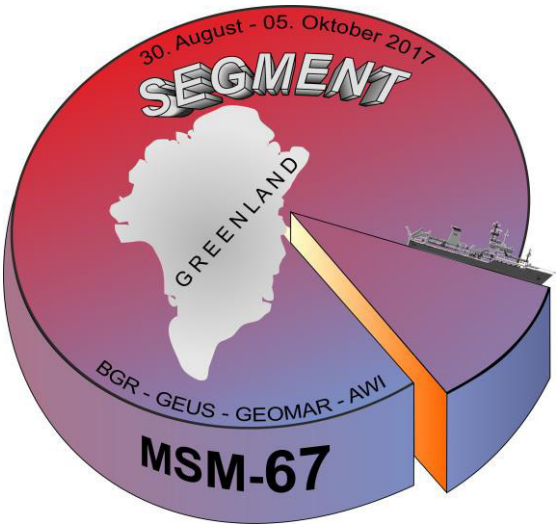

FS MARIA S. MERIAN

August 31st – October 4th, 2017,
Reykjavik (Iceland) –
Longyearbyen (Svalbard)

Bundesanstalt für
Geowissenschaften
und Rohstoffe

MARIA S. MERIAN-Berichte

SEGMENT

Cruise No. MSM67

31. August 2017– 04.October 2017
Reykjavik(IC) − Longyearbyen(SV)

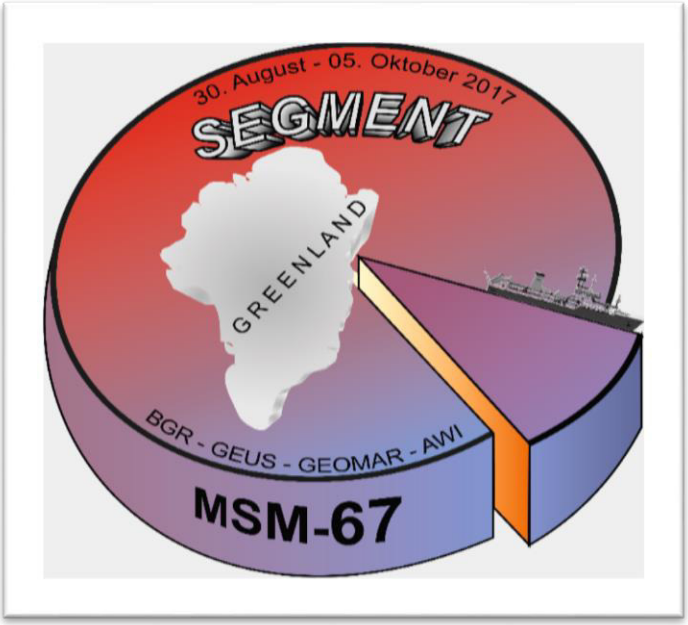

Volkmar Damm, Dieter Franke,
Udo Barckhausen, Stephanie Barnicoat, Thomas Behrens, Kai Berglar, Anke Dannowski, Ümit Demir, Timo Ebert, Berenice Ebner, Martin Engels, Thomas Funck, Boris Hahn, Peter Klitzke, Andreas Madsen, Lorenzo Scala, Michael Schnabel, Martin Thorwart, Peter Steinborn, Per Trinhammer

Editorial Assistance:
DFG-Senatskommission für Ozeanographie
MARUM – Zentrum für Marine Umweltwissenschaften der Universität Bremen

2017

Table of Contents

1 Summary

Survey MSM67 SEGMENT it is intended to study the architecture of the rifted continental margin off East Greenland around the Jan Mayen fracture zone. Key issues to be addressed are margin segmentation and the location of the continent-ocean transition (COT). Both subjects are highly debated. Symmetric segmentation of conjugate margins has significant implications on our general understanding of continental rifting processes, and a margin-parallel COT off East Greenland would indicate an N-S opening in the Norwegian/Greenland Sea. The latter challenging most publications on the early evolution of the North Atlantic. A major open question is also the timing, duration and distribution of magmatism that resulted in the formation of the North Atlantic large igneous province. Previous suggestions of very short (~3 Myr) periods of intense magmatism have been challenged and a much longer duration and/or a post-breakup origin are under discussion. Here, we want to establish the amount of post-breakup magmatism as evident in high-velocity lower crust and test the dependence of magmatism with distance from the proposed hot-spot under Iceland and the influence of major fracture zones on volcanism.

Das Projekt MSM67 SEGMENT zielt auf die Untersuchung der Architektur des Kontinentrandes Ostgrönlands um die Jan Mayen Bruchzone. Zentrale Untersuchungsziele sind die Segmentierung des Kontinentrandes und die Bestimmung der Kontinent-Ozean Grenze (COT), beides umstrittene Themen mit weitreichenden, grundlegenden Implikationen zum Aufbruch von Kontinenten. Eine an beiden Kontinenträndern identifizierte und damit symmetrische Segmentierung würde zum Verständnis des Spreizungsprozesses beitragen und eine COT, die parallel zum Kontinentrand verläuft impliziert eine Nord-Süd Öffnung der Norwegisch-Grönländischen See und wäre damit entgegengesetzt zur gegenwärtigen Vorstellung. Eine weitere zentrale Frage ist die Zeitlichkeit, Dauer und regionale Verteilung des starken Vulkanismus während der Öffnung des Nordatlantiks. Die ursprünglich angenommene sehr kurze Dauer (etwa 3 Millionen Jahre) des intensiven Magmatismus wird inzwischen angezweifelt und eine wesentlich längere Dauer diskutiert. Wir wollen den Anteil des Magmatismus ermitteln, der sich nach dem Aufbrechen des Nordatlantiks als Hochgeschwindigkeitskruste manifestiert und die Abhängigkeit der Volumina von der Entfernung zur thermischen Anomalie unter Island untersuchen, sowie den Einfluss von großen ozeanischen Bruchzonen auf den Magmatismus überprüfen.

Abbreviations:

FZ	fracture zone
COT	continent-ocean transition; COB continent-ocean boundary
SDRs	seaward dipping reflectors
MCS	multi-channel reflection seismic

2 Participants

Name	Discipline	Institution
Volkmar Damm	Geophysicist/Chief Scientist (until Sep. 8th)	BGR
Dieter Franke	Geophysicist/Chief Scientist (since Sep. 9th)	BGR
Udo Barckhausen	Geophysicist	BGR
Stephanie Barnicoat	MMO	Seiche
Thomas Behrens	Technician	BGR
Kai Berglar	Geophysicist	BGR
Anke Dannowski	Geophysicist	GEOMAR
Ümit Demir	Technician	BGR
Timo Ebert	Technician	BGR
Berenice Ebner	Student	AWI
Martin Engels	Physicist	BGR
Thomas Funck	Geophysicist	GEUS/GEUS
Boris Hahn	Technician	BGR
Peter Klitzke	Geophysicist	BGR
Andreas Madsen	Student	Univ. Aarhus
Lorenzo Scala	MMO	Seiche
Michael Schnabel	Geophysicist	BGR
Peter Steinborn	Technician	BGR
Martin Thorwart	Geophysicist	GEOMAR/CAU
Per Trinhammer	Technician	Univ. Aarhus/GEUS

AWI	Alfred Wegener Institute, Bremerhaven
BGR	Bundesanstalt für Geowissenschaften und Rohstoffe, Hannover
CAU	Christian-Albrechts-Universität zu Kiel
GEOMAR	Helmholtz-Zentrum für Ozeanforschung, Kiel
GEUS	Geological Survey of Denmark and Greenland, Copenhagen K, Denmark
Seiche	Seiche Ltd., Bradworthy, Holsworthy Devon, United Kingdom
Univ. Aarhus	Aarhus University

3 Research program

Introductory remarks:

Besides bad weather conditions and sea ice, unforeseen circumstances made considerable changes in the proposed work program necessary.

1. Only one day prior departure a survey license was finally granted by Greenland authorities, however with some unforeseen requirements. Among others (see 3.3.1, p. 16), we were requested not to commence our activities in Greenland waters before September 10th. Thus we had to plan for an alternative program for the first 10 days of the cruise. We were prepared for this situation and had already elaborated an alternative survey in the area around the Norwegian Jan Mayen Island, situated 500 km east of Greenland. An appropriate application for research permission was submitted to the Norwegian authorities well in advance and approved within very short time. Therefore, we were able to acquire a seismic refraction line across the Jan Mayen ridge and skipped the originally planned seismic refraction line across the Jan Mayen Fracture Zone in Greenlandic waters. We are confident that this line will substantially contribute to the success of the project.
2. Medical circumstances required to drop the chief scientist in the port of Akureyri/Iceland, before the research cruise continued toward the most remote areas of east Greenlandic waters. Therefore we skipped the planned MCS survey along the refraction line across the Jan Mayen ridge and sailed from Akureyri to Greenland. We hope to get access to some existing commercial reflection seismic data in the vicinity of our line, in order to support the modelling of the refraction seismic data.
3. When sailing off East Greenland, medical circumstances required again to drop one scientist in the port. Therefore, we had another three days transit to drop the scientist in the port of Longyearbyen/Spitsbergen.

The work program has been adopted accordingly. However, the circumstances necessitated to predominantly concentrate on data acquisition; there was little room for data processing and only minimal data interpretation was possible during this cruise.

3.1 Geological evolution and tectonic setting of the Norway-Greenland Sea

3.1.1 Geology of the East Greenland shelf

Subsequent to the Caledonian orogeny, several periods of extensional deformation affected the northern North Atlantic region before break-up of the continent (Eldholm et al., 1987; Mosar et al., 2002; Ziegler et al., 1998). However, Late Paleozoic and Mesozoic basin formation was not accompanied by significant magmatism, except around breakup time and from there on (Meyer et al., 2007). It is generally accepted that the final separation of Greenland from Eurasia took place during Chron 24r, at the Paleocene-Eocene transition (c. 54 Ma) (Eldholm et al., 1989; Gaina et al., 2009; Gaina et al., 2017; Tsikalas et al., 2002). After breakup, sea-floor spreading occurred simultaneously along the Mohns and Aegir Ridges that are offset along the Jan Mayen Fracture Zone. In large parts of the North Atlantic, the magnetic seafloor anomalies are well defined and are of little or no controversy. While most authors proposed symmetric spreading and a south to north directed opening of the Norwegian-Greenland Sea, Voss et al. (2009) suggested a southward propagation of the break-up at the northeast Greenland margin, starting at the Greenland FZ at 54.2 Ma and ending at 50 Ma off the location of the Jan Mayen FZ. Also the evolution of the Norway Basin, south of the Jan Mayen FZ turns out to have been more complicated than previously thought. Gernigon et al. (2012) suggest that breakup initiated

in the central part of the Møre margin. Based on a dense magnetic grid, these authors identified faster early spreading in the central part of the Møre Marginal High that decreased towards the north and south. The fan-shaped magnetic anomaly pattern initiated at around 49-46 Ma (chrons C22n-C21n) in the Norway Basin (Gernigon et al., 2012). The key location for solving this controversy is the NE Greenland margin around the Jan Mayen FZ.

The shelf in the proposed study area (see Fig. 3.1-1) is characterized by flood basalt units forming the acoustic basement, a situation that is mirrored at the conjugate margin, the Vøring Plateau. The Vøring Margin has been extensively investigated by MCS data (e.g. Berndt et al., 2001; Le Breton et al., 2012; Mjelde et al., 2009; Skogseid and Eldholm, 1989), seismic refraction data (e.g. Berndt et al., 2000; Breivik et al., 2009; Faleide et al., 2008; Mjelde et al., 2009), commercial drilling on the continental shelf (e.g. Dalland et al., 1988), scientific drilling on the Vøring Plateau (Eldholm et al., 1987; Eldholm et al., 1989; Faleide et al., 1991 ; Planke, 1994; Skogseid and Eldholm, 1989) and modeling (van Wijk et al., 2004). The conjugate NE Greenland margin is not studied in the same detail as the Vøring Margin.

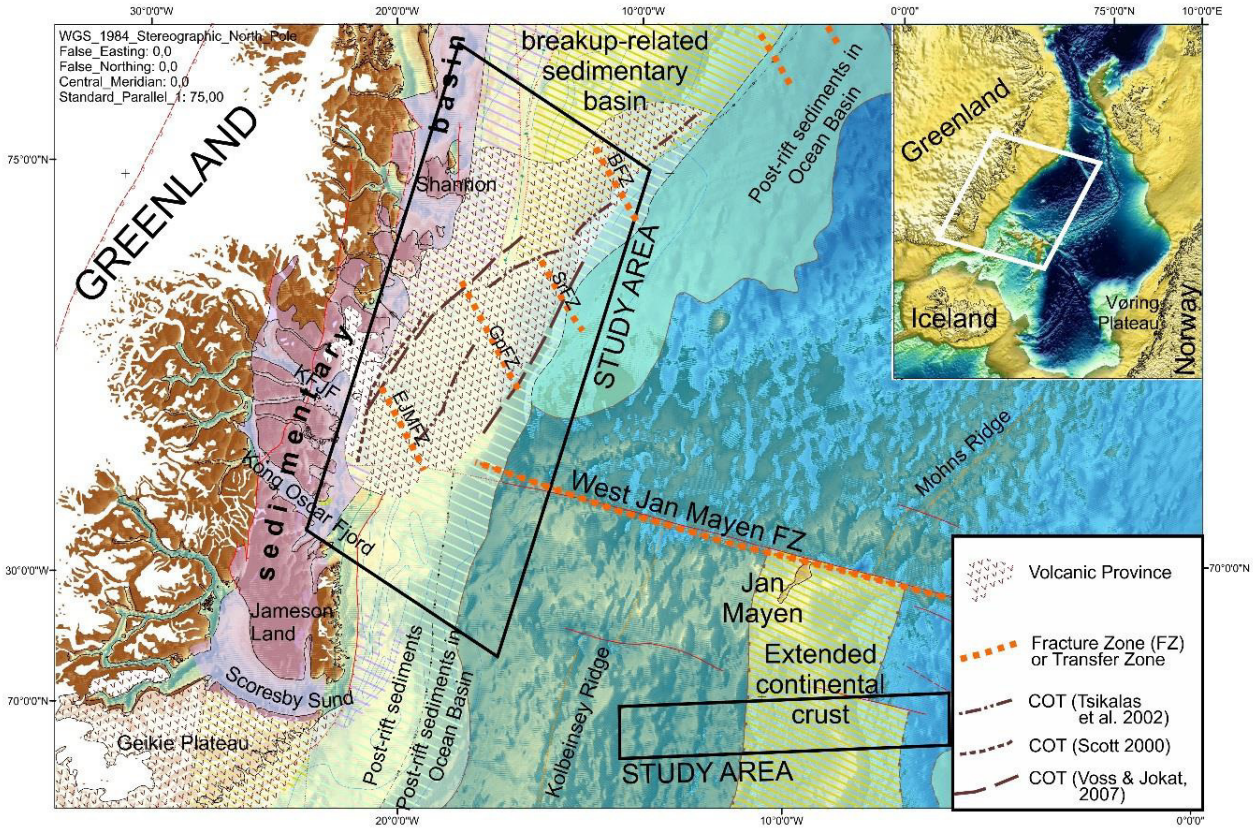

Figure 3.1 1*: The study area comprises the NE Greenland shelf and deep sea around the intersection with the Jan Mayen fracture zone (FZ). In addition, the conjugate continental margin of the Jan Mayen microcontinent was studied by means of a seismic refraction line. Shown are interpreted COT positions in Greenland (Scott, 2000; Tsikalas et al., 2002; Voss and Jokat, 2007). The COT either follows the shelf-break or crosses the shelf towards the Kejser Franz Joseph Fjord (KFJF). Suggested structural lineations resulting in margin segmentation comprise the Gleipne FZ/transfer zone (GpFZ), the Bivrost FZ/transfer zone (BFZ), the Surt FZ/transfer zone (SrFZ), and the East Jan Mayen FZ/transfer zone (EJMFZ) (Tsikalas et al., 2002). Geological interpretation is from Grantz et al. (2011).*

The NE Greenland margin is only sparsely explored. Rare studies in the 1980ies and early 1990s identified a narrow window off Northeast Greenland, to the north of the Jan Mayen FZ showing weak indications of faulted and tilted Cretaceous sediments truncated by the rift unconformity similar to observations from the Norwegian continental margin. Hinz et al. (1987) suggested that an inner SDR sequence marks the beginning of an excessive volcanic episode resulting in the emplacement of the East Greenland plateau basalts. The presence of widespread SDRs was confirmed by Mutter and Zehnder (1988) on the basis of two-ship expanded spread and wide aperture CDP profiling and a classification as volcanic rifted margin is obvious. Results from a commercial seismic reconnaissance survey, mostly across the inner East Greenland shelf to the north of the proposed study area were summarized by Hamann et al. (2005), leading to the interpretation of the proposed study area as "volcanic province". Based on the same data set, Tsikalas et al. (2005) interpreted conjugate sets of transfer zones on the NE Greenland shelf and the Vøring Plateau. Berger and Jokat (2008) provide a first view of the sediment distribution and tectonic features along the East Greenland continental margin. However, available scientific multichannel seismic data are sparse and lack penetration. In addition, the records suffer from seafloor multiples hindering a concise crustal-scale interpretation. Commercial data (e.g. Kanumas) concentrates on the inner shelf and seldom reaches out on the oceanic crust, hindering a conclusive interpretation of the COT. Most structural interpretations on the NE Greenland shelf and margin thus are derived from magnetic data or extrapolation of conjugate structures (e.g. Tsikalas et al., 2002). Commercial exploration focused mainly on the Danmarkshavn Basin, to the north of the proposed study area (Christiansen, 2011; Granath et al., 2010). A couple of refraction seismic lines have been acquired by the Alfred Wegener Institute, revealing a wide range of crustal geometries. While Schlindwein and Jokat (1999) modelled an about 80 km-wide and less than 8 km thick high-velocity lower crustal body in the prolongation of Kejser Franz Josef Fjord (and did not reach the eastern end of the margin), Voss and Jokat (2007) derived a body ~225 km wide and 16 km thick, implying a major asymmetry when compared to the conjugate Vøring margin. With respect to the Vøring margin the Moho is 10 km deeper in the continental unit of the East Greenland margin, a wider COT, and a larger high-velocity lower crustal body, interpreted as magmatic underplating, are proposed.

3.1.2. Margin segmentation and the evolution of the North Atlantic Rift

Transfer zones or rift segment boundaries have long been recognized and represent structures dissecting a propagating rift at high angles (see Koopmann et al. (2014) for a recent review). Debate continues over if transfer zones are inherent in the rifting process and if there is a link between continental transfers and oceanic fracture zones. The term transfer zone is widely used, particularly where cross-margin structural elements on the shelf are spatially related to onshore zones of strike-slip faulting.

In the northernmost Atlantic, there is consensus that the East Jan Mayen FZ is a major shear zone with an about 160 km-wide left-stepping offset in the COB at the Norwegian margin (e.g. Olesen et al., 2007). However, the origin of major and long-lived transform boundaries, segmenting mid-oceanic ridges such as the Jan Mayen FZ are poorly understood. From a similar NW–SE trend of the Jan Mayen FZ and Caledonian and/or Paleoproterozoic shear zones, Doré et al. (1999) and Fichler et al. (1999) conclude that the fracture zone has even been influenced by much older inherited structures. However, it is unclear how far the conjugate West Jan Mayen FZ continues below the shelf. In fact we should expect the western end of the East Jan Mayen FZ at the Greenland continental margin (Gernigon et al., 2009), which strikes at considerable angle to the present FZ. The presence of fracture zones and continental transfer zones farther north at the East Greenland margin is also under discussion.

In the continental margin segment under discussion, potential fracture zones and transfer zones comprise the Gleipne FZ/transfer zone, the Bivrost FZ/transfer zone, the Surt FZ/transfer zone, and the Jan Mayen transfer zone (Figure 3.1 1, Figure 3.1 *2*). Tsikalas et al. (2002) and Mjelde et al. (2005) interpret such lineaments at the Vøring Margin and infer a connection between the continental transfers and the oceanic fracture zones. In addition, Tsikalas et al. (2002; 2005) proposed that such FZ and transfer zones are conjugate features being present at both sides of the Norwegian-Greenland Sea resulting in a symmetric segmentation of the continental margins. Other authors partly or completely rejected this interpretation. Olesen et al. (2007) argue that the Bivrost Lineament is well expressed in the basement structure; however, there is no outboard fracture zone in this position. Berger and Jokat (2008) concluded that their seismic dataset off NE Greenland does not provide evidence for the existence of any major fracture zone. Hence, their data do not support margin segmentation. However, the seismic coverage is coarse and Berger and Jokat (2008) show a seismic example (Line AWI-2003-0585) that reveals a major vertical offset in the oceanic crust of about 1 km, pretty close to the proposed Bivrost FZ.

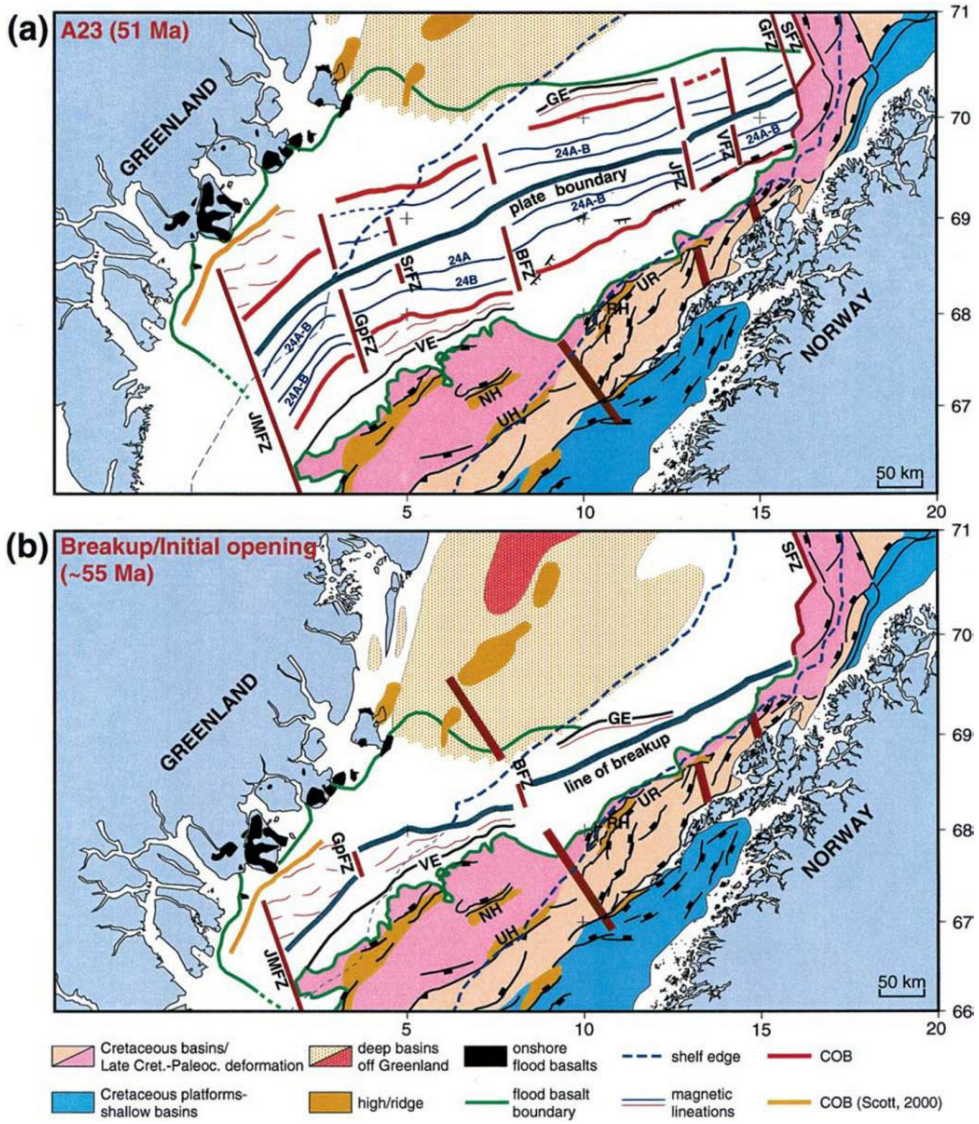

Figure 3.1 2: *The proposed study area where the Jan Mayen fracture zone (JMFZ, red) intersects with the NE Greenland margin reconstructed to (a) Chron 23n.2n, and (b) break-up time (from Tsikalas et al. (2005)). GpFZ denotes the Gleipne Fracture Zone, BFZ the Bivrost Fracture Zone. Offsets of >10 km are proposed to occur along the crustal lineaments. Please note also major differences in various proposed COB locations.*

3.1.3 The Continent-ocean-transition (COT) at the East Greenland continental margin

A key issue related to rifted continental margins is the structure and architecture of the COT, which is still not fully understood. Debate continues over whether there is a COT or a COB and whether this boundary is located at the lithosphere or at the crust (e.g. Franke et al., 2011; Mjelde et al., 2007). The width, thickness, and nature of the COT are important parameters in order to understand the processes leading from continental rifting to seafloor spreading. The seaward termination of the COT is generally defined by the location of the oldest oceanic crustal magnetic anomaly and/or the seaward termination of the wedge of seaward dipping reflectors, whereas the landward extent is related to the seaward termination of clearly identifiable rotated continental fault blocks (Mjelde et al., 2005; Whitmarsh and Miles, 1995). Although highly variable, volcanic rifted margins tend to show a significantly smaller width of the COT than magma-poor margins (Clift, 1997).

Reconstructions of the North Atlantic typically provide a good fit along the Reykjanes Ridge and the northern part of the Mohns Ridge (Gaina et al., 2002; Mosar et al., 2002). However, the same is not true for the southern Mohns Ridge, close to the Jan Mayen FZ, where a gap occurs between the SW Vøring Margin and the conjugate NE Greenland margin (Olesen et al., 2007). This may be explained either by more complex rifting including the formation of a highly extended or even fragmented Jan Mayen microcontinent (Gaina et al., 2009; Gaina et al., 2017), or by a COT that may be placed close to the NW Greenland shore (Olesen et al., 2007; Scott, 2000). The proposed COT/COB locations thus differ considerably. The COB as proposed by Scott (2000) is located 75 km landward of the COB as interpreted by Tsikalas et al. (2005). The COT as suggested by Voss and Jokat (2007) covers a wide region with the seaward end being located about 130 km away from the interpretation by Scott (2000).

While a COT running across the NE Greenland shelf is geometrically elegant, there are some conflicts with structural observations. Schlindwein and Jokat (1999) and Schmidt-Aursch and Jokat (2005) show that the crust is relatively thick there and does not display velocities that are compatible with typical oceanic crust. Voss and Jokat (2007) argue for a 120 to 130 km wide COT, based on refraction seismic velocities and the extent of interpreted Cretaceous syn-rift sediments mixed with basaltic intrusions. This is in contrast to the typically sharp transition at volcanic rifted margins in the vicinity of the SDRs (Clift, 1997; Franke, 2013). Alternatively, the COT may be located at the continental slope, where several authors (Abdelmalak et al., 2016; Geissler et al., 2016; Hinz et al., 1991) interpreted the presence of SDRs which can be used to constrain the position of the COT. At the conjugate Vøring Plateau, modeling of a seismic refraction profile, with 5 km receiver spacing, indicates the presence of stretched continental crust and anomalously thick oceanic crust, separated by a 25 km wide COT with an inner SDR wedge (Mjelde et al., 2005).

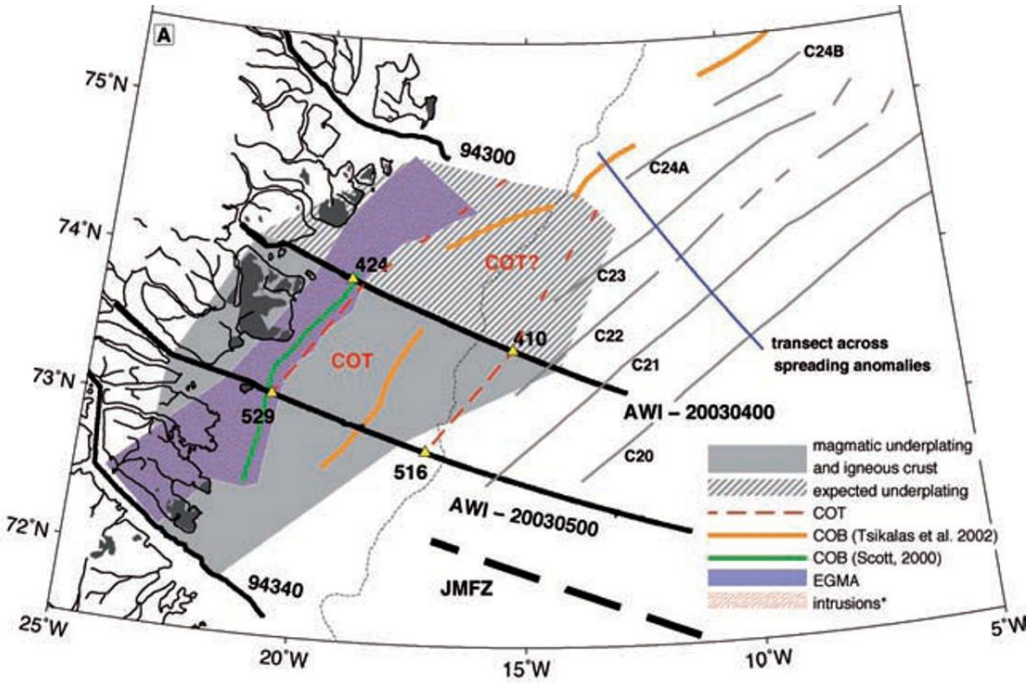

Figure 3.1 3: *The proposed study area where the Jan Mayen fracture zone (JMFZ, dashed) intersects with the NE Greenland margin. The Figure is from Voss and Jokat (2007). Black lines show existing seismic profiles with a spacing of c. 100 km. Locations of three different continent–ocean boundaries (COB) are shown: The orange line indicates the COB as interpreted by Tsikalas et al. (2002), the green line the COB as proposed by Scott (2000), and the red dashed lines outline the COT from Voss and Jokat (2007). Magnetic anomalies C24 to C21 pinch out against the NE Greenland continental slope.*

If the COT is indeed located at the continental slope, the magnetic spreading anomalies in the oceanic domain would terminate against the NE Greenland continental slope, in favor of a southward propagating seafloor spreading system using the current interpretation of spreading anomalies (cf. Figure 3.1 3). Break-up started with chron C24B in the north and there is an oblique angle of the anomalies C24A, C23 and C22 along the margin between Shannon Island and the Jan Mayen FZ (Figure 3.1 3). In consequence spreading must have propagated southward, an idea which had been proposed earlier by Voss and Jokat *(2007)* and Voss et al. (2009). In contrast to available plate tectonic models, this would indicate that the Norwegian-Greenland Sea opened from north to south. Recent interpretations suggest that anomaly 25 (58 Ma) is the oldest anomaly in the Eurasian Basin of the Arctic Ocean (Berglar et al., 2016; Brozena et al., 2003). If this is correct, it appears possible that the formation of the North Atlantic started in the Arctic Ocean and migrated to the south, i.e. towards the proposed Iceland thermal anomaly, changing our present understanding of the early evolution of the North Atlantic.

3.1.4. Distribution and timing of magmatism

There is consensus that the final Late Cretaceous/Paleocene rift phase, which resulted in continental separation, was accompanied by a significant and well-known magmatic event (see Meyer et al. (2007) for a review). However, it is unclear if all of the magmatic intrusives and extrusives of the North Atlantic large igneous province can be related to this event. After several decades of studies on the NE Atlantic margins, the causes of initiation of volcanism and break-up and their relationship are still debatable (Gaina et al., 2009).

Early authors proposed a short period of intensive magmatism and suggested that volcanic activity ceased about 3 m.y. after break-up (Eldholm, 1991; Hinz et al., 1987). However, according to Meyer et al. (2007), there is solid evidence of prolonged magmatism after continental separation on Iceland and the northern parts of the West and East Greenland margins, while the southern part of the NE Atlantic margins seem devoid of post-breakup magmatism. Two or three main phases of post-Mesozoic igneous activity occurred in the study region (Price et al., 1997; Tegner et al., 2008). Intermittent pre-breakup (~61 Ma), volcanic activity occurred at widely spaced localities along the rift zone occurred in West Greenland, East Greenland and the British Isles from 61–56 Ma (Storey et al., 2007). At 56–54 Ma, eruption rates rose by an order of magnitude. However, there was another, alkaline magmatic episode from 37–35 Ma (Price et al., 1997). Other authors have asked challenging questions about the timing, variability and origin of the atypical magmatic events that affected the Norwegian-Greenland Sea after the break-up phase (e.g. Breivik et al., 2008; Breivik et al., 2006; Gernigon et al., 2006; Greenhalgh and Kusznir, 2007; Olesen et al., 2007). For example, Clift (1997) argued from subsidence data from ODP Site 918 and from the structure of the Greenland-Iceland Ridge that the Iceland thermal anomaly did provide significant thermal input into the region only after about 44 Ma. Also the lower crust reveals some asymmetry that may be explained by delayed magmatism. The lower crust at the NE Greenland margin shows thick layers of high velocity (Voss and Jokat, 2007), typically interpreted as magmatic underplating or intrusions. However, the conjugate margin of the western Jan Mayen microcontinent shows no high-velocity lower crust at all (Kodaira et al., 1998). Also the "mantle plume" concept has been challenged. The melting anomalies that have been classified as "hot spots", including Iceland, exhibit extreme variability (Foulger, 2007). This highlights the necessity for a precise description and definition of what kind of structure is referred to with the term "hot spot". Further, a local context appears essential and also a distinction between data and models. E.g. a "hot spot trail" from West Greenland, across Greenland to the present position of Iceland on the Atlantic spreading ridge is neither proven nor even supported by the evidence (Doré and Lundin, 2005). The rapid post-volcanic cooling period 52–45 Ma seen in Jameson Land is difficult to reconcile with the classical model of a major thermal anomaly (Mathiesen et al., 2000). Also, local tectonic overprinting such as the presence of a fracture zone may change the amount of magmatic crustal thickening (Berndt et al., 2001; Gernigon et al., 2009), emphasizing the importance of comprehensive geophysical data sets. The alternative models available have strong implications for our understanding of mantle convection and for extension processes. Courtillot et al. (1999) pointed out that key observations for either hypothesis are the magnitude of extension and the temporal relationship between volcanism and extension.

3.1.5 Structure and evolution of the Jan Mayen Microcontinent (JMMC)

The JMMC is 400–450 km long, and varies in width from 100 km in the north to 310 km in the south (Blischke et al., 2016). The most prominent seafloor expression of the JMMC is the Jan Mayen Ridge, a 10-30 km wide elevation that extends over 150 km in N-S direction in the center of the North Atlantic. The Jan Mayen Ridge is likely underlain by continental crust (Blischke et al., 2016; Peron-Pinvidic et al., 2012), with a thickness of 11-15 km (Kodaira et al., 1998).

The eastern flank of the Jan Mayen Ridge was formed during breakup of the Norway Basin and seafloor spreading along the, nowadays extinct, Aegir Ridge just prior to magnetic anomaly 23 (Eldholm et al., 1986). Early seafloor spreading (C24r and C22n) rates in the Norway Basin are moderate to fast (<50 mm/year) and resulted in a relatively smooth oceanic top basement (Gernigon et al., 2012).

The oceanic spreading is supposed to have started between the Faeroe–Shetland Escarpment and the eastern flank of the Jan Mayen Ridge (Eldholm et al., 1986). Because of faster early spreading in the central part of the Møre Marginal High that decreased towards the north and south, Gernigon et al. (2012) suggest that breakup initiated in the central part of the Møre margin. To explain the fan-shaped magnetic anomalies of the Norway Basin, already Talwani and Eldholm (1977) suggest that the JMMC must have rotated counter-clockwise. From a new dense magnetic grid, Gernigon et al. (2012) conclude that the fan-shaped magnetic anomaly pattern initiated at around 49-46 Ma (chrons C22n-C21n) in the Norway Basin.

A refraction seismic line indicates the presence of highly attenuated continental crust from the Jan Mayen Ridge to the western end of the Jan Mayen Basin. While the continental upper crust shows a relatively uniform thickness of 3 km, the lower continental crust decreases significantly down to almost zero thickness towards the western part of the Jan Mayen Basin (Kodaira et al., 1998). Above, the presence of an up to 5 km deep sedimentary basin is indicted with a thin basaltic layer deposited within the sediments. This volcanic flow unit is interpreted as shallow-marine landwards flows emplaced during chrons C13–C6b (33–21.56 Ma) (Blischke et al., 2016). Intense extensional deformation (e.g. line npd-JM85-11) may indicate an early formation within this frame. Seaward the flow unit terminates against oceanic crust with an inferred age of 14.6 Ma (line BGR-75-05). Below Cenozoic sediments at the eastern flank of the Jan Mayen Ridge, and at the conjugate Møre margin, a flood basalt unit is interpreted. Skogseid & Eldholm (2015) interpret the basalt unit as seaward dipping reflectors (SDRs). However, this is controversial and also the character of the lower crust at the Jan Mayen Ridge is still disputed. Modelling of refraction seismic data by Kodaira et al. (1998) resulted in lower crustal velocities not exceeding 6.8 km/s. A more recent work of Breivik et al. (2012) analyzed refraction seismic data just 10-30 km further to the south. Their model document lower crustal velocities exceeding 7.0 km/s in the area of the eastern COT.

The volcanic phase, resulting in the formation of conjugate volcanic overprinted margins was likely short-lived; refraction seismic data indicate 10–11 km thick igneous crust at the Møre margin, tapering off to magma-starved seafloor spreading along the extinct Aegir Ridge by C23 time (51.4 Ma) (Breivik et al., 2006). The latter is probably associated with slow to ultra-slow seafloor spreading (Breivik et al., 2006).

On the western side of the JMMC rifting gradually propagated northward, likely from chron C21 onward (Blischke et al., 2016). This is interpreted to have been accompanied by large-scale extension of the southern Jan Mayen Ridge complex, crustal thinning across the Iceland Plateau and listric normal faulting along the western flank of the Jan Mayen Ridge (Blischke et al., 2016). However, the Oligocene development of the conjugate East Greenland – JMMC margins remains unclear. Breakup at the SW corner of the JMMC is interpreted to have occurred in the earliest Oligocene, at around chron C13n time (Blischke et al., 2016), but this is still a controversial topic. From magnetic data, Gernigon et al. (2012) propose that breakup between the JMMC and Greenland was finalized in the earliest Miocene (C6b, 23-22.5 Ma). Subsequently the JMMC was rifted away from the East Greenland margin. During Oligocene times, a deformation zone within the continental and/or transitional domain may have developed in the southern JMMC (Gernigon et al., 2012).

3.2 Scientific aims

One of the projects goals is a conclusive interpretation of the Continent-Ocean Transition (COT). Scott (2000) and Olesen et al. (2007) proposed a COT close to the Greenland shore, far inboard the continental shelf. However, from refraction seismic and magnetic data it was shown by Schlindwein and Jokat (1999) and Voss and Jokat (2007) that the crust is comparable thick there and does not yield velocities of typical oceanic crust. For locating the COT, we acquired

MCS data, complemented by ship-borne magnetic and gravity data. The MCS data will be used to identify a continental crustal architecture that is dominated by rotated fault blocks and grabens, filled with wedge shape deposits. SDRs in the COT mark the transition to the typical fault-block fabric of oceanic crust. Structural observations will be complemented by refraction seismic modeling. At the Vøring Margin, which is conjugate to the NE Greenland margin, P wave velocities of ~6.0 km/s in the top of the main crustal layer are conformable with granitic basement, whereas velocities of 6.9 km/s seaward of the COT (~6.9 km/s) show the presence of gabbroic rocks typical of oceanic crust (Mjelde et al., 2005). The COT is characterized by intermediate velocities of 6.5 km/s, interpreted as heavily intruded continental crust (Mjelde et al., 2005). The refraction seismic line we acquired along the Greenland shelf crosses the critical area of disputed COT locations. Magnetic data and gravity modelling will be used to validate the interpretations. By combining the different geophysical methods we are confident that we will be able to locate the COT much better than previously done. Further, we plan to compare the structures (e.g., dipping wedges of reflectors, basement ridges) from the East Greenland margin with those from the outer edge of the Vøring Plateau to further constrain this interpretation. If indeed the COT is located at the continental slope, the consequence is that spreading along the Mohns Ridge likely propagated southward in the Norway-Greenland Sea, an idea which had been proposed earlier by Voss and Jokat (2007).

The widely magma-poor continental margins on the western side of the JMMC and the conjugate East Greenland margin, south of the Jan Mayen FZ will be addressed by using the new refraction seismic profile across the Jan Mayen Ridge, supplemented by existing MCS data and the new MCS data off Greenland. Existing deep seismic data (Breivik et al., 2012; Hermann and Jokat, 2013) will be incorporated. Here we plan to contribute in particular to the unclear Oligocene development of the conjugate East Greenland – JMMC margins. Our intention is to better constrain the northern extent of the Oligocene deformation zone within the continental and/or transitional domain that is proposed to have gradually developed in the southern JMMC (Gernigon et al., 2012).

Our new grid of geophysical profiles will contribute to assess along-strike variations at the East Greenland continental margin. From distinct basement offsets, local abnormal volcanism and variations in the potential field data, we will identify continental transfer zones at the East Greenland margin. Margin segmentation can be deduced from (1) major lateral offsets in the distribution of the SDR wedges, (2) steep basement slope angles often associated with deeply penetrating faults, and (3) a drastic change in the architecture and style of the SDRs wedges including local absence of SDRs (Franke et al., 2007). Such structural data will be complemented by high-resolution gravity and magnetic data, as well as deep seismic data to validate the interpretation. Such lineaments will be compared to the conjugate Lofoten-Vesterålen margin. Conjugate features being present at both sides of the Norwegian-Greenland Sea would indicate symmetric segmentation of the continental margins.

The new data across the onshore prolongation of the Jan Mayen Ridge shows that oceanic transform faults indeed can continue into the continental domain. The northern portion of the inferred continental Jan Mayen Ridge shows considerable offsets in prolongation of fracture zones. However, at the Greenland shelf, the Jan Mayen FZ is not a straight structure across the shelf but the new data reveals considerable N-S offsets. It appears likely that the western onshore Jan Mayen FZ developed in a south-north-stepping pattern. In between we assume the development of pull-apart grabens, bounded by steeply dipping normal faults.

To address the question of distribution, timing and origin of basaltic intrusives and extrusives, we complement existing refractions seismic profiles across the shelf with a key line along the Greenland shelf. The line runs across the prolongation of the Jan Mayen FZ on the shelf. We aim for a re-evaluation of different rift models and of the mechanisms for the emplacement of

the basalts. Existing wide-angle reflection/refraction data reveal the deep structure of the crust and especially the amount of magmatic underplating/intrusions during the rifting and initial seafloor-spreading phase at the Paleocene-Eocene transition (c. 54 Ma) (Schlindwein and Jokat, 1999). However, likely more magmatic material was emplaced with the separation of the Jan Mayen microcontinent from East Greenland in Oligocene/Miocene times (Gudlaugsson et al., 1998; Scott, 2000). Our new data will allow to test the hypothesis that the major Oligocene plate boundary reorganization was preceded by various ridge jumps and/or short-lived triple junctions NE and possibly SW of the Jan Mayen microcontinent between break-up (54 Ma) and magnetic chron C18 (40 Ma) (Blischke et al., 2016; Gaina et al., 2017; Peron-Pinvidic et al., 2012; Voss and Jokat, 2007). With a margin-parallel line along the shelf we will study how the presence of the major Jan Mayen FZ did affect volcanism and magmatism. The line will provide a detailed image on the distribution and thickness of the high-velocity lower crustal body with increasing distance from the FZ, as well as from the distance to the proposed thermal anomaly of Iceland. Further this line will provide geophysical constraints on the nature of the COT and on the deep structure of potential transfer zones and thus margin segmentation. Our working hypothesis is that a vast part of volcanic intrusives and extrusives at the location, where the West Jan Mayen Fracture Zone intersects with the NE Greenland margin, is either pre-rifting or post-rifting and may have partly its origin in the intersection with this fracture zone.

3.3 Marine mammal observation (MMO) to comply with environmental best practice standards

3.3.1 Preconditions for impact mitigation during seismic surveying by Norwegian and Greenlandic authorities

The research program for the MSM67 cruise involved seismic operations in Norwegian and Greenlandic waters. Special preconditions for impact mitigation during seismic surveying were given by authorities from both states.

The **Norwegian Government** in their "Standard answer to research cruises in 2017" requested that acoustic equipment and seismic operations remain outside protected areas,

(1) To minimize impact, active transmission should be limited to 24 hours within a range of 50 .km
(2) In addition, a "soft start" should be used if possible, and there should also be personnel with biological expertise on the boat who can look out for and assess effects on marine mammals. (…) As a precaution, the use of any type of seismic sources is subject to the same restrictions.
(3) Provided that the guidelines above are followed, the Governor considers that no separate permission for use of bottom penetrating sounder is required in relation to the Svalbard Environmental Protection Act

For all seismic operations carried out in Norwegian waters, the standard JNCC mitigation procedures were followed to ensure the survey conformed to the regulatory framework concerning marine fauna mitigation and precautionary measures for the Norwegian authorities (Table 3.3 1). Marine mammal observers (MMOs) were not explicitly requested aboard seismic survey vessels. However, to complete the survey according to international standards and in compliance with BGR's best practice regime to protect the marine environment during seismic surveying, a dedicated MMO regime was implemented for all activities involving the use of a noise array aboard the RV Maria S. Merian.

The **Government of Greenland** Environmental Agency for Mineral Resource Activities (EAMRA) has set out guidelines for seismic activities pursuant to the Mineral Resources Act section 3c, sub section 3. According to these guidelines, "EAMRA decides, based on a preliminary scope (draft scope) of the seismic activities, whether an EIA (Enviromental Impact Assessment) or an EMA (Enviromental Mitigation Assessment) must be prepared". In accordance with the United Nations Convention for the Laws of the Sea articles 56, 1, a, article 240 c) and d) as well as article 246 paragraph 8, EAMRA has assessed measures necessary to mitigate impacts of the activity based on scientific recommendations. Consequently, according to the assessment of EAMRA and recommendations of GINR and DCE the following mitigation measures were requested and met for all seismic activities carried out in Greenland waters (see also Table 3.3 1):

- The activities in the area between 70° N and 80° N may not commence before the 10th of September 2017.
- No activities may be performed inside the closed walrus area before 30th September 2017
- 2 trained and skilled MMSO's shall take part in the operation with a special focus on observations of walruses, narwhals and bowhead whales.

In the East Greenland area, three species have been identified by the EAMRA as species of concern in relation to the cumulative impacts of seismic activities since 2011. These include narwhal, walrus, and *t*he critically endangered bowhead whale (Figure 3.3 1).

Greenlandic guidelines for seismic surveys have therefore designated areas where seismic surveys are either prohibited in certain periods or can be regulated to reduce impacts on marine mammals. The survey area is within designated areas of concern for narwhal and bowhead whale, and close to a designated closed area for walrus (area closed 1st June to 31st September).

It was therefore recommended by EAMRA that the MMO's concentrate their efforts to actively search for bowhead whales and narwhals and when these are encountered within 2 km of the airgun array, to shut down the array, move 50 km away before a new ramp up is commenced and the survey line continued. The vessel is not permitted to return to the sighting location until 24 hours after the whales were observed.

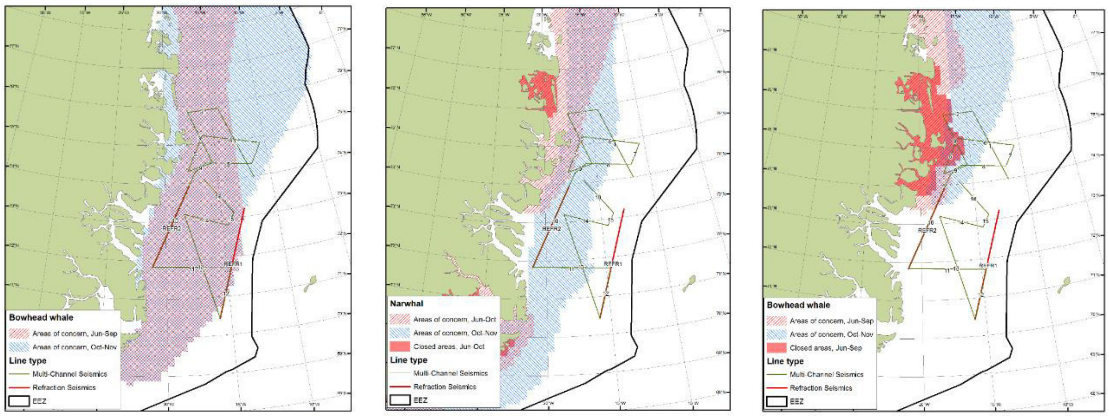

Figure 3.3 1: *Maps showing initially proposed survey lines within designated area of concern for bowhead whales (a), narwhals (b), and designated closed area for walruses (c). The survey lines have been modified to acknowledge the restricted areas that have not been entered.*

Table 3.3 1: *Mitigation procedures summary.*

	NORWAY	GREENLAND
Source mitigation zone	500 m	500 m
Pre-watch period	30 minutes (depth < 200m), 60 minutes (depth > 200m)	30 minutes (depth < 200m), 60 minutes (depth > 200m)
Soft start length	20 – 40 minutes	20 - 40 minutes
Soft-start delays	Yes	Yes
Shut-down during production	No	Yes, if a marine mammal enters mitigation zone, airguns reduced to mitigation output until marine mammal has left the area and MMO/PAM instructs to resume at full operating power
Species covered	Marine mammals	Marine mammals including Polar bears
Special requirements	Passive acoustic monitoring (PAM) during darkness & reduced visibility	2000 m mitigation zone for bowhead whales and narwhals. If seen within 2000m, shut down operations, move 50 km away before resuming seismic operations and do not return to sighting location for 24 hours. Passive acoustic monitoring (PAM) during darkness & reduced visibility

Marine mammal observations within Greenlandic waters followed procedures outlined in the Manual for Seabird and Marine Mammal Survey on Seismic Vessels in Greenland (4th revised

edition, March 2015) to ensure that data fit into the databases of MMSO observations kept by the Greenland authorities. The specific role of the MMO during the survey was to focus on marine mammal monitoring and mitigation which correspond closely to the Joint Nature Conservation Committee (JNCC) standards, described in the guidelines to EIA/EMA of seismic surveys in Greenland waters. These data are recorded and reported to EAMRA and their scientific advisors (DCE and GINR) on JNCC Marine Mammal Recording forms which were downloaded from the JNCC website (http://jncc.defra.gov.uk/page-1534).
In addition to marine mammal visual observations, the MMO's were also tasked with operating the Passive Acoustic Monitoring (PAM) system on board the seismic vessel. This required that both MMO's are also certified and experienced PAM-operators.

3.3.2 Marine mammals in the survey areas

The SEGMENT project investigates the East Greenland continental margin located within the Greenland Sea and includes survey locations south of Norwegian Jan Mayen Island and at the Knipovich ridge south west of Svalbard within the Norwegian Sea (Figure 3.3 2). Collectively, these two regions constitute an important area of the Arctic Ocean for marine life. Marine productivity around North East Greenland is limited by the persistent cover of sea ice which inhibits the growth of plankton and other small marine organisms. However, marine productivity can be found in places where the pack ice has fractured to expose large areas of open water (polynyas) which offer a winter refuge for marine mammals and seabirds. Areas where the Arctic Ocean mixes with warmer waters of the North Atlantic are rich in marine organisms and support great numbers of marine mammals and seabirds.
While many species of cetaceans occur seasonally within arctic waters, typically during summer months, there are several species which are native to the arctic and occur year-round. Bowhead whales (*Balaena mysticetus*) are circumpolar in arctic pack ice and around polynyas and spend their entire life in arctic waters, making seasonal movements into higher latitudes in the spring and summer as the ice recedes. They are sexually mature at about 20 years of age and females give birth to one calf every 3-4 years. The bowhead whale stocks in the survey area are assessed as critically endangered by the International Nature Conservation Organisation (IUCN). Small populations of narwhals (*Monodon monoceros*) occur in the Greenland Sea, aggregating in coastal areas when the ice breaks up in spring, and moving further offshore when the sea freezes in winter.
In summer months, they can form herds of hundreds of animals which are segregated by age and sex. Walruses (*Odobenus rosmarus)* are distributed in pack ice and coastal waters of Greenland, are gregarious and haul out in great numbers on beaches and ice flows around openings in the sea ice. Females mature sexually at 4-8 years of age and breed in spring between April and May, delivering a single calf after one-year gestation.
Other marine mammals may occur seasonally over the Greenland continental shelf and slope and in the Norwegian Sea. These include rorquals (humpback whale, fin whale, blue whale, sei whale and minke whale) which are attracted by the triggering of the early blooming of phytoplankton and zooplankton to undertake a northerly migration to their summer feeding grounds in the cooler, high latitude waters of the Arctic where they feed for 3-4 months on the rich supply of krill and other food. After this they will migrate south to tropical breeding and calving waters. Several species of odontocetes (dolphins, beaked whales, and sperm whales) occur in the Norwegian Sea and in the Greenland Sea. Sperm whales and beaked whales occur in the Southern Greenland Sea and in Norwegian waters, primarily found over continental slopes, deep canyons and edges of ocean banks. Oceanic dolphins are resident all year round and can be observed both in the Greenland Sea as far north as the pack ice and in the Norwegian Sea with overlapping calving seasons throughout the year. In the winter months, they are found father offshore away from the ice.

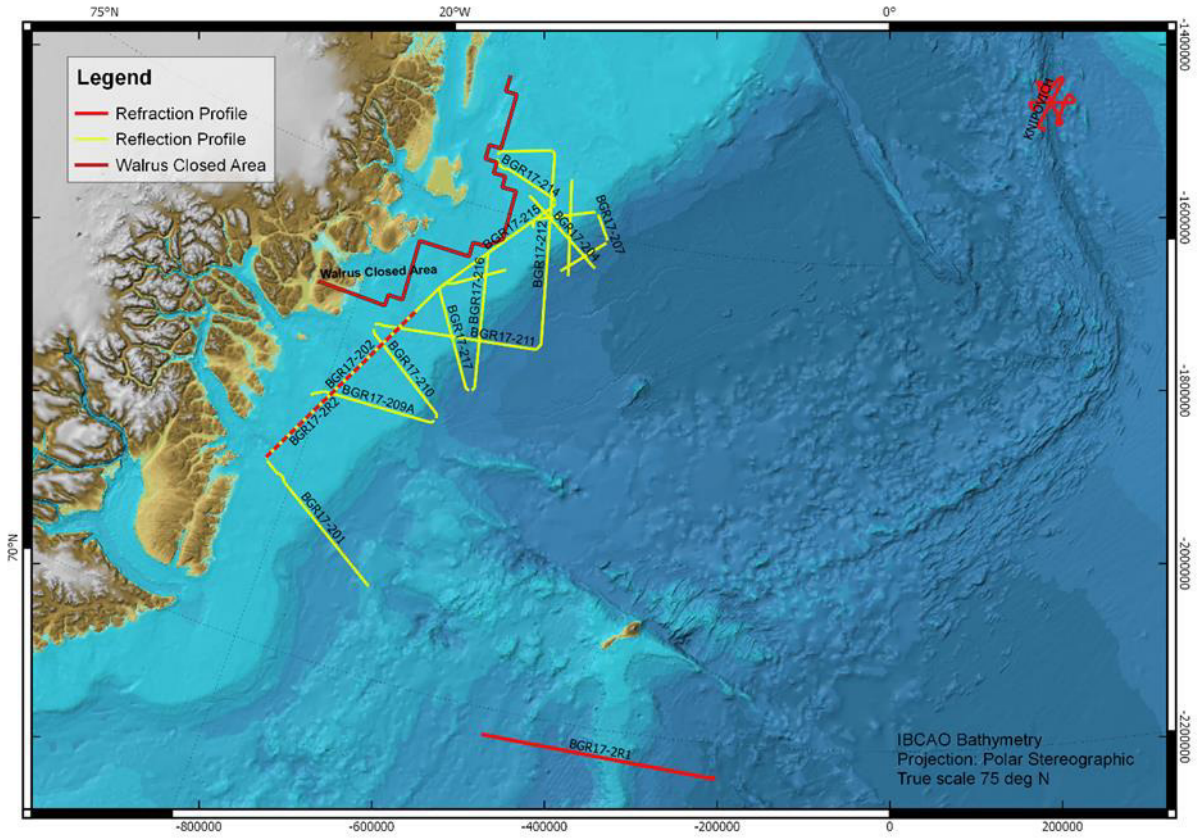

Figure 3.3 2*: Overview of MSM67 SEGMENT project seismic data acquisition profiles and survey area.*

Several other pinniped species occur year-round throughout the Arctic Ocean, making seasonal movements further north in response to receding ice cover, while the polar bear occurs circumpolar on the Arctic Ocean sea ice and adjacent land masses. A list of all species found in the survey areas are listed in Table 3.3 2.

Table 3.3 2*: Marine Mammals in Survey Areas*

Species common name	Species Latin name	Distribution
Bowhead whale	*Balaena mysticetus*	Resident, Greenland Sea
Humpback whale	*Megaptera novaeangliae*	Migration, Norwegian and Greenland Sea
Blue whale	*Balaenoptera musculus*	Migration, Norwegian and Greenland Sea
Fin whale	*Balaenoptera physalus*	Migration, Norwegian and Greenland Sea
Sei whale	*Balaenoptera borealis*	Migration, Norwegian and Greenland Sea
Northern Minke whale	*Balaenoptera acutorostrata*	Migration, Norwegian and Greenland Sea
Sperm whale	*Physeter macrocephalus*	Resident, Norwegian Sea
Narwhal	*Mondon Monoceros*	Resident, Greenland Sea
Northern Bottlenose whale	*Hyperoodon ampullatus*	Resident, Norwegian and Greenland Sea
Orca/Killer whale	*Orcinus orca*	Resident, Norwegian and Greenland Sea
long fin pilot whale	*Globicephala meals*	Resident, Norwegian and Greenland Sea
White-beaked dolphin	*Lagenorhynchus albirostris*	Resident, Norwegian and Greenland Sea
Walrus	*Odobenus rosmarus*	Resident, Greenland
Ringed seal	*Pusa hispida*	Resident, Greenland
Bearded seal	*Eringathus barbatus*	Resident, Greenland
Polar bear	*Ursus maritimus*	Resident, Greenland

3.3.3 Conventional visual observations and passive acoustic monitoring

Visual observations

Dedicated visual observations were carried out during hours of daylight and when weather conditions permitted. Observer effort was recorded with environmental data. Wind speed was classified to the Beaufort wind scale. Other classifications for sea state, swell, visibility and glare followed the JNCC recording forms (Appendix-A 2). A new record was entered every time environmental conditions or the source status changed, or at least every hour.
Observations were carried out from the observation deck above the bridge (17 m). The MMOs scanned the sea with the naked eye, using 7x50 binoculars to closer investigate any visual cues seen, such as circling seabirds, dark shapes, splashes or blows. If marine mammals were observed, the distance to the sighting was estimated, using reticules from binoculars and a range estimation stick. The time, location and other data required for the completion of the JNCC sightings forms were also recorded, as well as the behavior of the animals in relation to the survey vessel.
Photographs of marine mammals were taken whenever possible to document the species identification (also sometimes providing information on group sizes and behavior). Photography is a useful tool in freezing the motion of fast-moving species such as delphinids, allowing later examination of their flank markings and facilitating identification. It also permits independent verification of sighting data. During this survey, the MMOs used a range of photographic equipment; Canon DSLR cameras 70 x 300 zoom lens.
During the survey, 113 h 02 min of dedicated visual observation for marine mammals were carried out by the MMOs. Visual watch was conducted in a slight or choppy sea when the beaufort scale was less than 6 and when the visibility was good. In poor visibility conditions or a beaufort scale higher than 6, Passive Acoustic Monitoring was carried out. Of the time spent on visual watch, the source was active for 45 h 55 min.

Passive acoustic monitoring (PAM)

Two Passive Acoustic Monitoring (PAM) systems were employed on the vessel during the cruise, the first one primarily for marine mammal mitigation and the second mainly for comparison purposes:

1. Seiche Ltd (UK) provided a four-channel 250 m towed array cable which consisted of two (H1 and H2) identical, spherical broadband hydrophones (200 Hz to 200 kHz, - 3 dB points); two (H3 and H4) identical spherical hydrophones (2 kHz to 200 kHz), and a depth gauge (2 Bar sensor). Channel sensitivity at the output from the pre-amplifier was -166 dB re: 1 V/µPa for the broadband channel and -157 dB re 1V/µPa for the low frequency channel.
2. 2. Sercel's QuietSea™ system which processes and analyses sound from both the seismic streamers and additional hydrophones on the gun arrays. QuietSea™ system is a new Sercel product which was recently purchased by BGR. It is fully integrated in the Sercel seismic acquisition units and operates automatically.

The 250 m Seiche Ltd (UK) array cable (1) was deployed from a hanging block suspended by crane arm and offset 5 m to the starboard side quarter. The cable was deployed and retrieved using the starboard auxiliary winch and reel. The array cable was connected to a PAM base station via a 100 m deck cable. The PAM Base was contained in a 19-inch rack housing and consisted of a buffer box with an internal card (NI DAQ USB-6251) for sampling high frequency (HF) sound (H3 and H4, 500 ks/s), an external sound card (Fireface 800) for digitally sampling Low Frequency (LF) sound (H1 and H2, 48 ks/s), a rack mounted PC ("PAMGuard PC") running PAMGuard64 version 1.15.11 CORE, Java (update 8 version 131), NI Device Monitor (version 17) and the Fireface 800 controller software.
Odontocetes (e.g. toothed whales and dolphins) emit echolocation clicks to navigate and find prey. Individual click energy broadly varies between species but generally, peak frequency may

range from 4 kHz to 200 kHz and are emitted in rapid sequences or trains. Mysticetes (e.g. baleen whales) and many odontocetes also emit frequency modulated (FM) tonal signals and pulsed calls that are used for communication. Marine mammal vocalisation signals were detected acoustically using a headset (Sennheiser HD280 pro) and the PAMGuard PC. Raw FFT data acquired by the LF sound card was displayed in real-time on spectrograms. A mid-frequency (MF) spectrogram displayed signals with a frequency range of 0 Hz to 24 kHz and was suitable for the detection of frequency modulated (FM) tonal signals (e.g. whistles, peak frequency 4 kHz to 24 kHz) and pulsed calls (e.g. buzz, squawk, bark, etc.) produced by odontocetes (e.g. dolphins, narwhals etc.) A low-frequency (LF) spectrogram displayed signals with a frequency range of 0 Hz to 3 kHz and was used to detect LF tonal signals (e.g. songs, moans, grunts, shrieks, pulses) produced by mysticetes (e.g. humpback whales, bowhead whales, etc.). A very low-frequency (VLF) spectrogram displayed signals with a frequency range of 0 Hz to 480 Hz for closer inspection of VLF tonal vocalisations (e.g. calls, pulses, moans, etc.) produced by large mysticetes (e.g. blue whales, fin whales, sei whales, etc.).
Data from the LF sound card were processed using a LF click detector (frequency range of 0 Hz to 24 kHz, trigger high pass 4 kHz, order 4) to identify echolocation click trains of dolphin species and sperm whales. Candidate clicks were verified by inspection of click waveform and spectrum characteristics. Sperm whales produce powerful broadband echolocation clicks with a peak energy (160 to 180 dB re 1 µPa @ 1m) at approximately 0.1 kHz to 30 kHz. Many odontocetes (e.g. dolphins, beaked whales, *Kogia*, etc.) produce clicks with energy exceeding the human hearing range (e.g. > 20 kHz). High frequency echolocation clicks were processed using an HF click detector (frequency range 0 Hz to 250 kHz, trigger band pass 15 kHz to 160 kHz, order 6) and classified by frequency sweep as MF Pulse (e.g. test band 20 kHz to 50 kHz, click length 0.04 to 1 ms), HF Pulse (e.g. test band 50 kHz to 100 kHz, click length 0.04 to 1 ms) and Narrow Band HF (e.g. test band 120 kHz to 150 kHz, click length 0.03 to 0.12 ms) to facilitate detection of target frequency bands (e.g. beaked whale clicks have a peak frequency of 30 kHz to 60 kHz). The vessels position was provided by the on-board GPS navigation system (NMEA GGA string, BAUD 4800) and displayed in PAMGuard on a map along with hydrophone positions, 500m exclusion zone, vessel heading, track and local bathymetry data.
The location of detected marine mammals are resolved by calculating the bearing and range of the received signals from pairs of grouped hydrophones (LF: H1 & H2, HF: H3 & H4) using a combination of automated detectors and manual localization techniques. The bearing of the target signal is calculated using a time of arrival difference (TOAD) cross-correlation function, which calculates the difference in the arrival times of the same signal when detected on two or more hydrophones of known separation distance (e.g. H1 and H2 have a separation of 2m, H3 and H4 have a separation of 0.25m) and the speed of sound in water (e.g. 1500 m/s). The bearings of detected vocalizations may be displayed on a map and the animal's location is resolved using Target Motion Analysis (TMA), where successive bearings begin to converge as the vessel advances along a track. FM tonal sounds may be detected using an automated whistle and moan detector, or manually selected using a clip generator. Automated detections are verified manually by inspecting the spectrogram display and aurally using the headset. False automated detections attributed to other noise sources (e.g. airguns, echosounders, sub-bottom profilers, etc.) are monitored and excluded from candidate marine mammal detections by the PAM operator. LF click trains (e.g. sperm whale echolocation clicks and coda, etc.) can be tracked and plotted automatically by running automated click train ID, or manually by selecting and assigning individual target clicks to a tracked acoustic event. HF clicks are automatically classified per pre-defined parameters (e.g. MF_Pulse, HF_Pulse, NBHF, etc.) and individually inspected by click waveform, spectrum, inter-click interval (ICI) and Wigner plots to identify vocalisations (e.g. beaked whales, *Kogia*, dolphins, etc.) and other noise sources. Verified HF click trains are tracked, labelled as an acoustic event and displayed on the map. LF and HF click

trains are localized automatically using the tracked click localizer function or manually using real-time TMA and the map measuring tool.
Where possible, acoustic detections were further processed offline, using PAMGaurd Viewer Mode and localized by TMA using four Distance Sampling models (Least Squares, 2D simplex optimisation, 3D simplex optimization, Markov Chain Monte Carlo (MCMC) localisation). The model with the best relative Goodness-of-fit between observed data and theoretical is chosen as the localized position of the animal. While TMA works well for stationary or slow-moving animals relative to vessel speed (e.g. foraging sperm whales or singing humpback whales), it is less effective for large groups of fast-moving, highly directional vocalizing species (e.g. dolphins). While instantaneous bearings of groups of dolphins can be measured using TOAD, range estimation is best achieved by correlating concurrent visual sightings, or (during darkness/poor visibility) by measuring the relative amplitude of the received signal (dB) using the headset, an amplitude radar display and spectrogram Gannier Scale value as a proxy for distance, while taking into consideration the background noise levels and local sound propagation conditions. While bearing estimates using TOAD and localization techniques by TMA represent the best practice for tracking marine mammals acoustically, algorithmic and mathematical assumptions on hydrophone spacing, biases associated with slant range in the 3D plain and left/right ambiguity in the 2D plain, inevitably induce some error in calculations associated with these techniques. Therefore, a conservative approach to localization is applied during real-time monitoring and mitigation.
Acoustic monitoring was available 24 h, while monitoring by the PAM operator was focused during the hours of darkness and poor visibility. A local monitoring station (LMS) comprising of a laptop with remote link via network connection (NetSupport Manager) to the main PAM PC was situated inside the observation room enabling the MMO to make acoustic recordings during visual sighting events, which could be analyzed in detail in post processing. Acoustic encounters were defined as different detections when it could be certain they were different groups of animals orspecies or when they were separated by at least 20 min without an acoustic detection. PAM effort and source operation logs were maintained and updated on standard JNCC recording forms. Sound recordings (.wav format) and screengrabs (.png) of PAMGuard displays were archived to catalogue detection events where possible. An SQLITE3 database logged GPS positional data, hydrophone depth and detection events continually throughout the project. Data acquired by the LF and HF click detectors, whistle and moan detectors and clip generators were stored in binary format and made available for offline processing in PAMGuard Viewer.
The contracted MMO/PAM operator was responsible for filling in all forms relating to seismic operations, visual and acoustic effort, sightings and acoustic detections with the PAM. Furthermore the MMO/PAM operator was responsible for providing advice on the application of the appropriate mitigation guidelines.

A total of 305 h 54 min of acoustic monitoring was carried out with 292 h 07 min of monitoring while the seismic source was active on full volume, reduced volume or during testing. There was a total of 13 h 41 min of PAM monitoring while the seismic source was inactive.

Communication and reporting

The MMO/PAM Operator liaised directly with the seismic crew using handheld VHF radios on the appropriate working channel (Ch 2). Notification of the 60-minute pre-shoot watch for every soft start was provided by the seismic crew, along with an ‘all clear’ check immediately prior to starting the airguns. In the case of a mitigation event, the MMO/PAM Operator informed the seismic crew immediately that any delay or shut down of the source was required, and communication was maintained regarding animal movements and the subsequent resumption of operations.

Throughout the survey, weekly reports were submitted to the chief scientist on board the RV *Maria S. Merian*. The reports included information on sightings, environmental conditions, mitigation, and seismic airgun activity.

3.3.4 Visual observations and passive acoustic detections

There were a number of visual observations on transit (Figure 3.3 3). In addition, on survey site there was a visual observation on Sept 11th of an *unidentified mysticete spp.* (sighting no. 11) and two sightings of Humpback whales (sightings no. 12 & 13) during multi-channel seismics acquisition line BGR17-201, on the East Greenland continental shelf. Sighting 11 was observed 2000 m away from the vessel, heading south and travelling parallel to the vessel in the opposite direction. Two tall blows were observed in the distance. Sighting 12 was first observed at 1500 m away from the vessel, crossing perpendicular ahead of the vessel heading northeast. The closest distance observed to the airguns was 700 m. Sighting 13, there were three whales, two at 2000 m from the vessel and one that was observed much closer at 800 m. The closest one dived, showing its tail fluke and was not observed again. The other two travelled away from the vessel heading south west. There was no mitigation action necessary for sightings no. 11, 12 & 13 as none of the whales were observed within 500 m of the airguns.

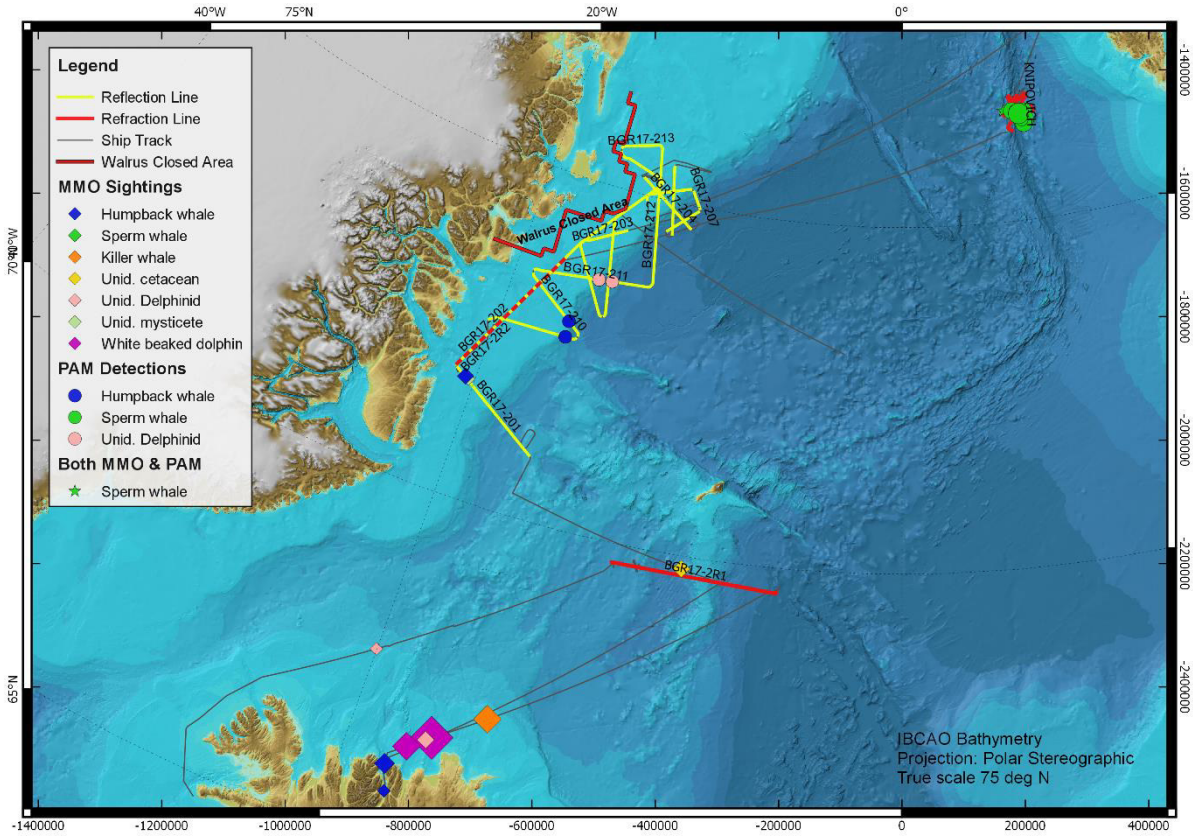

Figure 3.3 3: *Overview of MSM67 marine mammal sightings.*

On Sept 19th, while the vessel was on survey at the Knipovich ridge, South of Svalbard in Norwegian waters, there were three sightings of Sperm whales (Physeter microcephalus), all of which were concurrently detected with the PAM system. Sighting 14 consisted of two Sperm whales, both observed 1500 m traveling away from the vessel heading north east. Sighting 15, was an individual Sperm whale at approximately 2500 m away travelling parallel to the vessel in the opposite direction heading west. Sighting 16, two Sperm whales were visually observed travelling away from the vessel heading south west. As the Knipovich survey site was within

Norwegian waters, standard JNCC guidelines were followed and no mitigation action was necessary as the airguns were already in full volume during all Sperm whale visual (and acoustic) encounters.

In total, there were fifteen acoustic detection events of marine mammals logged during the MSM67 research cruise. Detections 501-511 (Sperm whales) took place between Sept 19th and Sept 20th in Norwegian waters around Knipovich ridge during refraction seismic operations at the AWI, Bremenhaven OBS site. Clicks from individual trains were marked and tracked in real-time, and displayed on the map. Bearings to individual sperm whales (subject to left/right ambiguity) were plotted relative to vessel track and using target motion analysis the distance to localized sperm whales were recorded. Detections 501-511 all took place while the RV Maria S. Merian was engaged in full volume airgun operations. Further analysis of sperm whale detections were processed offline in PAMGuard viewer mode, to confirm distances of localised sperm whales using TMA and to determine group sizes, click characteristics and start and end times of detections.

On Sept 26th on the Greenland continental shelf-edge, during multi-channel seismic lines BGR17-209a and BGR17-210, two Humpback whale detections were observed at 10:35 UTC (512) (Figure 3.3 4) and at 15:35 UTC (513). On both detections, repeated calls (1.5 kHz) and associated harmonics (up to 18 kHz) were seen on the LF spectrogram and heard aurally over the headset. Detection 512 was assessed by the PAM operator, and considered to be within 500 m of the airguns due to the intensity (amplitude, dB) of the calls relative to background noise, and bearing estimates from the Baleen Moan Detector which indicated the whale was approaching the vessel from ahead.

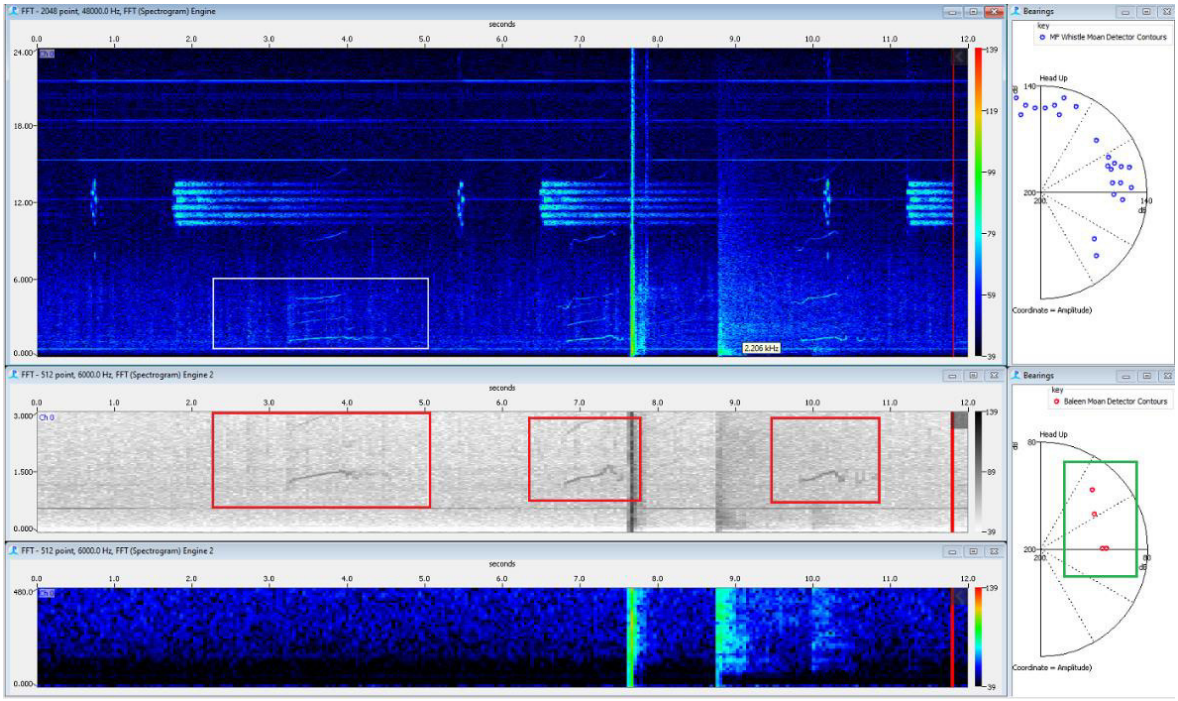

Figure 3.3 4: *Detection 512, PAMGuard spectrogram displays showing humpback whale calls (red boxes) at 1.5 kHz and associated harmonics (upper spectrogram). Radar display shows bearings to calls detected by the Baleen Moan detector (green box) showing whale approaching from ahead. Airgun shot and multi-beam echo-sounder also seen on spectrograms.*

The PAM operator notified the seismic operators of the whales presence and the airguns were immediately powered down to mitigation gun until 20 minutes after the last vocalisation, to ensure the animal had left the exclusion zone. Twenty minutes after the last detection of the whale, the PAM operator gave the clearance to resume firing of the airgun array according to the Greenlandic mitigation protocol. On detection 513, the sounds heard and displayed on the spectrogram although very similar (1.5 kHz calls), were much fainter in intensity, more irregular and without harmonics and therefore not considered to be within proximity to the airguns (estimated 2000 m). Therefore, no mitigation action was necessary.
On Sept 27th on the Greenland continental shelf edge, during multi-channel seismic line BGR17-211, there were two separate detections of unidentified delphinid spp. (514 & 515). Faint, frequency modulated (4 kHz to 8 kHz) sinusoidal whistles were heard over the headset and displayed on the spectrogram. Both detections lasted only a few minutes, and no clicks were observed. Due to the brief and faint sounds, bearing and location to the dolphins was unresolved but judged to be over 3000 m away. No mitigation action was necessary.

3.3.5 Conclusions regarding MMO mitigation and compliance

Marine mammals were both visually sighted and acoustically detected over a widely distributed area of the N Atlantic Arctic region in both Norwegian waters and Greenlandic waters during the MSM67 research cruise. On the continental shelf and slope of East Greenland, Humpback whales were the most commonly identified marine mammals. In the Norwegian waters near Knipovich ridge, several groups of deep-diving Sperm whales where seen and detected by PAM. In the coastal areas North of Iceland, a variety of species were observed, including Humpback whales within the picturesque Eyjafjordur close to Akureyri, and further offshore, White-beaked dolphins and a pod of Killer whales.

It is possible that many of the migratory species had already moved South towards warmer waters where they will spend the winters months breeding and mating, as there were very few occurrences of those species that often occur in large numbers in the Arctic waters during the summer months. There were no recorded sightings of the critically endangered Bowhead whale, Narwhals or Walruses.

Although none of the deep-diving beaked whales were observed, such as the Northern Bottlenose whale, these species are notoriously elusive and spend relatively short time at the surface, spending the majority of their time on long foraging dives.

There was one occasion where mitigation action was necessary during the survey. In this instance, on Sept 26th on the Greenland continental shelf-edge, during multi-channel seismic line BGR17-209a, a Humpback whale was detected by the PAM operator and determined to be within 500m of the airguns. The PAM operator advised the seismic operators to power-down the airgun array and activate the mitigation gun until the animal had cleared the exclusion zone. Twenty minutes after the last detection of the whale, the PAM operator gave the clearance to resume firing of the airgun array according to the Greenlandic mitigation protocol.

4 Narrative of the cruise

Research vessel MARIA S. MERIAN berthed in Reykjavik, Island harbor on Monday morning (August 28th). Members of the scientific crew of MSM67 arrived on the same day and started the loading of scientific equipment and mobilization onboard. There were 6 containers of BGR, plus one container each of both partners Geomar and GEUS (Geological Survey for Denmark and Greenland), all containing scientific equipment for survey MSM67. After unpacking the containers, straightaway the installation of the scientific equipment on deck and in the labs took place. By Wednesday evening all installations of scientific equipment onboard R/V MARIA S. MERIAN were completed and the vessel departed from Reykjavik in the morning of August 31st, as scheduled.

Processing of our application for research permission by the Greenland authorities took longer than expected. Three days prior departure, a survey license was finally granted, however with some unforeseen requirements. Among others, we were requested not to commence our activities in Greenland waters before September 10th. Thus we had to plan for an alternative survey program for the first 10 days of the cruise. Fortunately we had elaborated an alternative survey program for the area around the Norwegian Jan Mayen Island, situated 500 km east of Greenland. An appropriate application for research permission was submitted to the Norwegian authorities well in advance and approved within very short time. We therefore were able to spend the allocated ship time fully for our research goals.

After 550 nautical miles of transit we arrived in the working area south of Jan Mayen Island, early in the morning on Sep 2nd. Here we acquired a seismic crustal transect in an area of unknown crustal nature. The results will contribute to the question of how far the Jan Mayen microcontinent, which was separated from Greenland only 26 Mio years ago, extends westwards. Older sediment basins in this area experienced the same geological evolution as the Greenland margin and this crustal investigations nicely complement our activities on the Greenland margin. However, this crustal transect replaces the planned seaward refraction seismic profile across the Jan Mayen Fracture Zone offshore Greenland. The latter had to be canceled for timing reasons.

Starting in the night from Friday to Saturday 20 ocean bottom seismometers (OBS) of GEUS and 10 OBS of Geomar were deployed along a 260 km long W-E line. After deploying airguns, magnetic sensors and a hydrophone for passive acoustic monitoring (PAM), we acquired refraction seismic data along this first profile from Sunday Sep. 3rd to Monday, Sep. 4th. On Wednesday, September 6th, all but one instrument were recovered.

Medical circumstances required to drop the chief scientist in the port of Akureyri/Iceland, before the research cruise continued toward the most remote areas of east Greenlandic waters. During the transit, the airguns were maintained and the seismic refraction data were evaluated. One of the OBS did not raise to the surface and we went back to the position of this instrument for the time of the automatic backup release set to September 9th at 7:00 am. However, all our efforts did not succeed and this instrument could not be retrieved.

After transit towards Greenland, we deployed all reflection seismic equipment next to the magnetometers and the passive acoustic marine mammal monitoring hydrophone (PAM). This operation was finished on Sunday morning, September 10th and from there acquired geophysical data across the NE Greenland shelf.

Bad weather encountered during the night from Tuesday to Wednesday (end Line 202, beginning Line 203) necessitated some maintenance on the outboard instruments. On Wednesday Sep. 13th, the weather improved, the outboard geophysical instruments were repaired. Problems with the streamer buoyancy induced by considerable movements of the vessel resulted in partly poor data quality on these two lines.

Profiling was again interrupted on early Thursday Sep. 14th morning due to drift ice. Strong winds over the last days had shifted the sea ice far south and the streamer end buoy was snapped off after contact. To recover the buoy, again all outboard equipment had to be taken in during Thursday morning. Around midnight we redeployed all instruments and restarted measurement. As the drift ice has since extended throughout the northern survey area, we skipped the investigation of this region.

On Saturday Sep. 16th, medical circumstances required again to drop one scientist in the port. Therefore, after retrieving the equipment, we were heading towards Longyearbyen on Spitsbergen. After dropping the patient in the harbor on Monday Sep. 18th at 8:30, we arrived at the area of the KNIPAS experiment in the Norway-Greenland Sea by Tuesday Sep. 19th. In order to support the interpretation of the passive seismic data, an active seismic refraction experiment was planned. For logistic reasons, the active part of the experiment was performed during cruise MSM67, while the instruments will be recovered during the next cruise with RV Maria S. Merian, MSM68. Initially this active part was planned for the end of cruise MSM67, on the way back to Longyearbyen. However, as the weather forecast for Greenland was not promising we started measurements already on Tuesday at 07:00. The five airgun-lines were completed by Wednesday evening Sep. 20th and we sailed back to Greenland.

After 1.5 days transit back to Greenland we deployed the OBS along the previously acquired line 202. Deployment started on Friday Sep. 22th, early morning and was finished by night time. Shooting the line took from Friday 22nd 20:30 to Sunday 24th 02:00. From there on, all the OBS were recovered until Monday Sep. 25th in the afternoon.

After two hours transit we redeployed the streamer and started geophysical profiling on Sep. 25th, at 22:30. Line 209 was completed by Sep. 26th at 11:00. A short interruption of acquisition was due to the presence of marine mammals. Line 210 was completed by Sep. 27th at 2:00, line 211 at 22:30. Stronger winds dominated during acquisition of line 212 until finalization on Thursday Sep 28th 22:00. However the vessel's course in wind direction enabled the acquisition of high-quality data. On Friday Sep. 29th, we had to go around floating icebergs, which occurred occasionally along lines 213 and 214. Thus, there a couple of kinks in the profiles. The remaining geophysical profiles 215-217 were acquired without problems. Profiling was successfully finished on Sunday Oct. 1st and from 12:00 to 21:00 the scientific equipment was recovered. Subsequently we headed for the harbor in Longyearbyen (SV).

During transit a faulty seaglider from Geophysical Institute, University of Bergen, Norway (P.I. Idar Hessevik) was recovered. The seaglider had a faulty pressure sensor and was unable/risky for further diving, and the University of Bergen was searching possibilities for assistance on recovery. The seaglider was recovered safely and without any damages on October 02nd 2017 at 15:10 UTC (Position 72°34.7930'N 1°33.0740'E) and subsequently transit was continued. RV Maria S. Merian berthed in Longyearbyen (SV) on Oct. 4th as scheduled.

5 Data acquisition and preliminary results

5.1 Gravimetry

5.1.1 Method and instruments

During the cruise MSM-67, the BGR owned sea gravimeter system KSS32-M (S/N 22) was used. The KSS32-M was installed in the gravimeter room one level below the main deck (Fig. 5.1-1, 5.1-2). The sea gravimeter was located approximately 1 m above the vessel's nominal water line, 0.5 m to portside from the centerline, and 54 m forward of the stern.

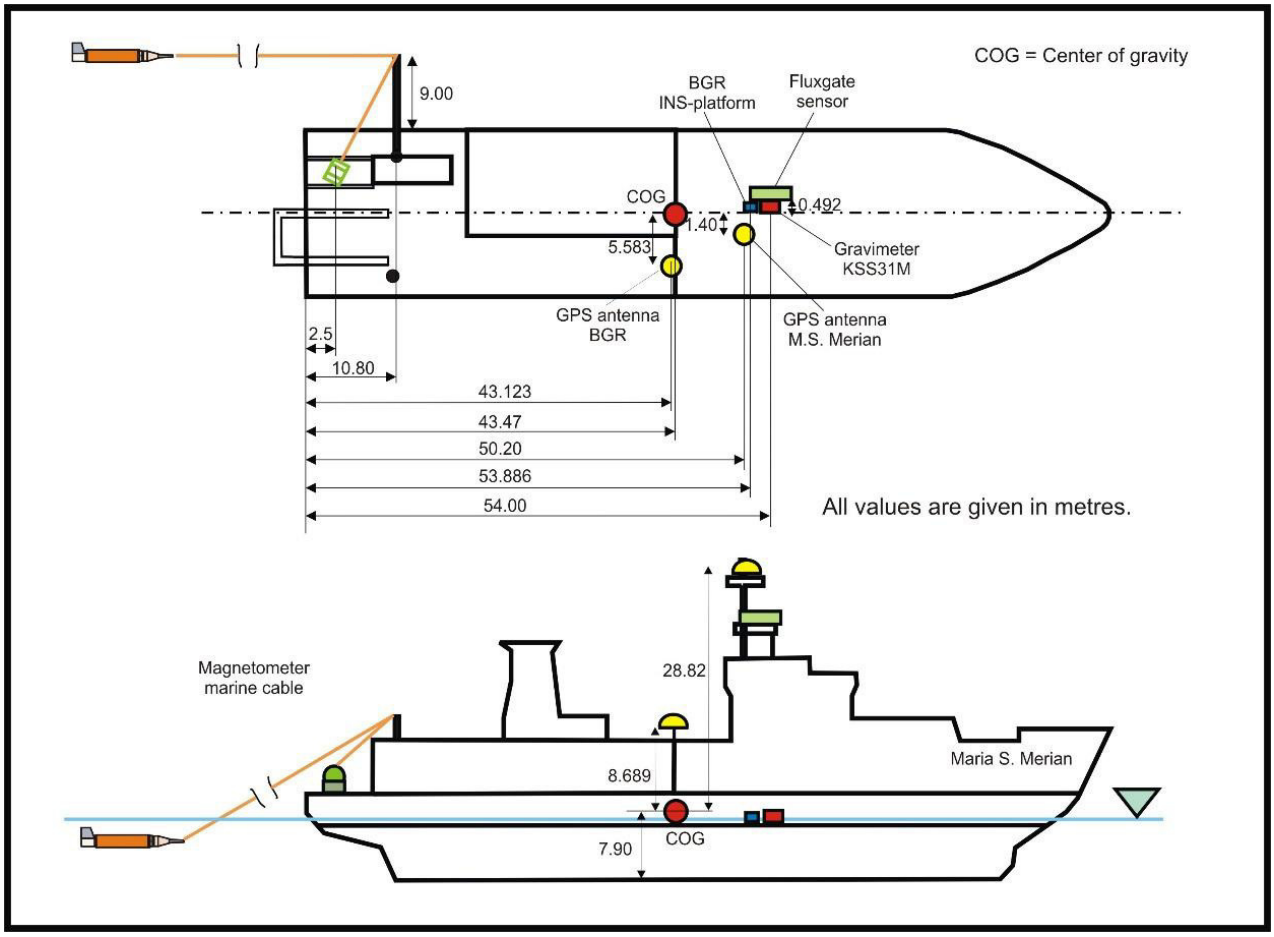

Figure 5.1 1: *The locations of the GPS antenna, magnetometer winch, outrigger port, shipboard fluxgate sensor and gravity meter on RV Merian during MSM-67. The magnetometer towfish distances from the ship's GPS position follow from the sketch, taking cable length on the winch, cable path along the outrigger, and GPS antenna position into account.*

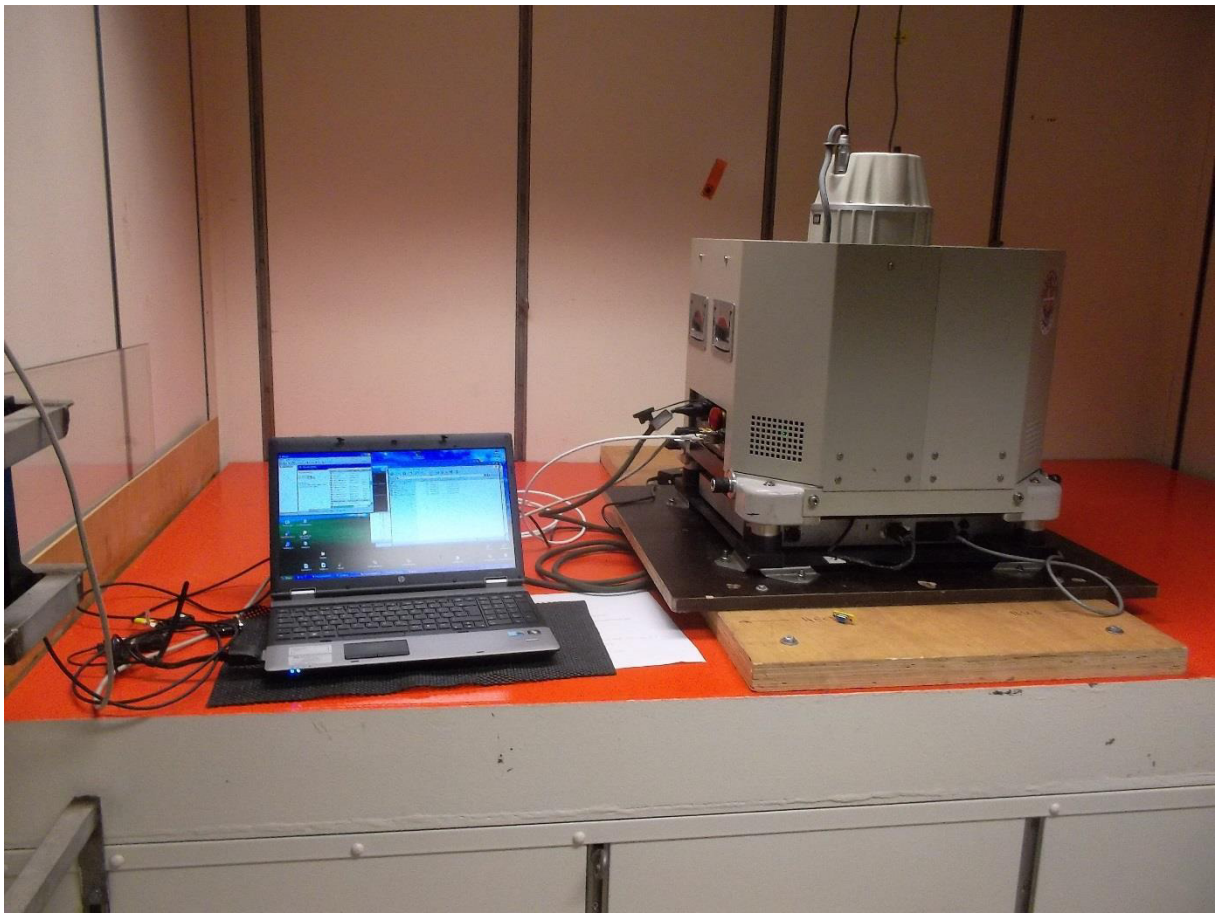

Figure 5.1 2: *KSS32-M gravimeter system in the gravimeter lab of RV Merian.*

The gravimeter system KSS32-M is a high performance instrument for marine gravity measurements, manufactured by the Bodenseewerk Geosystem GmbH. While the sensor is based on the Askania type GSS3 sea gravimeter designed by Prof. Graf in the 1960ties, the development of the horizontal platform and the corresponding electronic devices took place at the Bodenseewerk Geosystem in the second half of the 1970ties. The system was completely modernized and modified in 2011 by the successor company Bodensee Gravitymeter Geosystem GmbH. Before, the system consisted of two main assemblies: the gyro-stabilized platform with the gravity sensor and a rack containing the control electronics, the data handling subsystem and the power supply. After the modernization the system electronics and the power supply are integrated in the platform. The system is controlled by a notebook (HP ProBook 6550B). The main software to operate the KSS32-M is DACQS developed by BGGS.

It allows to change a number of settings (for example: parameters of the Bessel Filter applied to the measured data) and provides detailed information about the status of the system. The data acquisition is also managed by DACQS, whereby a wide range of values not only the gravity but also for example the attitude and horizontal accelerations of the platform could be recorded.

The gravity sensor GSS30 (Fig. 5.1-3) was not affected by the modernization. It consists of a tube-shaped mass that is suspended on a metal spring and guided frictionless by 5 threads. It is non-astatized and particularly designed to be insensitive to horizontal accelerations. This is achieved by limiting the motion of the mass to the vertical direction. Thus it is a straight line gravity meter avoiding cross coupling effects of beam type gravity meters. The main part of the total gravity acceleration is compensated by the mechanical spring, but gravity changes are compensated and detected by an electromagnetic system. The displacement of the spring-mass

assembly with respect to the outer casing of the instrument is measured using a capacitance transducer.

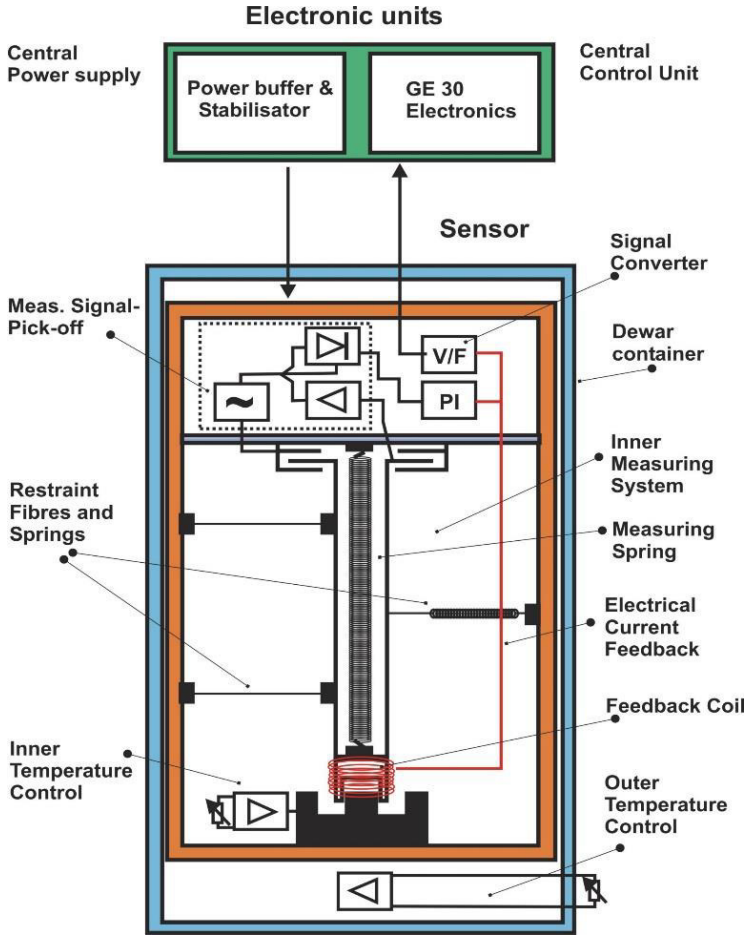

Figure 5.1 3: *Principle sketch of the gravity sensor GSS30 of the gravimeter system KSS32-M.*

The leveling subsystem consists of a platform stabilized in two axes by a vertical, electrically erected gyro. The stabilization during course changes can be improved by providing the system with online navigation data. The stabilized platform will keep the sensor in an upright position with an accuracy of leveling in the order of 0.5 arc-minutes. This is particularly important as the sensor is very sensitive to tilting and the corresponding effects of horizontal accelerations. Vertical accelerations, however, cannot be eliminated. Luckily on a ship the vertical acceleration oscillates symmetrically with the ship's motion. The period of the oscillation is in the order of several seconds. This signal can be eliminated easily by means of low-pass filtering.

The data are transmitted via the notebook to the BGR data acquisition and processing system in the magnetic lab on the main deck and online navigation data from this system are sent with a rate of 1 Hz to support the stabilizing platform. The support is realized as follows: The horizontal position of the gyro-stabilized platform is controlled by two orthogonal horizontal accelerometers. The platform is leveled in such a manner that the horizontal accelerations are zero. If the ship describes a curve, the additional horizontal acceleration will cause the platform to be leveled according to the resulting apparent vertical axis. This axis may differ substantially from the true vertical axis and will result in reduced gravity values and additionally in an effect of horizontal accelerations on the measured gravity. This error, named Harrison effect, is eliminated by supplying the KSS32-M system with online navigation data. A microprocessor

calculates the leveling errors from this input and enters them into the platform electronics which corrects the platform accordingly.

5.1.2 Gravity data processing

Processing of the gravity data consists essentially of the following steps:

- a time shift of 76 seconds due to the overcritical damping of the sensor
- conversion of the output from reading units (r.u.) to mGal by applying a conversion factor of 0.94542 mGal/r.u., on this cruise this was done in the system itself by hardware setting
- connection of the harbour gravity value to the world gravity net IGSN 71 (see 5.1.3)
- correction for Eötvös effect using the navigation data
- correction for the instrumental drift (not performed until completion of the cruise)
- subtraction of the normal gravity (WGS67)

As a result, we get the so-called free-air anomaly (FAA) which in the case of marine gravity is simply the Eötvös correceted observed absolute gravity minus the normal gravity. According to the selectable time interval of the data acquisition system, gravity values are available every 1 second.

Additionally the gravity anomalies, which are provided every second directly by the data handling subsystem of the KSS32-M, were recorded with a separate computer. Free-air gravity anomalies are obtained when the KSS32-M is supplied with the necessary navigation data (geographical latitude and longitude, speed, course over ground and heading). These data are available every second. The differences in both data sets are small. For the display and interpretation of gravity data the 1s processed values were used. However, outliers were removed manually in both data sets. Also the gravity data collected during the deployment and recovery of OBS were usually disregarded.

5.1.3 Gravity ties to land stations

To compare the results of different gravity surveys, the measured data have to be tied in a world-wide accepted reference system. This system is represented by the International Gravity Standardization Net IGSN71 (Morelli, 1974). The IGSN71 was established in 1971 by the International Union of Geodesy and Geophysics IUGG as a set of world-wide distributed locations with known absolute gravity values better than a few tenths of mGal. According to the recommendations of the IUGG, every gravity survey, marine or land, should be related to the datum and to the scale of the IGSN71.

Therefore, land gravity measurements have to be carried out to connect the gravity measurements at sea with the IGSN71. The marine geophysical group of BGR uses for gravity connections a LaCoste&Romberg gravity meter, model G, no. 480 (LCR G480).

RV MARIA S. MERIAN moored at the northern side of central pier of Vesturhöfn harbour in Reykjavik, Iceland (Fig. 5.1-4). On Aug. 30 and 31, 2017, tie measurements to point A on the pier opposite the gravimeter room on MERIAN have been made. Point A is located between the fourth and fifth bollard 48 m from the eastern corner of the pier.

The connection measurements resulted in an average absolute gravity value of 982267.9 mGal (with water level –3.8 m, IGSN71) for point A at the water level. That results in an absolute gravity value of 982267.61 mGal for the location of the gravity sensor. The reading of the KSSM32-M at the leaving time (Aug. 31, 2017, 08:30 UTC) from the pier was 2274.3 mGal.

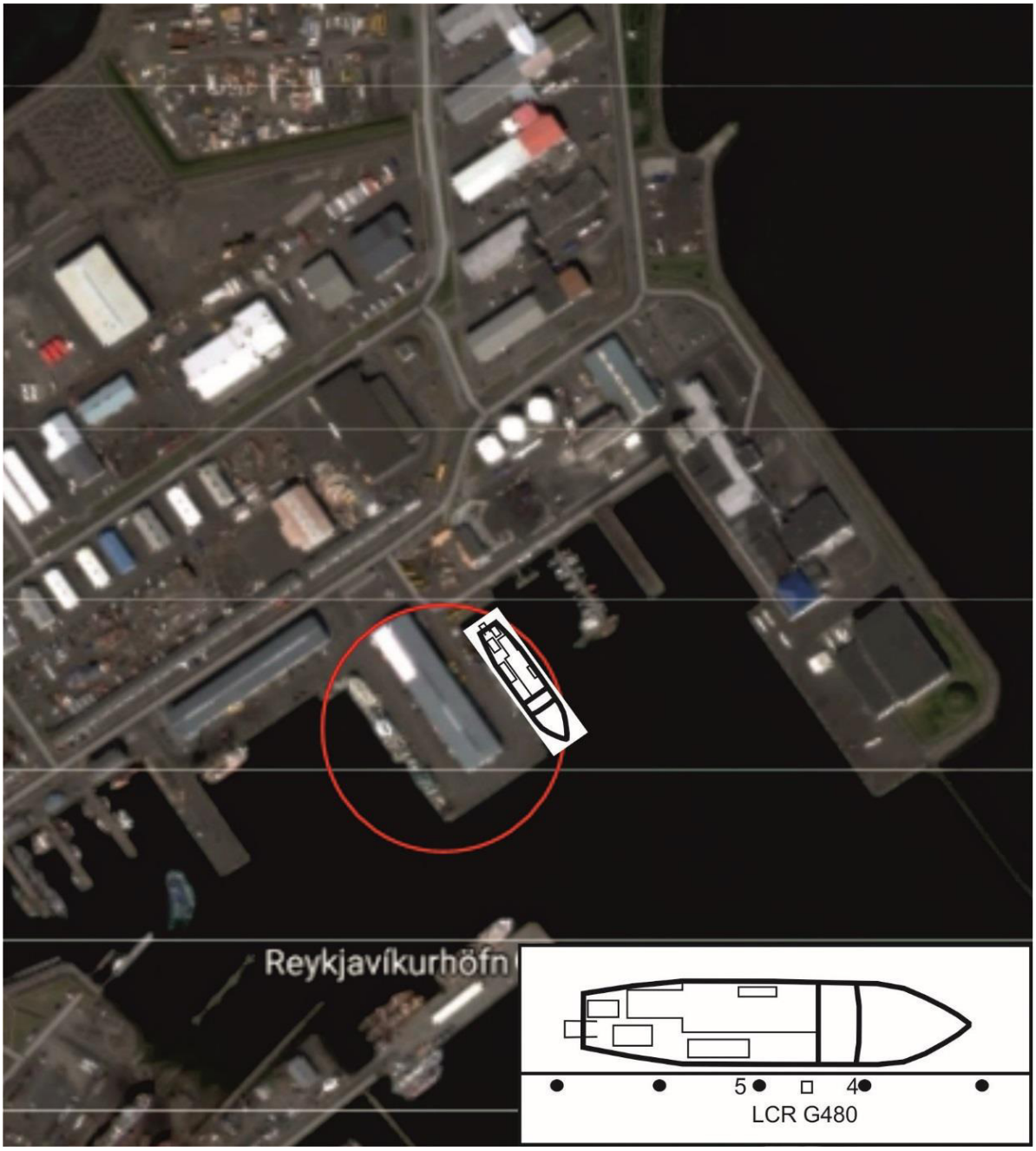

Figure 5.1 4: *Location of the docking site of RV MARIA S. MERIAN at the central pier in Vesturhöfn harbour (Reykjavik, Iceland) with site of dock-side gravity tie point.*

Station	Observer	Date	Time UTC	Reading units	Gravity value [mGal]
A	B	30.08.17	12:50	5800.18	5901.20
01	B	30.08.17	13:30	5792.24	5893.11
02	B	30.08.17	13:55	5796.09	5896.74[1)]
03	B	30.08.17	14:55	5909.68	5910.75[2)]
A	B	30.08.17	15:30	5800.14	5901.17
B	B	04.10.17	10:40	6481.67	6596.55
04	B	04.10.17	11:05	6480.10	6594.95

Table 5.1 1: *Observation summary of the gravity tie measurements in Reykjavik (Iceland) and Longyearbyen (Spitsbergen) during MSM-67. Gravity in mGal was calculated using LCR G 480 scaling table. B = U. Barckhausen (observer). 1) corrected for the height of the no longer existing pillar (1 m); 2) corrected for height above water table.*

Reference Stations:

01: Hallgrimskirkja, Reykjavik
BGI Station No. 21941 B 982258.79 mGal (IGSN71)

02: Landakotskirkja, Reykjavik
BGI Station No. 21941 C 982262.46 mGal (IGSN71)

03: Sundahöfn, mooring location of RV Polarstern ARK XXV/2, 07/2010
(64°09.241'N, 21°51.589'W) 982276.46 mGal (IGSN71)

04: Airport, Longyearbyen
Station No. GI 803 of KMS Gravity Net 982963.00 mGal (IGSN71)

Gravity stations:

A: Vesturhöfn, central pier, 48 m from the eastern corner of the pier
(64° 09.267'N, 21° 56.423'W)

B: Longyearbyen

Differences between reference and gravity stations:

A – 01 = +8.09 mGal

A – 02 = +4.46 mGal

A – 03 = –9.58 mGal

Absolute gravity at A (from 01):	982266.87 mGal
Absolute gravity at A (from 02):	982266.92 mGal
Absolute gravity at A (from 03):	982266.88 mGal
Absolute gravity for A	982266.89 mGal (IGSN71 system)
Absolute gravity at gravity sensor	982267.61 mGal

(1.1 m above water level, water level at -3.8 m) used for the gravity tie on 31.08.2017 (08:30 UTC)

Reading of sea gravimeter KSS31 at that time: 2274.3 mGal

B – 04 = –1.60 mGal

Absolute gravity at B (from 04):	982964.60 mGal
Absolute gravity for B (reduced to water level –3.1 m)	982965.43 mGal (IGSN71 system).
Absolute gravity at gravity sensor	982964.98 mGal

(1.7 m above water level, water level at -3.1 m) used for the gravity tie on 04.10.2008 (08:30 UTC).

Reading of sea gravimeter KSS31 at that time: 2950.4 mGal.

On Oct. 4, 2017, RV MARIA S. MERIAN docked at the Longyearbyen Kaier in Longyearbyen, Spitsbergen (Fig.5.1-5). Tie measurements to reference station 04, which is located at the airport of Longyearbyen, have been made. The point description and absolute gravity value of the reference station was kindly provided by Kort- og Matrikelstyrelesen (KMS, Copenhagen, Denmark). Point B is located near the center of the pier. The connection measurements resulted in an average absolute gravity value of 982965.43 mGal (with water level –3.1 m, IGSN71) for point B at the water level. That results in an absolute gravity value of 982964.98 mGal for the location of the gravity sensor. The reading of the KSSM32-M on Oct. 4 (08:30 UTC) was 2950.4 mGal.

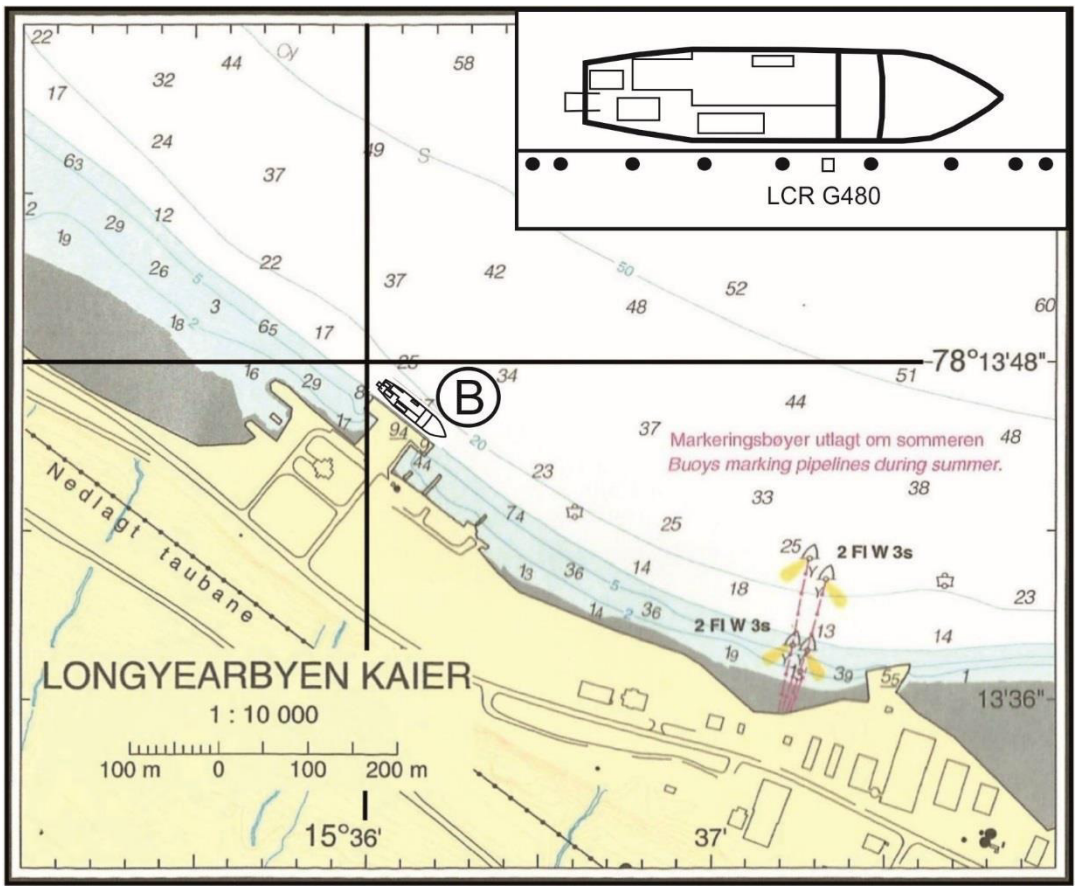

Figure 5.1 5: *Location of the docking site of R/V MARIA S. MERIAN in Longyearbyen (Spitsbergen) and gravity tie points.*

The instrumental drift for the cruise MSM-67 can be derived from the readings in Reykjavik and Longyearbyen to -21.27 mGal in 35 days or -0.608 mGal/day. This drift rate is very high and could possibly be explained by the fact that rough weather with high sea states and related ship motion was encountered during much of the cruise. However, the evaluation of gravity differences along profiles sailed repeatedly indicates a very small instrumental drift during the cruise at least for the time interval between the profiles. A comparison of global satellite gravity data to the shipboard gravity data show a rather large, but almost perfectly constant offset of -14 mGal. This number is in the range of the inferred total instrumental drift between Reykjavik and Longyearbyen. We suspect that data acquisition problems which occurred at the beginning of the cruise during the transit to the first survey area caused a permanent shift in the gravity data by roughly -14 mGal. Therefore it was decided to tie the gravity data to the absolute gravity of Reykjavik with a correction factor of +14 mGal and to abstain from a drift correction. Further investigation of the cause of the offset to the level of the satellite gravity will be necessary during post-cruise processing.

5.1.4 Data quality

In order to check the accuracy of the data quantitatively, the values along one profile measured repeatedly and at crossovers of gravity profiles were compared. Fig. 5.1-6 shows the comparison for profiles BGR17-202 and BGR17-2R2.

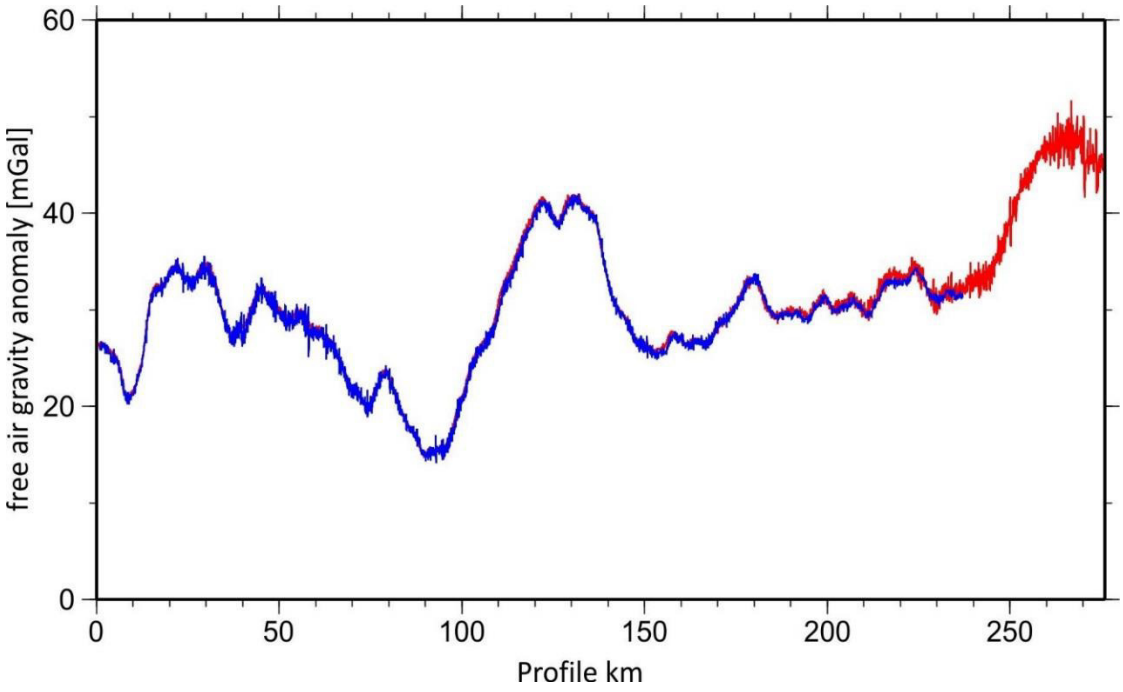

Figure 5.1 6: *Comparison of free-air gravity anomalies along profiles BGR17-202 (red curve) and BGR17-2R2 (blue curve).*

The coincidence is nearly perfect and the differences amount to less than 1.5 mGal. The second run (BGR17-2R2, blue curve) did not cover the entire length of the first profile (BGR17-202, red curve). Both profiles have a relatively high noise level due to rough seas. The last 50 km of profile BGR17-202 show very high data noise due to particularly bad weather with wind speeds of more than 25 m/s. Fig. 5.1-7 shows the same profiles after a mild median filtering.

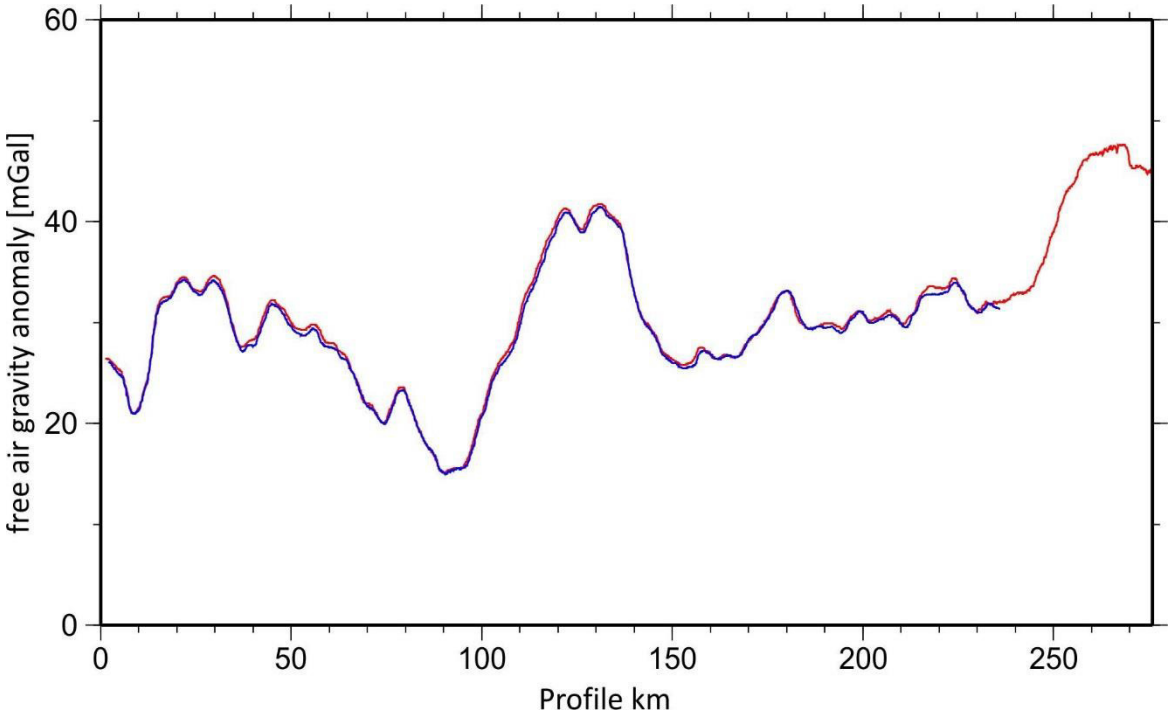

Figure 5.1. 7: *Comparison of free-air gravity anomalies along profiles BGR17-202 (red curve) and BGR17-2R2 (blue curve) after median filtering.*

5.2 Hydroacoustic systems

RV MARIA S. MERIAN has hull mounted sediment echosounder and swath bathymetry systems which were used during the cruise.

5.2.1 Swath bathymetry

In order to get detailed information about the seafloor morphology of the study area, the seafloor was surveyed by the SIMRAD EM122 (deep water) and SIMRAD EM712 (shallow water) multi-beam systems.

The SIMRAD EM122 system is a multibeam swath sonar designed for all ocean depth ranges. The angular coverage sector of the echo system may reach 150° in shallow water or a swath width up to 25 km in depths greater than 5000 m. 432 beams are generated for each ping. The angular coverage, beam pointing angles and ping rate adapt to varying depth ranges. The ping rate depends merely on the overall round trip travel- and processing time. In shallow waters the ping rate may reach 3 Hz, whereas in 5000 m water depth a ping is generated about every 12 sec. The beam spacing has been set to equidistant beam footprint, thus allowing for uniform sampling of the seafloor across the track.

The seafloor is detected using amplitude and phase information for each beam sounding. Phase detection allows for high accuracy bottom determination even with high incidence angles of the soundings at large slant ranges. Depth and position calculation is then performed per beam taking account of the beam angles and refraction in the water column using the corresponding sound velocity profile, the vessel's attitude and movement (MRU) and the vessel's position via the system-position sensor, which was the DGPS system. Additionally, backscatter and amplitude data of the seafloor are recorded.

Operation of the EM122 was controlled by a workstation running the Seafloor Information Software by Kongsberg Maritime AS (SIS Version 4.3.2).

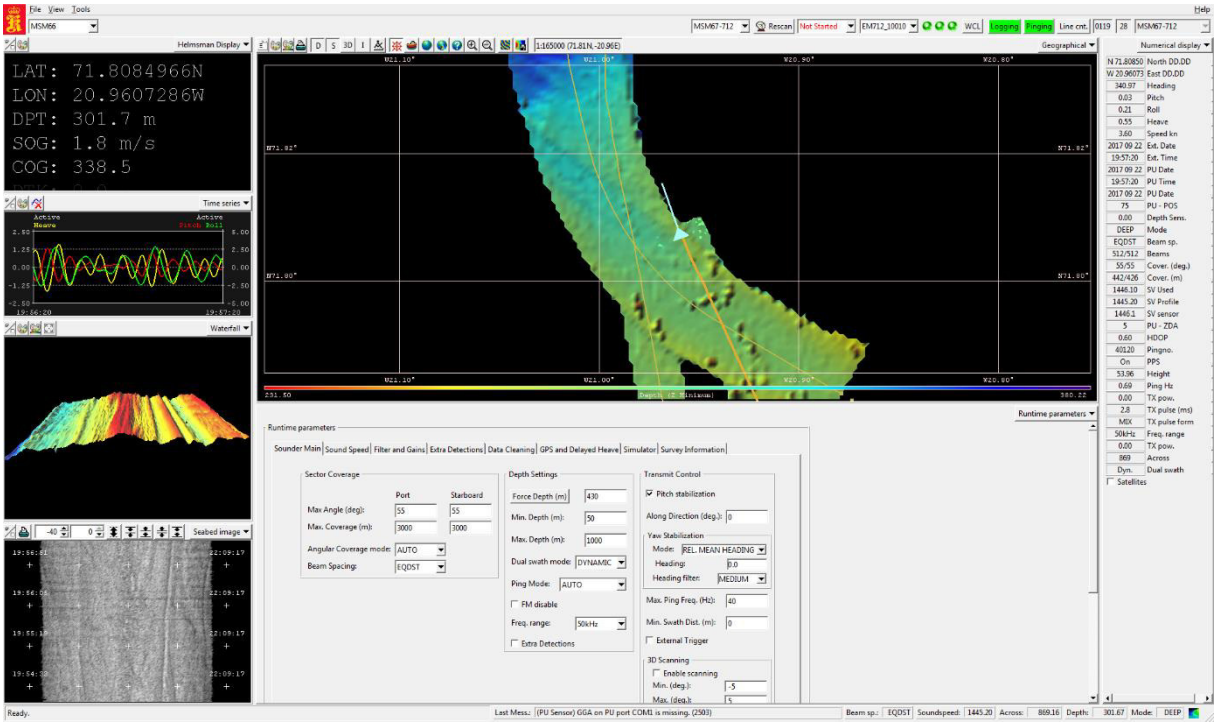

Figure 5.2 1: *Quality control and access to the swath bathymetry system sensors.*

The Simrad EM712 works on frequencies from 40 Hz – 100 Hz with 512 beams generated per ping. It is controlled by the Seafloor Information Software by Kongsberg Maritime AS (SIS Version 4.3.3). The software performs all depth and position calculations in real-time. Several online displays allow quality control and access to the system sensors (Figure 5.2 1). It was used in water depths above 1000 m, to achieve a higher resolution of the seafloor compared to the data acquired by the Simrad EM122. Best results were achieved with a frequency of 50 Hz and an opening angle of 55 to 60 degrees. However, the data get poor during bad weather conditions which were common during the cruise. Due to interferences, the Simrad EM712 could not be used together with the subbottom profiler Parasound.

5.2.2 Sub-bottom profiler

The PARASOUND DS III-P70 system (Atlas Hydrographic, Bremen) installed on RV MARIA S. MERIAN combines a high-frequency deep-sea echosounder (NBS, narrow-beam system) for water depth sounding with a low-frequency sediment echosounder (SBP, sub-bottom profiler). Because the SIMRAD EM122 and EM712 were used for water depth sounding, only the SBP capabilities and settings of the Parasound system are described here.

The system simultaneously transmits two independent pulse-modulated harmonic signals via the same transducer array. The seawater does not only serve as a propagation medium for the original signals, but also generates additional new signal components at different frequencies. This parametric or non-linear propagation effect of sound in seawater allows for a narrow transmission beam angle of 4.5° x 5° which leads to a high spatial and vertical resolution. A disadvantage of the small footprint (7% of the water depth) is the loss of a return signal over areas of greater water depths and over slopes steeper than 4°, where the reflected signal is not captured by the ship's detectors.

To achieve best data accuracy and best sediment layer resolution, the transmission and reception beams are fully motion-compensated with respect to the roll, pitch and heave movement of the vessel.

Parasound settings and data acquisition

During cruise MSM67 the two primary frequencies (PHF1 and PHF2) were chosen to 19.8 kHz und 23.8 kHz to utilize the parametric effect efficiently for sediment investigations. These two PHF result in a secondary parametric low frequency (SLF) of 4 kHz, which is sufficiently low to allow for deep bottom penetration in soft sediments of more than 200 meters depending on the sediment characteristics. System configuration options only allow an input of the PHF1 and the desired SLF. The PHF2 value is set internally using these two values PHF2=PHF1+SLF). Maximum transmission voltage was set to 120 V. For the signal transmission, we used the quasi-equidistant transmission mode with a desired time interval of 800 ms.

The Atlas Parastore software package for controlling the echo sounder and for acquisition, visualisation, processing and storage of the data is implemented onboard on RV MARIA S. MERIAN. The acquired data is stored using the ASD, SEG-Y and PS3 formats. The ASD (Atlas Sounding Data) is a raw data file format for the storage of the complete sounding profiles. In contrast, the SEG-Y and PS3 files provide the option only to save the data within the Parasound reception window.

During the MSM67 cruise we recorded a time window of 200 ms. Because the signal was generated in two periods of 0.5 ms to achieve higher penetration, a sampling frequency of 6,135 kHz (sampling interval 0,163 ms) was sufficient. The time delay, i.e. the start time of the Parasound depth window was automatically set based on the detected water depth provided by the PHF signal. The recording window is moved automatically when the seafloor reflection gets

close to the top or bottom of the window limits. (Time delay changes when the absolute distance is less than 10% of the total time window).

SLF data were stored in SEG-Y and PS3 format. File length was limited to 30 minutes of recording time. The Parasound sediment echosounder was continuously operated in deep water (see data examples Figure 5.2 3and Figure 5.2 **4**). Due to interferences with the SIMRAD EM712 multibeam system which was used for high resolution bathymetry, it was shut down in shallow waters. As soft sediments are mostly abundant on the Greenland shelf (Figure 5.2 12), acquisition of high resolution bathymetry instead was preferable.

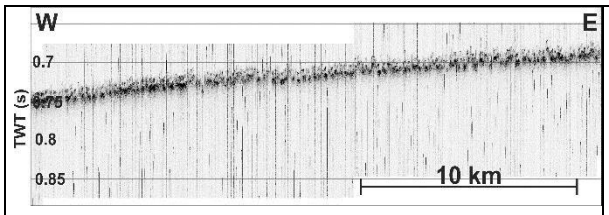

Figure 5.2 2*: Data example – East Greenland shelf*

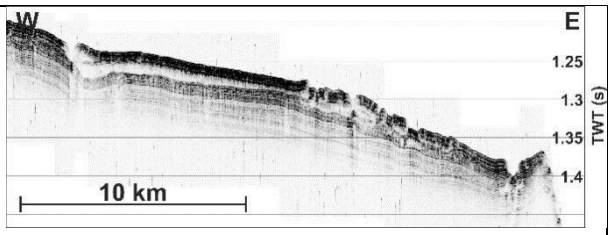

Figure 5.2 3*:Data example – Jan Mayen Ridge*

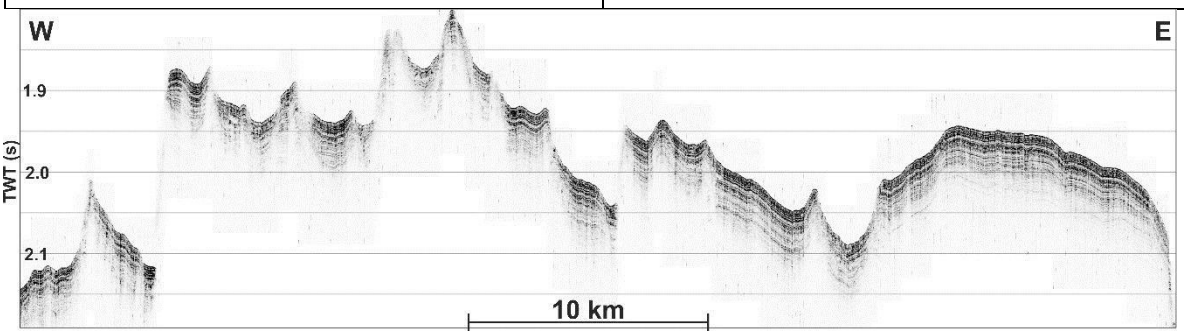

Figure 5.2 4: *Data example – faulting, oceanic domain.*

5.2.3 Sound velocity profile (SVP)

Water depths are calculated from beam travel times using a sound velocity model of the water column. Since sound velocities, especially of the upper water masses, are subject to considerable annual and local variation, accurate depth calculations in a given survey area require the knowledge of the sound velocity profile of the water column for that specific region at the time of measurement.

The sound velocity in the water column was measured with Lockheed Martin XSV-2 probes. They have a maximum operation depth of 2000 m and were used in deep water regions of the survey area.

Three SVPs were measured during the cruise in deep water areas (Figure 5.2 **5**). For shallow waters of up to 400 meter depth on the Greenland shelf, a simple velocity profile was constructed, based on the different runtime of inner and outer beams of the SIMRAD EM712 multi-beam system

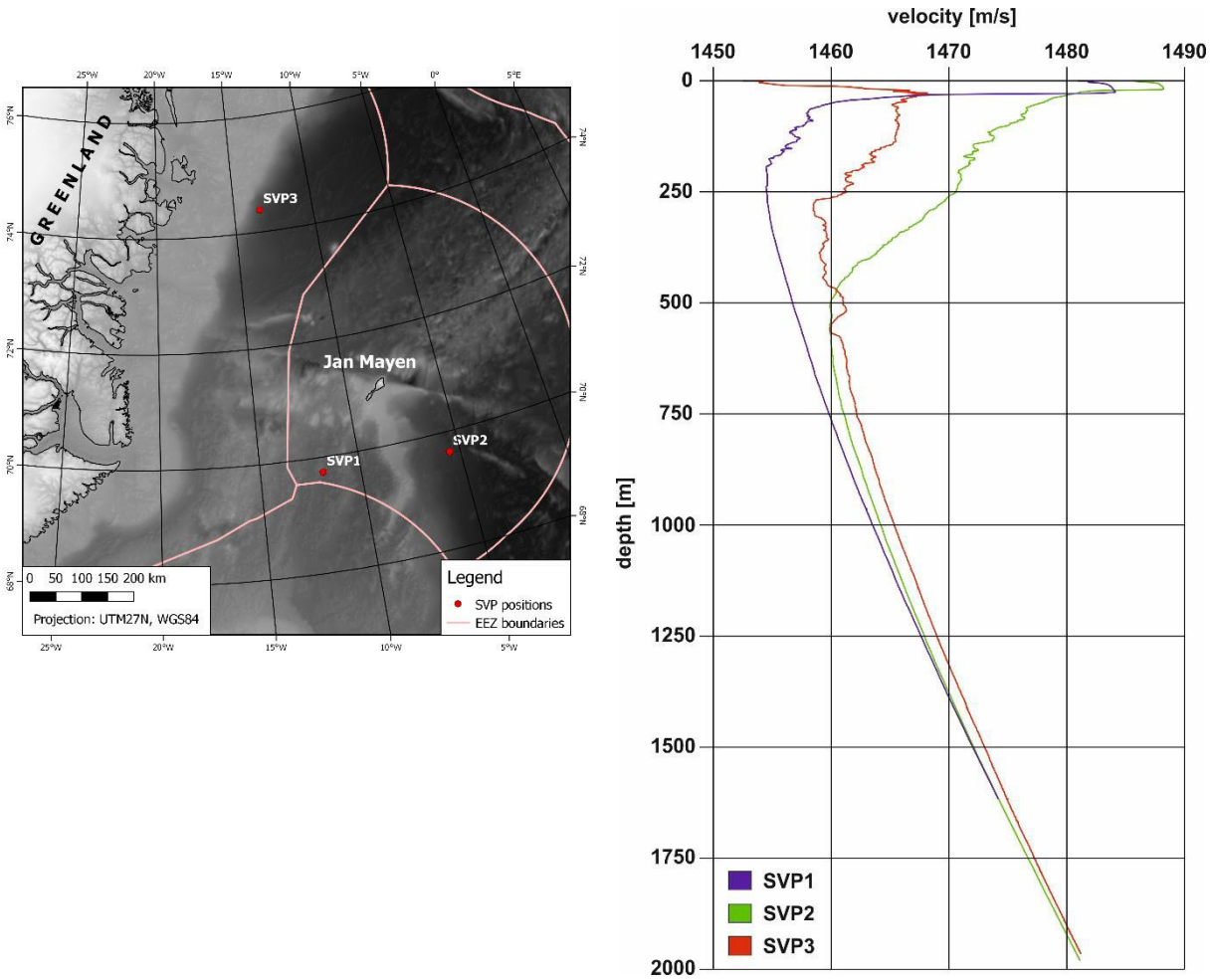

Figure 5.2 5: *Sound velocity profiles and locations.*

5.3 Magnetics

5.3.1 Method, instruments and operation

The BGR magnetometer systems used during cruise MSM-67 consisted of two independent magnetometer types which were operated simultaneously on one cable:

(1) the SeaSpy system with one or two Overhauser magnetometer sensors and

(2) an oriented Magson fluxgate sensor.

Overhauser sensors measure the scalar absolute value of the total magnetic field while fluxgate magnetometers measure the magnetic field vector in its three components.

Marine Magnetics SeaSpy™ Gradiometer

The SeaSpy™ Marine Gradiometer System manufactured by Marine Magnetics Corp. normally consists of two proton precession magnetometers, enhanced with the Overhauser effect. In its original configuration two exactly equivalent magnetometers are towed 150 meters apart as a longitudinal array 550 meters astern of the ship (Figure 5.3 1). Both sensors measure the total intensity of the magnetic field simultaneously. The difference between the two measurements is an approximation for the longitudinal gradient of the field in the direction of the profile line. Provided that the time variations are spatially constant over the sensor spacing, the differences are free from temporal variations and their integration restores the variation-free total intensity or magnetic anomaly (apart from a constant value).

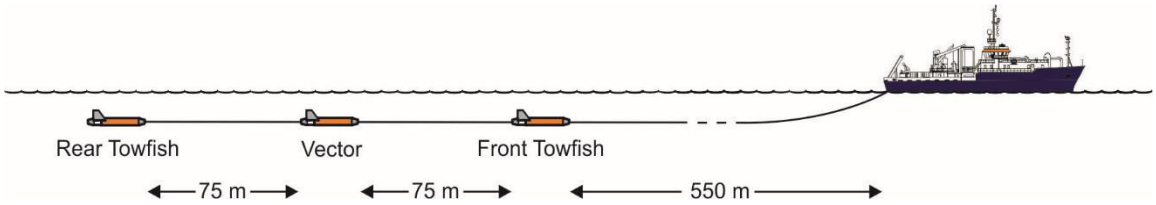

Figure 5.3 1: *Schematic sketch of the towed gradiometer system towed gradiometer system (front and rear Overhauser sensor) and one fluxgate towfish in-between.*

A standard proton precession magnetometer uses a strong DC magnetic field to polarize itself before a reading can be taken. Overhauser sensors work similar to proton magnetometers with the exception that the excitement of the proton spin (polarization) is done by radio waves which excite the spin of the electrons in an organic fluid within the sensors. The electrons then transfer their spin to the protons in the fluid via a quantum mechanical process called Overhauser effect. Similar to every other proton magnetometer the relaxation frequency of the protons is a measure for the magnitude of the ambient magnetic field. The polarization power required is much smaller than that needed by normal proton magnetometer systems and the AC field may be left active while the sensor is producing a valid output signal. This allows the sensor to cycle much faster and to produce more precise results than a standard proton magnetometer. The signal is digitized by the electronics assembly within the tow fishes which then transmit digital data strings via a two conductor tow cable to the vessel. The tow cable is connected to a deck leader which is in turn connected to the power supply and the logging computer. As configured for this survey, the Overhauser sensors had a cycle time of one second. The sensors are specified with a noise level of 0.01 nT/√Hz, a resolution of 0.001 nT, and an absolute accuracy of 0.2 nT.

Magson™ Fluxgate Magnetometer

The Magson fluxgate towfishes were designed by the BGR marine geophysics group and built by the Magson company in Berlin. The system consists of i) a digital 3-axis Magson fluxgate magnetometer yielding excellent precision, ii) a two-axis tilt-meter, type 900H made by Applied Geomechanics Ltd., iii) a two-axis and single axis accelerometer, types ADXL203 and ADXL103 made by Analog Devices, iv) sensors for temperature, pressure, and humidity, and v) a data acquisition microprocessor built by Magson as well. Fluxgate and inclinometers are mounted on a common platform. All components, shown in Figure 5.3 2, are placed inside a pressurized glass-fibre tube of the same brand as the sensors of our standard SeaSpy™ gradiometer.

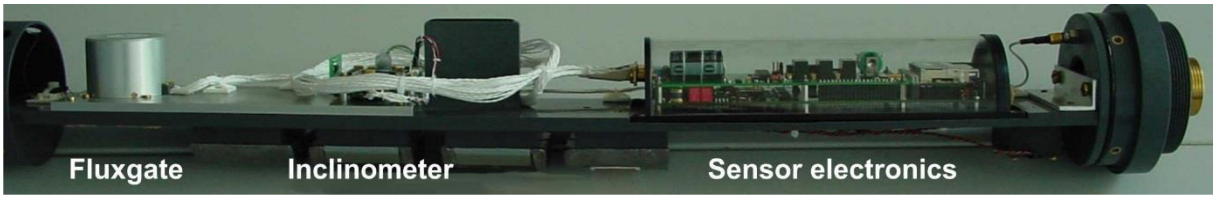

Figure 5.3 2*: Components inside the fluxgate magnetometer towfish.*

The Magson fluxgate uses the principle of vector-compensating all three ring-core-sensors by means of three independent Helmholtz-coils. The internal feedback circuit, using digitally controlled DC-currents fed into the Helmholtz-coils maintains precise nulling of the field inside the ring-core. Thus the amplitude of this current can be used as a signal to measure the vector components of the magnetic field. A factory calibration is required to provide offset, scale factor and non-orthogonality angle for each axis. All electronic components are integrated on the board of the data acquisition microprocessor. The Magson fluxgate sensor is specified with a noise level of 0.02 nT/√Hz, a resolution of 0.008 nT and a long term stability < 10 nT/year.

Inside the tow fish a special platform is used to mount the fluxgate and both tilt-sensors. The first tilt-sensor by Applied Geomechanics (900H) measures pitch and roll angles by a conductive liquid in a half filled glass vial. The tilt angle is derived by the height of liquid covering five electrodes. This inclinometer covers an angular range of ± 25°/± 40° (first/second Magson towfish) with an accuracy of about 0.01° of arc (noise level 0.005°).

The second tilt-sensors are dual axis accelerometers by Analog Devices (ADXL203), measuring pitch and roll angles over a span of ± 50°/± 20° (first/second Magson towfish) resolving 0.05° of arc (noise level 0.095°). A third accelerometer for the vertical axis (ADXL103) allows to detect an unintended upside down position of the towfish.

The accuracy of the Applied Geomechanics sensor is significantly higher, but the calibration function is non-linear and temperature dependent. The Analog Devices sensor has a faster response (cross correlation results in 0.1 s difference), the calibration function is linear and almost temperature independent, but it suffers the noise level increased by factor 2. Both tiltmeters measure not only the static acceleration, which would provide the needed true roll and pitch angles. Instead, they measure also the dynamic acceleration due to the angular accelerations of the continuously moving towfishes. This source of error can partly be reduced by filtering but remains a limiting factor of tilt estimation.

A high precision of angle measurement is necessary to rotate the field components measured in the sensors coordinate system of the moving fluxgate towfish into the horizontal geomagnetic coordinate system. By Euler rotation it is possible to separate the vertical from the horizontal field vector components. The accuracy of the vector data is limited by the accuracy of the rotation angles. For example, a 0.01° tilt deviation may result in up to 10 nT component error

in the survey area. Without any yaw angle estimation, the orientation of the horizontal field vector (i.e. the north and east component) remains unknown. A crude approximation might be ship's course. Utilising magnetic heading from the fluxgates themselves removes seafloor anomalies by default, however, a numerical yaw approximation has been introduced by Engels et al. (2008), demonstrating the advantages of vector component data analysis.

An embedded microprocessor with a flash disc is used to store all fluxgate and tilt-meter readings. The storage capacity of 1 GB is sufficient to allow for 11 days of continuous operation at a sampling rate of 10 Hz.

Magnetometer array configurations

All magnetometer array configurations which have been applied during cruise MSM-67 are listed in Table 5.3 1. Sensor type is identified by a serial number. S/N 13141, S/N13545 and S/N 13546 are Overhauser sensors while S/N13142 denotes the Magson sensor. Usually BGR has four Overhauser sensors and two Magson sensors available. Due to another cruise that overlaps with the MSM-67 cruise only the four sensors mentioned above were available. For technical reasons and due to adverse weather conditions on one line (BGR17-212) only one Overhauser sensor could be deployed. During Profile BGR17-203, very bad weather was encountered which lead to noisy data and finally to the failure of the entire Gradiometer system due to a defective tow cable.

Table 5.3 1: *Magnetometer configurations applied during cruise MSM-67.*

Profile	Main cable	S 1	Connect 1	S 2	Connect 2	S 3
BGR17-2R1 - BGR17-211	600-2	13545	75-6 AB	13142	75-7 AB	13546
BGR17-212	600-2	13141				
BGR17-213 - BGR17-217	600-2	13545	75-7 AB	13142	75-12 AB	13546

Fluxgate sensors require calibrations which are typically performed as loops (circles sailed by the ship for this purpose. However, sailing full circles while towing a seismic streamer is difficult and very time consuming. One full circle was performed during the cruise while deploying the streamer with the magnetometer array already measuring on Sept. 3, 2017. One more full circle was surveyed at the end of the scientific operations when all outboard gear had been retrieved already for the purpose of calibration the onboard magnetometers on Oct. 1, 2017.

Shipboard Magson™ Fluxgate Magnetometer

Another vector magnetometer system was installed on the observation deck of the vessel. It consists of two separate waterproof housings that contain orthogonal digital ring core fluxgate sensors and two-axis inclinometers, a data acquisition box and a GPS mouse. The system was built by MAGSON GmbH in Berlin for BGR and delivered January 2010 as an onboard system for research vessels. The electronics and software based on a Linux board is a new development compared to the older towed system described above. The sensors have a dynamic range of +/- 100000 nT and a long-term stability of <10 nT/year and were fixed to the railing on the port and starboard sides of the observation deck (Figure 5.3 3). The data are recorded internally on a CF memory card and optionally online on a laptop. Two different types of data files are stored separately for each hour. The first file type (file extension M60) contains the values of the three orthogonal vector components and the inclination values together with UTC time marks. The sampling rate can be chosen between 1 and 20 Hz. On this cruise we used 10 Hz. The second

file type (file extension S60) contains time marks and latitude and longitude from the GPS receiver and temperature values for both sensors. The sensors are internally heated to a selectable temperature, on our cruise to 15°C. Additionally we also recorded the values from the ship's motion reference units (heave, roll, pitch, and azimuth). Experience shows that roll and pitch values from the vessel sensors are much more reliable than the inclinometer values from the fluxgate sensors that are less precise due to dynamic accelerations.

The vector magnetometer data from the two sensors installed on the observation deck of the ship do not suffer from the orientation problems of the towed vector magnetometers because the orientation sensors of the ship can be used. On the other hand, the measured vector components are heavily influenced by the induced and remanent magnetization of the ship which may also be time dependent. The three components of the remanent magnetic field of the ship and the nine matrix elements of the susceptibility tensor can be determined by a least squares fit of the measured magnetic field components against the values of a magnetic reference field during a calibration loop (Isezaki, 1986; König, 2006). After the determination of all 12 parameters that describe the magnetic field of the ship for all azimuthal directions, the measured vector components of the ship based magnetometers can be corrected for the field of the vessel.

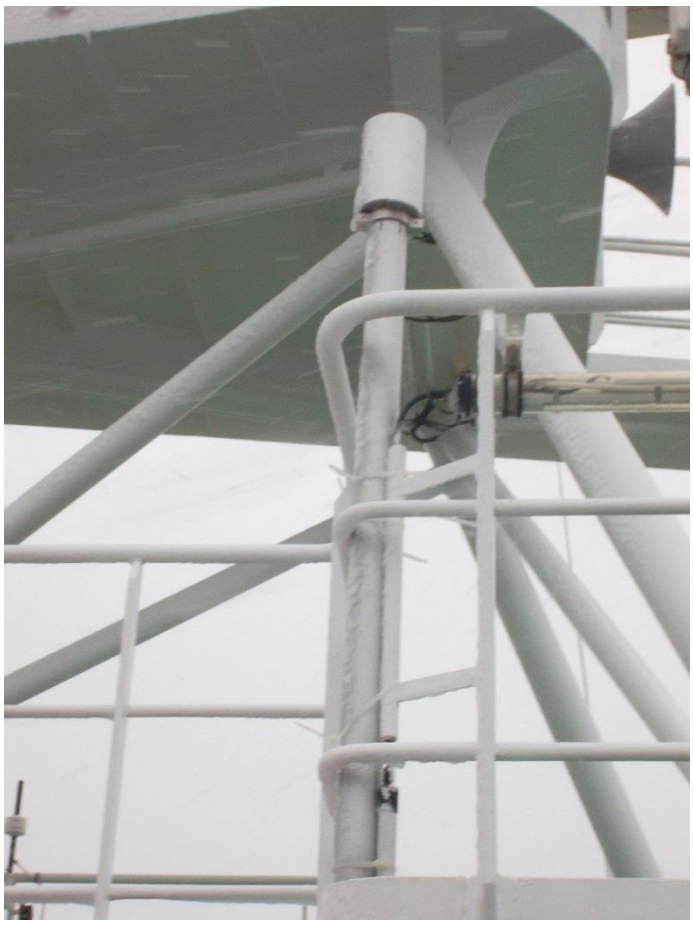

Figure 5.3 3*: Fluxgate magnetometer installed on the observation deck of RV Merian, starboard side.*

5.3.2 Data processing and calibration

The magnetic raw data recorded by the Overhauser and fluxgate magnetometers were processed in time domain in order to obtain high quality magnetic data which are essential for further data analyses. Processing of total magnetic field gradients results in reconstructed variation free total field values. Single sensor fluxgate data provide anomalies in vector components which may still contain a variation contribution. Further processing of the vector component data with time and spectral domain methods will be part of the post-cruise work.

We use two standard processing sequences for total field magnetic data. The first one contains of a simple algorithm for cleaning erroneous data of one Overhauser sensor before the magnetic reference field (IGRF 2015) is removed. The resulting magnetic anomalies are stored using a 20 second sampling rate. Later in this chapter these values are used to display preliminary anomaly curves in several figures.

The second processing sequence is more sophisticated and uses the records of two Overhauser sensors and one towed Magson sensor. The philosophy is to pre-process raw data in the time domain in a comprehensive straight-forward and transparent way before gradiometer anomaly reconstruction and further component analysis. In the following the current status of the processing codes (version 10) is summarized briefly:

1. Code READMAG reads all data formats from the individual sensors and the ship's GPS recordings. Gaps, erroneous data records and unphysical data exceeding certain thresholds are replaced by dummy values. From GPS positions which are smoothed by a running mean, control parameters like waypath kilometers, velocity, and azimuth are derived for each sample which is accepted as having reasonable values. The time delay of each sensor according to its position behind the vessel and the ship's velocity is taken into account. Clock deviations (shift and drift) of the individual instruments are being corrected. Fluxgate raw data are calibrated firstly by the factory scalar calibration parameters (including temperature calibration) and secondly by the results from the calibration circle. Tiltmeter angles are calibrated as well. Vector component data are obtained by applying roll, pitch and yaw angles in an Euler rotation prior to rotation into the geographic coordinate system. The magnetic heading of the fluxgates is used as a first approximation of the yaw angles.
2. Code INTERMAG interpolates all data gaps marked by dummy values either linear or by cubic splines. In order to despike and resample the scattered raw data, a median filter provides a robust mean. All data which were recorded at different sampling rates are decimated to equidistant 50 m samples which is the window length of the median filter. For gradiometer data, the median applies to the differences in order to preserve simultaneous measurements of rear and front sensors.
3. Code IGRFMAG subtracts the ambient main field using IGRF model 2015 up to degree and order 13 (195 coefficients) with secular variation prediction (80 coefficients). From the dot product projection of the measured total field into the IGRF direction the absolute value of the IGRF is subtracted. This IGRF subtraction is done for each gradiometer sensor individually in order to remove the main field gradient. From the vector components the IGRF components are subtracted directly. Optionally a band pass filtered yaw angle can be subtracted from the fluxgates' magnetic headings before IGRF subtraction in order to eliminate yaw angles due to water currents from yaw angles due to magnetic anomalies.
4. Code FILTMAG applies a band pass filter in the time domain in order to limit purely on wavelengths related to realistic anomalies originating from crustal sources in some cases. Routinely, wavelengths shorter 6 km are removed by the lowpass filter (LP) and eliminate the high frequency scattering due to orientation errors, e.g. misleading tilts by towfish dynamics. The highpass filter (HP) gently cuts longer wavelengths and removes long period trends, fluxgate baseline instabilities, and even partly external daily geomagnetic variations. In order to

avoid a loss of data at the beginning and end of each profile until all recursive filter coefficients are defined, profile boundaries are wrapped at both ends.

5. Code GRADMAG sums up total field differences between both Overhauser sensors or other arbitrary sensor pairs. The differences can be obtained either from the LP or band pass filtered data. For two sensors which are operating simultaneously in gradiometer mode, temporal external variations are constant over a horizontal spacing of 150 m. Consequently, taking differences of simultaneous readings approximates the small gradient of crustal anomalies with values often below one nT per 150 m. Summing up these small differences ('integrating the gradient') and correcting for the off-axis gradient reconstructs the stationary internal anomaly – free of external geomagnetic variations. Any constant offset between both sensors and any linear trend of the anomalous field is removed by subtracting the mean of all gradiometer differences. Consequently, anomaly profiles start and end centred at the baseline. Subtracting the trend obtained by linear regression of the reconstructed anomaly and adding the trend obtained by linear regression of the LP filtered curve helps to preserve a true anomaly trend.

For most of the profiles the gradient data were processed during the cruise and reasonable results were obtained, one example is shown in Figure 5.3 4. However, as many parameters can be set in the processing sequence, it will be necessary to adjust the processing according to regional characteristics of the magnetic anomalies and to the actual disturbances of Earth's magnetic field at the time of the data acquisition. For the latter, digital data from magnetic observatories in Greenland and Jan Mayen will be used to identify times with magnetic variations and to correct our measurements.

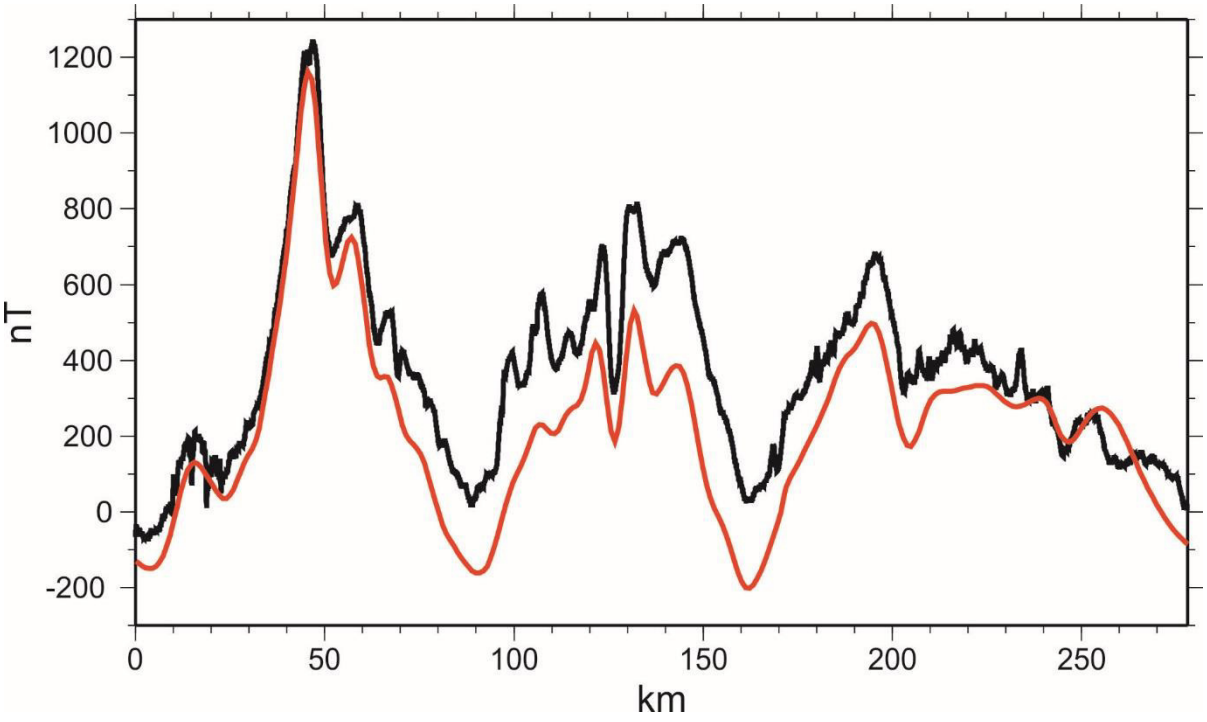

Figure 5.3 4: *Comparison of single sensor magnetic total field data (black line) and gradiometer processed data (red line) acquired along profile BGR17-202.*

5.3.3 Data quality

The magnetic data observed during the cruise are in general of good quality. The instruments performed well during most of the cruise and the Earth magnetic activity was low to moderate during much the cruise while magnetic measurements have been carried out with the towed magnetometer system. However, the effect of daily variations and magnetic disturbances is much stronger at high latitudes than at lower latitudes and even at times of low magnetic activity can reach the amplitude of typical crustal magnetic anomalies. Figure 5.3 5 shows the Earth magnetic activity represented by Kp values after Bartels (1957) for the time between June and early October 2017. The red line shows the times when the towed magnetometer system was in use parallel to the acquisition of refraction seismic or reflection seismic data.

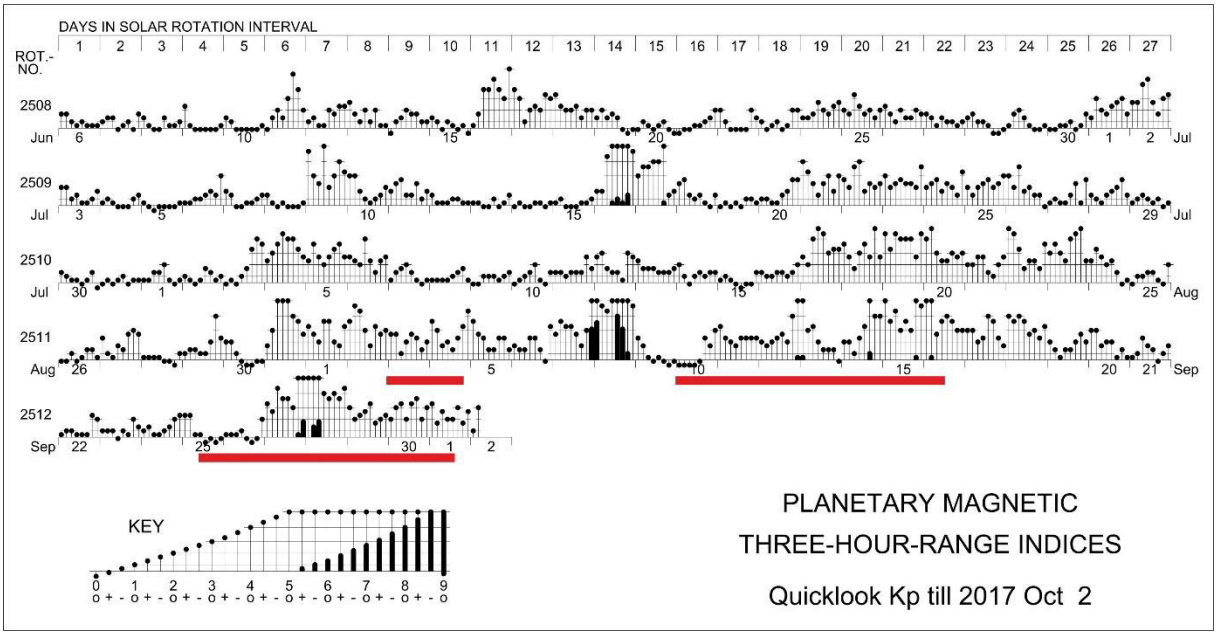

Figure 5.3 5*: Planetary magnetic three-hour-range indices for summer and fall of 2017. Low indices indicate low Earth magnetic activity and thus only moderate disturbance of magnetic measurements. The time period of magnetic measurements with the towed magnetometer array during cruise MSM-67 is shown by the red bar.*

5.4 Multichannel reflection seismic equipment and survey setup

5.4.1 Seismic sources

During the cruise BGR's 2D airgun array was installed on board RV Maria S. Merian. The airgun array includes 16 G-guns subdivided into two gun strings with eight guns each (Figure 5.4 1). Each gun string consists of four two-gun clusters. The individual gun volumes of the port side array range from 380 in^3, 250 in^3, 180 in^3 to 100 in^3 whereas the starboard array volumes vary from 250 in^3, 200 in^3, 120 in^3 to 70 in^3. Each gun string has a total length of 15.56 m. The maximum total volume sums up to 3100 in^3 (50.8 l) throughout the survey for all MCS reflection profiles. M.S.Merian's three compressors with a primary volume of 10 m^3/min each (without supercharger) provided the working pressure of 2172 psi (150 bar). It takes 15.2 seconds to recharge the volume sufficient for the standard shot time spacing of 18 s (50 m @ 5.4 kn).

Only for the second refraction profile BGR17-2R2 the guns no. 7 & 8 and 15 & 16 (Figure 5.4 1) were replaced by GEOMAR's four 520 in^3 G-guns. Therefore, the total volume increased to 4840 in^3 (79.31 l).

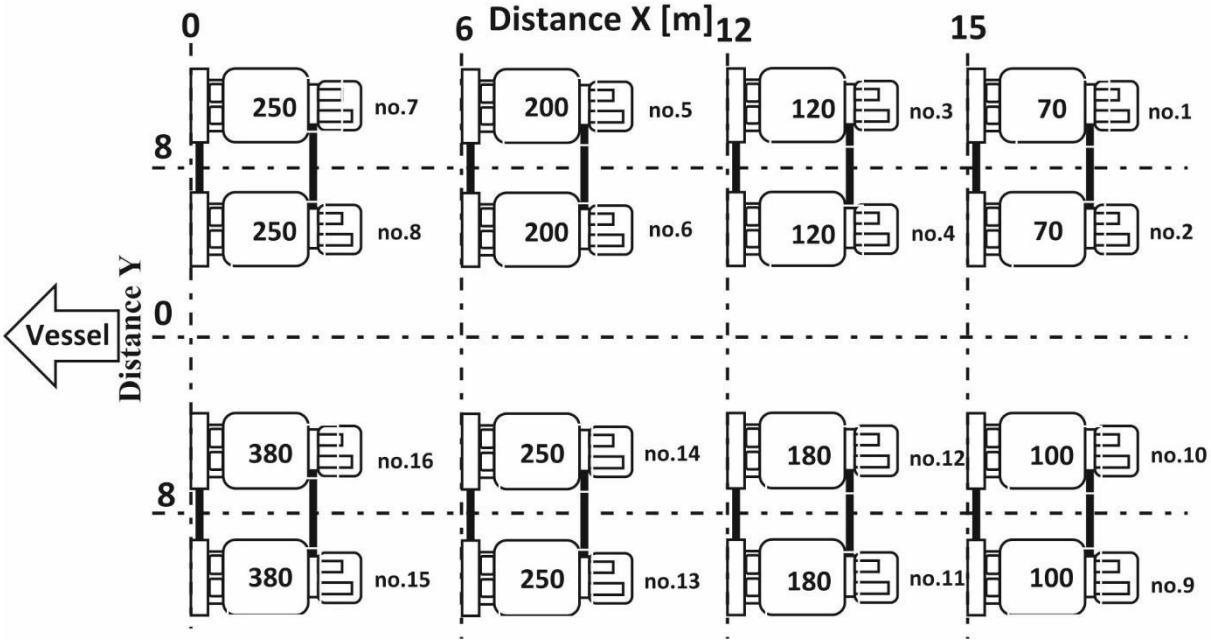

Figure 5.4 1: *BGR's airgun system during cruise MSM67 towed by the vessel at the left hand side.The individual volumes are given for each gun (in in^3).*

The towing depth of the airguns was 6 m throughout the survey. The towing distance between the vessel and the first gun sums up to 45 m (4 m from the stern to the cable grip, 40 m umbilical and 1 m gun trailer). Therefore the center of each gun string is 52.5 m behind the stern of the vessel and the lateral spacing between the arrays amounts 16.40 m.

Triggering and synchronization are controlled by the BigShot gun-system from "Real Time Systems". It is capable to control up to 32 airguns. The input trigger signal comes from the navigation system SPECTRA controlling the equidistant shot point spacing at 50 m. For lines BGR17-2R1 and BGR17-2R2 shots were triggered at 50 / 60 sec interval using a Master PC (LabView 8.6) synchronized with GPS over a Meinberg GPS 170 interface. The timing of all guns was controlled using the software package BigShot GUI (see Figure 5.4 2). Additionally, the pressure on each gun string displayed in the watch room made it possible to identify malfunctions of the compressors immediately.

Before starting profile measurements we enlarged the airgun power stepwise by a soft-start (ramp-up). The ramp-up was performed by shooting intervals of 16 s. Starting with the smallest airgun we added every 5 shots one additional gun. The soft start was completed after 20 minutes. The smallest airgun also operated as mitigation gun during turns less than 1 hour.

Figure 5.4 2*: Shot timing of all 16 G-guns for BigShot.*

5.4.2 Seismic data recording

BGR's ***SEAL 428*** seismic recording system and a towed sensor cable with an active length of 4500 m were used to record the seismic data. The bird controlling system (DigiCOURSE System3) and the streamer control system are interfaced with the navigation system (see chapter 5.4.3, p. 52).

The SEAL 428 seismic recording system is a high-resolution seismic data acquisition system designed for marine towed streamers acquisition. The SEAL recording system is capable to handle a maximum recording capacity of 960 channels (@ 12.5 m; 2 ms) per streamer, a maximum record length of 47 s (navigation triggered, SR = 2 ms). The sampling interval may vary from 1/4 ms, 1/2 ms, 1 ms, 2 ms to 4 ms. During the cruise we sampled the data at 2 ms. The HP DL380 G7 Server is capable to support a maximum of 17500 channels (SR 2 ms). Figure 5.4-3 shows the screen used for controlling the physical data acquisition along the cable as well as the data recording.

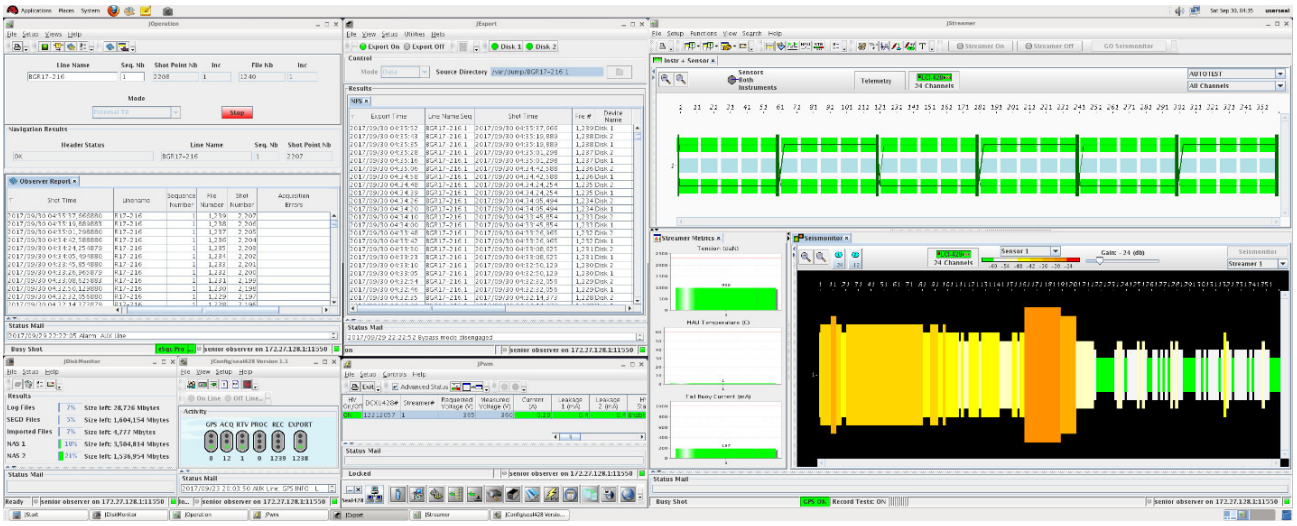

Figure 5.4 3*: Example screen image of the SEAL control software.*

The positioning controlling system ***DigiCOURSE System 3*** managed the vertical streamer position (depth) and measured the heading along the cable by compass birds. Further on, the offset to the first active section was measured using DigiRANGE by acoustic transponders. DigiCOURSE System 3 is a hardware and software package that controls and collects data from a network of acoustic sensors and streamer positioning devices (Figure 5.4.-4). The system has online command, diagnostic, and performance-monitoring capability. System 3 employs a modular architecture which provides a variety of configurations and levels of functionality. The minimum system equipment configuration includes two real-time processors: an Operator Interface (OI) and a Data Management Unit (DMU), a Line Interface Unit (LIU), and cable-mounted measuring devices. Further on, a recovery system which has a self-triggering mechanism at a depth of 50 m were attached to the streamer. We operated the cable at a depth of 12 m.

Figure 5.4. 4: *Streamer devices: DigiBirds for depth control and compass heading (red), CMX units for acoustic measurements (yellow), and recovery system (green).*

BGR's ***SEAL digital streamer*** during cruise MSM67 consisted of 30 Sentinel Solid Active Sections (SSAS-RD, group interval 12.5 m) with 360 channels (Figure 5.4 5-5). It has a flexible architecture with redundant data transmission modes, i.e. data transmission may be reconfigured on-line in case of a failure. Each channel has an individual 24 bit, Sigma Delta A/D converter. The active streamer sections have a diameter of 55 mm.

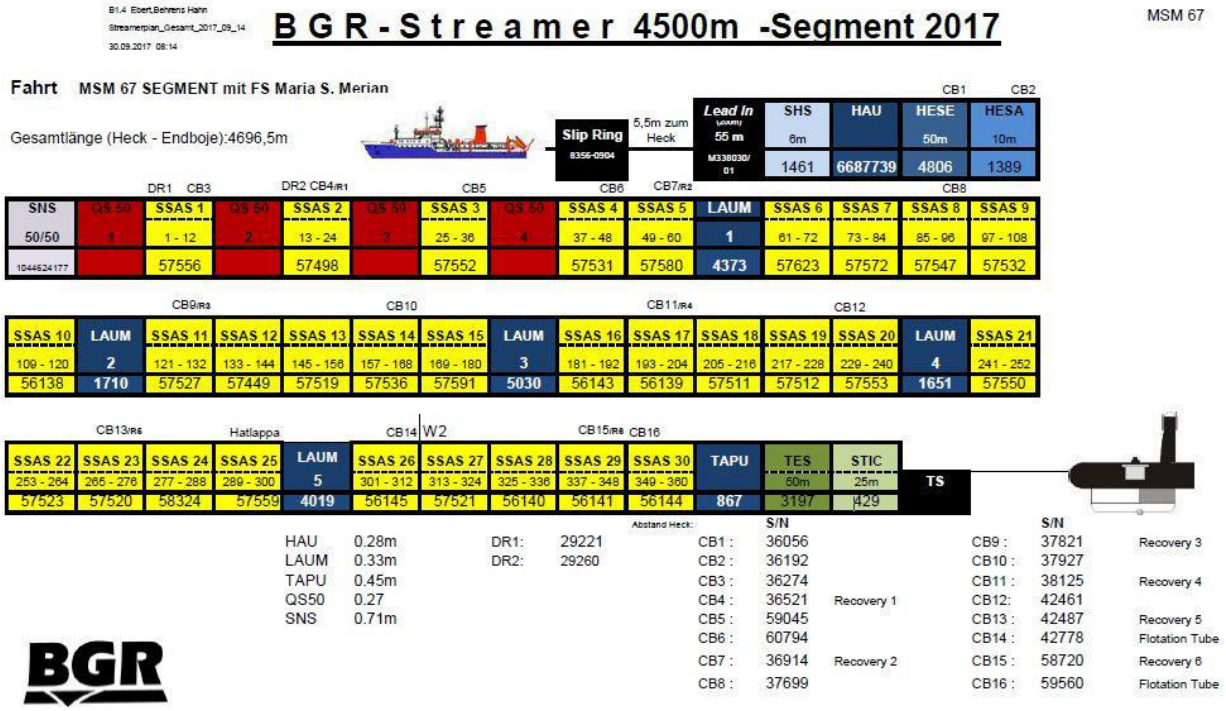

Figure 5.4 5: *Streamer configuration during MSM67.*

During profiling, the data quality is checked in real time (***QC***) – (see Fig. 5.4-6). Continuous online seismic data quality control is performed using an eSQC-Pro client 'HP Z420' connected directly to the eSQC-Pro Server "HP DL380" without slowing down the acquisition. Three main windows are used for quality control:

- The Normal display window shows the latest incoming SEGD shot record. The traces are displayed in the time/distance range.
- The Single Trace window shows the data of one selected channel from the streamer. With each new shot the display is updated with the new acquired trace added to the window. Four single trace windows may be opened simultaneously.
- The auxiliary channel recording the waterbreak hydrophone.

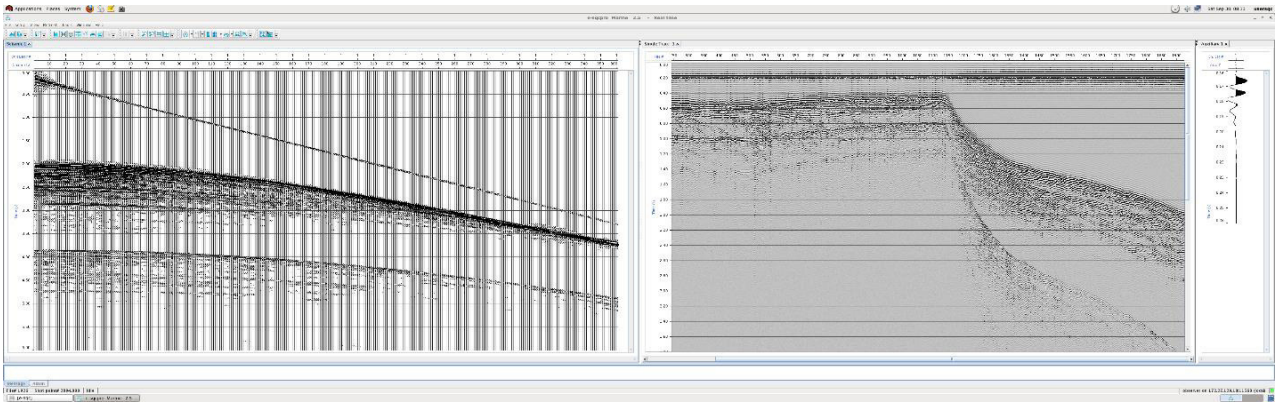

Figure 5.4 6: *QC display example for line BGR17-216.*

After initial deployment of the new streamer first time, bird angles up to -5 degrees have been observed along the whole streamer. Therefore, we changed the ***buoyancy*** of the streamer in the break between lines BGR17-209 and BGR17-209A. SSAS with bird number 8 to 16 were equipped with an additional weight block each. The corresponding wing angles are given in Table 5.4 1, documenting the resulting change in buoyancy.

Table 5.4 1: *Mean bird angles for whole profiles without (lines BGR17-204 and BGR17-205) and with (lines BGR17-214 and BGR17-215) additional weight blocks.*

	Bird 10	Bird 11	Bird 12	Bird 13
BGR17-204	-3.7°	-2.1°	-1.6°	-4.5°
BGR17-205	-3.5°	-1.8°	-1.7°	-4.4°
BGR17-214	+0.5°	+2.7°	+1.4°	-0.3°
BGR17-215	-0.5°	+1.7°	+0.7°	-1.6°

5.4.3 Navigation and positioning

Proper seismic processing requires (e.g. for offset calculation and binning) the exact position of the gun array and all receiver groups in the curved and feathered streamer. For managing all types of navigation data and in order to control all systems for seismic data acquisition we used the software package Spectra (ION Concept Systems) which is together with the later version Orca the standard navigation software in the exploration industry. This software has four main tasks:

- collection of all kind of sensor positioning data with accurate timing including input/output trigger signals
- calculating online network solutions (position of the ship and all sensors)
- real-time visualization of predicted and past shot locations
- generation of P1/90 and P2/94 navigation files according to UKOOA standards

The mobile BGR seismic equipment can be mounted on different research vessels. The vessel and survey specific geometry parameter used by Spectra are sketched in Appendix A1.

Figure 5.4 7: *Example for Spectra operation using the Display Node.*

The design of Spectra employs a central Data Server process which acts as the information bank and data broker for the system. All produced data (i.e. configuration data, raw data or positional solution data) are stored by the data server and made available on demand. Further parts of Spectra are the following components (so-called Nodes):

- Line Management Node (LMN): defines survey lines and controls shooting when online
- Real Time Configuration Node (RTCN): configures interfaces and triggers for the real time unit
- Spectra Configuration Node (SCN): configures the nominal positions of all nodes, sensors and observations between nodes
- Network Calculation Node (NCN): calculates the positions of all sensors on the vessel (the ncc network) every second and the positions of all other sensors (the main network) at the time of the shot. Further on, the NCN delivers the estimated time of the next shot
- Data Logging Node (DLN): writes both P1/90 and P2/94 files to disk
- Navigation Logging Node (NLN): reports summary navigation data in the form of a shot log
- Display Node (DN): provides user configurable numerical and graphical displays of network solution, real time binning and raw data (example shown in Figure 5.4 7).

We used Spectra version 14.12.1, patch level 638, installed on a Dell Precision R5400 with Red Hat Linux 5. A second Dell R5400 in the lab allowed the plug-in of 2 additional screens and to log the navigation data to a second hard disk. A third machine installed on the bridge exported information about the streamer shape to the ship's officers, which proved useful during evasion maneuvers due to floating icebergs. Further on, this display helped during recovery of the lost tail buoy on profile BGR17-204.

As real time unit we used a PowerRTNU II (RTNU) manufactured by ION Concept Systems. This unit receives all positioning information via RS-232 or Ethernet interfaces and sends and receives trigger signals. It is connected to the Spectra machine via Ethernet switch. The RTNU has an own GPS antenna to obtain a correct time signal.

Table 5.4 2: *Interfaces and data types of the RTNU.*

Port	Interface Name	Sensor (data type)	I/O	COMM
1	DG_GGA_NMEA	DGPS	I	9600 N 8 1
2	XX_NMEA_ANY	Seapath 200 (pitch, roll, heave)	I	9600 N 8 1
3	GY_NMEA_GYRO	Gyro	I	9600 N 8 1
4	EC_NMEA_DPT	Simrad EM-120 (water depth)	I	9600 N 8 1
5	XX_NMEA_ANY	DOLOG-22 (speed through water)	I	9600 N 8 1
6	DG_NMEA_GGA	Kongsberg Seatrack	I	9600 N 8 1
7	GN_SYNTRON_V2	BigShot (GCS-90)	I/O	9600 N 8 1
8	RG_SEATRACK	Kongsberg Seatrack	I	9600 N 8 1
9	HDR_LABO	SEAL (SEG-D header)	O	9600 N 8 1
10	XX_NMEA_ANY	SV&T (sound velocity)	I	9600 N 8 1

Table 5.4 2 gives an overview about all data interfaces at the RTNU located in room "Deck Lab". Data about DGPS and Gyro was delivered via RS-232 directly from the Seapath 200 in room "Data Processing". In Spectra's node RTCN, the interface DG_GGA_NMEA decoded the DGPS information. The acceptable quality was set to 5 (Float Real Time Kinematic). Furthermore, the ship's system operator delivered via Ethernet pitch, roll, heave, water depth, speed through water and sound velocity. A MOXA NPort 5410 converted these data to RS-232. In the RTCN, the standard interface XX_NMEA_ANY was adapted to decode this information.

Additionally, we interfaced BGR's seismic equipment (see chapter 5.4.2, p. 49) to the RTNU. In order to receive airgun data (pressure, status and delta times of single guns) from the gun controller we applied the interface GN_SYNTRON_V2 on port 7. With this interface, a GCS90 control string (containing the line name and the next shot number) and the 'Begin Line' (BL) message (option "Incorporate 'BL' command") were sent to the gun controller. For the Kongsberg relative GPS (RGPS) system we used the interface RG_SEATRACK on port 8 to obtain range and bearing to the tail buoy. In order to have a spare GPS position we interfaced the reference position of this system to channel 6. This interface was configured in extended mode. The acceptable quality has to be set to "1234" since this position is not DGPS. The SEAL header was sent to the seismic recording system via port 9 together with the sequence number (which was set in the LMN by the option "Add Sequence Number"). This number has to be entered manually at the SEAL before the start of the profile.

Most of the serial interfaces were connected via a Data Distributor to the RTNU. This provides full electrical and optical isolation between the sensor and the RTNU as well as additionally LED indication of RX & TX data activity for each channel. Examples for the format of the data strings are given in Appendix-A 3.

The Positioning Control System (PCS, System 3) was connected to the Spectra machine via Ethernet. Data from the birds and acoustic were decoded by the virtual interface 'vid' – a process running on the Spectra machine. The virtual interface DG_V_PRTNU was used to obtain the GPS position of the RTNU receiver. The virtual interface GN_V_TRIGGERS supplied additional timing information, e.g. the time difference to the last shot ('Shottime Diff').

The RTNU also creates and receives triggers. All times are referenced to the next shot (a data item which is called @SHOTPREDICT@). At -120 ms the recording system obtains a trigger to start the system (TTL active high, 100 ms duration, output port 2). At -50 ms a trigger is sent to the gun controller (TTL active high, 100 ms duration, output port 1). The RTNU receives an

input trigger (the time break) from the gun controller (TTL, active low, 10 ms duration, input port 1). At -1000 ms the PCS receives a Contact Closure trigger (output port 4) from the RTNU. With a certain delay, the PCS submits the bird data to the Spectra system.

At the SCN, we configured an acoustic network. A DigiRANGE CTX unit was installed at keel position in the moon pool within the hangar. Two CMX units were attached to the first and second active section of the streamer. With this configuration, the dynamic stretch during profiling could be estimated. Further on, we defined a "user defined observation" containing the sound velocity within the water. Therefore, this data value was logged to the P2/94 files as item T7010.

At the end of each line, a shot log was produced containing basic information (e.g. distance across (DC), bottom speed (BSP), heading (HDG)). This log also contains manual comments protocolled by the navigators (e.g. gun failures). The record delay was found to be very stable at 120.08 ms, with small spikes in the range of 0.02 ms. These values (record delay per shot) can be exported to a text file which can be used during seismic processing.

During post-processing, a special focus was given to the offset of the first channel. Therefore, the measured distances delivered by the DigiRANGE system for profile BGR17-212 were analyzed in detail. In Figure 5.4 -8, upper panel, the measured traveltime between the ship-based CTX transponder and the CMX mounted to the first SSAS is shown. The middle panel of Figure 5.4 8 shows the corresponding sound velocity at the keel of the vessel. A clear correlation can be seen along the profile. Using these in-situ velocities, the measured traveltimes can be converted to a distance around 219 m, staying constant for the whole profile. Assuming a static/fixed geometry (Appendix-A 1), this distance would be estimated to be about 208 m. Therefore, the front stretch is about 11 m. The analysis of the tail buoy range gives a mean distance of 4759 m (range V1RG1-TB1RG1, Figure 5.4 -8, lower panel). The assumed static range would be 4746 m, resulting in a difference of about 13 m mainly due to the front stretch of 11 m. The remaining difference of 2 m might represent a residual tail stretch (TES section). The fact that the front stretch (HESE section) totals to more than 20 % of the active stretch length should be kept in mind for future cruises.

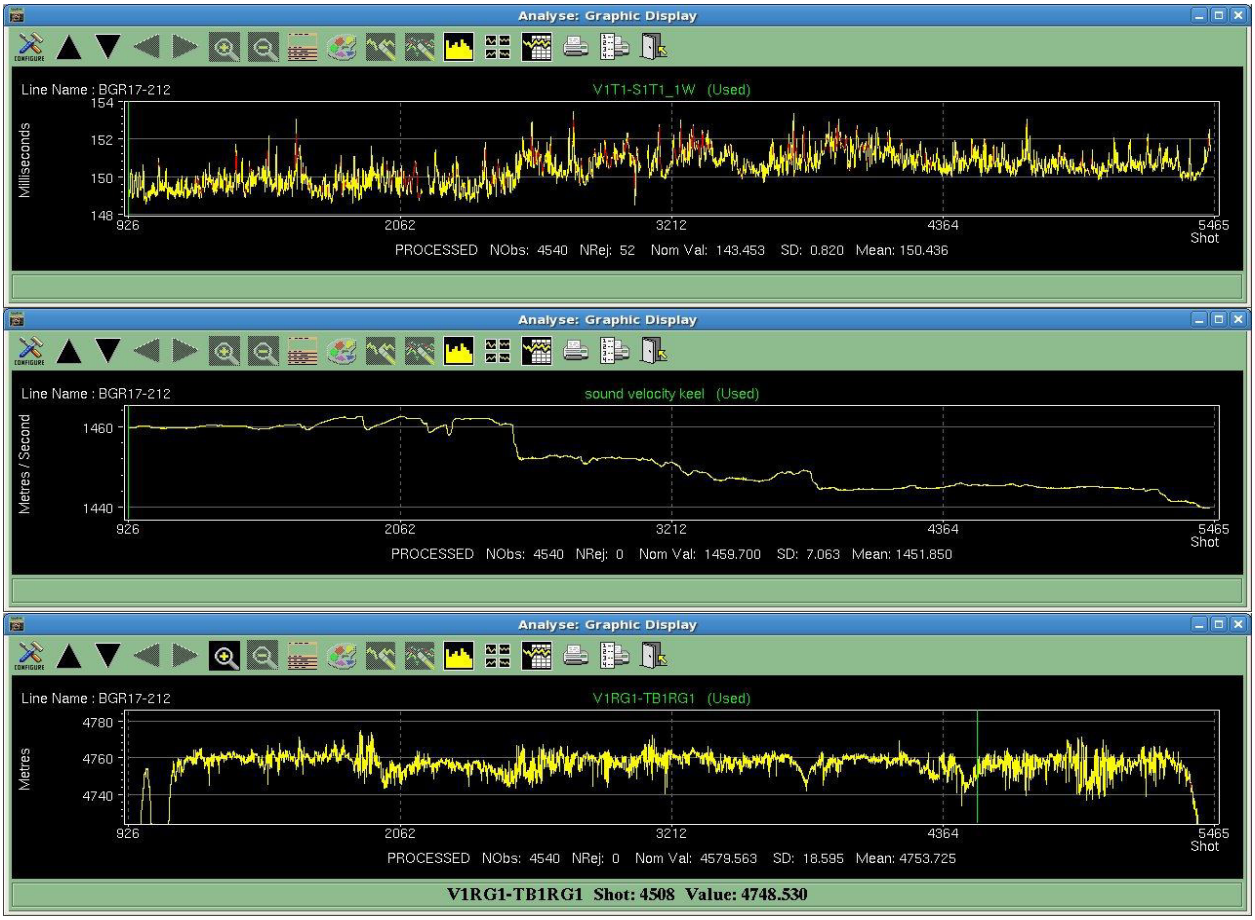

Figure 5.4 8: *Selected values for line BGR17-212, analyzed during post-processing. The upper panel shows the measured traveltime between CTX in moon pool and CMX-1 at the streamer (V1T1-S1T1). The middle panel shows the sound velocity in water, measured at the keel of the vessel. The lower panel displays the range to the tailbuoy (V1RG1-TB1RG1).*

Navigation post-processing (Sprint software)

The software Spectra produces online solutions for the whole network. This is mainly done to visualize the position and shape of the streamer during the profile and to command space equidistant shooting. A P1/90 file containing these positions is also generated online. Anyhow, a post-processing of the navigation data is needed to produce proper positions. Sometimes online solutions fail showing artifacts in the streamer geometry, e.g. when the radio transmission to the tail buoy is interrupted for some minutes and the tail buoy position got lost. During post-processing, all positioning data can be corrected for instance by cutting out bad data, interpolating gaps, de-spiking and filtering. Furthermore, the post-processing solution is much more sophisticated, it is using all sensor information, is knowing 'past and future' along a complete profile, and offers many tools for quality control. Post-processing was done during the cruise by using the software package Sprint (ION Concept Systems) installed on a Dell Precision R5400 with Red Hat Linux 5. The main steps of this post-processing are described by the following modules:

Module DataBase: Used to create a new database which may contain several profiles. However, every change in sensor geometry (e.g. we added two compass birds) requires a new database.

Module Import: Here, the P2/94 files are imported, containing all sensor positions and observations. Option 'Import All Positions' allows the comparison between the online solution (calculated by Spectra) and the post-processing solution (calculated by Sprint). Pitch, roll and heave corrections were calculated. The 'Shot Time Increment' for the QC-Report was set to 18 sec.

Module EditSurvey: For each profile, magnetic declination and the range of valid shot points (FGSP to LGSP) were adjusted. In the shot table bad shots have to be deleted. In the Nodes tab, gun nodes have to be 'freed' in order to become a variable shotpoint position. The flags for the GPS-Nodes from the RTNU and from the Kongsberg Seatrack were changed from "BODYFIXED" to "FREE" (only the more precise DGPS was used during processing). At the vessel's towpoint, the flag was changed to "BODYFIXED" oriented according to the vessel's gyro, while the gun and streamer references were rotated by compass 3.

Module PreProcess: In the 'Edit Groups' window, information from the Seatrack system was split into two groups, because values for range (RGPS_R) and bearing (RGPS_B) have different processing parameters. An acoustic group '1W/2W_front' was defined with selected 1-way and 2-way observations. The pre-processing consisted mainly of three steps: de-spiking, filtering and interpolating/ extrapolating missing data. Our final processing parameter including selected standard deviations (SD) are listed in Table 5.4 3. Additional standard graphics properties applied for all groups were standard plot, metres/radians, corrected 0-360 flips, nominal, scale on processed an inverted Neg Data. Pitch roll heave corrections were applied to GPS and RGPS positions. An important step is the visual scan of all observations: Bad sensors have to be rejected as well as the deselected GPS sensors, bad data values have to be edited and spikes must be removed. Especially, RGPS data needed intensive data editing during bad weather conditions. Finally, the processed data of the groups Compass, Depthsensor, Echosounder, GPS, Gyro, RGPS_B and RGPS_R were written to the data base using 'Batch Process Data'.

Table 5.4 3: *Pre-Processing parameter selected for cruise MSM67.*

Groups	SD	scale	gating	filter	int./extrapol.	graphics properties
1W/2W_front	2 m	1.480 (sound velocity)	ROC 0.1	300 s	100/20	-
Compass	0.5°	0.017453	ROC 0.1	300 s	100/20	-
Depthsensor	1 m	1	ROC 0.2	120 s	50/20	(fixed scale ±5) inverted
Echosounder	1 m	1	(pregate absolut 0-3000)	30 s	50/20	inverted
GPS	2 m	1	RM 10	30 s	50/20	polynomial delta
Gyro	0.1°	0.017453	-	20 s	50/20	detrend
Pitch/Roll	0.1°	0.017453	-	-	50/20	-
Heave	0.1 m	1	-	-	50/20	-
RGPS_R	4 m	1	RM 10	120 s	400/20	-
RGPS_B	0.02°	0.017453	RM 10	120 s	400/20	-

Module NetAdjust: First of all, 2D manual observations have to be created according to Table 5.4 linking the nominal positions of the gun, the first active section on the streamer (streamer reference) and the tail buoy to the network solution. It was computed using a Chebyshev polynominal streamer shaping model of order 8 (long streamer), applying streamer stretch, auto gate observations to 10 SD and including streamer rotation. The NetAdjust solution was first calculated in demo mode - this allows for the identification of areas and instances with non-consistent data – and finally in batch mode.

Table 5.4 4: *Manual observations during cruise MSM67 required for 2D-Sprint.*

man obs	**sensor node**	**target node**	**SD**	**nominal value**	**rotation**
MOX-G1	G1	Gun_V1_G001_Ref	2	0	Cmp3
MOY-G1	G1	Gun_V1_G001_Ref	2	0	Cmp3
Tail_Strm_1_ORDX	TB1	S001_T_2D	1	0	Cmp14/16
Tail_Strm_1_ORDY	TB1	S001_T_2D	1	+83.8	Cmp14/16
TowPt_V1_G001-G1-ordX	TowPt_V1_G001	G1	2	0	Cmp3
TowPt_V1_G001-G1-ordY	TowPt_V1_G001	G1	2	-52.5	Cmp3
TowPt_V1_G001-S1-ordX	TowPt_V1_G001	S1	2	0	Cmp3
TowPt_V1_G001-S1-ordY	TowPt_V1_G001	S1	2	-135.59	Cmp3

Module Reports: A shot report, a compass calibration report and a processing QC report was generated for each profile. These reports point out data and processing problems which require to repeat previous steps with improved parameter.

Modules Analyse: This module allows a detailed analyses of the network solution. For each profile, we plotted the i) calculated range of RGPS, ii) raw data differences between vessel reference and gun reference, streamer reference and tail buoy reference, iii) streamer feather, rotation and stretch as well as iv) the depth for the front, middle and rear streamer section.

Module Export: With this module the adjusted data were exported to the database and to the final new processed P1/90 files.

Modules Compare: This module allows a comparison between P190 files from the Spectra online solution with the Sprint post-processing solution. Deviations for receiver groups are typically in the range of 10 m to 20 m but might be much higher in cases where the online solution failed (e.g. the dynamic stretch increased far too much for the first profiles and required to restart Spectra without the stretch option in the NCN node).

5.4.4 Processing of MCS data

Preliminary onboard processing was conducted using the SeisSpace/ProMAX software package version 5000.10.0.0 running on a Supermicro server system with a 16 core AMD Opteron 6376 processor, 64 GB ram and an internal 24 TB raid. Focus was on the reduction of surface noise due to bad weather conditions and subsequent streamer updrift (Figure 5.4 9-9 and Figure 5.4-10), multiple suppression in shallow water areas, deconvolution and time migration. Line BGR17-202 is located along the refraction line BGR17-2r2 and in addition was depth migrated to allow constraining the sedimentary layers in refraction seismic modeling. Following is the example processing flow of line BGR17-202 with figures of selected processing steps (see Figs. 5.4-11 to 5.4-16). All stacked sections shown in the figures have an AGC 800 ms filter applied for better visualization of deeper parts of the profile. Except for lines BGR17-201, 02 and 03, most profiles were processed up to step 9 (srme) and then stacked, post-stack processed (steps 19-22) and exported to segy-format for a timely availability for first interpretation.

Processing flow BGR17-202

Receiver depth: 12 m, Source depth: 6 m, No. channels: 360

Group spacing: 12.5 m, cdp spacing: 6.25 m, shotpoint distance: 50 m, cdp fold: 45

Offset channel 1: 188 m, offset channel 360: 4570.5 m, offset source: 105 m

Shotfile: UTM 27 N, shots 967-6570

On Import to ProMAX: Y-coordinate - 8,000,000 for preservation of decimal accuracy

Wrong shots with 720 traces: shots 1001-1006

Bad weather conditions, streamer on 2 m depth from shot 5800

Processing: shots 1007-5800 used, Record length: 15 s, used for processing: 10 s

1. Geometry setup
2. Segd- and geometry load, remove 120 ms pre-shot recording
3. Minimum phase bandpass filter 4 Hz - 18 dB, 120 Hz - 72 dB
4. Surface wave noise attenuation
   Velocity: 750 m/s, Frequency: 0-30 Hz, Panel size: 60
5. TDF noise rejection, common offset domain
   Window length: 46 ms, Frequency: 4-30 Hz, 7 traces aperture, Threshold multiplier: 2
6. TDF noise rejection, cdp domain
   Window length: 46 ms, Frequency: 4-30 Hz, 5 traces aperture, Threshold multiplier: 2
7. Direct arrival suppression: Coherent noise attenuation, velocity of 1460 m/s
8. Velocity analysis 1
9. Surface related multiple estimation SRME (2 runs)
   Regularization with picked velocity field
   Match Filter: 4 s window length, 200 ms filter length
   Adaptive subtraction: 800 ms window length, 120 ms filter length, spacial averaging 120 m, filter coefficient 6
10. TauP-deconvolution (cdp-domain)
    Beam steer trace interpolation

AGC 400 ms
TauP transformation: -1400/1400 ms/km slowness, inc. 2ms/km
Minimum phase predictive deconvolution: 400 ms operator length, 64 ms prediction distance
TauP inverse transform
AGC removal
Interpolated traces removal

11. Velocity analysis 2
JavaSeis framework create (CMP, cdp-seq.no framework)
CVS analysis
12. Common reflection surface (CRS)
2D CRS ZO search: search aperture 1000 m, cdp search spacing 10, time search spacing 8 ms, max. dip 0.1, 3 stages
2D CRS stack: no stretch mute, offset bin 1st center 50 m, max. offset 4600 m, offset bin size 100 m, stacking aperture 150 m
13. True amplitude recovery, 1/dist spherical spreading
14. F-X decon in common offset domain: Horizontal window length 10, filter samples 5, time window length 500 ms, overlap 300 ms, 4 Hz – 120 Hz
15. Kirchhoff pre-stack time migration
No trace binning necessary, CRS output is regular
Migrating all panels to regular cdp spacing of 6.25 m, max. frequency 120 Hz, aperture 8000 m

15a. Kirchhoff pre-stack depth migration
No trace binning necessary, CRS output is regular
Conversion of rms-velocities to interval velocities: smoothing, reducing velocities by 90% (900 ms) to 85% (2 s) to 80% (10 s)
Migrating all panels to regular cdp spacing of 6.25 m, max. frequency 120 Hz, aperture 2000 m
Max. depth 15 km

16. Far offset top mute
17. Residual moveout
18. Stack
19. Zero phase bandpass filter 4 Hz - 18 dB, 120 Hz - 72 dB
20. Trace equalization
21. F-X decon
22. AGC 800 ms
23. SEGY-export

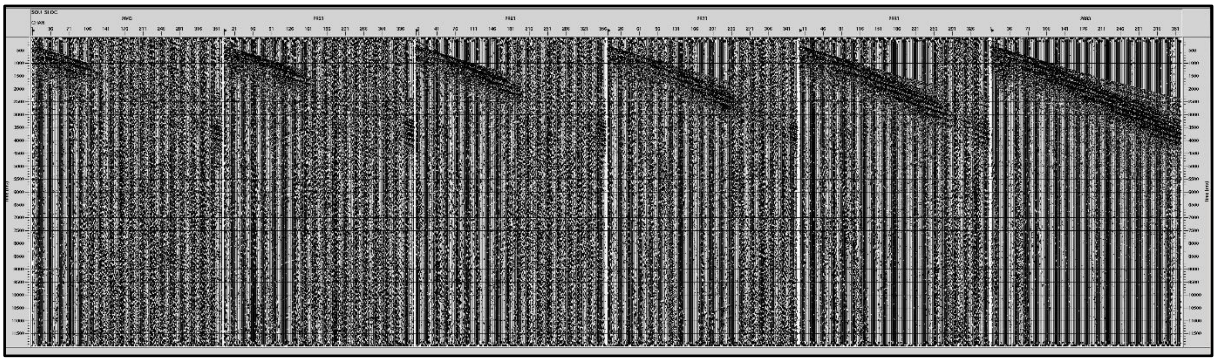

Figure 5.4 9: *Surface wave noise from 2 m streamer depth (left) to 12 m streamer depth (right), acquired during bad weather conditions.*

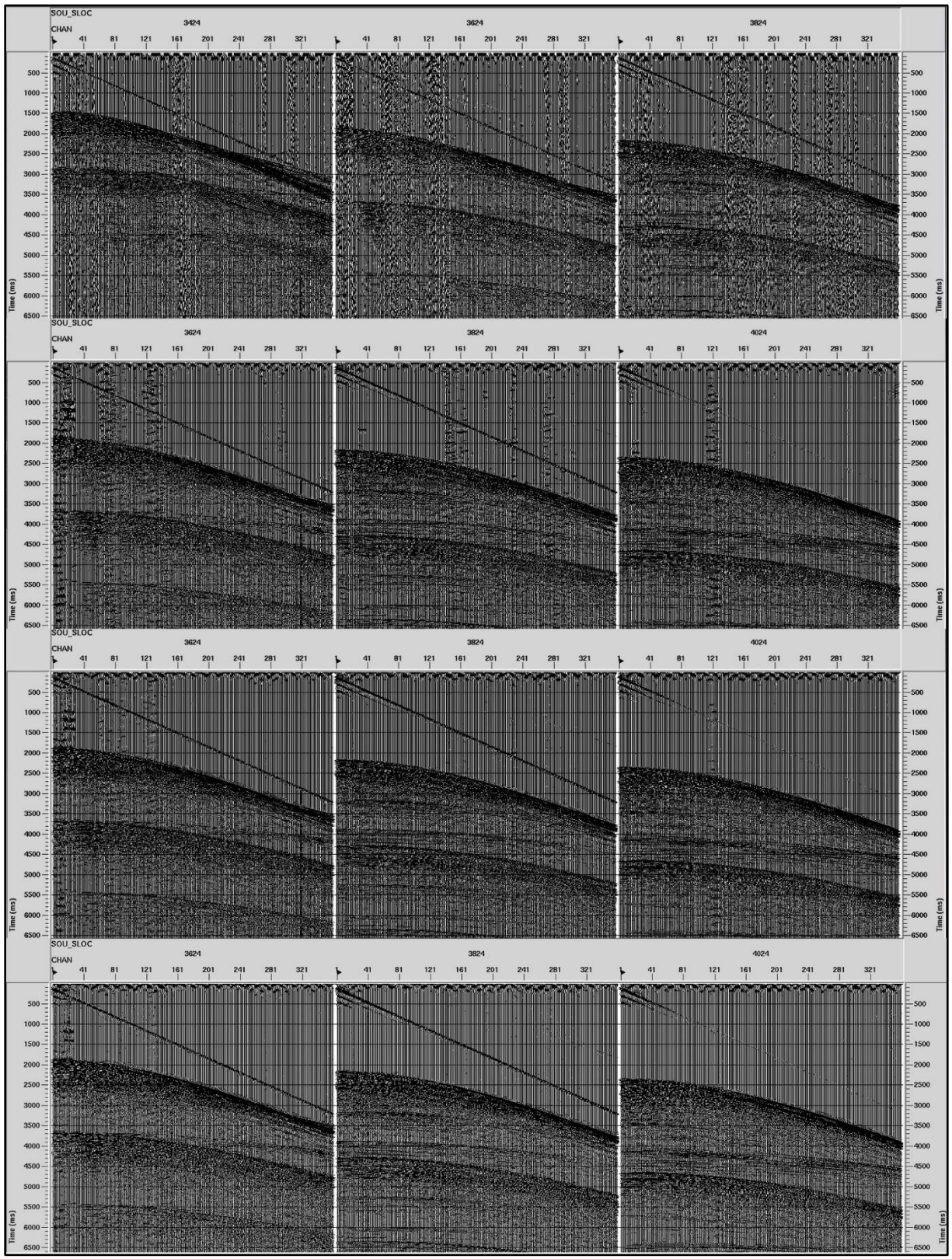

Figure 5.4 10: *Suppression of surface noise. A: raw data, B: surface wave noise attenuation, C: surface wave noise attenuation and TDF noise rejection (common offset domain), D: surface wave noise attenuation and 2x TDF noise rejection (common offset domain, cdp domain). See No. 4.-6 in the example processing flow.*

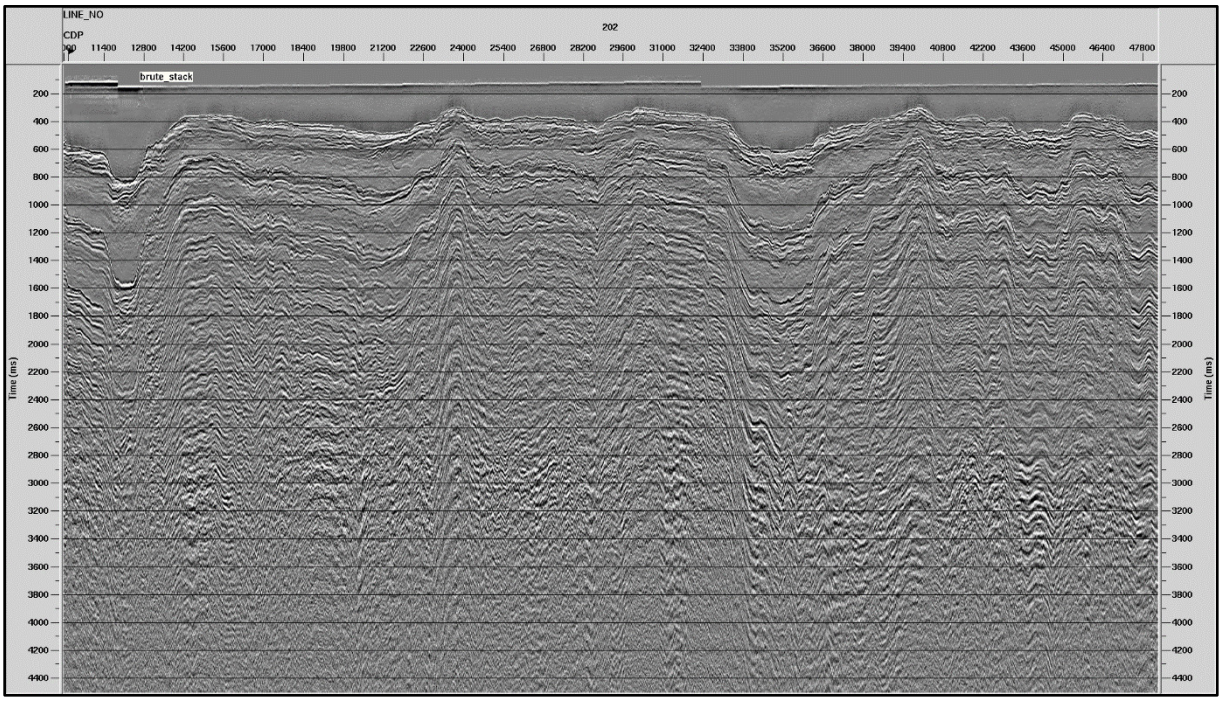

Figure 5.4 11: *Brute stack of bandpass filtered raw data with constructed velocities.*

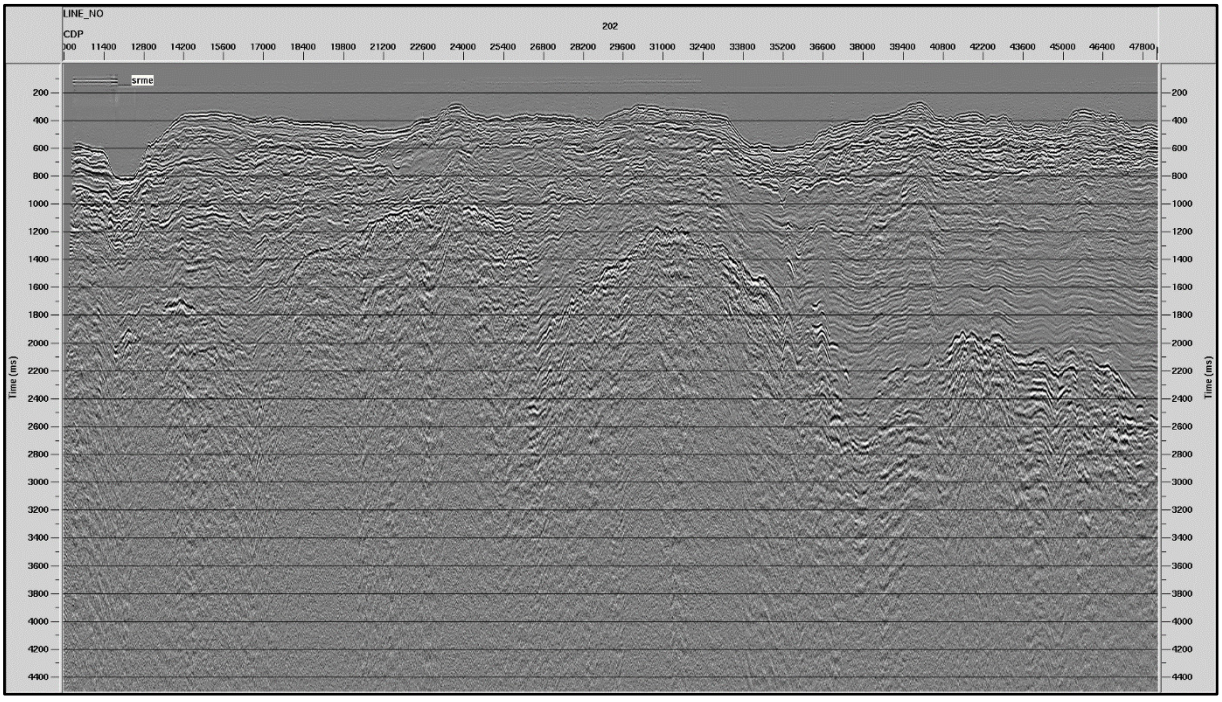

Figure 5.4 12: *Surface related multiple estimation (SRME) applied. See No. 9 in the example processing flow.*

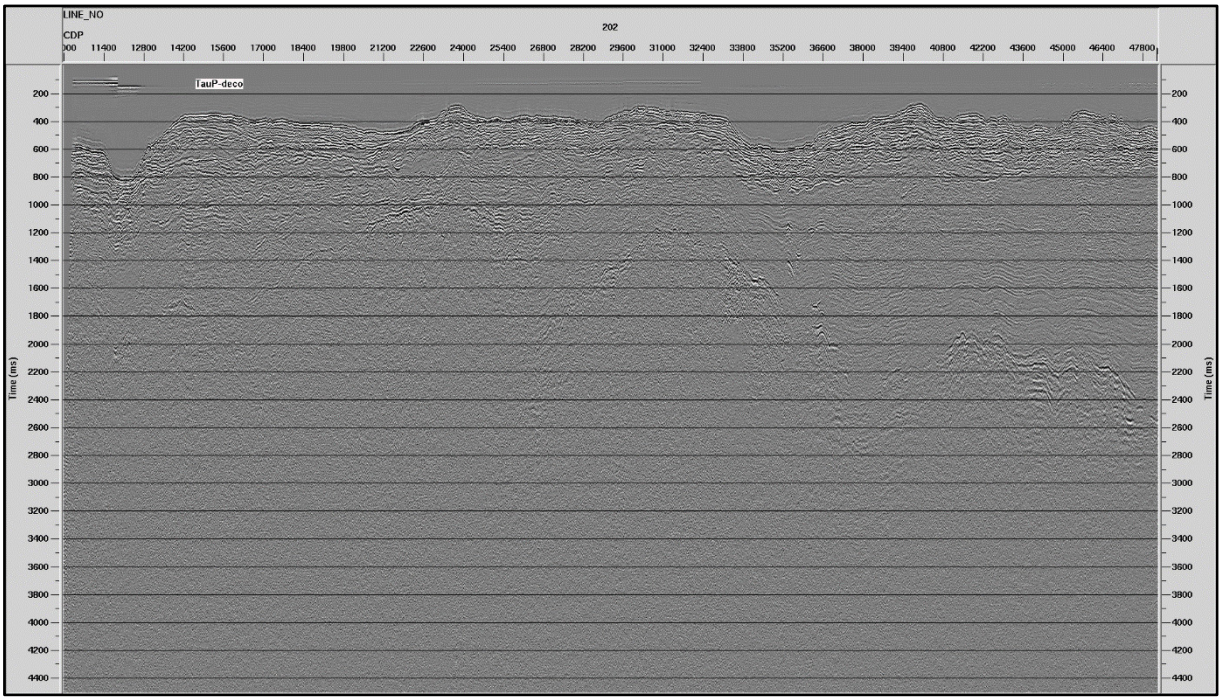

Figure 5.4 13*: Minimum phase predictive deconvolution in the TauP domain. See No. 10 in the example processing flow.*

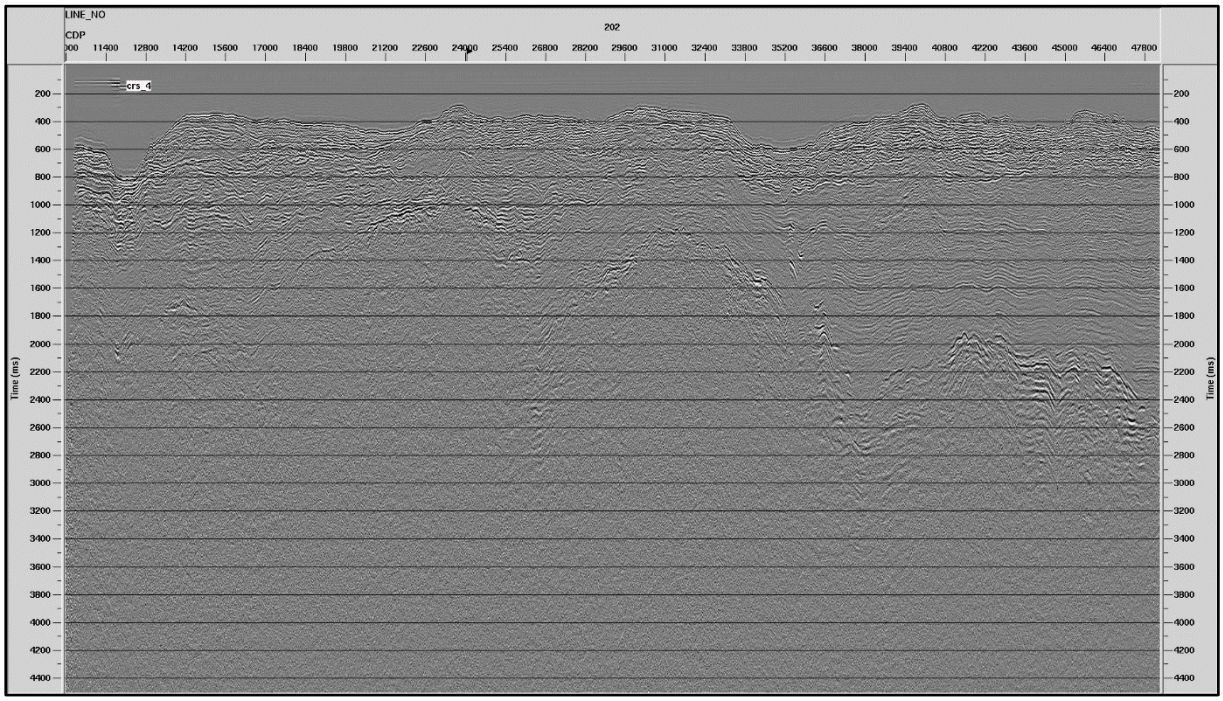

Figure 5.4 14: *Common reflection surface (CRS) applied to improve lateral continuity of reflectors. See No. 12 in the example processing flow.*

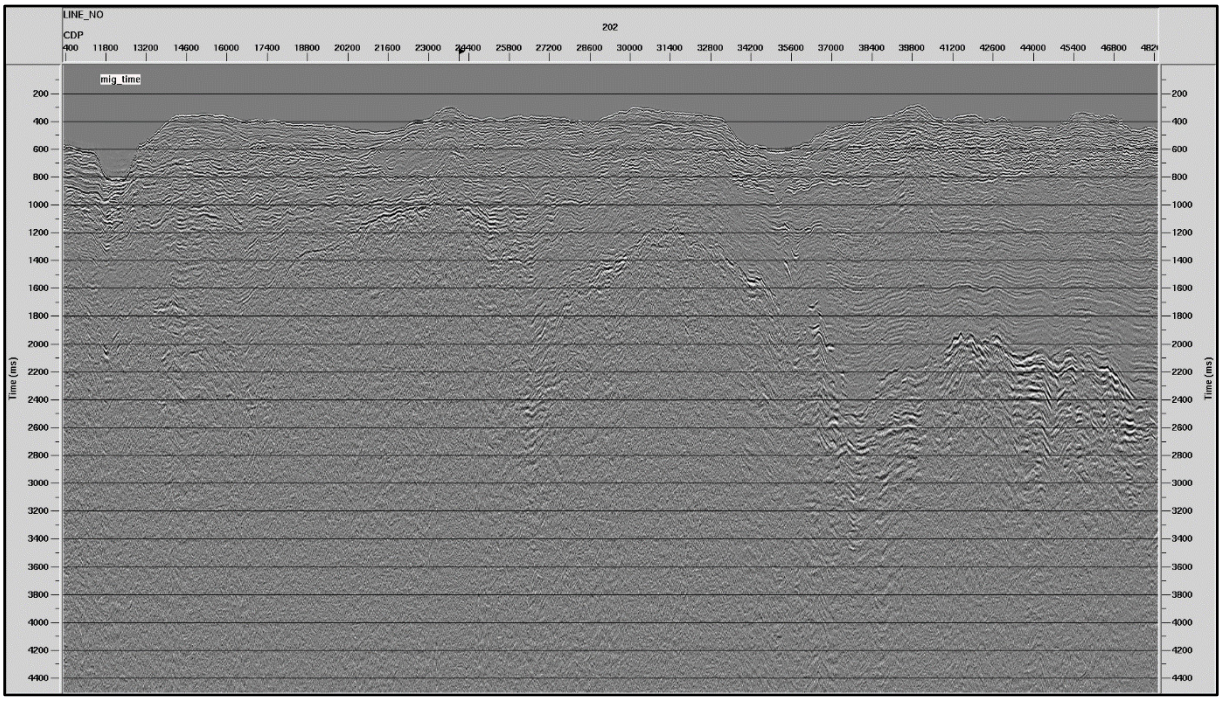

Figure 5.4 15*: Kirchoff pre-stack time migration of line BGR17-202. See No. 15 in the example processing flow.*

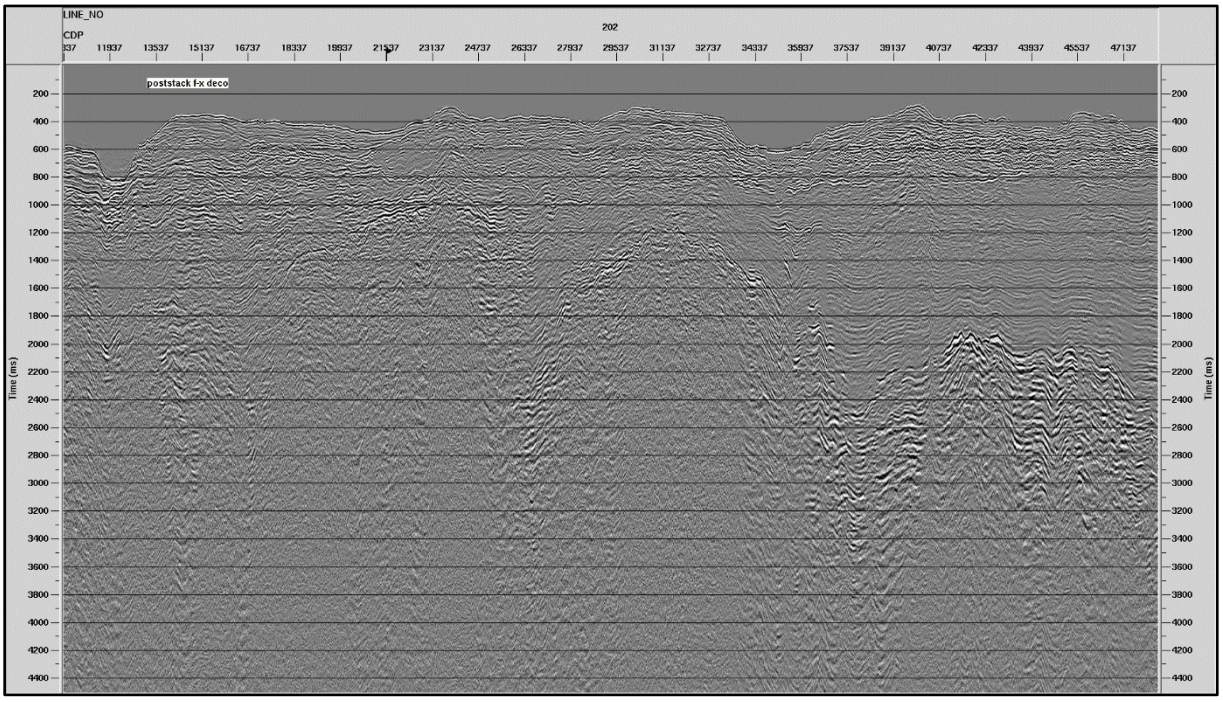

Figure 5.4 16: *Migrated section with residual moveout and post-stack F-X deconvolution applied. See No. 17-21 in the example processing flow.*

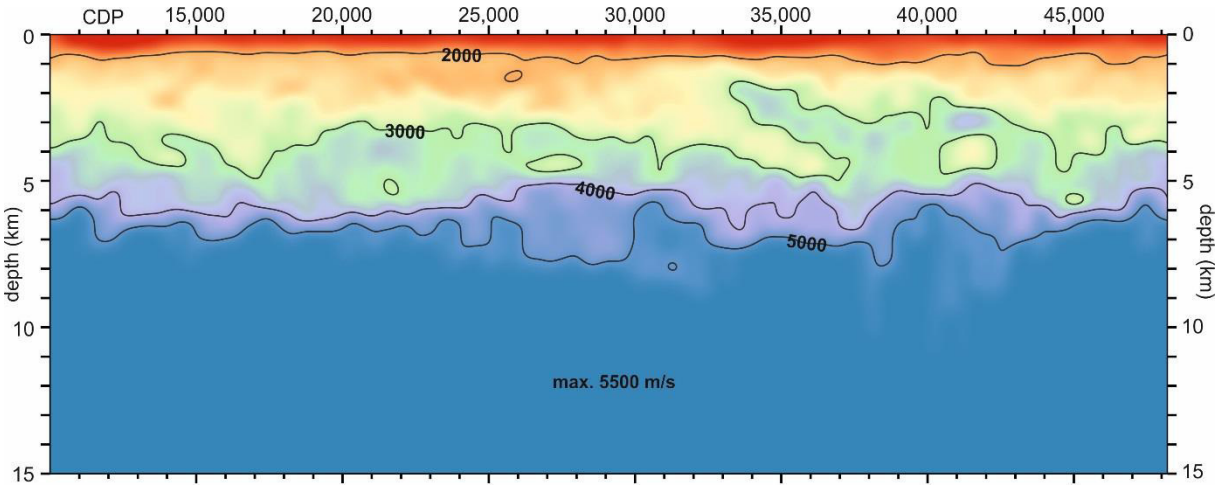

Figure 5.4 17: *Interval velocities used for depth migration of line BGR17-202. The velocities are derived from smoothed rms-velocities, reduced to 95% (shallow) down to 80% (deep). Maximum allowed velocity is 5.5 km/s. See No. 15a in the example processing flow.*

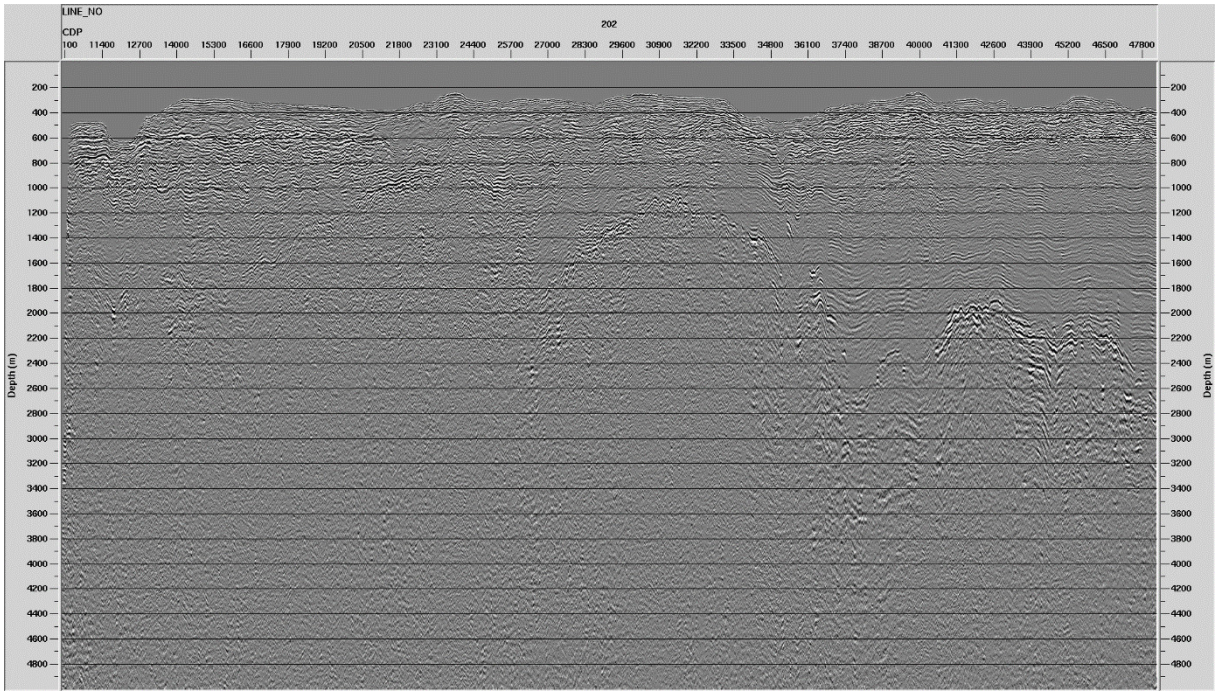

Figure 5.4 18: *Pre-stack Kirchoff depth migrated section BGR17-202. Interval velocities for migration are shown in Figure 5.4 17. See No. 15a in the example processing flow.*

5.5 Wide-angle reflection and refraction seismics

The main research focus of cruise MSM67 was the investigation of the volcanic passive margin off Northeast Greenland around the West Jan Mayen Fracture Zone. Of particular interest are the margin segmentation as well as the timing, duration and distribution of magmatism that resulted in the formation of the North Atlantic large igneous province. Two wide-angle seismic refraction profiles were acquired, one of which had to be moved from Greenland to the conjugate Jan Mayen microcontinent due to restrictions that came with the research permit for Greenland. The Greenlandic authorities requested to delay the seismic work until September 10, 2017 to avoid interference with a whale study carried out in the same area. The first seismic refraction line (BGR17-2R1) was a transect across the Jan Mayen microcontinent covering both the western and eastern continent-ocean transition zone. Line BGR17-2R2 was parallel to the coast of East Greenland and crossed the interpreted landward extension of the West Jan Mayen Fracture Zone.

5.5.1 Seismic instrumentation

A total of 31 ocean bottom seismometers (OBS) were made available for the expedition MSM67. Of those, 20 instruments were provided by the Danish seismometer pool DanSeis and 10 OBS came from the GEOMAR pool. BGR contributed one OBS that was not used for data acquisition. In total, the OBS were deployed on 59 sites located along the two seismic refraction lines

Sercel MicroOBS_Plus

In 2002 IFREMER in Plouzané, France, began designing a new generation of small, low-cost ocean bottom seismometers for wide-angle seismic use, which are easy to deploy (Figure 5.5-1).

Figure 5.5 1: *Sercel MicrOBS_Plus during deployment along line BGR17-2R1 (photo: Thomas Funck).*

The 20 OBS from the DanSeis pool were manufactured in 2016 and 2017 and are of the type Sercel MicrOBS_Plus. These instruments are an advancement of the previous model MicrOBS. The development of the MicrOBS is based on four conceptual ideas:

1. Integration of acquisition and instrument release: This integration is possible due to the use of a broadband hydrophone which allows recording of the low-frequency signal

from air gun shots or earthquakes (from 0.1 Hz up to several 100 Hz) as well as the high-frequency release signal (about 10 kHz). This significantly reduces the weight of the instrument and therefore facilitates its handling.

2. Rechargeable batteries: To avoid the opening and resealing of the instrument, which remains a delicate operation at sea, a rechargeable battery pack is used in the MicroOBS.
3. Data download by USB cable: The data are downloaded from the instrument via a USB 1.1 cable connection, to avoid opening and closing the instrument between successive deployments at sea.
4. Size reduction: The substantial size reduction of the MicrOBS compared to older OBS was possible due to the three points mentioned above, the integration of the electronics with the release, the reduction of the battery weight and the download of the data. Thus, it was possible to fit the complete instrument into a 13-inch glass sphere. The complete mass of the instrument is only 20 kg plus 20 kg for the anchor.

In 2006, Sercel started producing a new generation of MicrOBS instruments with the objective to allow for longer deployments during wide-angle seismic surveys. In order to contain a larger amount of batteries, the instrument named MicrOBS_Plus (Fig. 5.5-1) is housed in a 17-inch glass sphere. The disk space was enlarged to 8 GB resulting in a deployment length of up to 31 days with 24 days of recording at a sampling rate of 4 ms (250 Hz). Acquisition electronics, geophone and hydrophone are identical with the original MicrOBS. The weight of the instruments is 36 kg and an anchor weight of 28 kg is used for the deployment.

GEOMAR OBS-2002

The GEOMAR Ocean Bottom Seismometer 2002 (OBS-2002) is a design based on experience gained with the GEOMAR Ocean Bottom Hydrophone (OBH; Flueh and Bialas (1996)) and the GEOMAR Ocean Bottom Seismometer (OBS, Flueh and Bialas (1999)). The basic system is constructed to carry a hydrophone and a small seismometer for higher frequency active-seismic profiling. However, due to the modular design of the front end it can be adapted to different seismometers and hydrophones or pressure sensors. The sensitive seismometer is deployed between the anchor and the OBS frame (Fig. 5.5-2), which allows good coupling with the sea floor. The three-component seismometer (Owen, 4.5 Hz), usually used for active seismic profiling, is housed in a titanium tube, modified from a package built by Tim Owen (Cambridge). Geophones with a natural frequency of 4.5 Hz were used during MSM67. When deployed to the sea floor, the entire system rests horizontally on the anchor frame. After releasing its anchor weight, the instrument turns into a vertical position and ascends to the surface with the floatation on top. This ensures a minimum system height and water current sensibility during data acquisition. At the same time, the sensors are well protected against damage during recovery and the transponder remains under water, which allows for continuous ranging.

G-Gun Array

For profile BGR17-2R1 the G-gun array was identical to the one used for the acquisition of the seismic reflection data (see section 5.4.1, p. 48 for more details). The total volume of the array was 3100 cubic inches (50.4 L) and the shot interval was initially 60 s but was changed to 50 s when the ship's speed increased due to weather conditions.

For profile BGR17-2R2 two G-guns with a volume of 70 cubic inches (guns number 9 and 10) and two with a volume of 100 cubic inches (numbers 1 and 2) were replaced by four G-guns with a volume of 520 cubic inches each. This resulted in a total volume of 4840 cubic inches (79.3 L) and the shot rate was set to 60 s. For both profiles the array was operated at a pressure of 150 bar.

Figure 5.5 2: *GEOMAR OBS (Design 2002).*

5.5.2 Acquisition of Seismic Refraction Data

Releaser Test

Before the deployment of the GEOMAR OBS-2002 a releaser test was carried out. For that purpose 15 KumQuad releasers (13 of Geomar and two of BGR) were attached with closed hooks to a steel EPAL box pallet. The box was brought to a depth of 1100 m. The individual release commands were sent to the releasers to open the hook. No releaser failed. Following this test, a Sercel MicrOBS_Plus OBS was lowered down to a depth of 20 m. The OBS was fully equipped with its anchor and after sending the release command, it took 13 minutes for the burn wire to break and the OBS returned to the surface. This test also showed that the deck unit of Sercel can be connected to the ship's retractable hydrophone, which saved a lot of time during the OBS recovery since no transducer had to be lowered manually over the side of the ship.

Profile BGR17-2R1

Profile BGR17-2R1 (Figure 5.5 3) crossed the Jan Mayen microcontinent at 69.7°N, whose western margin is conjugate to East Greenland. The 254 km long line extends from oceanic crust in the Norway Basin, across the microcontinent and into oceanic crust that formed at the presently active mid-oceanic Kolbeinsey Ridge.

20 MicroOBS_Plus and 10 OBS-2002 were deployed at a spacing of 8.6 km. The deployment coordinates and depths are listed in Table 5.5 1. The backup release time was set to 23:45 UTC on September 8, 2017 for the easternmost instrument (station 097) and to 20.40 UTC a day later for the westernmost OBS (station 126).

Deployment of the OBS started on September 2, 2017 at 04:54 UTC and was completed by 21:44 UTC on the same day. After deploying the air gun array, the shooting started on September 3, 2017 at 01:47 UTC. The coordinate of the first shot point is 69.649028°N and 5.200774°W. The shot interval was 60 s at an average speed of 4.5 knots leading to an average shot distance of 140 m. Due to weather conditions the speed hat to be increased to over 5 knots. To maintain the shot spacing, the shot interval was then reduced to 50 s starting at 17:22 UTC. The shooting ended with shot number 2280 on September 4, 2017 at 12:02 UTC. The last shot took place at 69.734553°N and 12.054864°W.

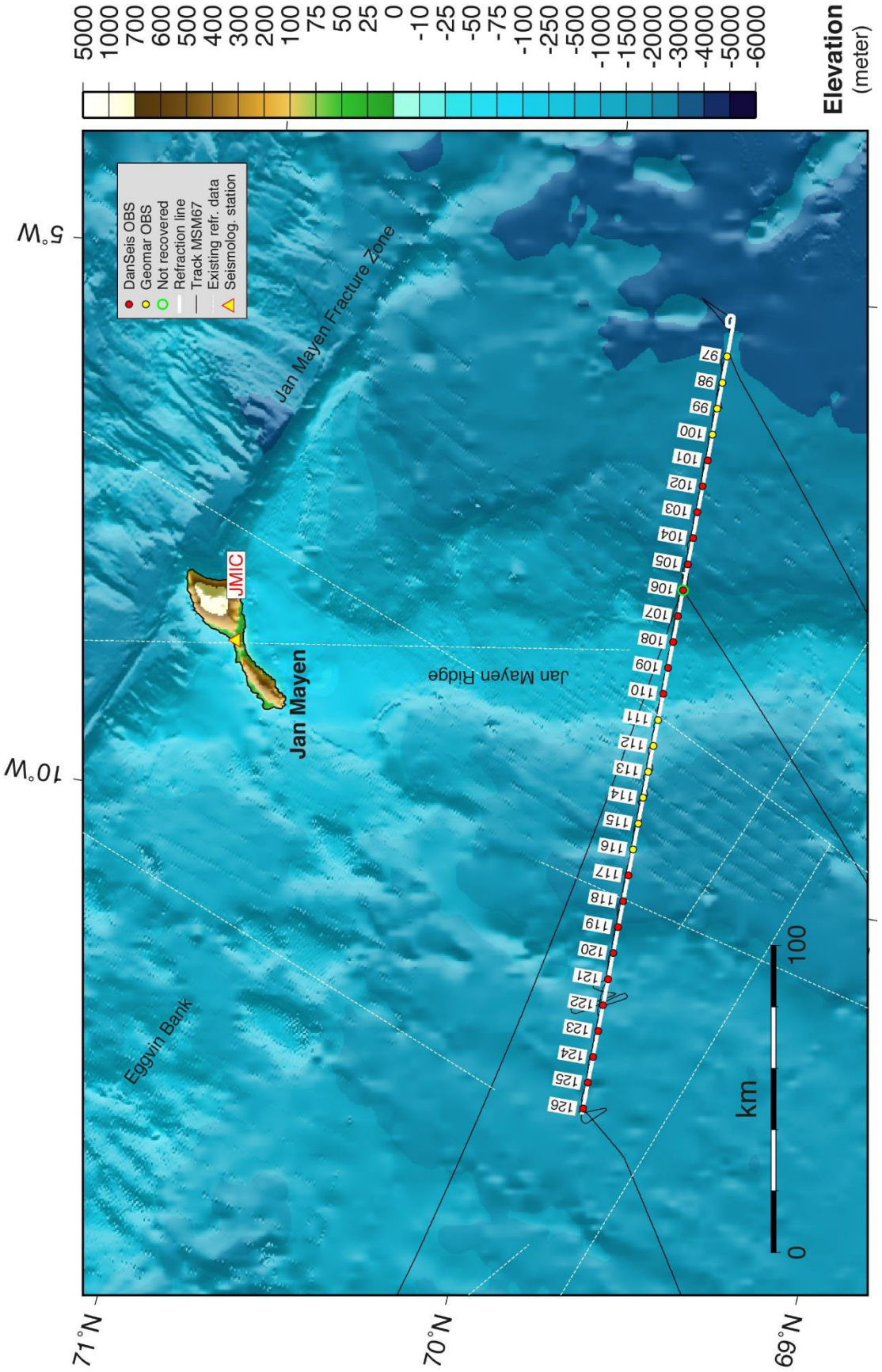

Figure 5.5 3: *Location map of seismic refraction profile BGR17-2R1. Bathymetric data are from the IBCAO 3.0 chart (Jakobsson et al., 2012).*

After recovering the air gun array, each OBS position was approached individually from west to east and the release command was transmitted several times. In order to save time, the next OBS was released after the recovery of the previous OBS. Then the ascent time of the OBS in the up to 3000 m deep water was used to sail to the released OBS. In the shallower water, this approach did not always work for the MicrOBS_Plus and they were then released a second time at the actual site. The recovery started on September 4, 2017 at 15:22 UTC but had to be halted at 22:00 UTC due to bad weather conditions. The recovery continued the next morning at 04:00 UTC and was completed by 14:23 UTC on September 6, 2017.
Except for OBS106 all OBS raised to the surface and could be recovered. No radio signal was received from OBS106 and also a visual search failed. It is not possible to range this type of instruments or get a feedback if the release worked. The ship returned back to the position of OBS106 in time for the backup release but there was no sign of the Sercel MicrOBS_Plus.

Table 5.5 1: *Deployment details of the OBS along line BGR17-2R1. All times are in UTC.*

MSM67 - SEGMENT - September 2017 Profile: BGR17_2R1

Station	Latitude		Longitude		Depth (m)	Deployment date/time		Recovery date	released	on surface	on deck	Sync date/time		Skew sync date/time		Skew ms
OBS126	69.73479	N	12.00082	W	1752	02.09.2017	4:54	04.09.2017	15:22	15:57	16:16	01.09.2017	19:06	04.09.2017	16.29	-8
OBS125	69.73662	N	11.77679	W	1871	02.09.2017	5:30	04.09.2017	16:23	17:03	17:35	01.09.2017	18:59	04.09.2017	17:44	2
OBS124	69.73692	N	11.55254	W	1898	02.09.1927	6:07	04.09.2017	18:21	18:53	19:07	01.09.2017	18:45	04.09.2017	19:17	5
OBS123	69.73745	N	11.32849	W	1884	02.09.2017	6:42	04.09.2017	19:51	20:33	20:47	01.09.2017	18:26	04.09.2017	20:58	-7
OBS122	69.73771	N	11.10448	W	1852	02.09.2017	7:17	04.09.2017	21:36	22:07	22:29	01.09.2017	13:49	04.09.2017	22:32	-21
OBS121	69.73732	N	10.88140	W	1719	02.09.2017	7:53	05.09.2017	04:11	04:48	05:06	01.09.2017	13:33	05.09.2017	05:14	-14
OBS120	69.73751	N	10.65655	W	1582	02.09.1927	8:30	05.09.2017	05:46	06:22	06:33	01.09.2017	13:13	05.09.2017	06:42	-33
OBS119	69.73689	N	10.43342	W	1813	02.09.2017	9:06	05.09.2017	07:13	07:50	08:00	01.09.2017	13:04	05.09.2017	08:09	-31
OBS118	69.73605	N	10.20975	W	2182	02.09.2017	9:40	05.09.2017	08:42	09:33	09:45	01.09.2017	12:44	05.09.2017	10:09	13
OBS117	69.73469	N	9.98494	W	2187	02.09.2017	10:13	05.09.2017	10:26	11:09	11:18	01.09.2017	12:27	05.09.2017	11:22	-12
OBS116	69.73369	N	9.76130	W	1969	02.09.2017	10:47	05.09.2017	11:21	11:47	12:07	02.09.2017	5:03	05.09.2017	13:09	-248
OBS115	69.73181	N	9.53834	W	2135	02.09.2017	11:20	05.09.2017	12:10	12:40	12:49	02.09.2017	5:44	05.06.2017	16:52	5
OBS114	69.72971	N	9.31358	W	2112	02.09.1927	11:53	05.09.2017	12:53	13:23	13:35	02.09.2017	5:54	05.09.2017	14:51	-25
OBS113	69.72747	N	9.09023	W	2013	02.09.2017	12:26	05.09.2017	13:40	14:04	14:25	02.09.2017	6:16	05.09.2017	14:44	-146
OBS112	69.72463	N	8.86715	W	1729	02.09.2017	13:01	05.09.2017	14:29	14:50	15:15	02.09.2017	6:35	05.09.2017	16:37	17
OBS111	69.72176	N	8.64311	W	1212	02.09.2017	13:38	05.09.2017	15:27	15:32	16:00	02.09.2017	6:55	05.09.2017	16:18	-4
OBS110	69.71885	N	8.41987	W	848	02.09.2017	14:14	05.09.2017	16:41	17:09	17:16	01.09.2017	11:35	05.09.2017	17:24	6
OBS109	69.71533	N	8.19633	W	917	02.09.2017	14:51	05.09.2017	17:55	18:10	18:20	01.09.2017	11:24	05.09.2017	18:28	-35
OBS108	69.71156	N	7.97257	W	1023	02.09.1927	15:27	05.09.2017	18:58	19:26	19:37	01.09.2017	11:06	05.09.2017	19:48	14
OBS107	69.70757	N	7.75027	W	1474	02.09.2017	16:05	05.09.2017	20:13	20:50	21:06	01.09.2017	10:24	05.09.2017	21:17	-4
OBS106	69.70319	N	7.52686	W	1965	02.09.2017	16:40	05.09.2017	21:44	no	no	01.09.2017	09:57	05.09.2017	no data	-
OBS105	69.69863	N	7.30325	W	2367	02.09.2017	17:12	06.09.2017	01:04	01:44	02:02	01.09.2017	09:38	06.09.2017	02:12	-28
OBS104	69.69373	N	7.07910	W	2503	02.09.1927	17:46	06.09.2017	02:06	02:58	03:20	01.09.2017	9:47	06.09.2017	03:30	-51
OBS103	69.68951	N	6.85668	W	2557	02.09.2017	18:20	06.09.2017	04:03	04:54	05:03	31.08.2017	21:00	06.09.2017	05:12	-25
OBS102	69.68333	N	6.63425	W	2634	02.09.2017	18:55	06.09.2017	05:06	06:00	06:12	31.08.2017	20:37	06.09.2017	07:14	34
OBS101	69.67788	N	6.41098	W	2716	02.09.2017	19:30	06.09.2017	09:45	10:43	11:01	31.08.2017	20:10	06.09.2017	11:07	22
OBS100	69.67165	N	6.18876	W	2814	02.09.2017	20:05	06.09.2017	11:03	11:39	12:00	02.09.2017	9:20	06.09.2017	12:20	-9
OBS099	69.66556	N	5.96727	W	2895	02.09.2017	20:37	06.09.2017	12:02	12:34	12:45	02.09.2017	8:20	06.09.2017	13:04	12
OBS098	69.65913	N	5.74407	W	2958	02.09.2017	21:11	06.09.2017	12:50	13:26	13:32	02.09.2017	8:38	06.09.2017	13:44	26
OBS097	69.65240	N	5.52113	W	2992	02.09.2017	21:44	06.09.2017	13:35	14:13	14:23	02.09.2017	9:44	06.09.2017	14:36	6

Profile BGR17-2R2

Profile BGR17-2R2 (Figure 5.5 4) was located on the shelf of the East Greenland continental margin running in a SW-NE direction. All remaining 19 MicrOBS_Plus and 10 OBS-2002 were deployed along the 239 km long line at a spacing of 8.4 km. Deployment details are specified in Table 5.5 2. The backup release time was set to 23:00 UTC on September 30, 2017 for the most southern instrument (station 201) and to 20:00 UTC on October 1, 2017 for the northernmost OBS (station 229).

All OBS were deployed during one day. The deployment of the instruments started on September 22, 2017 at 03:39 UTC and lasted until 17:37 UTC. After deploying the G-gun array, the shooting started on September 22, 2017 at 20:43 UTC. The coordinates of the first shot are 71.8532207°N and 21.014816°W. The shot interval was 60 s at an average speed of 4.5 knots resulting in an average shot distance of about 140 m. The shooting lasted until 01:10 UTC on September 24, 2017. The position of the last shot is 73.7706723°N and 17.793288°W.

After recovering the air gun array, each OBS station was visited to send the release command. Due to the shallow water, the instruments were released near its location. The recovery started at 03:01 UTC on September 24, 2017 but had to be halted at 21:00 UTC due to bad weather conditions. The recovery was resumed at 05:00 UTC on September 25, 2017 to be completed on the same day at 14:42 UTC. All 29 OBS could be recovered.

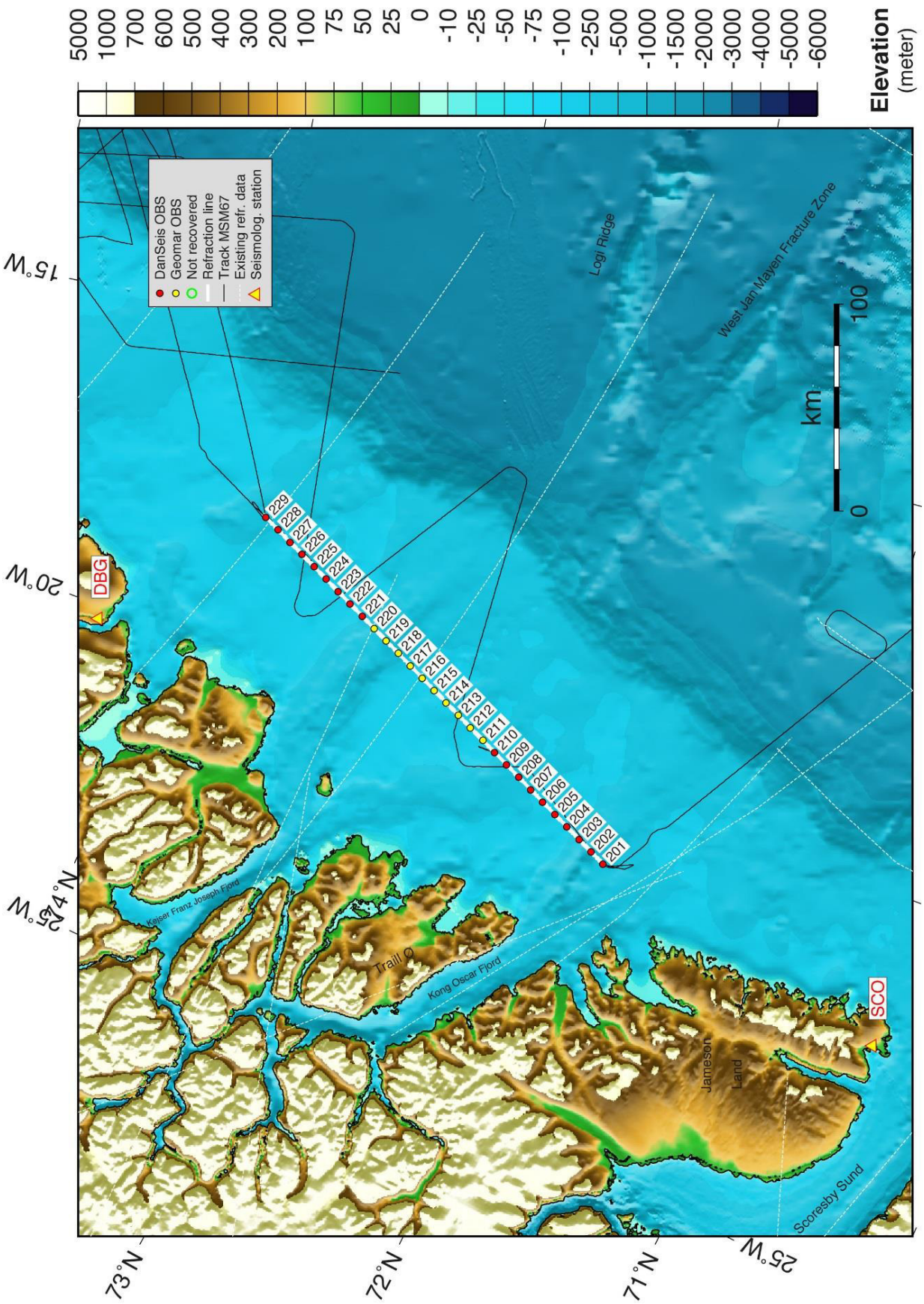

Figure 5.5 4: *Location map of seismic refraction profile BGR17-2R2. Bathymetric data are from the IBCAO 3.0 chart (Jakobsson et al., 2012).*

Table 5.5 2: *Deployment details of the OBS along line BGR17-2R2. All times are in UTC.*

MSM67 - SEGMENT - September 2017 Profile: BGR17_2R2

Station	Latitude		Longitude		Depth (m)	Deployment date/time		Recovery (date)	released	on surface	on deck	Sync date/time		Skew sync date/time		Skew ms
OBS229	73.75673	N	17.81872	W	285	02.09.2017	05:30:00	24.09.2017	3:01	3:10	3:24	20.09.2017	13:48	24.09.2017	3:00	22
OBS228	73.69035	N	17.94398	W	233	02.09.1927	06:07:32	24.09.2017	4:01	4:09	4:18	20.09.2017	13:39	24.09.2017	4:23	12
OBS227	73.62374	N	18.07270	W	195	02.09.2017	06:42:31	24.09.2017	4:56	5:46	5:56	20.09.2017	13:23	24.09.2017	6:02	9
OBS226	73.55695	N	18.19263	W	285	02.09.2017	07:17:04	24.09.2017	6:30	6:44	6:52	20.09.2017	13:12	24.09.2017	6:58	1
OBS225	73.48953	N	18.31499	W	223	02.09.2017	07:53:46	24.09.2017	7:55	8:05	8:12	20.09.2017	12:59	24.09.2017	8:18	33
OBS224	73.42242	N	18.43801	W	215	02.09.1927	08:30:20	24.09.2017	8:43	8:53	8:59	20.09.2017	12:41	24.09.2017	9:10	30
OBS223	73.35587	N	18.56127	W	174	02.09.2017	09:06:24	24.09.2017	9:31	9:39	9:47	20.09.2017	09:41	24.09.2017	10:02	32
OBS222	73.28809	N	18.68347	W	218	02.09.2017	09:40:47	24.09.2017	10:19	10:30	10:39	20.09.2017	09:29	24.09.2017	11:03	-6
OBS221	73.22041	N	18.80200	W	263	02.09.2017	10:13:43	24.09.2017	11:10	11:29	11:45	20.09.2017	09:13	24.09.2017	11:58	56
OBS220	73,15411	N	18,91901	W	360	02.09.2017	10:47:00	24.09.2017	12:27	12:32	12:40	22.09.2017	04:36	24.09.2017	13:13	-152
OBS219	73,08630	N	19,03390	W	390	02.09.2017	11:20:00	24.09.2017	13:25	13:00	13:45	22.09.2017	04:51	24.09.2017	14:12	12
OBS218	73,01914	N	19,15126	W	295	02.09.1927	11:53:00	24.09.2017	14:26	14:30	14:42	22.09.2017	05:07	24.09.2017	14:56	-1
OBS217	72,95157	N	19,26750	W	206	02.09.2017	12:26:00	24.09.2017	15:22	15:27	15:36	22.09.2017	05:18	24.09.2017	15:59	-12
OBS216	72,88412	N	19,38158	W	186	02.09.2017	13:01:00	24.09.2017	16:14	16:17	16:24	22.09.2017	05:30	24.09.2017	16:56	8
OBS215	72,81625	N	19,49832	W	203	02.09.2017	13:38:00	24.09.2017	17:03	17:06	17:12	22.09.2017	05:40	24.09.2017	17:32	-105
OBS214	72,74919	N	19,60937	W	243	02.09.2017	14:14:21	24.09.2017	17:51	17:55	18:04	22.09.2017	05:53	24.09.2017	18:25	4
OBS213	72,68106	N	19,72066	W	220	02.09.2017	14:51:03	24.09.2017	18:44	18:48	18:56	22.09.2017	06:03	24.09.2017	19:15	-150
OBS212	72,61411	N	19,83333	W	238	02.09.1927	15:27:33	24.09.2017	19:36	19:39	19:45	22.09.2017	06:15	24.09.2017	20:25	17
OBS211	72,54333	N	19,94189	W	197	02.09.2017	16:05:46	24.09.2017	20:37	20:40	20:47	22.09.2017	06:26	24.09.2017	21:16	9
OBS210	72.47655	N	20.05260	W	247	02.09.2017	16:40:13	25.09.2017	5:12	5:28	5:40	20.09.2017	14:02	25.09.2017	5:46	22
OBS209	72.40948	N	20.16012	W	301	02.09.2017	17:12:08	25.09.2017	6:20	6:37	6:51	20.09.2017	14:14	25.09.2017	6:55	25
OBS208	72.34119	N	20.26821	W	282	02.09.1927	17:46:06	25.09.2017	07:33	07:40	07:58	20.09.2017	14:24	25.09.2017	8:03	-1
OBS207	72.27292	N	20.37681	W	262	02.09.2017	18:20:43	25.09.2017	08:39	08:48	08:57	20.09.2017	14:35	25.09.2017	9:10	-15
OBS206	72.20506	N	20.48015	W	243	02.09.2017	18:55:03	25.09.2017	09:33	09:47	09:53	20.09.2017	12:33	25.09.2017	10:19	10
OBS205	72.13668	N	20.58756	W	220	02.09.2017	19:30:46	25.09.2017	10:28	10:36	10:43	20.09.2017	11:23	25.09.2017	11:32	56
OBS204	72.06840	N	20.69115	W	212	02.09.2017	20:05:00	25.09.2017	11:20	11:27	11:33	20.09.2017	11:15	25.09.2017	12:40	-12
OBS203	71.99997	N	20.79453	W	352	02.09.2017	20:37:00	25.09.2017	12:11	12:31	12:37	20.09.2017	11:04	25.09.2017	13:50	-5
OBS202	71.93186	N	20.89591	W	540	02.09.2017	21:11:00	25.09.2017	13:17	13:35	13:44	20.09.2017	10:23	25.09.2017	15:30	56
OBS201	71.86366	N	21.00096	W	378	02.09.2017	21:44:00	25.09.2017	14:25	14:35	14:42	20.09.2017	10:00	25.09.2017	17:00	22

Sink and Rise Velocity on Profile BGR17-2R1

The time of deployment, arrival at the sea bottom, the start of the ascent and the return to the sea surface could be determined by analyzing the data of the OBS. Together with the water depth, the ascent and descent velocities of the OBS can be calculated. All Geomar OBS-2002 sank with a velocity between 0.56 m/s and 0.63 m/s with exception of OBS099. This OBS descended only with a velocity of 0.49 m/s (Figure 5.5 5). The Sercel MicrOBS_Plus sank with an average velocity of 0.48 m/s (total range between 0.44 m/s and 0.52 m/s).

The ascent velocities (Figure 5.5 6) of the Sercel MicroOBS_Plus varied between 1.01 m/s and 1.13 m/s with an average of 1.07 m/s. The average burn time of the burn wires of the Sercel instruments was 9.5 minutes but varied between 2 and 16 minutes for individual instruments. The ascent rates for the Geomar OBS-2002 averaged 1.32 m/s with a total range between 1.17 and 1.51 m/s.

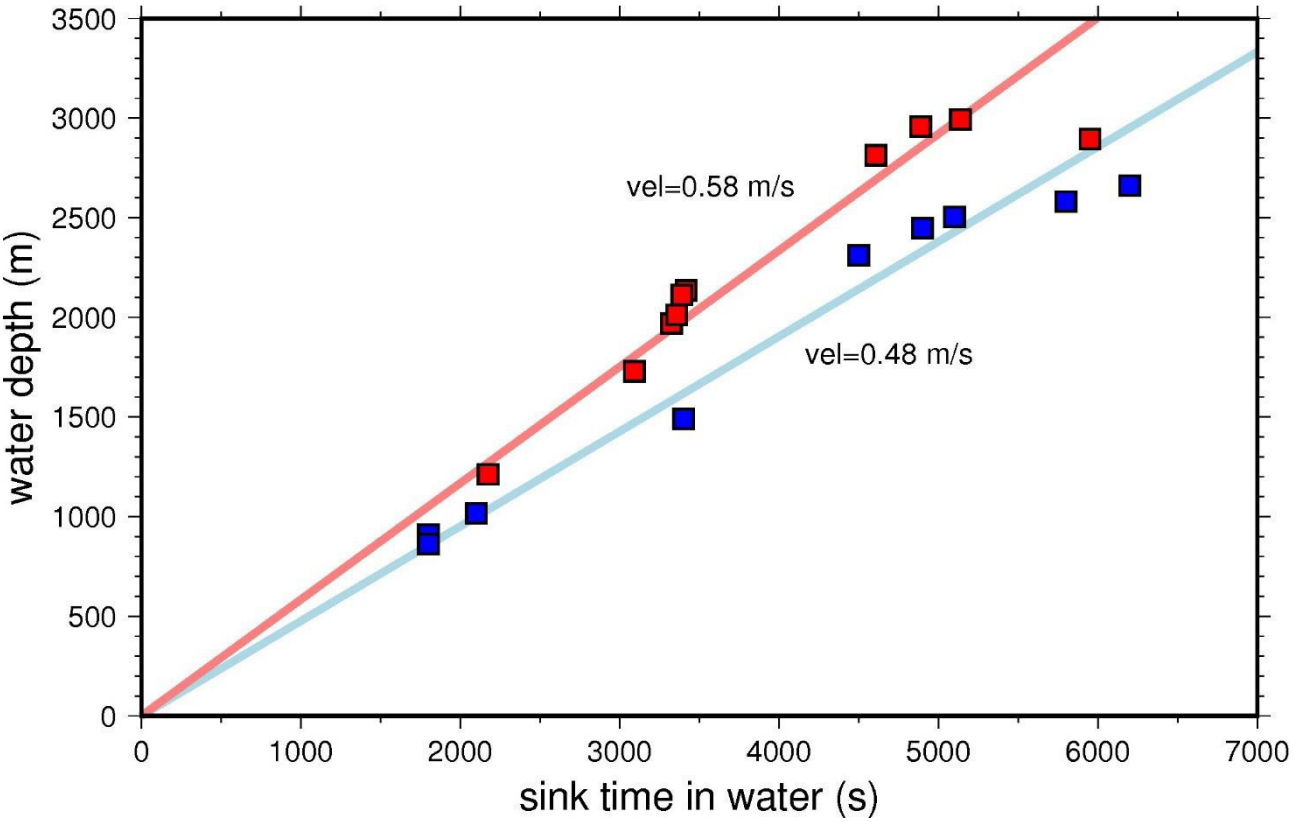

Figure 5.5 5: *Sink time vs. water depth for all OBS. Red squares indicate Geomar OBS-2002 while blue squares mark the Sercel MicrOBS_Plus.*

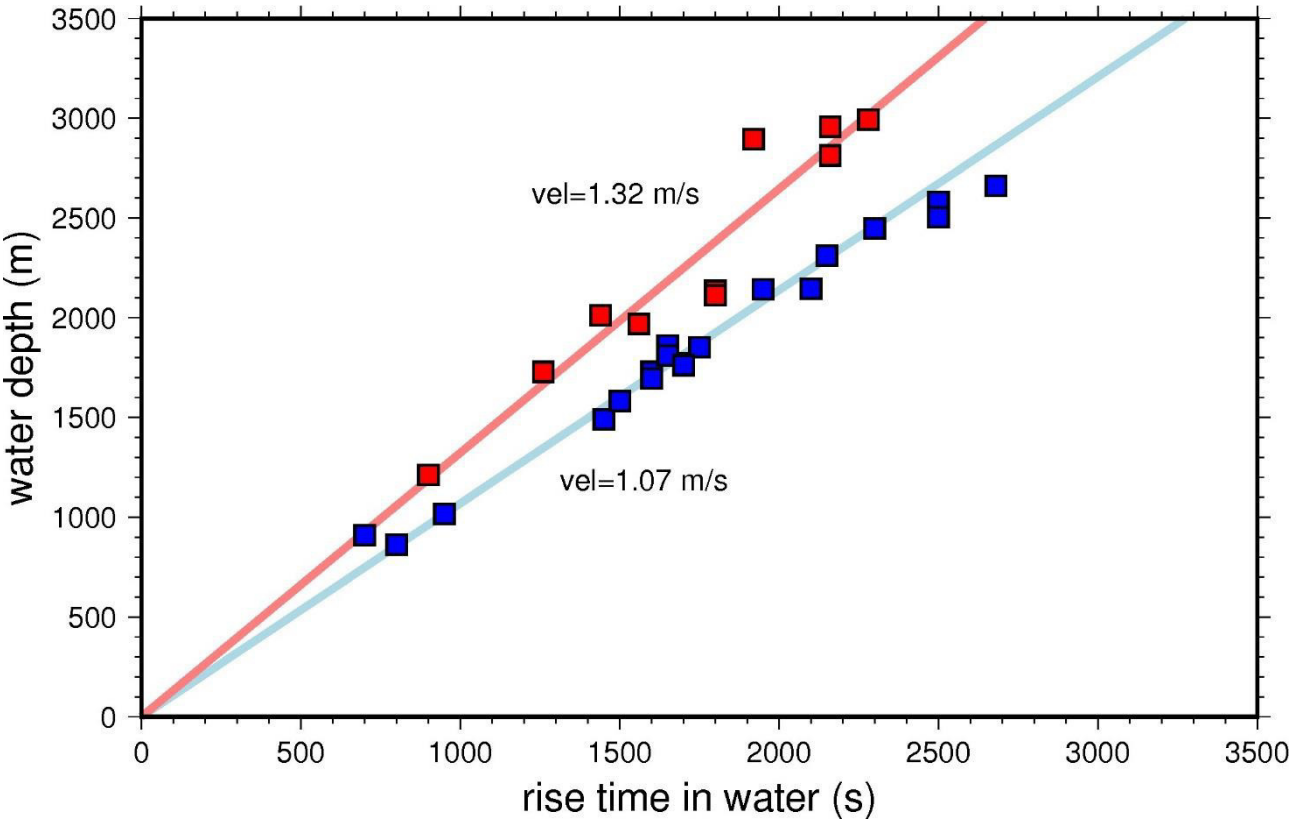

Figure 5.5 6: *Rise time vs. water depth for all OBS. Red squares indicate Geomar OBS-2002 while blue squares mark the Sercel MicrOBS_Plus.*

Data Preprocessing

Before deployment and after recovery the recorders are synchronized with the GPS time signal to determine the time drift (skew time) during the experiments. The drift of the OBS clock is assumed to be linear and the skew time is then applied to correct the data for this drift. Then a resampling of the data is carried out. The shot times are used to extract a 60-s-long data window for each shot that are then exported to SEGY data files. At the same time, the shot and OBS coordinates are added to the SEGY headers.

Data Quality Control

A quality control was performed by visual inspection of the pseudo SEGY files. On profile BGR17-2R1 one geophone component of GEOMAR OBS098 failed and lacks data after the first quarter of the recording time. For profile BGR17-2R1, one GEOMAR hydrophone (OBH113) was replaced, which improved the data quality. The malfunctioning horizontal geophone component (channel 4) could not be replaced (OBS212) due to missing spare parts. All other instruments out of the 59 deployments showed good data quality.

5.6 Preliminary results

5.6.1 Gravity

Figs. 5.6-1 through 5.6-4 show the gravity anomalies for all relevant lines of cruise MSM67 combined with synthetic profile lines from a satellite gravity data grid (Andersen et al., 2010) and with the bathymetry along the profile lines from a predicted bathymetry data grid (Jakobsson et al., 2012). A striking feature on all profiles crossing the shelf edge is a prominent gravity high close to the position of the shelf break. The high noise level in the data along a number of profiles correlates with rough weather conditions and the associated accelerations the gravity meter experienced through the motion of the ship.

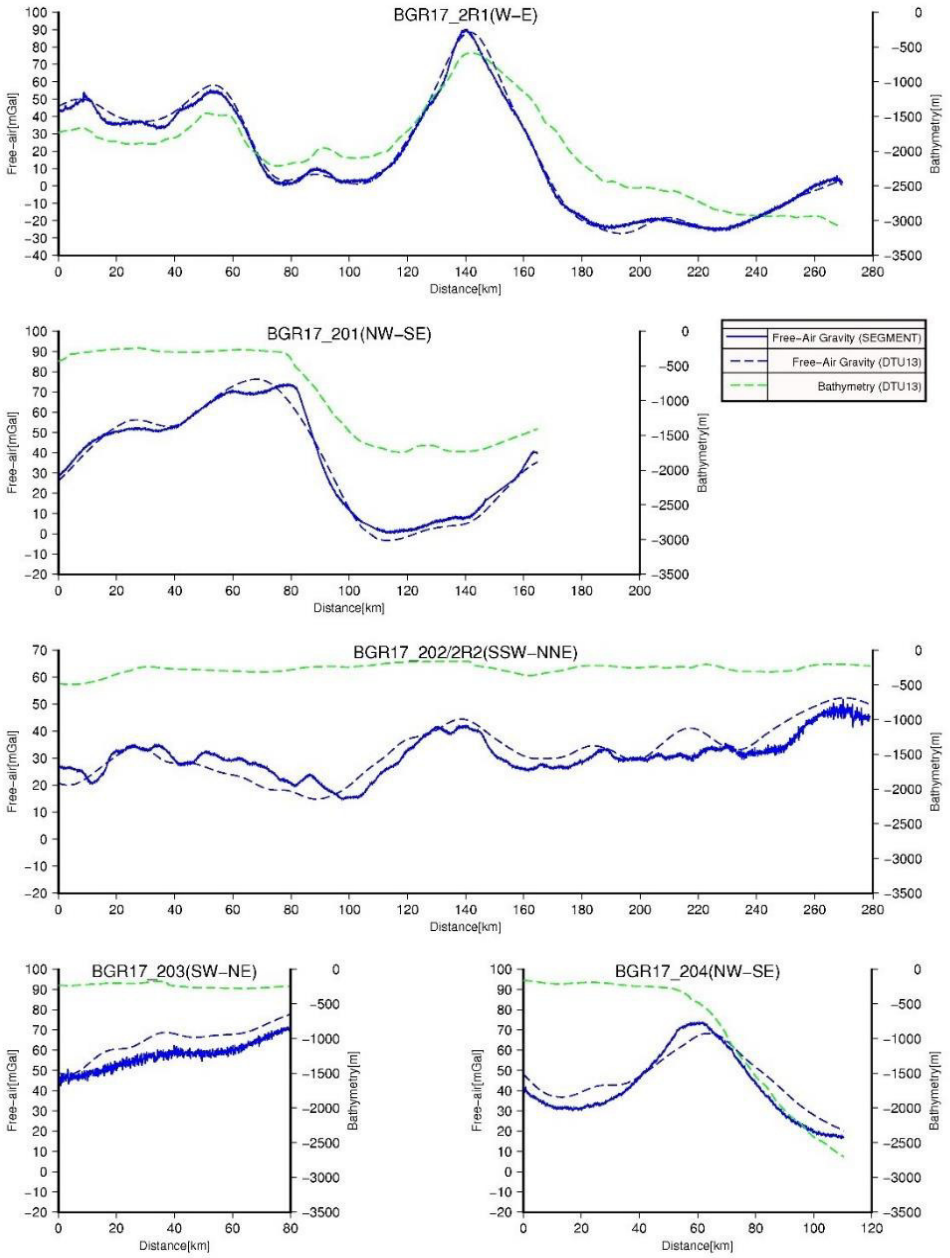

Figure 5.6 1*: Gravity profiles 2R1 through 204 of cruise MSM-67 (solid lines) combined with synthetic lines from satellite gravity data grid (blue dashed lines) and bathymetry from a predicted bathymetry data grid (green dashed lines). Note the high noise levels on profiles 202 and 203 which are due to bad weather during acquisition.*

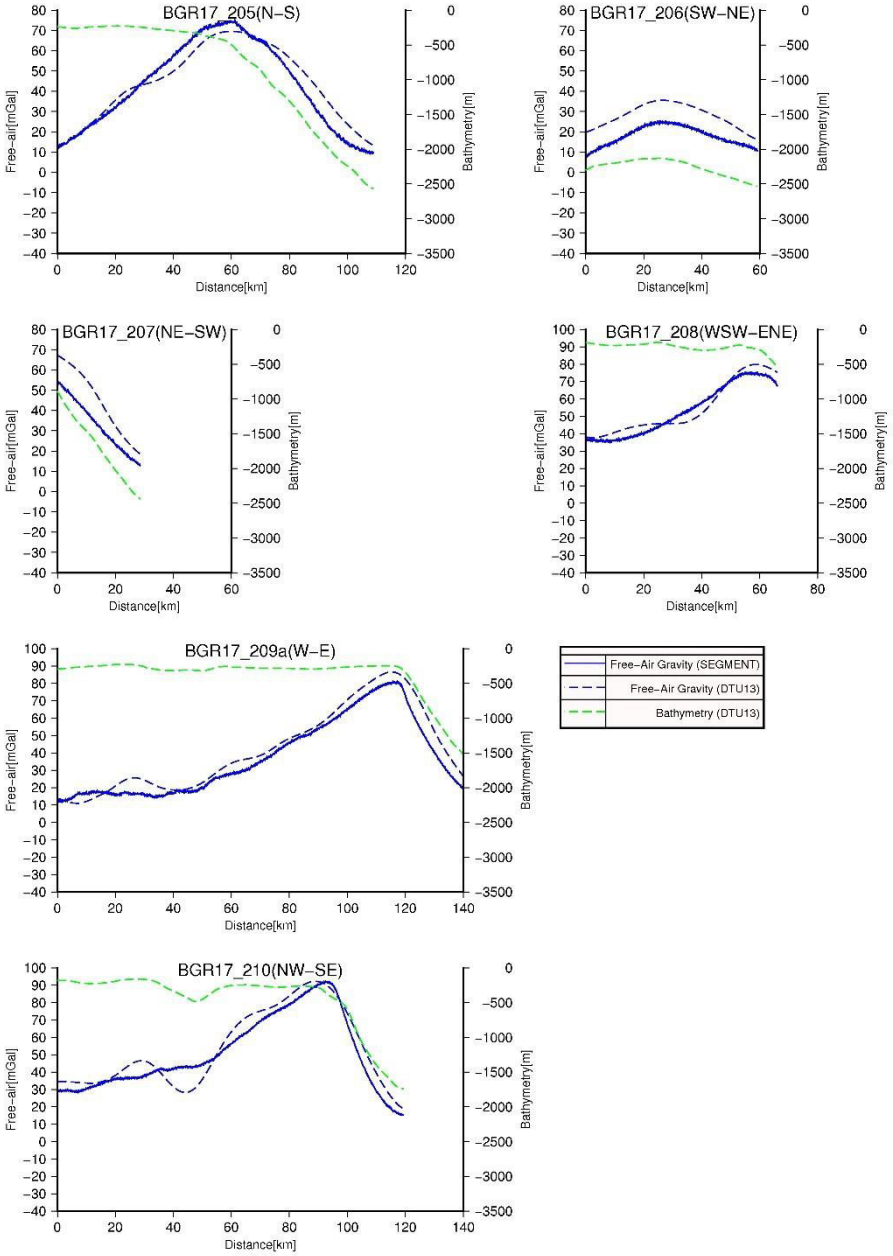

Figure 5.6 2: *Gravity profiles 205 through 210 of cruise MSM-67 (solid lines) combined with synthetic lines from satellite gravity data grid (blue dashed lines) and bathymetry from a predicted bathymetry data grid (green dashed lines).*

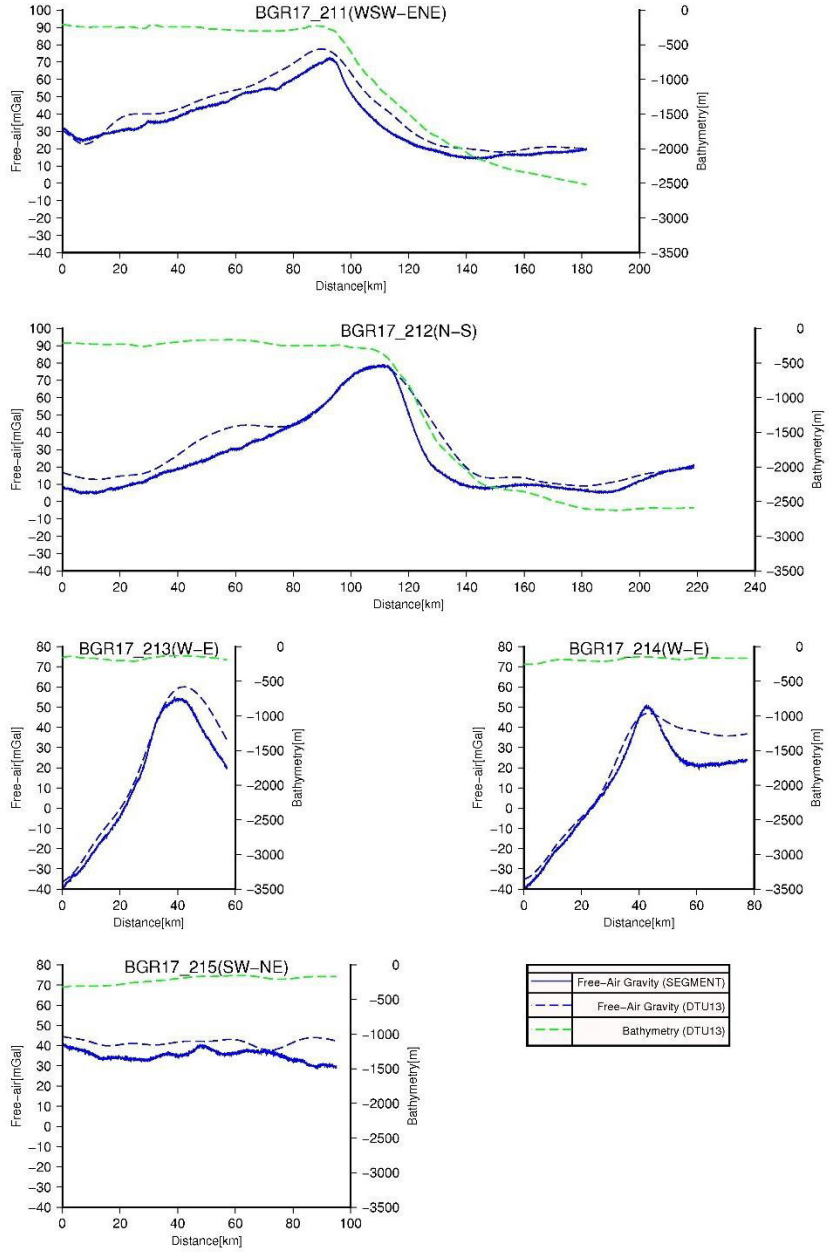

Figure 5.6 3: *Gravity profiles 205 through 215 of cruise MSM-67 (solid lines) combined with synthetic lines from satellite gravity data grid (blue dashed lines) and bathymetry from a predicted bathymetry data grid (green dashed lines).*

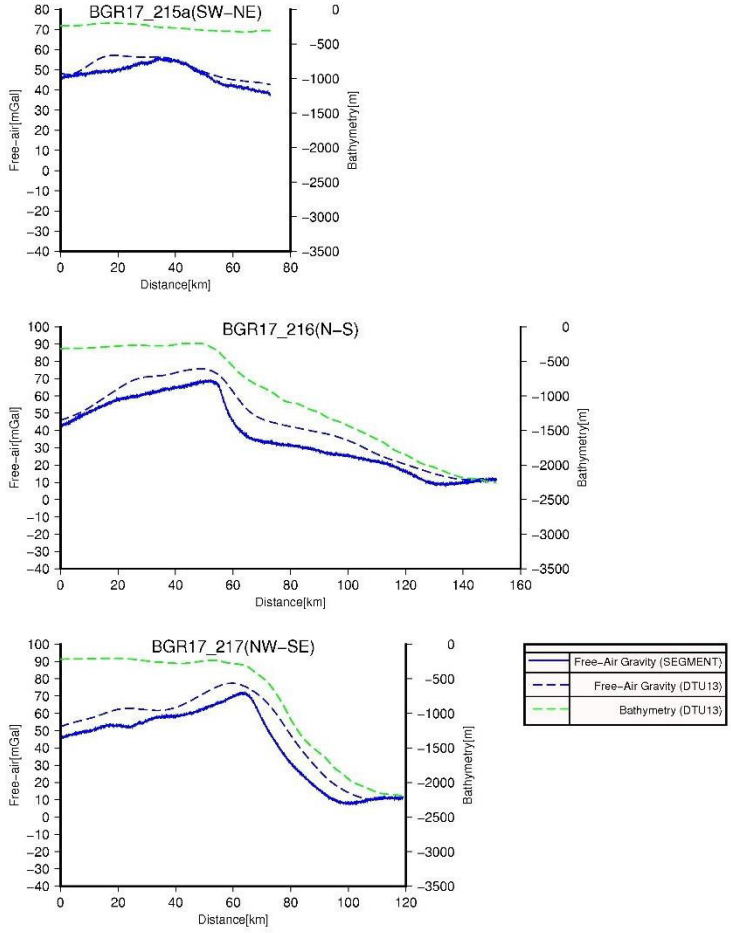

Figure 5.6 4: *Gravity profiles 215a through 217 of cruise MSM-67 (solid lines) combined with synthetic lines from satellite gravity data grid (blue dashed lines) and bathymetry from a predicted bathymetry data grid (green dashed lines).*

5.6.2 Magnetics

Figure 5.6 5 and Figure 5.6-6 show the magnetic anomalies for all relevant lines of cruise MSM-67 as wiggle traces along the profile lines.

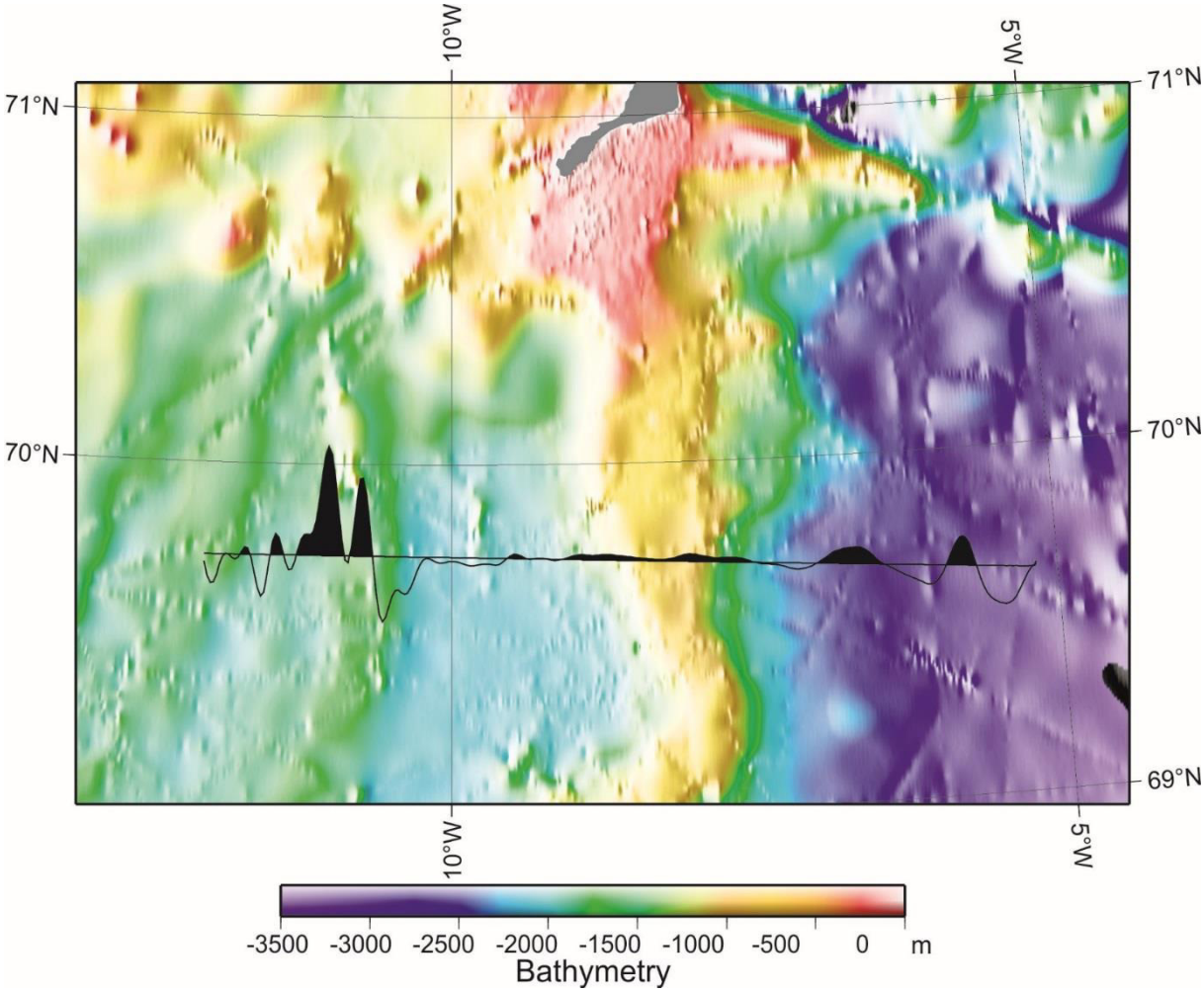

Figure 5.6 5: *Magnetic anomalies shown as wiggle traces for profile BGR17-2R1 south of Jan Mayen. Positive anomalies filled black, negative anomalies blank.*

South of Jan Mayen, a long refraction seismic profile was acquired over the Jan Mayen Ridge. The magnetic profile shows old seafloor spreading anomalies in the east (likely Anomaly 24), then low amplitude magnetic anomalies which are typical for many plutonic continental rocks in its central part above the ridge. In the western part of the profile, this pattern terminates sharply against high amplitude magnetic anomalies of younger oceanic crust (likely Anomalies 5C through 6). – (for comparision see Fig. 5.6-7).

On the profiles obtained offshore Greenland, only a few profiles clearly indicate seafloor spreading anomalies on their seaward ends. Profile BGR17-201 is located south of the Jan Mayen fracture zone and at its seaward end shows high amplitude seafloor spreading anomalies which are supposedly the mirror image of those imaged at the western end of profile BGR17-2R1 und thus represent Anomalies 5D and 6. Further north, profiles 209 and 210 did not reach oceanic crust at their eastern ends. On profiles 211, 212, 216, and 217 most likely Anomaly 22 is imaged at the eastern ends.

Older seafloor anomalies cannot be identified on these profiles, instead it seems likely that the adjacent anomalies in western direction represent SDR sequences of different intensity. Even

further to the north, Profiles 204, 205, and perhaps also the very short Profile 207 may have imaged Anomaly 24 at their eastern ends.

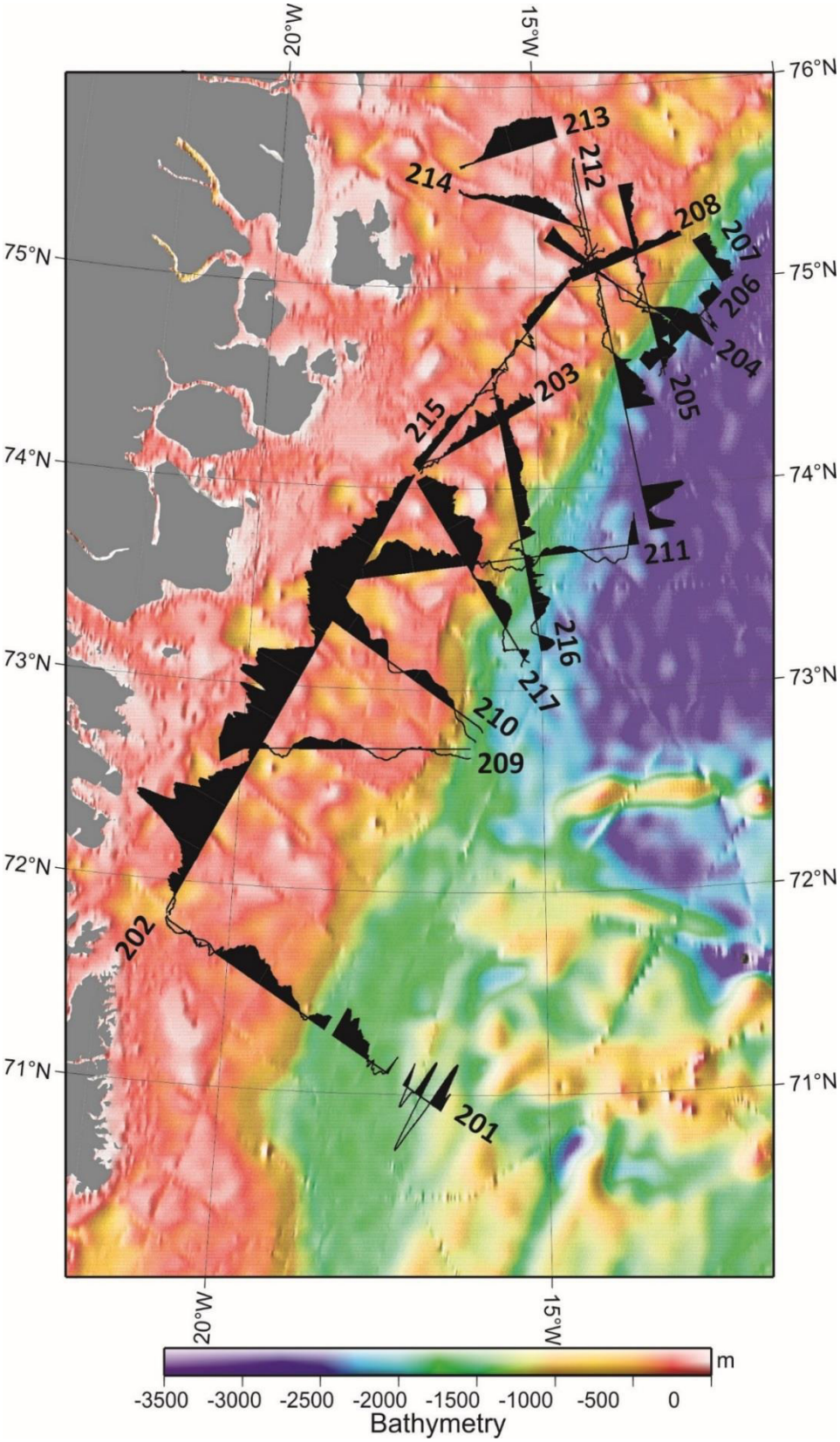

Figure 5.6-6: *Magnetic anomalies shown as wiggle traces for MSM-67 profiles at the continental shelf of East Greenland, positive anomalies filled black, negative anomalies blank.*

Most parts of the Greenland shelf area are dominated by positive anomalies of high amplitudes which hint at the presence of massive volcanics at shallow depths in this area. Where the water is shallow, especially on profile 202, the close distance from the source rocks to the magnetic sensors result in very high values of the positive anomalies. On the other hand, lower values and even negative values in some places could be associated with structures where the basement is encountered at much greater depths.

Many profiles show a pattern of low amplitude, short wavelength, noise-like anomalies seemingly superimposed to the longer wavelength high amplitude anomalies. In some cases like profile 203 this is due to sensor noise because the data were acquired in very rough weather conditions. In most cases, the origin will be disturbances of the Earth's magnetic field with frequencies on the order of minutes. However, shallow lying volcanic basement structures with a rough surface topography can also result in the observed anomaly patterns. Further processing and modelling of the magnetic data will have to distinguish between the different possible origins of the short wavelength anomalies.

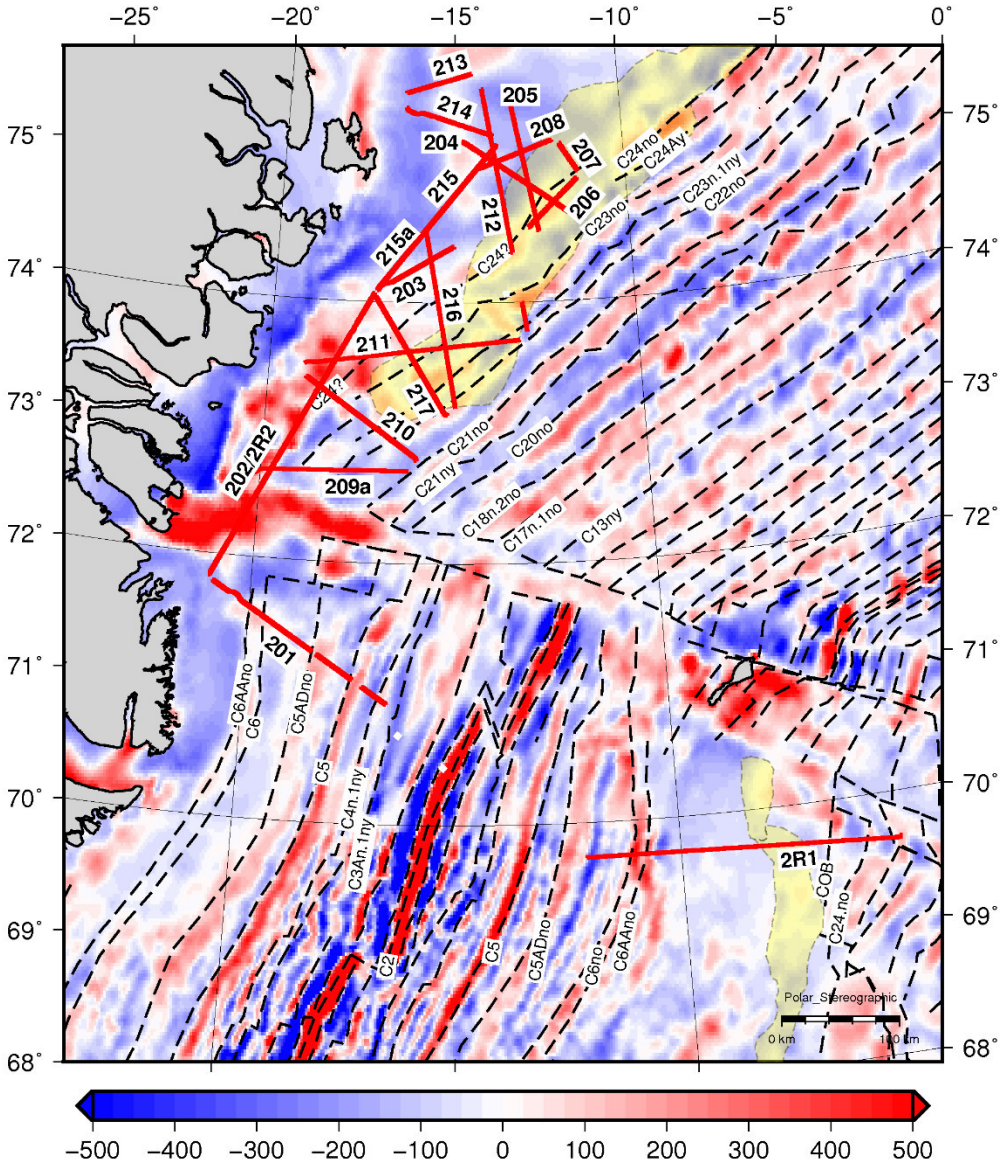

Figure 5.6 7: *Magnetic anomaly map of the Northwest Atlantic (CAMP data) and location of magnetic profiles of cruise MSM-67 (red lines). Dashed lines are magnetic Chrons from Gaina et al. 2017. Yellow shaded areas denote SDRs (Hopper et al. 2016).*

Figure 5.6 **8**- through

Figure **5.6 11** show the magnetic anomalies for all relevant lines of cruise MSM67 combined with synthetic profile lines from the CAMP magnetic data grid (Gaina et al., 2011) and with magnetic anomalies reconstructed from the gradient where available.

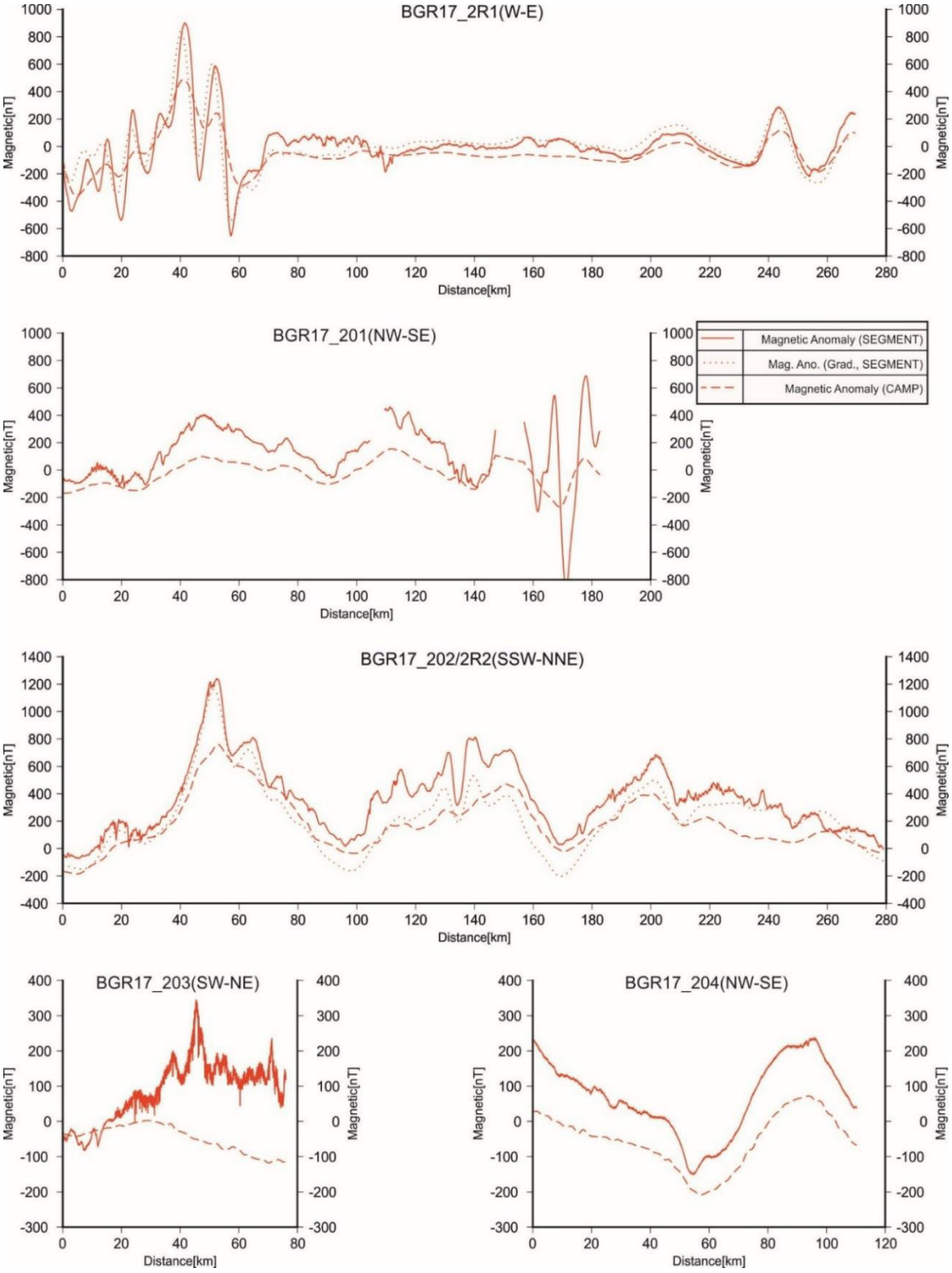

Figure 5.6 8*: Magnetic profiles 2R1 through 204 of cruise MSM-67 (solid lines) combined with synthetic lines from the CAMP magnetic data grid (dashed lines) and magnetic data reconstructed from gradient measurements (where available, dotted lines).*

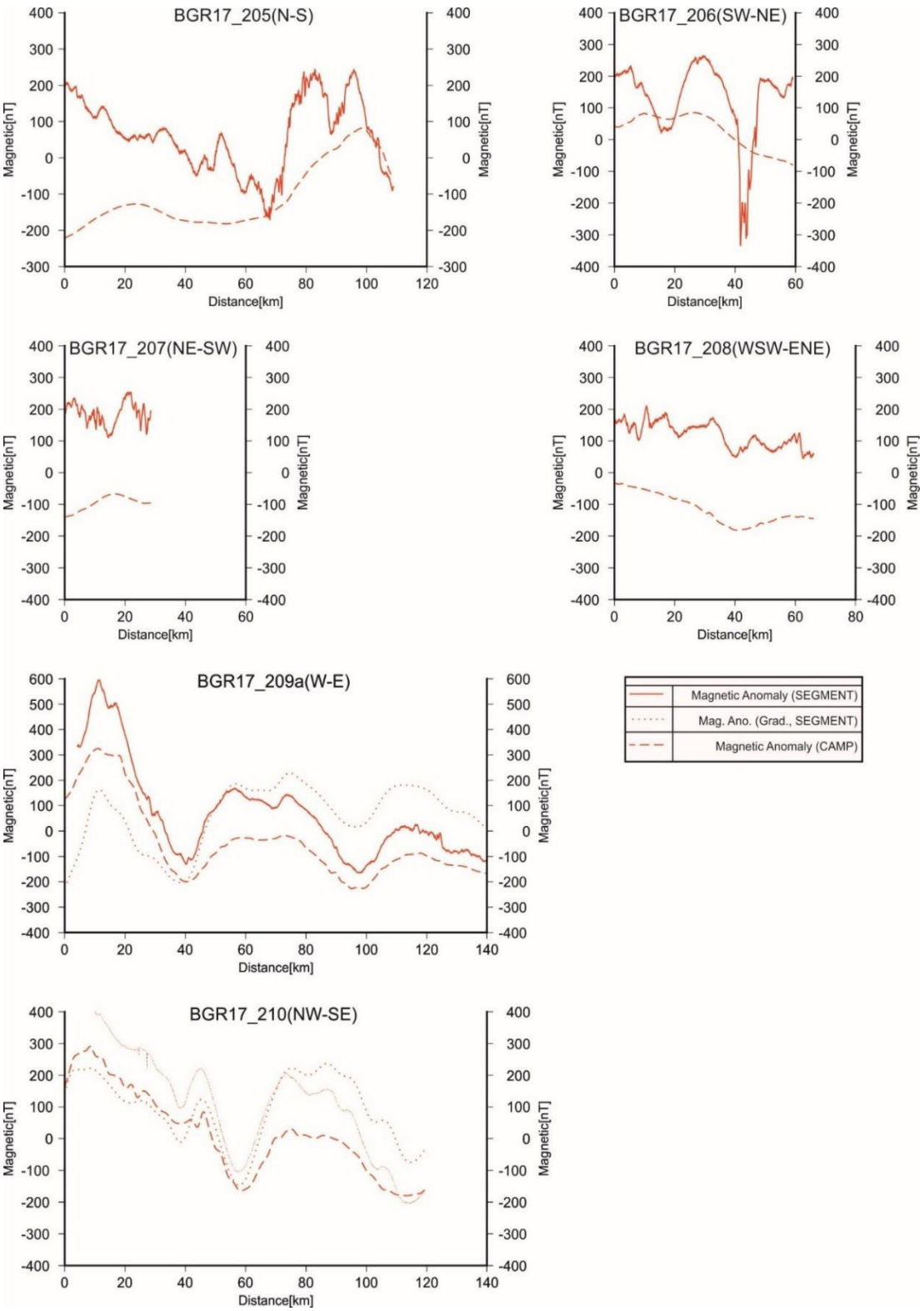

Figure 5.6 9: *Magnetic profiles 205 through 210 of cruise MSM-67 (solid lines) combined with synthetic lines from the CAMP magnetic data grid (dashed lines) and magnetic data reconstructed from gradient measurements (where available, dotted lines).*

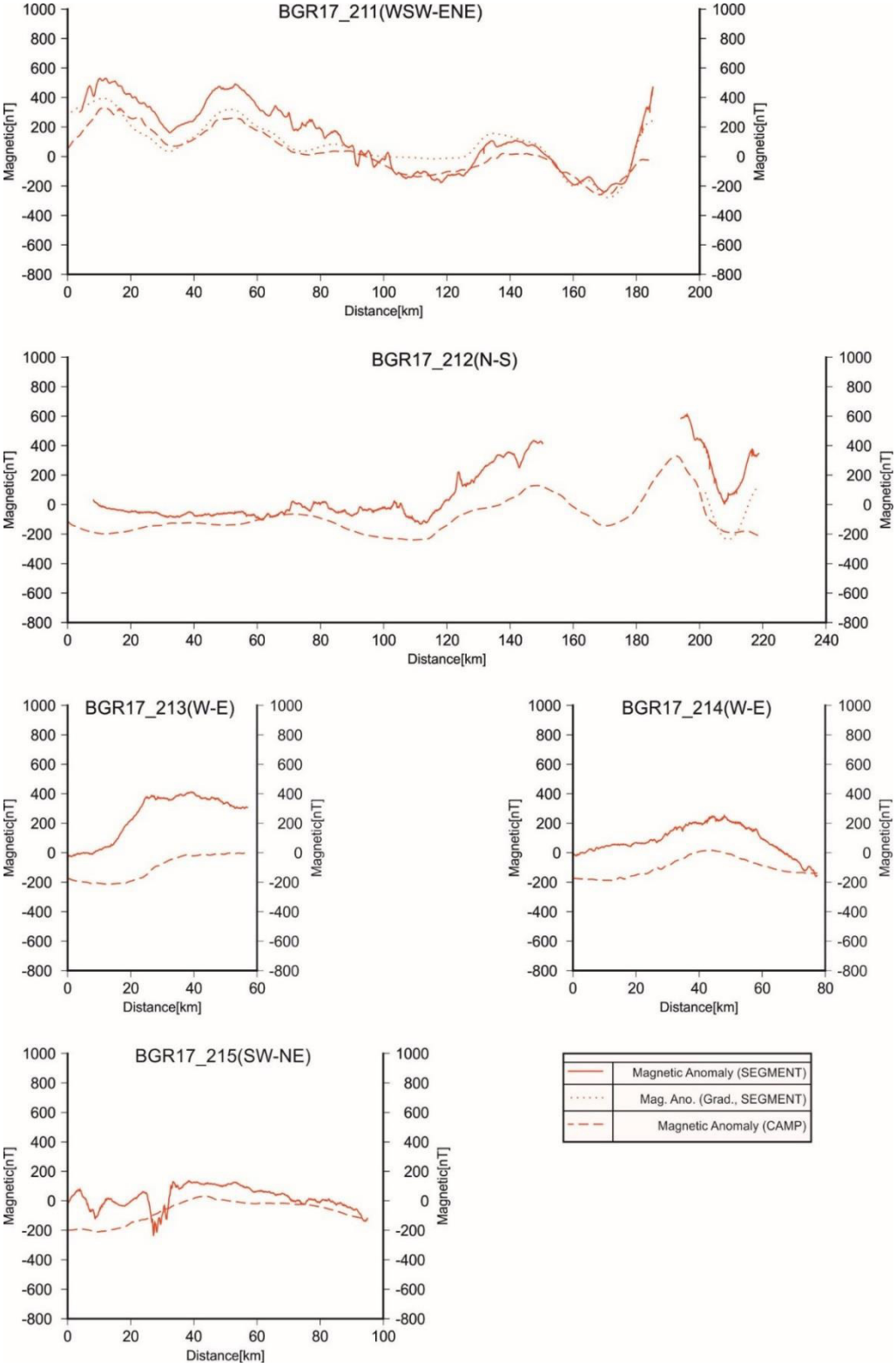

Figure 5.6 10*: Magnetic profiles 211 through 215 of cruise MSM-67 (solid lines) combined with synthetic lines from the CAMP magnetic data grid (dashed lines) and magnetic data reconstructed from gradient measurements (where available, dotted lines).*

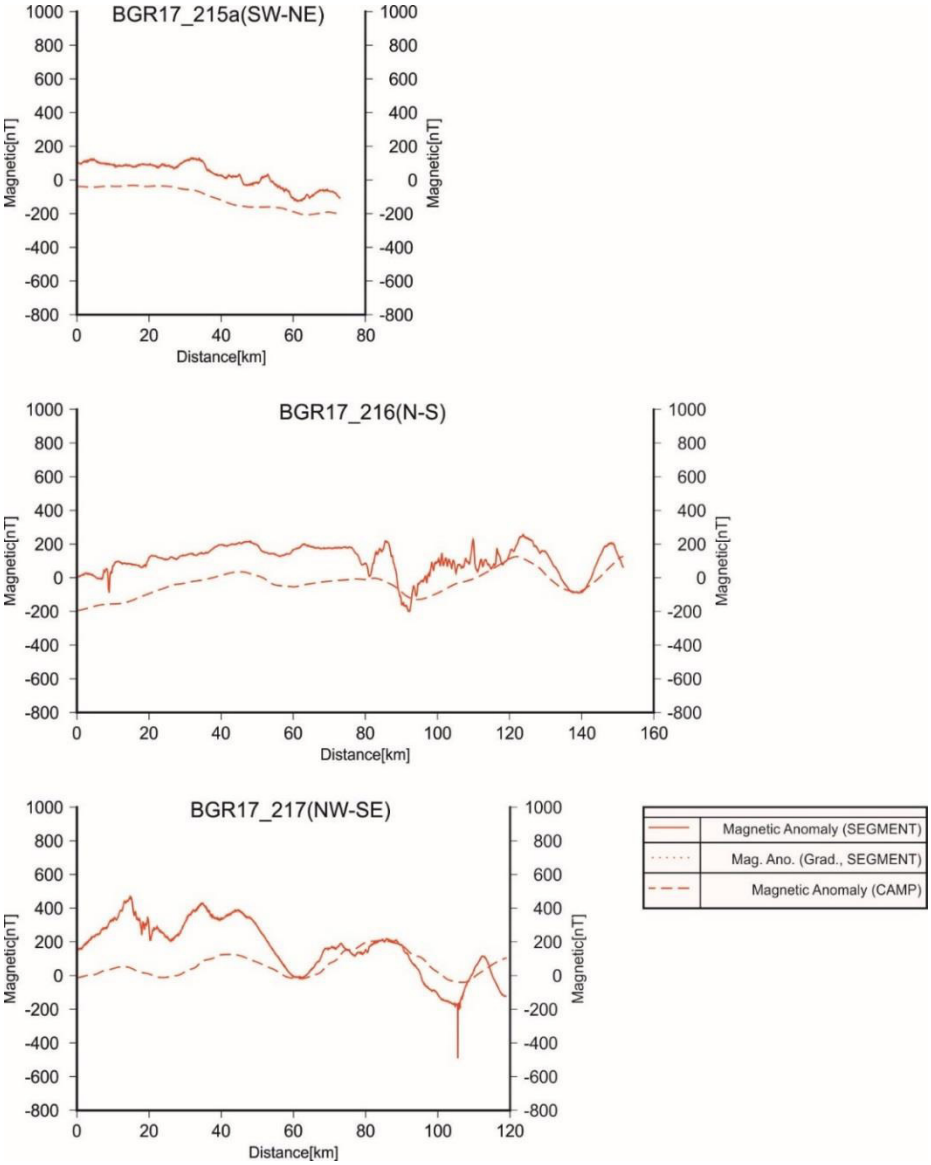

Figure 5.6 11: *Magnetic profiles 215a through 217 of cruise MSM-67 (solid lines) combined with synthetic lines from the CAMP magnetic data grid (dashed lines.)*

5.6.3 Multichannel reflection seismics

The 240 km long, N25°E striking profile BGR17-202, along the NE Greenland shelf (Figure 5.6 12) elucidates the structural configuration in the vicinity of the Jan Mayen fracture zone. A couple of incisions and valleys on the seafloor are likely due to glacial erosion, which formed when the ice sheet reached possible the shelf edge during the Last Glacial Maximum (e.g. Arndt et al., (2015)). The valleys are found in prolongation of the major fjord systems along the NE Greenland shore. Based on the seismic stratigraphic concepts of Berger and Jokat (2008), Hamann et al. (2005) and Tsikalas et al. (2005), we subdivide the underlying sedimentary succession into two units, separated by an inferred Early-Middle Miocene unconformity. These sedimentary units with comparably high frequency reflectivity are clearly distinguished from the underlying succession from which they are separated by a major unconformity. This unconformity is associated with distinct low-frequency patterns, typical for volcanic deposits. We thus interpret the unconformity as the breakup unconformity of the Norway-Greenland Sea, with an age of ~54 Ma, and the associated low-frequency patterns as expression of the flood basalt units forming the acoustic basement, a situation that is mirrored at the conjugate margin, the Vøring Plateau. So far the flood basalts are distinct only on top of elevated fault blocks and not in the grabens itself. However, this may be due to preliminary processing and conclusions from this observation may be premature.

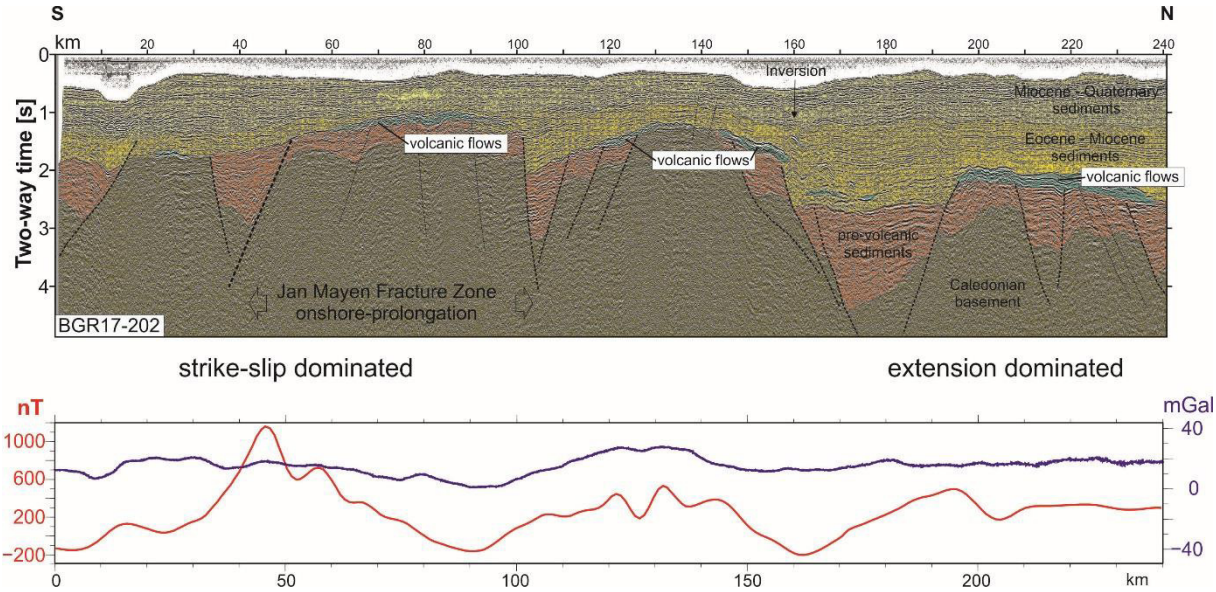

Figure 5.6 12: *Preliminary interpreted brute stack of reflection seismic line BGR17-202.*

The grabens and half-grabens below the breakup unconformity exhibit wedge-shaped layered successions of unknown age. However, from the depositional pattern, a syn-deformational infill is evident. Onshore, in the southern prolongation of the profile, the Jameson Basin is situated. This Triassic rift basin is bounded by the N-S trending Liverpool Land to the east and is filled with Paleozoic to Mesozoic sedimentary successions (Guarnieri et al., 2017). The eastern margin of the Jameson Land Basin is represented by the N-S elongated Liverpool Land high that is characterized by Caledonian basement rocks and Palaeozoic sediments. In this area, a prominent NE-SW trending escarpment, cuts through Liverpool Land (Guarnieri et al., 2017) that might reach the position of profile BGR17-202. However, the Triassic rift is typically dissected by NW-SE to WSW-ENE trending fault systems, interpreted as transfer faults accommodating the differential movement associated with NW-SE extension. Additional work

is needed before a conclusive tie to the onshore area will be possible. A difference in the infill pattern between the individual grabens is not evident so far.

The basement is reasonably imaged below the elevated fault blocks, and can be inferred in the grabens by the diminishing reflectivity. We observe a predominance of steeply dipping faults at the position, where the onshore prolongation of the Jan Mayen fracture zone is situated. The deep grabens around this structural high are possibly pull-apart graben systems. In contrast, along the northern portion of the profile, listric faulting is the dominant structural style. Surprisingly, to the north of the inferred onshore Jan Mayen fracture zone, the younger, inferred Eocene to Miocene, sediments successions are affected by faulting, while in the south these successions drape the graben structures. Expected would be the contrary, renewed faulting associated with the ?Oligocene separation of the Jan Mayen microcontinent from the East Greenland shelf, while the final rupture of the Norway-Greenland Sea took place already in the Early Eocene. It might be speculated that the onshore (East) Jan Mayen fracture zone developed in a gradual process with prograding deformation. Magnetic chrons seaward of the conjugate Vøring margin indicate a NW–SE spreading direction (N°150), but south of the West Jan Mayen fracture zone the anomalies between C23n and C21n rather suggest a N°100–120 direction (Gernigon et al., 2009). Gernigon et al. (2009) suggest that this difference explained by two regional stress directions resulting in faulting and block rotation. In any case, plate motion history and local reorganisation of plate boundaries around the Jan Mayen fracture zone are likely more complex than previously anticipated.

The major half-graben in the center of the profile exhibits additionally a mild inversion phase at about the time the inferred Early-Middle Miocene unconformity developed. In the seismic data the inversion is indicated by a distinct fold in the strata overlying the half-graben. Along that fault sill intrusions are distinct.

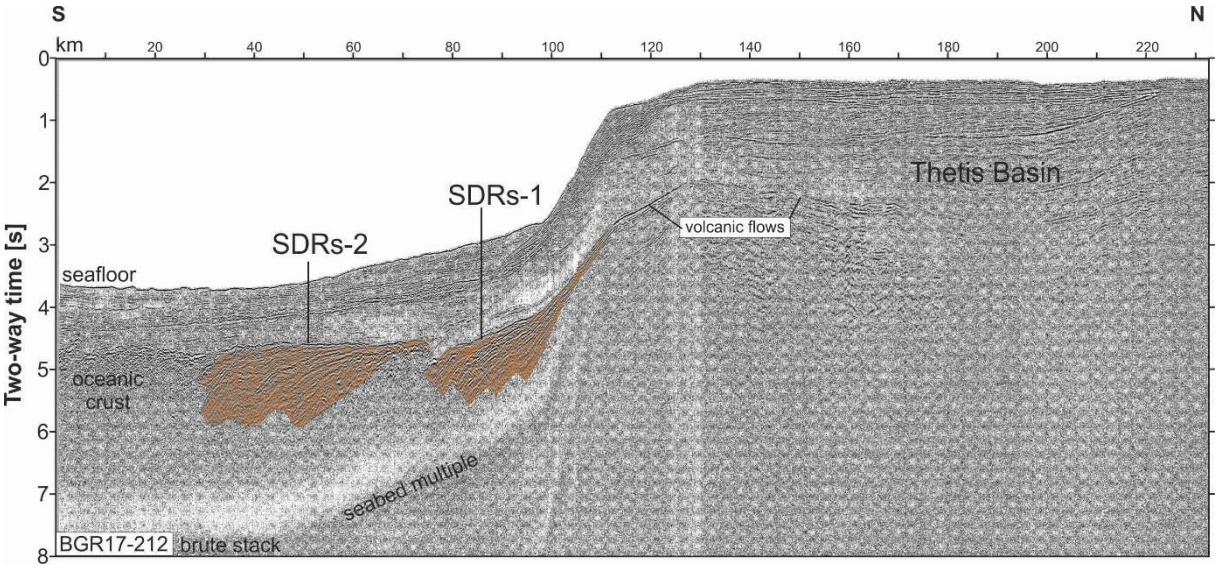

Figure 5.6 13: *Preliminary interpretation of seaward dipping reflectors (SDRs) at the brute stack of reflection seismic line BGR17-212.*

An example of a reflection seismic imaging the continental slope is provided in Figure 5.6 13. The brute-stack of line BGR17-212, running in an S-N direction from the deep sea onto the shelf shows distinct seaward dipping reflectors (SDRs). These are found at the continental slope, merely at the position predicted from the literature (Abdelmalak et al., 2016; Geissler et

al., 2016; Hinz et al., 1987). We interpret two distinct and separated SDR wedges. So far the inner wedges have often been shown with a question mark, as these are frequently masked by seabed multiples. This example highlights that the SDRs, typically interpreted as thick lava flow units, the expression of abundant volcanism during breakup can be conclusively imaged. The two separated, and consecutive wedges may be interpreted sensu Planke et al (2000) as transition from subaerial emplacement to deposition under shallow or deep marine conditions. Only the inner SDRs are thought to overly (partly) continental crust and thus it is essential to clearly identify both types, inner and out SDRs, in order to assess the position of the COT. The distinct difference in subsidence between the two wedges may support the idea that the inner wedge covers partly continental basement. Interestingly, along this profile, the thickness of the lava flows increases with time. This might be an indication for increased volcanism in the early post-breakup phase.

5.6.4 Wide-angle reflection and refraction seismics

The data are of generally high quality. On line BGR17-2R1 where the smaller air gun array was used, the maximum offsets to which seismic energy can be observed range between 60 km and 80 km. This is sufficient to map the crust and uppermost mantle and in particular the record sections within the oceanic crust (Figure 5.6 14-14) show clear Moho reflections P_mP and mantle refractions P_n. The stations located on the Jan Mayen microcontinent itself have a lower signal-to-noise ratio than the ones in oceanic crust. There are numerous examples of clear converted shear waves on the horizontal components, best again in the oceanic domain.
For line BGR17-2R2 the larger 4840 cubic inches array was used and the maximum offsets increased to >200 km. Figure 5.6 15 shows an example with a clear P_mP and P_n phase. Given the shallow water of 200-550 m along the line, there are a number of reverberations following the first arrival but the relevant seismic phases can be easily identified.

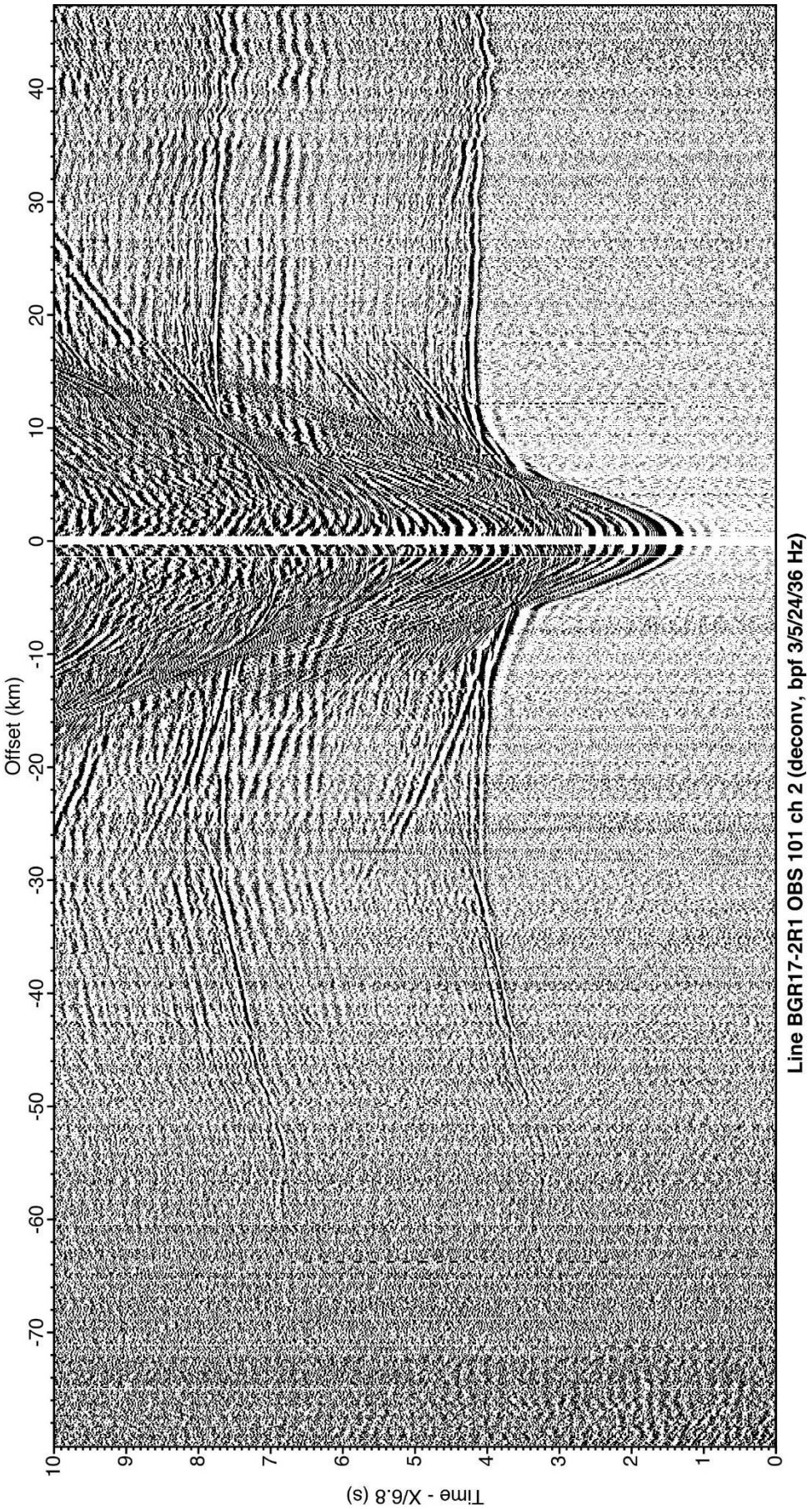

Figure 5.6 14: *Record section of the vertical geophone of OBS 101 (Sercel MicrOBS_Plus) on line BGR17-2R1. The record is displayed with a reduction velocity of 6.8 km/s.*

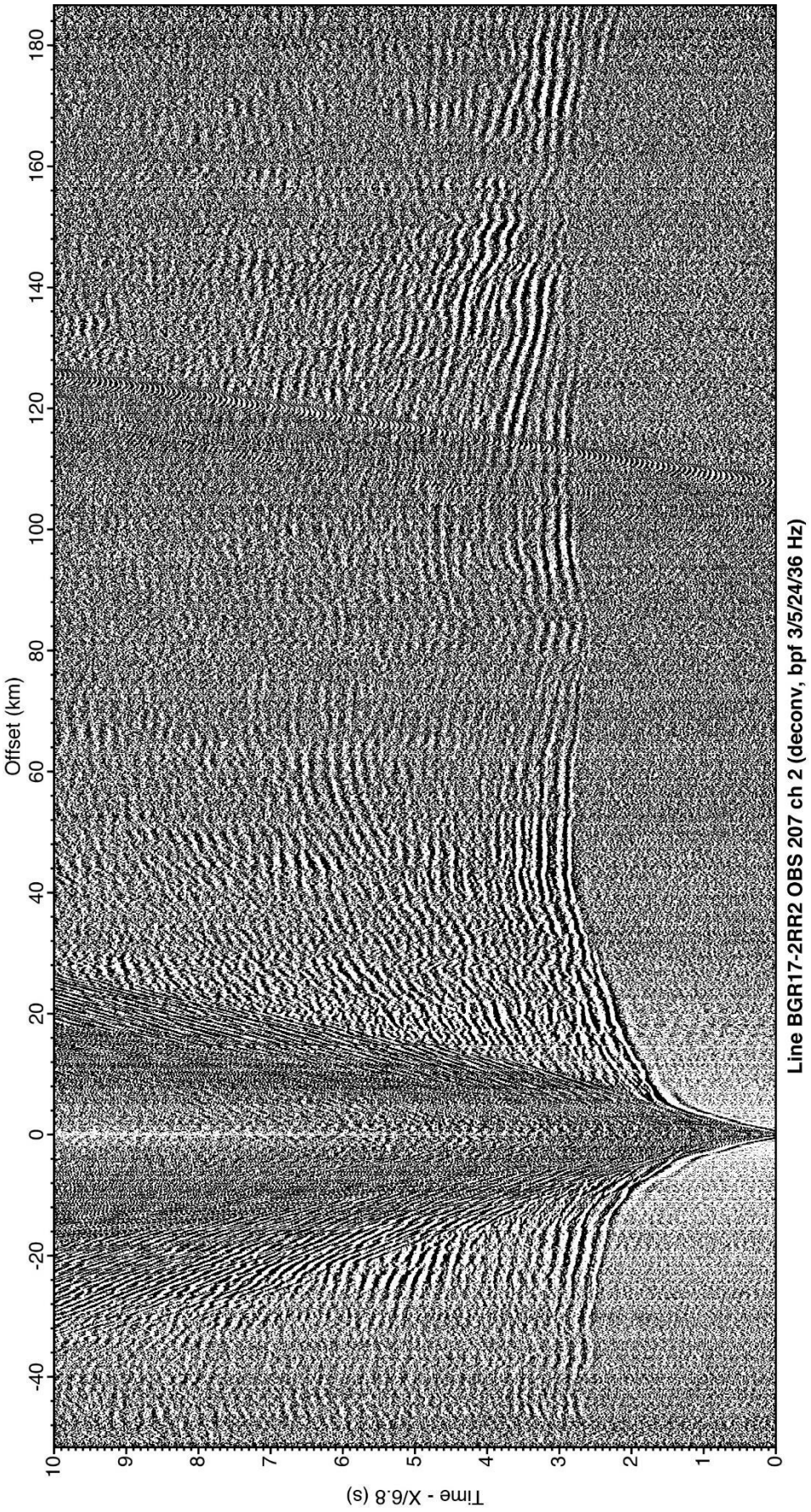

Figure 5.6 15: *Record section of the vertical geophone of OBS 207 (Sercel MicrOBS_Plus) on line BGR17-2R2. The record is displayed with a reduction velocity of 6.8 km/s.*

5.7 References

Abdelmalak, M.M., Planke, S., Faleide, J.I., Jerram, D.A., Zastrozhnov, D., Eide, S., and Myklebust, R., 2016, The development of volcanic sequences at rifted margins: New insights from the structure and morphology of the Vøring Escarpment, mid-Norwegian Margin: Journal of Geophysical Research: Solid Earth, v. 121, p. 5212-5236.

Andersen, O. B., P. Knudsen and P. Berry, 2010, The DNSC08GRA global marine gravity field from double retracked satellite altimetry, Journal of Geodesy, Volume 84, Number 3, DOI: 10.1007/s00190-009-0355-9.

Arndt, J.E., Jokat, W., Dorschel, B., Myklebust, R., Dowdeswell, J.A., and Evans, J., 2015, A new bathymetry of the Northeast Greenland continental shelf: constraints on glacial and other processe: Geochemistry, Geophysics, Geosystems, p. n/a-n/a.

Bartels, J., 1957, The geomagnetic measures for the time-variations of solar corpuscular radiation, described for use in correlation studies in other geophysical fields: Ann. Intern. Geophys., v. 4, p. 227-236.

Berger, D., and Jokat, W., 2008, A seismic study along the East Greenland margin from 72°N to 77°N: Geophysical Journal International, v. 174, p. 733-748.

Berglar, K., Franke, D., Lutz, R., Schreckenberger, B., and Damm, V., 2016, Initial opening of the Eurasian Basin, Arctic Ocean: Frontiers in Earth Science, v. 4.

Berndt, C., Mjelde, R., Planke, S., Shimamura, H., and Faleide, J.I., 2001, Controls on the tectono-magmatic evolution of a volcanic transform margin: the Vøring Transform Margin, NE Atlantic: Marine Geophysical Researches, v. 22, p. 133-152.

Berndt, C., Skogly, O.P., Planke, S., Eldholm, O., and Mjelde, R., 2000, High-velocity breakup-related sills in the Vøring Basin, off Norway: Journal of Geophysical Research, v. 105, p. 28443-28454.

Blischke, A., Gaina, C., Hopper, J.R., Péron-Pinvidic, G., Brandsdóttir, B., Guarnieri, P., Erlendsson, Ö., and Gunnarsson, K., 2016, The Jan Mayen microcontinent: an update of its architecture, structural development and role during the transition from the Ægir Ridge to the mid-oceanic Kolbeinsey Ridge: Geological Society, London, Special Publications, v. 447.

Breivik, A.J., Faleide, J.I., and Mjelde, R., 2008, Neogene magmatism northeast of the Aegir and Kolbeinsey ridges, NE Atlantic: Spreading ridge–mantle plume interaction?: Geochemistry Geophysics Geosystems, v. 9, p. 1-15.

Breivik, A.J., Faleide, J.I., Mjelde, R., and Flueh, E.R., 2009, Magma productivity and early seafloor spreading rate correlation on the northern Vøring Margin, Norway -- Constraints on mantle melting: Tectonophysics, v. 468, p. 206-223.

Breivik, A.J., Mjelde, R., Faleide, J.I., and Murai, Y., 2006, Rates of continental breakup magmatism and seafloor spreading in the Norway Basin–Iceland plume interaction: Journal of Geophysical Research, v. 111, p. B07102.

Breivik, A.J., Mjelde, R., Faleide, J.I., and Murai, Y., 2012, The eastern Jan Mayen microcontinent volcanic margin: Geophys. J. Int., v. 188, p. 798-818.

Brozena, J.M., Childers, V.A., Lawver, L.A., Gahagan, L.M., Forsberg, R., Faleide, J.I., and Eldholm, O., 2003, New aerogeophysical study of the Eurasia Basin and Lomonosov Ridge: Implications for basin development: Geology, v. 31, p. 825-828.

Christiansen, F.G., 2011, Chapter 42 Greenland petroleum exploration: history, breakthroughs in understanding and future challenges, *in* Spencer, A.M., Embry, A.F., Gautier, D.L., Stoupakova, A.V., and Sørensen, K., eds., Arctic Petroleum Geology. Geological Society, London, Memoirs, Volume 35: London, p. 647-661.

Clift, P.D., 1997, Temperature anomalies under the Northeast Atlantic rifted volcanic margins: Earth and Planetary Science Letters, v. 146, p. 195-211.

Courtillot, V., Jaupart, C., Manighetti, I., Tapponnier, P., and Besse, J., 1999, On causal links between flood basalts and continental breakup: Earth and Planetary Science Letters, v. 166, p. 177-195.

Dalland, A., Worsley, D., and Ofstad, K., 1988, A lithostratigraphic scheme for the Mesozoic and Cenozoic succession offshore Norway north of 62 N, NPD-Bull., Volume 4, p. 67-84.

Doré, A.G., and Lundin, E.R., 2005, Challenges and Controversies in Exploration of the Northeast Atlantic Margin, Petroleum Systems of Divergent Continental Margin Basins: 25th Annual Gulf Coast Section SEPM Foundation, p. 18-21.

Doré, A.G., Lundin, E.R., Jensen, L.N., Birkeland, Ø., Eliassen, P.E., and Fichler, C., 1999, Principal tectonic events in the evolution of the northwest European Atlantic margin: Geological Society, London, Petroleum Geology Conference series, v. 5, p. 41-61.

Eldholm, O., 1991, Magmatic tectonic evolution of a volcanic rifted margin: Marine Geology, v. 102, p. 43-61.

Eldholm, O., Faleide, J.I., and Myhre, A.M., 1987, Continent-ocean transition at the western Barents Sea/Svalbard continental margin: Geology, v. 15, p. 1118-1122.

Eldholm, O., Thiede, J., and Party, O.L.S., 1986, Formation of the Norwegian Sea: Nature, v. 319, p. 360-361.

Eldholm, O., Thiede, J., and Taylor, E., 1989, Evolution of the Vøring Volcanic Margin: Proceedings of the Ocean Drilling Program, Scientific Results, v. 104, p. 1033-1065.

Engels, M., Barckhausen, U., and Gee, J.S., 2008, A new towed vector magnetometer: methods and results from a Central Pacific cruise: Geophys. J. Int., v. 172, p. 115-129.

Faleide, J.I., Gudlaugsson, S.T., Eldholm, O., Myhre, A.M., and Jackson, H.R., 1991, Deep seismic transects across the sheared western Barents Sea-Svalbard continental margin: Tectonophysics, v. 189, p. 73-89.

Faleide, J.I., Tsikalas, F., Breivik, A.J., Mjelde, R., Ritzmann, O., Engen, Ø., Wilson, J., and Eldholm, O., 2008, Structure and evolution of the continental margin off Norway and the Barents Sea: Episodes, v. 31 p. 82-91.

Flueh, E.R., and Bialas, J., 1999, Ocean bottom seismometers: Sea Technology, v. 40, p. 41-46.

Flueh, E.R., and Bialas, J.A., 1996, Digital, high data capacity ocean bottom recorder for seismic investigations: Int. Underwater Systems Design, v. 18, p. 18-20.

Foulger, G.R., 2007, The "Plate" model for the genesis of melting anomalies, *in* Foulger, G.R., and Jurdy, D.M., eds., Plates, Plumes, and Planetary Processes GSA Special Paper 430, GSA, p. 1-25.

Franke, D., 2013, Rifting, lithosphere breakup and volcanism: Comparison of magma-poor and volcanic rifted margins: Marine and Petroleum Geology, v. 43, p. 63-87.

Franke, D., Barckhausen, U., Baristeas, N., Engels, M., Ladage, S., Lutz, R., Montano, J., Pellejera, N., Ramos, E.G., and Schnabel, M., 2011, The continent-ocean transition at the southeastern margin of the South China Sea: Marine and Petroleum Geology, v. 28, p. 1187-1204.

Franke, D., Neben, S., Ladage, S., Schreckenberger, B., and Hinz, K., 2007, Margin segmentation and volcano-tectonic architecture along the volcanic margin off Argentina/Uruguay, South Atlantic: Marine Geology, v. 244, p. 46-67.

Gaina, C., Gernigon, L., and Ball, P., 2009, Palaeocene–Recent plate boundaries in the NE Atlantic and the formation of the Jan Mayen microcontinent: Journal of the Geological Society, v. 166, p. 601-616.

Gaina, C., Nasuti, A., Kimbell, G.S., and Blischke, A., 2017, Break-up and seafloor spreading domains in the NE Atlantic: Geological Society, London, Special Publications, v. 447.

Gaina, C., Roest, W.R., and Muller, R.D., 2002, Late Cretaceous-Cenozoic deformation of northeast Asia: Earth and Planetary Science Letters, v. 197, p. 273-286.

Gaina, C., Werner, S. C., Saltus, R., and Maus, S., 2011, Circum-Arctic mapping project: new magnetic and gravity anomaly maps of the Arctic. Geological Society, London, Memoirs, 35(1), 39–48. Geissler, W.H., Gaina, C., Hopper, J.R., Funck, T., Blischke, A., Arting, U., Horni, J.Á., Péron-Pinvidic, G., and Abdelmalak, M.M., 2016, Seismic volcanostratigraphy of the NE Greenland continental margin: Geological Society, London, Special Publications, v. 447.

Gernigon, L., Gaina, C., Olesen, O., Ball, P.J., Péron-Pinvidic, G., and Yamasaki, T., 2012, The Norway Basin revisited: From continental breakup to spreading ridge extinction: Marine and Petroleum Geology, v. 35, p. 1-19.

Gernigon, L., Lucazeau, F., Brigaud, F., Ringenbach, J.-C., Planke, S., and Le Gall, B., 2006, A moderate melting model for the Voring margin (Norway) based on structural observations and a thermo-kinematical modelling: Implication for the meaning of the lower crustal bodies: Tectonophysics, v. 412, p. 255-278.

Gernigon, L., Olesen, O., Ebbing, J., Wienecke, S., Gaina, C., Mogaard, J.O., Sand, M., and Myklebust, R., 2009, Geophysical insights and early spreading history in the vicinity of the Jan Mayen Fracture Zone, Norwegian–Greenland Sea: Tectonophysics, v. 468, p. 185-205.

Granath, J.W., Whittaker, R.C., Singh, V., Bird, D.E., G., M., and Dinkelman, 2010, Full crustal seismic imaging in northeast Greenland: First Break, v. 28, p. 79-83.

Grantz, A., Scott, R.A., Drachev, S.S., Moore, T.E., and Valin, Z.C., 2011, Chapter 2 Sedimentary successions of the Arctic Region (58–64° to 90°N) that may be prospective for hydrocarbons: Geological Society, London, Memoirs, v. 35, p. 17-37.

Greenhalgh, E.E., and Kusznir, N.J., 2007, Evidence for thin oceanic crust on the extinct Aegir Ridge, Norwegian Basin, NE Atlantic derived from satellite gravity inversion: Geophysical Research Letters, v. 34, p. 1-5.

Guarnieri, P., Brethes, A., and Rasmussen, T.M., 2017, Geometry and kinematics of the Triassic Rift basin in Jameson Land (East Greenland): Tectonics, v. 36, p. 602-614.

Gudlaugsson, S.T., Faleide, J.I., Johansen, S.E., and Breivik, A.J., 1998, Late Palaeozoic structural development of the South-western Barents Sea: Marine and Petroleum Geology, v. 15, p. 73-102.

Hamann, N.E., Whittaker, R.C., and Stemmerik, L., 2005, Geological development of the Northeast Greenland Shelf, *in* Doré, A.G., and Vining, B.A., eds., Petroleum Geology: North-West Europe and Global Perspectives - Proceedings of the 6th Petroleum Geology Conference: London, Geological Society, p. 887-902.

Hermann, T., and Jokat, W., 2013, Crustal structures of the Boreas Basin and the Knipovich Ridge, North Atlantic: Geophysical Journal International.

Hinz, K., Meyer, H., and Miller, H., 1991, North-east Greenland Shelf north of 79°N: results of a reflection seismic experiment in sea ice: Marine and Petroleum Geology, v. 8, p. 461-467.

Hinz, K., Mutter, J.C., and Zehnder, C.M., 1987, Symmetric conjugation of continent-ocean boundary structures along the Norwegian and East Greenland Margins: Marine and Petroleum Geology, v. 4, p. 166-187.

Hopper, J.R., Funck, T., Stoker, M., Arting, U., Peron-Pinvidic, G., Doornenbal, H., and Gaina, C., eds., , 2016, Tectonostratigraphic atlas of the North-East Atlantic region: Copenhagen, Denmark, Geological Survey of Denmark and Greenland, p. 338.

Isezaki, N., 1986, A new shipboard three-component magnetometer: Geophysics, v. 51, p. 1992-1998.

Jakobsson et al., 2012, The International Bathymetric Chart of the Arctic Ocean (IBCAO) Version 3.0: Geophysical Research Letters, v. 39, p. L12609.

Kodaira, S., Mjelde, R., Gunnarsson, K., Shiobara, H., and Shimamura, H., 1998, Structure of the Jan Mayen microcontinent and implications for its evolution: Geophysical Journal International, v. 132, p. 383-400.

König, M., 2006, Processing of shipborne magnetometer data and revision of the timing and geometry of the Mesozoic break-up of Gondwana, Berichte zur Polar- und Meeresforschung, 525, 137 p.

Koopmann, H., Franke, D., Schreckenberger, B., Schulz, H., Hartwig, A., Stollhofen, H., and di Primio, R., 2014, Segmentation and volcano-tectonic characteristics along the SW African continental margin, South Atlantic, as derived from multichannel seismic and potential field data: Marine and Petroleum Geology, v. 50, p. 22-39.

Korenaga, J., 1995, Comprehensive analysis of marine magnetic vector anomalies, J. Geophys. Res., 100 (B1), 365-378.

Le Breton, E., Cobbold, P.R., Dauteuil, O., and Lewis, G., 2012, Variations in amount and direction of seafloor spreading along the northeast Atlantic Ocean and resulting deformation of the continental margin of northwest Europe: Tectonics, v. 31, p. TC5006.

Mathiesen, A., Bidstrup, T., and Christiansen, F.G., 2000, Denudation and uplift history of the Jameson Land basin, East Greenland—constrained from maturity and apatite fission track data: Global and Planetary Change, v. 24, p. 275-301.

Meyer, R., van Wijk, J.W., and Gernigon, L., 2007, North Atlantic Igneous Province: A review of models for its formation, *in* Foulger, G.R., and Jurdy, D.M., eds., Plates, Plumes, and Planetary Processes, Volume 430, Geological Society of America Special Paper, p. 525-552.

Misra, A.A., Sinha, N., and Mukherjee, S., 2015, Repeat ridge jumps and microcontinent separation: insights from NE Arabian Sea: Marine and Petroleum Geology, v. 59, p. 406-428.

Mjelde, R., Raum, T., Kandilarov, A., Murai, Y., and Takanami, T., 2009, Crustal structure and evolution of the outer Møre Margin, NE Atlantic: Tectonophysics, v. 468, p. 224-243.

Mjelde, R., Raum, T., Murai, Y., and Takanami, T., 2007, Continent-ocean-transitions: Review, and a new tectono-magmatic model of the Voring Plateau, NE Atlantic: Journal of Geodynamics, v. 43, p. 374-392.

Mjelde, R., Raum, T., Myhren, B., Shimamura, H., Murai, Y., Takanami, T., Karpuz, R., and Næss, U., 2005, Continent-ocean transition on the Vøring Plateau, NE Atlantic, derived from densely sampled ocean bottom seismometer data: Journal of Geophysical Research, v. 110, p. B05101.

Morelli, C., 1974, The International Standardization Net 1971. Intern. Ass. Geodesy Spec. Public. 4, 194.

Mosar, J., Eide, E.A., Osmundsen, P.T., Sommaruga, A., and Torsvik, T.H., 2002, Greenland – Norway separation: A geodynamic model for the North Atlantic: Norwegian Journal of Geology, v. 82, p. 281-298.

Mutter, J.C., and Zehnder, C.M., 1988, Deep crustal and magmatic processes: the inception of seafloor spreading in the Norwegian-Greenland Sea: Geological Society London Special Publications, v. 39, p. 35-48.

Olesen, O., Ebbing, J., Lundin, E., Mauring, E., Skilbrei, J.R., Torsvik, T.H., Hansen, E.K., Henningsen, T., Midbøe, P., and Sand, M., 2007, An improved tectonic model for the Eocene opening of the Norwegian-Greenland Sea: Use of modern magnetic data: Marine and Petroleum Geology, v. 24, p. 53-66.

Parker, R.L. and O'Brien, M.S., 1997, Spectral analysis of vector magnetic field profiles, J. Geophys. Res., 102 (B11), 24815-24824.

Peron-Pinvidic, G., Gernigon, L., Gaina, C., and Ball, P., 2012, Insights from the Jan Mayen system in the Norwegian–Greenland sea—I. Mapping of a microcontinent: Geophysical Journal International, v. 191, p. 385-412.

Planke, S., 1994, Geophysical response of flood basalts from analysis of wire line logs: Ocean Drilling Program Site 642, Vøring volcanic margin: Journal of Geophysical Research, v. 99, p. 9279–9296.

Planke, S., Symonds, P.A., Alvestad, E., and Skogseid, J., 2000, Seismic volcanostratigraphy of large-volume basaltic extrusive complexes on rifted margins: J. Geophys. Res., v. 105, p. 19,335–19,351.

Price, S., Brodie, J., Whitham, A., and Kent, R., 1997, Mid-Tertiary rifting and magmatism in the Traill Ø region, East Greenland: Journal of the Geological Society, v. 154, p. 419-434.

Schlindwein, V., and Jokat, W., 1999, Structure and evolution of the continental crust of northern east Greenland from integrated geophysical studies: Journal of Geophysical Research B: Solid Earth, v. 104, p. 15227-15245.

Schmidt-Aursch, M.C., and Jokat, W., 2005, The crustal structure of central East Greenland—I: From the Caledonian orogen to the Tertiary igneous province: Geophysical Journal International, v. 160, p. 736-752.

Scott, R.A., 2000, Mesozoic-Cenozoic evolution of East Greenland: Implications of a reinterpreted continent-ocean boundary location.: Polarforschung v. 68, p. 83-91.

Skogseid, J., and Eldholm, O., 1989, Vøring plateau continental margin: seismic interpretation, stratigraphy and vertical movements: Proceedings of the Ocean Drilling Program, Scientific Results, v. 104, p. 993- 1030.

Storey, M., Duncan, R.A., and Tegner, C., 2007, Timing and duration of volcanism in the North Atlantic Igneous Province: Implications for geodynamics and links to the Iceland hotspot: Chemical Geology, v. 241, p. 264-281.

Talwani, M., and Eldholm, O., 1977, Evolution of the Norwegian-Greenland Sea: GSA Bulletin, v. 88, p. 969-999.

Tegner, C., Brooks, C.K., Duncan, R.A., Heister, L.E., and Bernstein, S., 2008, 40Ar–39Ar ages of intrusions in East Greenland: Rift-to-drift transition over the Iceland hotspot: Lithos, v. 101, p. 480-500.

Tsikalas, F., Eldholm, O., and Faleide, J., 2002, Early Eocene sea floor spreading and continent-ocean boundary between Jan Mayen and Senja fracture zones in the Norwegian-Greenland Sea: Marine Geophysical Researches, v. 23, p. 247-270.

Tsikalas, F., Faleide, J.I., Eldholm, O., and Wilson, J., 2005, Late Mesozoic–Cenozoic structural and stratigraphic correlations between the conjugate mid-Norway and NE Greenland continental margins, *in* Doré, A.G., and Vining, B.A., eds., Petroleum Geology: North-West Europe and

Global Perspectives, Volume 6: London, Geological Society, London, Petroleum Geology Conference series, p. 785-801.

van Wijk, J.W., van der Meer, R., and Cloetingh, S.A.P.L., 2004, Crustal thickening in an extensional regime: application to the mid-Norwegian Voring margin: Tectonophysics, v. 387, p. 217-228.

Voss, M., and Jokat, W., 2007, Continent-ocean transition and voluminous magmatic underplating derived from P-wave velocity modelling of the East Greenland continental margin: Geophysical Journal International, v. 170, p. 580-604.

Voss, M., Schmidt-Aursch, M.C., and Jokat, W., 2009, Variations in magmatic processes along the East Greenland volcanic margin: Geophysical Journal International, v. 177, p. 755-782.

Whitmarsh, R.B., and Miles, P.R., 1995, Models of the development of the West Iberia rifted continental margin at 40°30'N deduced from surface and deep-tow magnetic anomalies: J. Geophys. Res., v. 100, p. 3789-3806.

Ziegler, P.A., van Wees, J.-D., and Cloetingh, S., 1998, Mechanical controls on collision-related compressional intraplate deformation: Tectonophysics, v. 300, p. 103-129.

6 Data storage and access

All raw data acquired during the cruise will be copied and archived onboard using external drives. After the cruise, raw data will be synchronized with the professional long term archives of BGR (two separate mirrored data centers). Metadata will be published in the web accessible database systems PANGAEA (WDC-MARE) and the European database Geo-Seas. This allows users to contact the responsible scientists. The period of restricted data access will expire latest 2022. Bathymetric data will be delivered to the BSH data centre and to GEOMAR.

7 Survey map and list of profiles

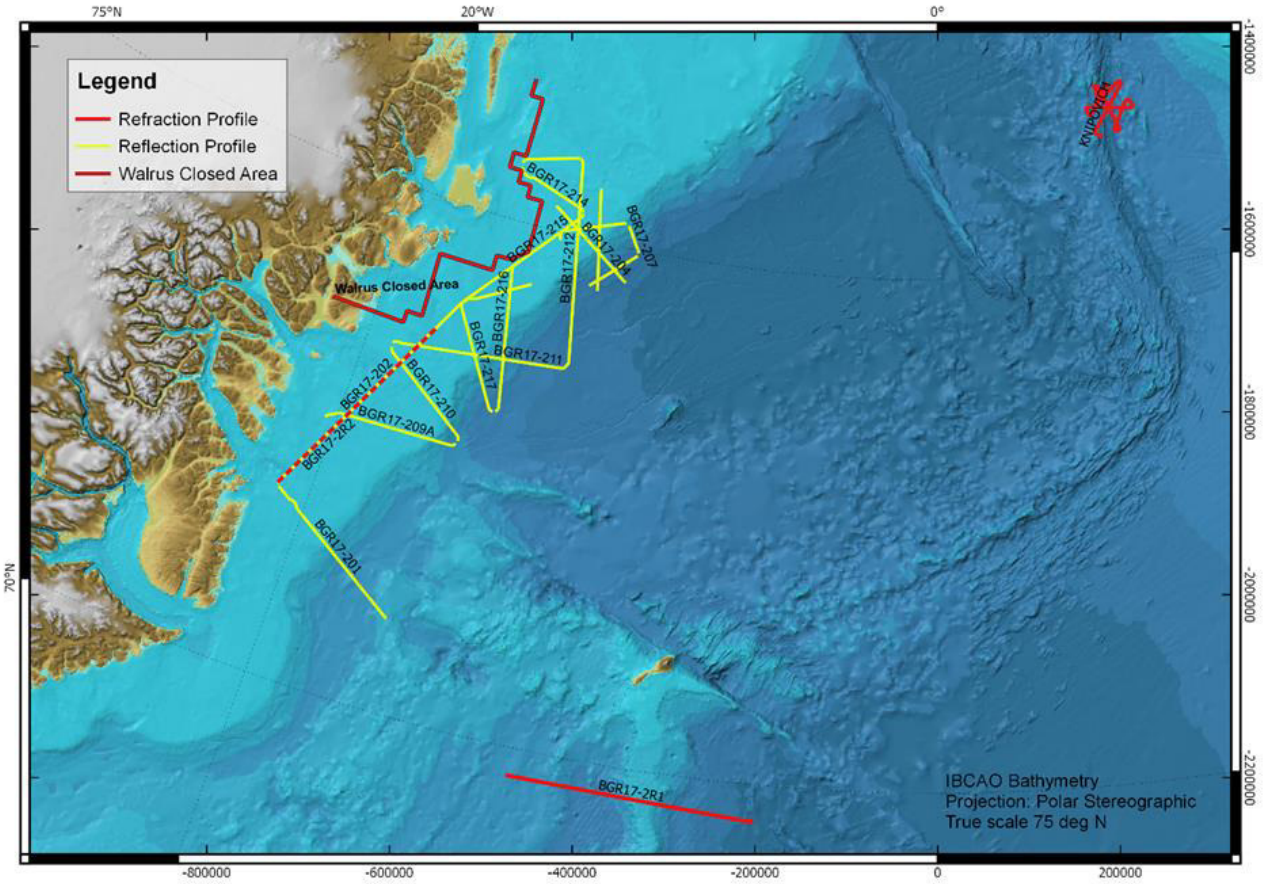

Figure 7 –1: Survey lines acquired during cruise MSM67

Table 7 - 1: *List of profiles acquired during MSM67.*

line	SEG-D filenb.	shotpoint P1 online	date	time (UTC)	latitude	longitude	course	length (km)
BGR17-2R1		1	2017.09.03	01:47:00	69.64849	-5.20281		
BGR17-2R1		2280	2017.09.04	12:02:30	69.73456	-12.05478	275°	264.25
BGR17-201-1	1	988	2017.09.10	08:30:07	70.88262	-16.53025		
BGR17-201-1	474	1491	2017.09.10	11:04:57	71.02206	-17.07468	308°	25.08
BGR17-200	1012	1011	2017.09.10	16:02:49	71.21214	-16.65331		
BGR17-200	1466	1464	2017.09.10	18:19:24	71.01876	-16.84441	198°	22.56
BGR17-201-2	1	1418	2017.09.10	18:53:47	71.00605	-16.98620		
BGR17-201-2	3395	4811	2017.09.11	12:04:40	71.82381	-21.00727	304°	168.85
BGR17-202	1	967	2017.09.11	12:08:27	71.82929	-21.01138		
BGR17-202	5604	6570	2017.09.12	16:29:54	74.07893	-17.20521	25°	278.86
BGR17-203		912	2017.09.12	16:33:39	74.08277	-17.18937		
BGR17-203	3338	4263	2017.09.13	09:52:50	74.81814	-12.30709	58°	166.72
BGR17-204	1	530	2017.09.13	17:53:55	74.67181	-11.68061		
BGR17-204	2201	2729	2017.09.14	05:11:41	75.23440	-14.79475	306°	109.41
BGR17-205	1	967	2017.09.15	01:41:22	75.49726	-13.30079		
BGR17-205	2260	3225	2017.09.15	13:39:59	74.49924	-12.65787	170°	112.41
BGR17-206	1	892	2017.09.15	14:38:34	74.51359	-12.93542		
BGR17-206	1353	2243	2017.09.15	21:42:52	74.96141	-11.38056	42°	67.4
BGR17-207	1	965	2017.09.15	21:47:41	74.96835	-11.38082		
BGR17-207	687	1651	2017.09.16	01:21:11	75.22595	-12.03298	327°	34.15
BGR17-208	1	971	2017.09.16	01:26:16	75.22841	-12.06087		
BGR17-208	1435	2404	2017.09.16	08:43:16	74.99802	-14.39240	250°	71.3
BGR17-209	1	971	2017.09.16	08:47:22	74.99256	-14.40240		
BGR17-209	117	1086	2017.09.16	09:25:07	74.93986	-14.37851	173°	5.9
BGR17-AWI		1	2017.09.19	07:12:00	76.81460	7.32797		
BGR17-AWI		2105	2017.09.20	18:16:00	76.37062	6.56840		
BGR17-2R2		1	2017.09.22	20:43:00	71.85406	-21.01365		
BGR17-2R2		1708	2017.09.24	01:10:00	73.77147	-17.79183	25°	237.76
BGR17-209A	1	567	2017.09.25	21:26:50	72.60235	-20.35198		
BGR17-209A	2856	3422	2017.09.26	12:08:31	72.72796	-16.07202	90°	142.33
BGR17-210	1	994	2017.09.26	12:48:52	72.78384	-16.00379		
BGR17-210	2458	3450	2017.09.27	01:15:15	73.43823	-19.05018	308°	122.26
BGR17-211	1	935	2017.09.27	02:04:51	73.50475	-19.04737		
BGR17-211	3779	4712	2017.09.27	21:07:08	73.73337	-13.10262	79°	187.91
BGR17-212	1	924	2017.09.27	21:10:44	73.73802	-13.09321		
BGR17-212	4543	5465	2017.09.28	20:16:32	75.74468	-14.36423	351°	226
BGR17-213	1	979	2017.09.28	20:22:06	75.74809	-14.39428		
BGR17-213	1249	2226	2017.09.29	02:54:53	75.57556	-16.53939	253°	62.05
BGR17-214	1	1104	2017.09.29	03:44:04	75.50603	-16.50066		
BGR17-214	1623	2721	2017.09.29	12:08:54	75.25893	-13.80214	109°	80.48
BGR17-215-1	1	988	2017.09.29	12:36:36	75.21956	-13.76263		
BGR17-215-1	1913	2900	2017.09.29	22:18:52	74.55113	-15.81670	220°	95.15
BGR17-216	1	969	2017.09.29	22:21:52	74.54679	-15.81898		
BGR17-216	3147	4114	2017.09.30	14:14:13	73.15506	-15.02603	171°	156.55
BGR17-217	1	1003	2017.09.30	14:50:22	73.13850	-15.19409		
BGR17-217	2427	3429	2017.10.01	03:07:32	74.06454	-17.20930	329°	120.73
BGR17-215-2	1	4274	2017.10.01	03:09:33	74.06759	-17.20892		
BGR17-215-2	1520	2754	2017.10.01	10:51:35	74.60824	-15.67593	37°	75.64

8 Acknowledgements

Many thanks go to Master Ralf Schmidt and the entire crew of RV Maria S. Merian for their great support during the cruise. Their experience and outstanding professional service contributed substantially to the final success of our survey.

Moreover, we highly appreciate the assistance by Briese Research for assistance and solving several unforeseen problems and we are finally grateful the Leitstelle Deutsche Forschungsschiffe for the coordination activities before and during the cruise.

Appendix-A 1: *Geometry of Spectra reference points on the vessel and in the water.*

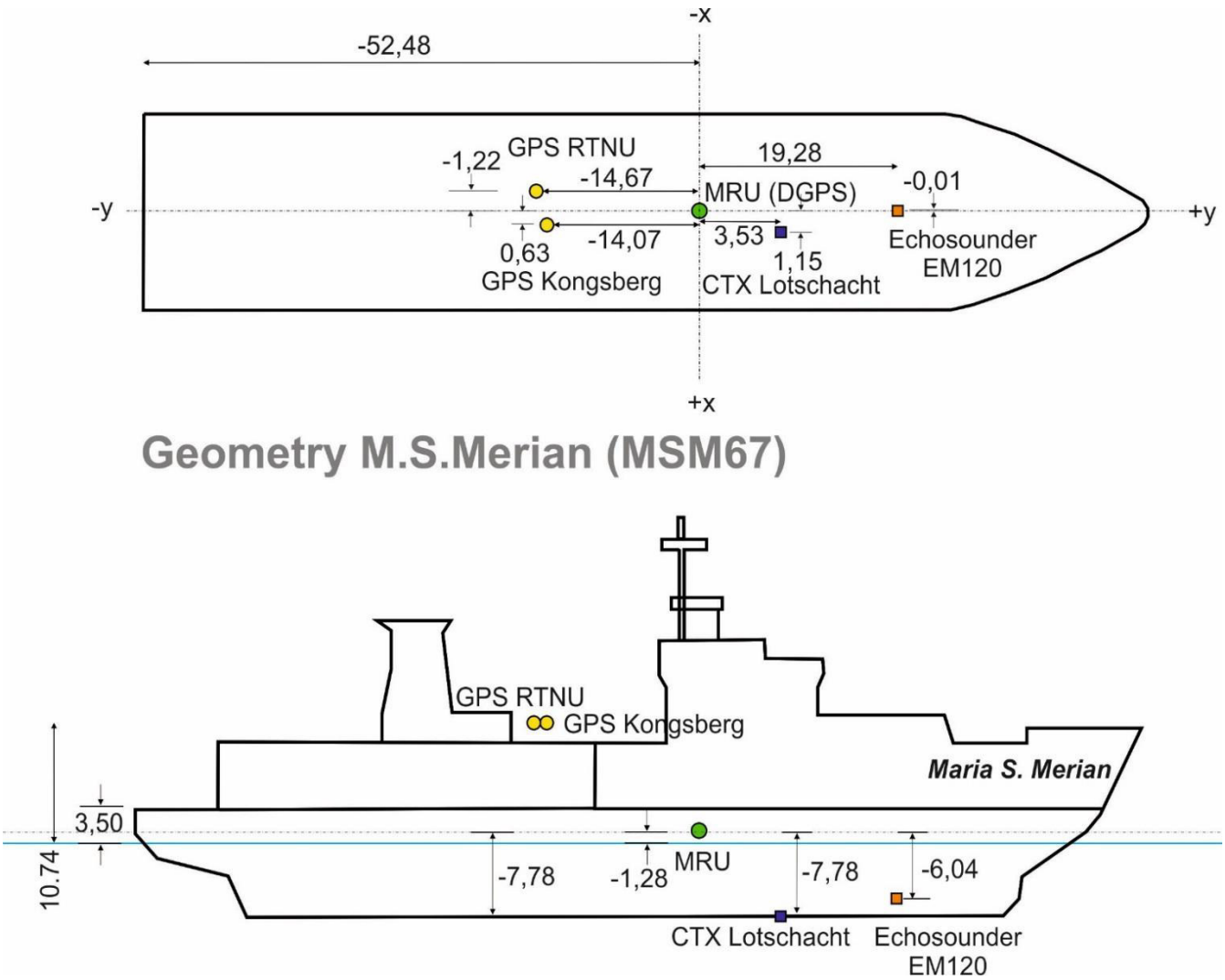

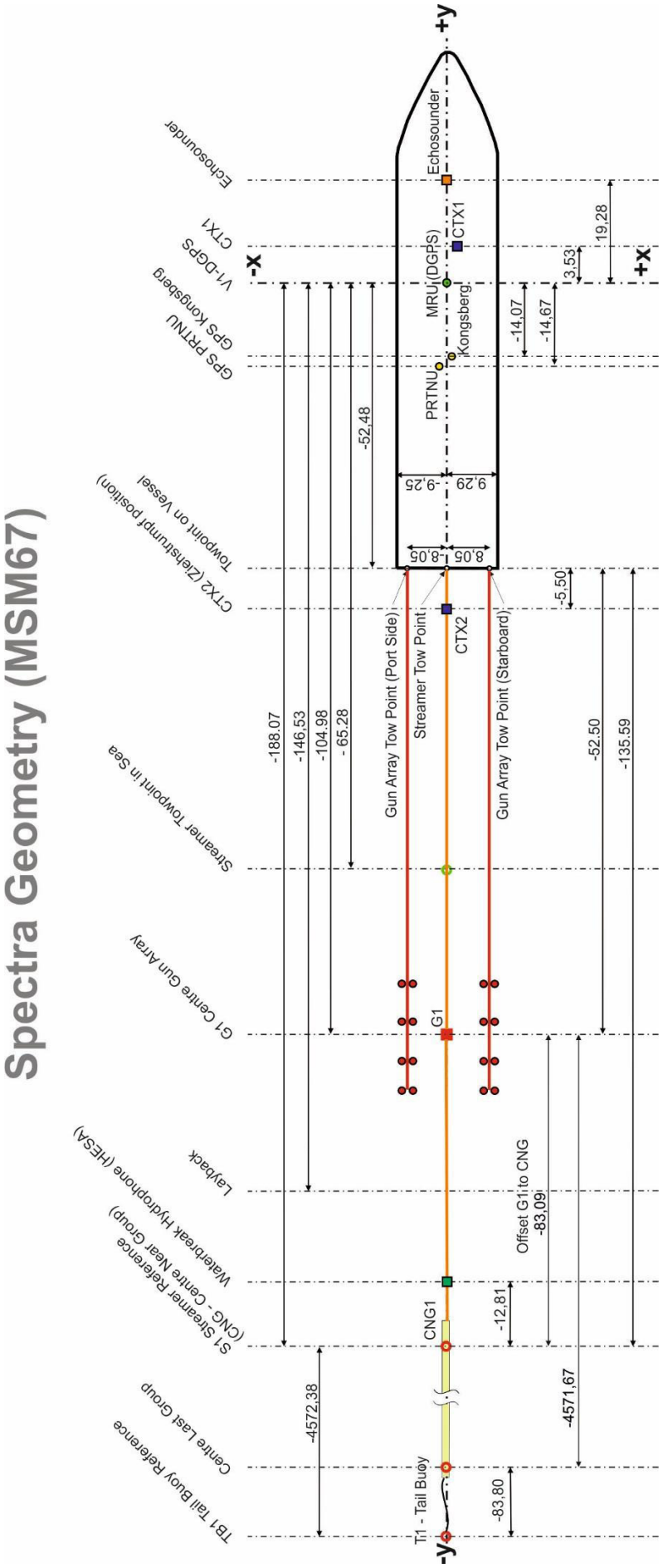
Spectra Geometry (MSM67)
+y
-y
-x
+x
Echosounder
CTX1
MRU (DGPS)
Kongsberg
PRTNU
9,29
-9,25
8,05
8,05
19,28
3,53
-14,07
-14,67
-52,48
-5,50
CTX2
Gun Array Tow Point (Port Side)
Streamer Tow Point
Gun Array Tow Point (Starboard)
-188.07
-146,53
-104.98
- 65.28
-52.50
-135.59
G1
CNG1
Offset G1 to CNG
-83,09
-12,81
-4572,38
-4571,67
Tr1 - Tail Buoy
-83,80
Echosounder
CTX1
V1-DGPS
GPS Kongsberg
GPS PRTNU
Towpoint on Vessel
CTX2 (Zielstrumpf position)
Streamer Towpoint in Sea
G1 Centre Gun Array
Leyback
S1 Streamer Reference (CNG - Centre Near Group)
Waterbreak Hydrophone (HESA)
Centre Last Group
TB1 Tail Buoy Reference

Appendix-A 2: *Wiring of Spectra's real-time system Power RTNU during cruise MSM67.*

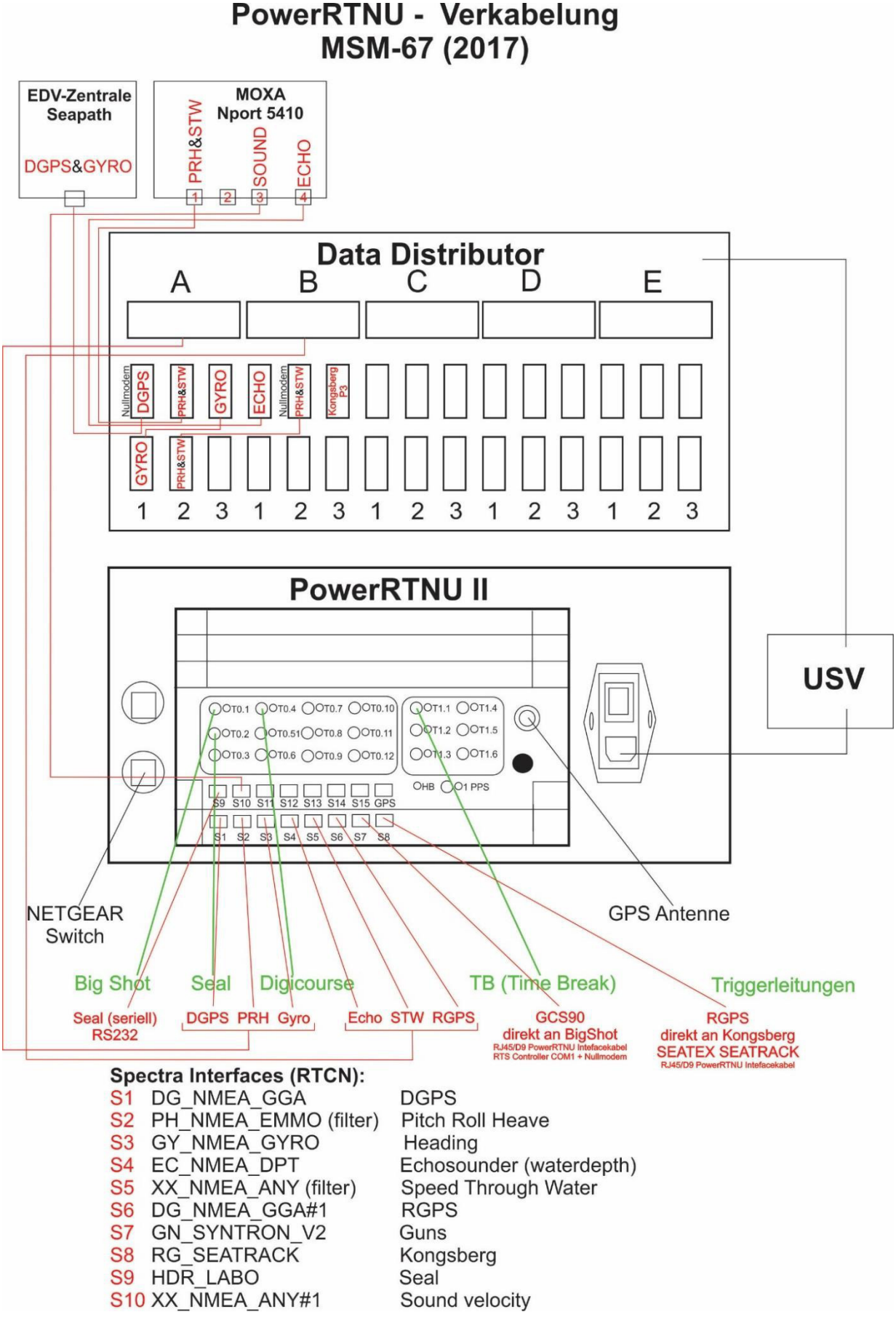

Spectra Interfaces (RTCN):

S1	DG_NMEA_GGA	DGPS
S2	PH_NMEA_EMMO (filter)	Pitch Roll Heave
S3	GY_NMEA_GYRO	Heading
S4	EC_NMEA_DPT	Echosounder (waterdepth)
S5	XX_NMEA_ANY (filter)	Speed Through Water
S6	DG_NMEA_GGA#1	RGPS
S7	GN_SYNTRON_V2	Guns
S8	RG_SEATRACK	Kongsberg
S9	HDR_LABO	Seal
S10	XX_NMEA_ANY#1	Sound velocity

Appendix-A 3: *Serial data interfaces used for seismic navigation.*

1 - DG_NMEA_GGA

```
$GPGGA,073223.5432,7334.867513,N,01720.877099,W,5,09,1.1,1.70,
M,50.56,M,1.0,0000*5A<CR><LF>
```

2 - PH_NMEA_EMMO

```
$PRDID,0.290,-0.06,81.340,0.380*6E<CR><LF>
```

3 - GY_NMEA_GYRO

```
$GPHDT,81.12,T*3F<CR><LF>
```

4 - EC_NMEA_DPT

```
$EMDPT,274.01*7A<CR><LF>
```

5 - XX_NMEA_ANY

```
$WATSP,2.67,0.05*47<CR><LF>
```

6 - DG_NMEA_GGA

```
$GPGGA,073504.10,7334.8954,N,01720.1641,W,1,06,01.6,+73.8,M,+0
0.0,M,00.0,0000*6C<CR><LF>
```

7 - GN_SYNTRON_V2

```
*GCS900452GR17-
211000000203403E17/09/27:00:35:3712161600000000503100
000000000000000000001AH1NN000114502002000002AH1NN0001135010010
0003AH1NN000120500000000004AH1NN000120500000000005AH1NN000116498
-
0100006AH1NN000120499000000007AH1NN000133501001000008AH1NN000128
50000000009AH1NN000115500000000010AH1NN000111499000000011AH1NN00
011649900000012AH1NN000117499000000013AH1NN000115503003000014AH1
NN000116498-
0100015AH1NN000117500000000016AH1NN000123502002000<CR><LF>
```

8 - RG_SEATRACK

```
073557.00S1     .0   .000   .0 0  .0S2     .0   .000   .0 0  .0S3
4757.3258.696-12.2 6 1.6S4     .0   .000   .0 0  .0<CR><LF>
```

9 - HDR_LABO

```
$10616000503073630.46087820170927UTC002037            BGR17-211
73.581965 -17.326635 273.6  73.581811 -17.329925 79.7 81.8 5.4
1000615822.3008168964.3-0102.6-0023.5080.1270*GCS900452GR17-
```

```
211000000203703E17/09/27:00:36:3212161600000000403100
000000000000000000001AH1NN000114500000000002AH1NN0001125020020
0003AH1NN000120500000000004AH1NN000119499000000005AH1NN000118501
00100006AH1NN000118500000000007AH1NN000131498-
0100008AH1NN000128499000000009AH1NN000116500000000010AH1NN000111
50000000011AH1NN000116499000000012AH1NN000116499000000013AH1NN00
011750200200014AH1NN000117501001000015AH1NN000117499000000016AH1
NN000122498-01000<CR><LF>
```

10 SP_NMEA_EMMO

```
$SVKEEL,1449.90*01<CR><LF>
```

Appendix-A 4: *Marine Mammal Observation Weekly Summaries.*

Observer Names: Lorenzo Scala, Stephanie Barnicoat

Marine Mammal Observation Weekly Summary

MSM67

31/08/2017 to 03/09/2017

Observer Names: Lorenzo Scala, Stephanie Barnicoat

Client	BGR	**Seismic Contractor**	BGR
Survey Location	Norwegian Sea	**Vessel Name**	FS Maria S. Merian
Regulator Reference Number		**Report Number**	001

Operations Summary Table

Description of Operations	Weekly	Project Total
Duration of full volume acquisition:	21:03	21:03
Duration of reduced volume acquisition operations:	-	-
Duration of soft starts:	00:29	00:29
Duration of source testing:	00:41	00:41
Total duration of source operations:	**22:13**	**22:13**

Monitoring Effort Summary Table

Visual and Acoustic Monitoring Efforts								
Monitoring Method	Source Inactive		Source Active		Total Monitoring Effort		Number of Soft Starts (per method)	
	Weekly	Project Total	Weekly	Project Total	Weekly	Project Total	Weekly	Project Total
Visual	22:01	22:01	02:25	02:25	24:06	24:06	0	0
Acoustic	1:00	1:00	17:28	17:28	18:28	18:28	1	1

Mitigation Actions Summary

There were no mitigation actions required.

Detection Summary

There was one visual sighting this week during the transit and no acoustic detections.

Sighting 1:

Three unidentified delphinids surfacing and travelling fast, changing direction of travel, 300 m from the vessel.

PAM Equipment Hardware/Software Status

PAM equipment was installed on the Maria S Merian 29th August and was deployed in the early hours on 3rd September ready for a pre-monitoring search for line BGR17-2R1.

Summary of Environmental Conditions

Environmental conditions for the week began with a slight sea state (no or few white caps) and a low swell (<2 m), Beaufort force scale 3 to 5. Towards the end of the week environmental conditions altered to a choppy sea state (lots of white caps) and a medium swell (2-4 m), with a Beaufort force scale of 5 to 7. The visibility has been good throughout the week (>5 km), altering to moderate (1-5 km) and poor visibility (<1 km) at the end of the week, making PAM a more suitable method for mitigation.

Marine Mammal Observation Weekly Summary

MSM67

04/09/2017 to 10/09/2017

Observer Names: Lorenzo Scala, Stephanie Barnicoat

Client	BGR	**Seismic Contractor**	BGR
Survey Location	Greenland waters	**Vessel Name**	FS Maria S. Merian
Regulator Reference Number		**Report Number**	002

Operations Summary Table

Description of Operations	Weekly	Project Total
Duration of full volume acquisition:	21:13	43:00
Duration of reduced volume acquisition operations:	00:32	00:32
Duration of soft starts:	00:43	01:12
Duration of source testing:	00:00	00:41
Total duration of source operations:	**22:28**	**44:53**

Monitoring Effort Summary Table

Visual and Acoustic Monitoring Efforts								
Monitoring Method	**Source Inactive**		**Source Active**		**Total Monitoring Effort**		**Number of Soft Starts** (per method)	
	Weekly	**Project Total**	**Weekly**	**Project Total**	**Weekly**	**Project Total**	**Weekly**	**Project Total**

Visual	35:54	57:55	00:00	02:25	35:54	60:00	0	0
Acoustic	06:39	07:39	22:46	39:15	28:26	46:54	2	3

Mitigation Actions Summary

There were no mitigation actions required.

Detection Summary

There were nine visual sighting events this week, all off transect, and no acoustic detections.

Visual and Acoustic detections			
Sighting/Detection number	**Date**	**Species**	**Distance from vessel**
2	07-09-17	Killer whale (*Orcinus orca*)	800
3	07-09-17	Delphinid	200
4	07-09-17	White beaked dolphin (*Lagenorhynchus albirostris*)	300
5	07-09-17	Delphinid	800
6	07-09-17	White beaked dolphin (*Lagenorhynchus albirostris*)	250
7	07-09-17	Humpback whale (*Megaptera novaeangliae*)	750
8	07-09-17	Humpback whale (*Megaptera novaeangliae*)	600
9	07-09-17	Humpback whale (*Megaptera novaeangliae*)	1500
10	09-09-17	Unidentified cetacean (*Megaptera novaeangliae*)	1200

PAM Equipment Hardware/Software Status

The PAM array was retrieved on 4th September at end of line, and has been on deck all week during the transit back to Iceland. The hydrophone array was deployed 10th September at 06:00 UTC, for seismic profiling.

Summary of Environmental Conditions

Environmental conditions for the week began with a choppy sea state (lots of white caps) and a medium swell (2-4m) with a Beaufort fore scale of 6 and 7, with a south easterly wind. In the middle of the week during transit, sighting conditions were very good with a slight sea state (no or few white caps), a low swell (<2m) and a Beaufort force scale of 2 to 3, excellent conditions for sighting marine mammals. Towards the end of the week in the survey area, environmental conditions consisted of a choppy sea state (lots of white caps) and a low swell (<2m), with a Beaufort force scale of 6 and 7, making PAM a more suitable method for mitigation.

Marine Mammal Observation Weekly Summary

MSM67

11/09/2017 to 17/09/2017

Observer Names: Lorenzo Scala, Stephanie Barnicoat

Client	BGR	**Seismic Contractor**	BGR
Survey Location	Greenland waters	**Vessel Name**	FS Maria S. Merian
Regulator Reference Number		**Report Number**	003

Operations Summary Table

Description of Operations	Weekly	Project Total
Duration of full volume acquisition:	96:34	139:34
Duration of reduced volume acquisition operations:	02:03	02:35
Duration of soft starts:	00:42	01:54
Duration of source testing:	00:00	00:41
Total duration of source operations:	**99:19**	**144:44**

Monitoring Effort Summary Table

Visual and Acoustic Monitoring Efforts								
Monitoring Method	Source Inactive		Source Active		Total Monitoring Effort		Number of Soft Starts (per method)	
	Weekly	Project Total	Weekly	Project Total	Weekly	Project Total	Weekly	Project Total
Visual	08:52	66:07	21:07	23:32	29:59	89:59	1	1
Acoustic	02:02	09:41	78:12	117:27	80:14	127:08	1	4

Mitigation Actions Summary

There were no mitigation actions required.

Detection Summary

There were three visual sighting events this week and no acoustic detections.

Visual and Acoustic detections			
Sighting/Detection number	Date	Species	Distance from vessel (m)
11	11-09-17	Unidentified mysticete	2000
12	11-09-17	Humpback whale (*Megaptera novaeangliae*)	1500, 700

13	11-09-17	Humpback whale (*Megaptera novaeangliae*)	2000, 900

PAM Equipment Hardware/Software Status

The PAM array was retrieved on two occasions this week whilst the crew retrieved the seismic equipment and on a third occasion as the vessel transects to port.

Summary of Environmental Conditions

Environmental conditions for the week has predominately consisted of northerly winds, with a varied sea state between a slight sea state (no or few white caps), and a choppy sea state (lots of white caps) consisting of a low swell (< 2m) but most often a medium swell (2-4m) with a Beaufort fore scale of ranging from 4 to 5 for the most part of the week peaking at 8 to 10 during the middle of the week.

Marine Mammal Observation Weekly Summary

MSM67

18/09/2017 to 24/09/2017

Observer Names: Lorenzo Scala, Stephanie Barnicoat

Client	BGR	**Seismic Contractor**	BGR
Survey Location	Greenland waters	**Vessel Name**	FS Maria S. Merian
Regulator Reference Number		**Report Number**	004

Operations Summary Table

Description of Operations	Weekly	Project Total
Duration of full volume acquisition:	39:34	179:08
Duration of reduced volume acquisition operations:	00:00	02:35
Duration of soft starts:	00:45	01:54
Duration of source testing:	00:00	00:41
Total duration of source operations:	**40:19**	**185:03**

Monitoring Effort Summary Table

Visual and Acoustic Monitoring Efforts								
Monitoring Method	**Source Inactive**		**Source Active**		**Total Monitoring Effort**		**Number of Soft Starts** (per method)	
	Weekly	**Project Total**	**Weekly**	**Project Total**	**Weekly**	**Project Total**	**Weekly**	**Project Total**
Visual	01:00	67:07	17:55	41:27	18:55	108:54	0	1

Acoustic	02:04	11:45	45:42	163:09	47:44	174:52	2	6

Mitigation Actions Summary

There were no mitigation actions required this week. During the Knipovich ridge lines were in Norwegian waters so we used JNCC guidelines to adhere to regulatory requirements and BGR best practice philosophy for minimising impact on environment and marine mammals during seismic operations. BGR17 R2 line was inside Greenlandic waters so JNCC with additional Greenland mitigation requirements including shut down for bowhead whale, narwhal and walrus and reduced power downs for other marine mammals were implemented. No marine mammals were detected during the refraction line, therefore no mitigation action was required.

Detection Summary

There were three concurrent visual and acoustic detections, and eight acoustics only detections all in the Norwegian Sea and all sperm whales (*Physter macrocpehalus*). (Table below). The sperm whales were first detected visually and then checked on the PAM Remote Local Monitoring Station that is set up in the observation deck. The other detections were first detected on PAMGaurd, broadband low to mid frequency clicks were visually detected on the spectrogram, and the click detector display (Figure 1).

Visual and Acoustic detections				
Sighting/Detection number	**Date**	**Species**	**Number**	**Distance from vessel**
14/501	19-09-	Sperm whale (*Physter macrocpehalus*)	2	1500
502	19-09-	Sperm whale (*Physter macrocpehalus*)	3	4500
503	19-09-	Sperm whale (*Physter macrocpehalus*)	2	4000
15/504	19-09-	Sperm whale (*Physter macrocpehalus*)	1	2500
505	19-09-	Sperm whale (*Physter macrocpehalus*)	3	1000
16/506	19-09-	Sperm whale (*Physter macrocpehalus*)	3	1500,
507	19-09-	Sperm whale (*Physter macrocpehalus*)	4	1000,
508	20-09-	Sperm whale (*Physter macrocpehalus*)	3	4000,
509	20-09-	Sperm whale (*Physter macrocpehalus*)	2	800, 400
510	20-09-	Sperm whale (*Physter macrocpehalus*)	1	800
511	20-09-	Sperm whale (*Physter macrocpehalus*)	4	1600,

PAM Equipment Hardware/Software Status

The PAM array was deployed on the 19th for the Knipovich refraction lines and was retrieved on the 20th. The PAM array was deployed again for on the 22nd for the OBS refractions lines and retrieved on the 24th for the retrieval of the OBS.

Summary of Environmental Conditions

Environmental conditions for the week has predominately consisted of northerly winds, with a slight sea state (no or few white caps), a low swell (< 2m) and with a Beaufort fore scale of ranging from 4 to 5 for the most part of the week. The visibility has been very poor for most of the week, making PAM the most practical tool for mitigation.

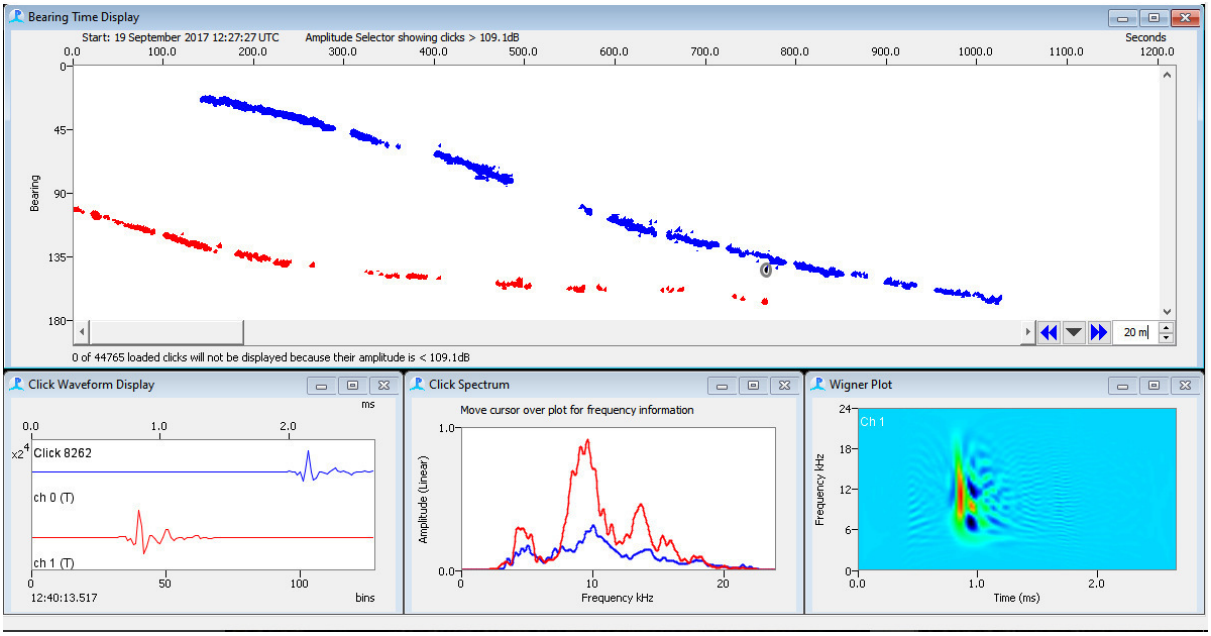

Fig 1: Output window from PAMGuard viewer analysis of acoustic detection 501 showing two individual sperm whales (blue and red tracks) bearing relative to PAM hydrophone array. Clear Click waveform, broadband spectrum with peak energy at 10 kHz and tight kernel of energy at expected click interval and freq. range of sperm whales.

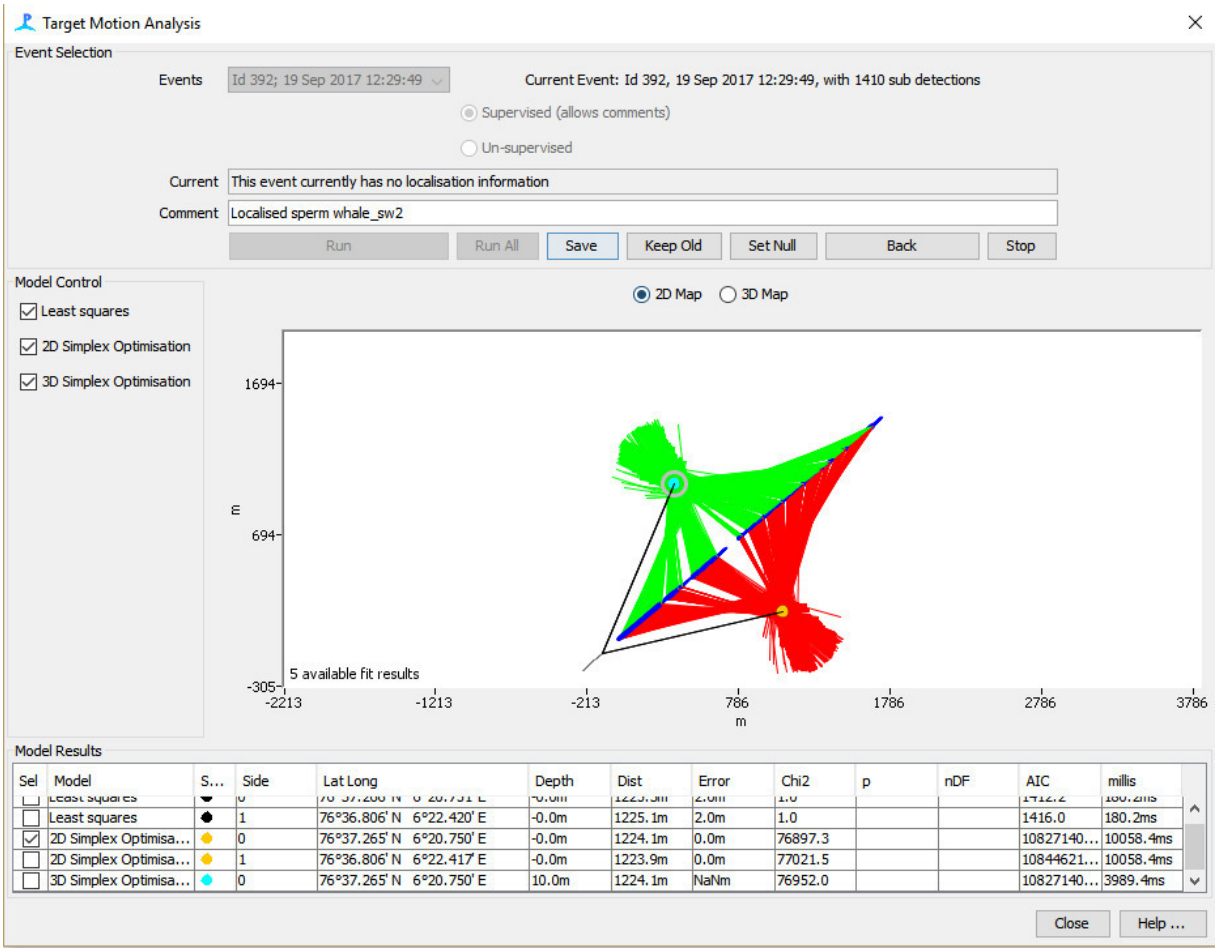

Fig 2: Output of Target Motion Analysis in PAMGuard viewer post processing to determine location of sperm whales relative to vessel and mitigation zone. 2D simplex model selected for best goodness of fit of data showing animal passed within approximately 1200m of vessel.

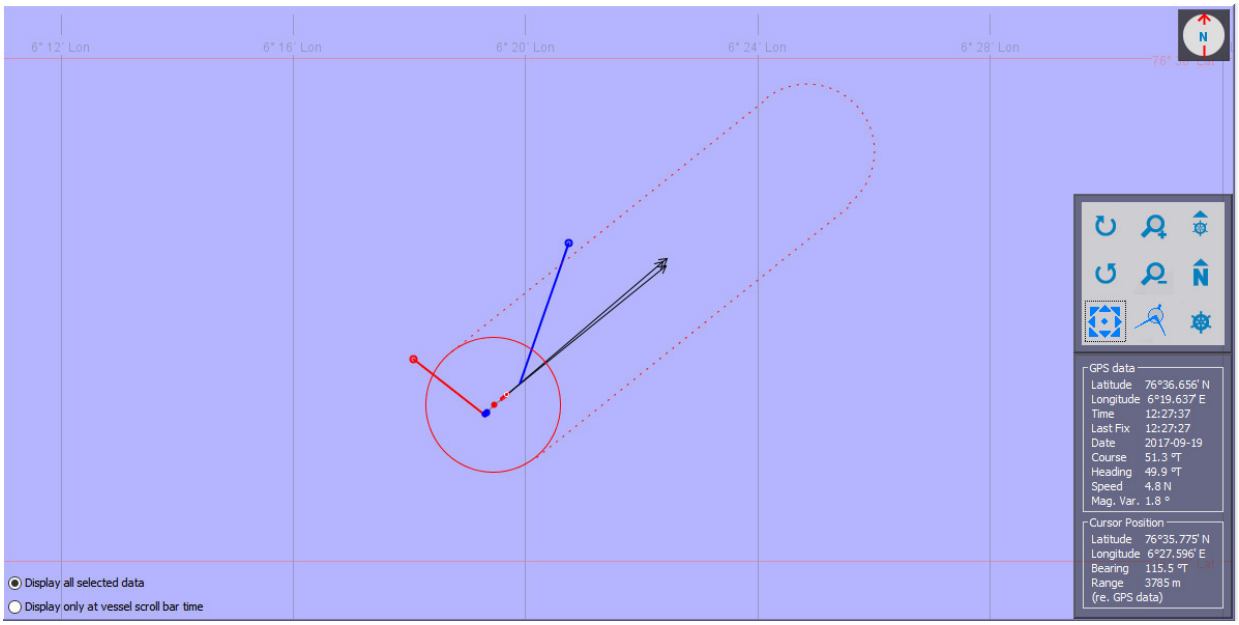

Fig 3: Map display showing localised positions of two sperm whales from detection 501 represented by red and blue line. Red circle is mitigation zone and back arrows are vessel track direction and heading.

Marine Mammal Observation Weekly Summary

MSM67

25/09/2017 to 01/10/2017

Observer Names: Lorenzo Scala, Stephanie Barnicoat

Client	BGR	**Seismic Contractor**	BGR
Survey Location	Greenland waters	**Vessel Name**	FS Maria S. Merian
Regulator Reference Number		**Report Number**	005

Operations Summary Table

Description of Operations	Weekly	Project Total
Duration of full volume acquisition:	129:58	309:06
Duration of reduced volume acquisition operations:	03:40	06:15
Duration of soft starts:	00:22	02:16
Duration of source testing:	00:00	00:41
Total duration of source operations:	**134:00**	**318:18**

Monitoring Effort Summary Table

Visual and Acoustic Monitoring Efforts								
Monitoring Method	**Source Inactive**		**Source Active**		**Total Monitoring Effort**		**Number of Soft Starts (per method)**	
	Weekly	**Project Total**	**Weekly**	**Project Total**	**Weekly**	**Project Total**	**Weekly**	**Project Total**
Visual	00:00	67:07	04:28	45:55	04:28	113:02	0	1
Acoustic	01:56	13:41	128:58	292:07	130:54	305:46	1	7

Mitigation Actions Summary

There were 1 mitigation actions required this week. Detection 512 was assessed by the PAM operator, and considered to be within 500m of the airguns due to the intensity (amplitude, dB) of the calls relative to background noise, and bearing estimates from the Baleen Moan Detector which indicated the whale was approaching the vessel from ahead. The PAM operator notified the seismic operators of the whales' presence and the airguns were powered down to mitigation gun until 20 minutes after the last vocalisation, to ensure the animal had left the exclusion zone.

Detection Summary

There were 4 acoustic detections during the week, 2 humpback whales and 2 unidentified dolphin species.

	Visual and Acoustic detections			
Sighting/Detection number	**Date**	**Species**	**Number**	**Distance from vessel**
512	26-09-17	Humpback whale (*Megaptera novaeangliae*)	1	< 500
513	26-09-17	Humpback whale (*Megaptera novaeangliae*)	1	4000
514	27-09-17	Unidentified dolphin (*Delphinidae spp*)	1	3000
515	27-09-17	Unidentified dolphin (*Delphinidae spp*)	1	3000

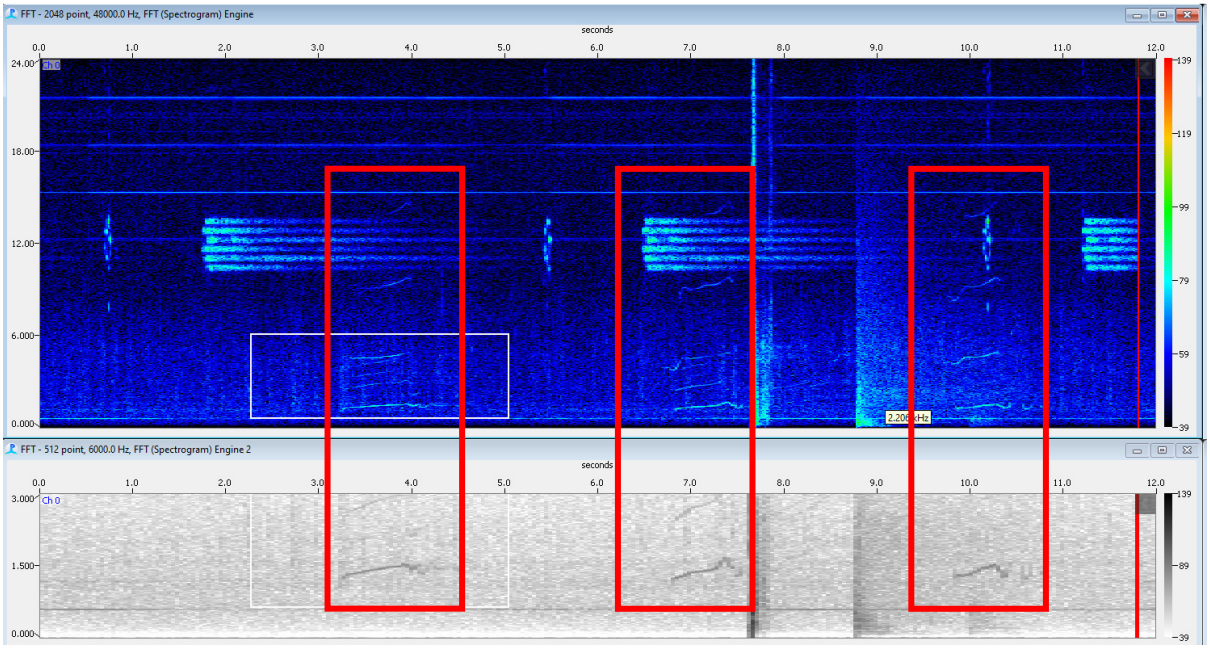

Figure 1: Spectrogram display in PAMGuard real time showing humpback whale LF tonal sounds (1.5 kHz) with harmonics (18 kHz). (Detection 512).

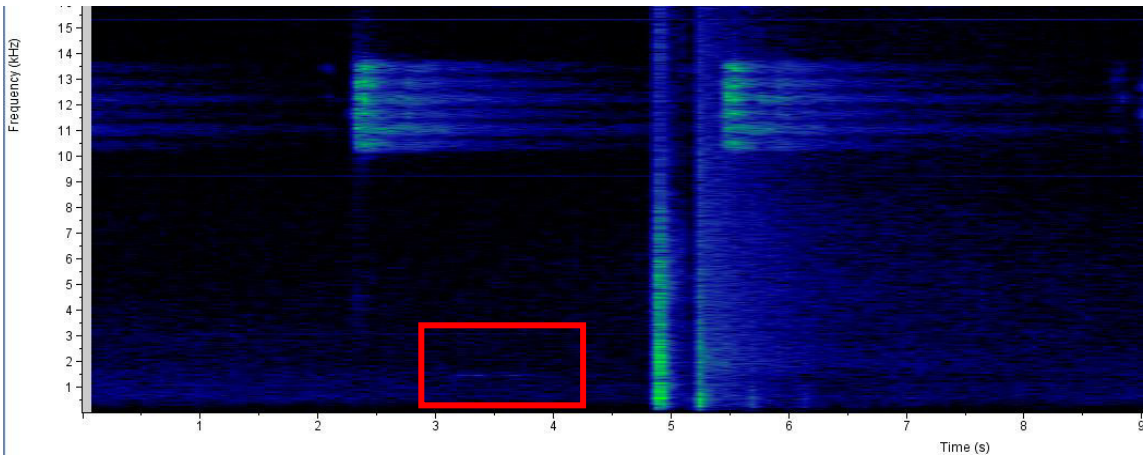

Figure 3: Spectrogram display in Raven Pro 1.5 showing post processing of humpback whale LF tonal sound (1.5 kHz). (Detection 513).

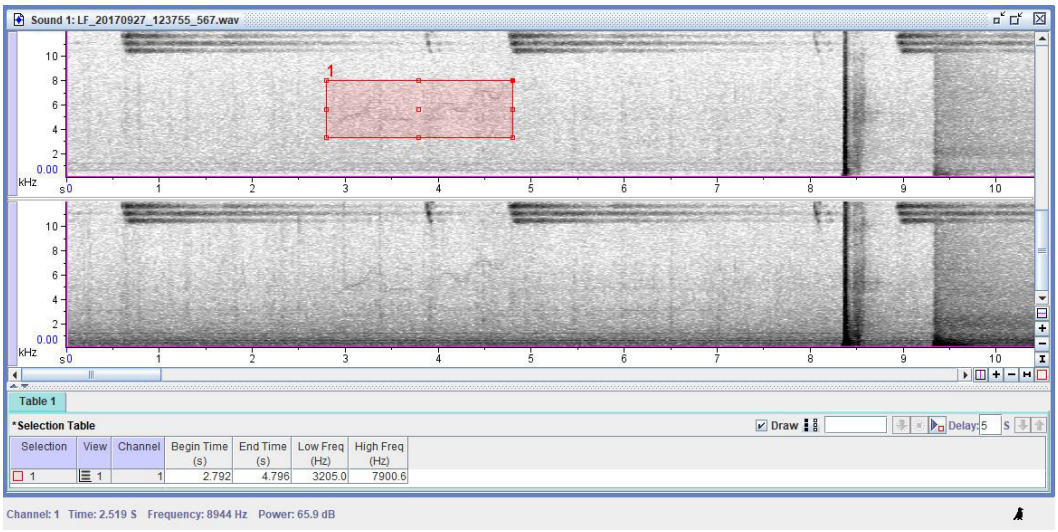

Figure 4: Spectrogram display in Raven Pro 1.5 showing post processing of unidentified delphinid spp. whistles (3-7.5 kHz). File time stamp indicates 27th sept 12:37 UTC (Detection 514).

PAM Equipment Hardware/Software Status

The PAM array was deployed on the 25th to continue with the seismic reflection lines. PAM has been the chosen tool to use for monitoring the presence of marine mammals this week due to poor visibility.

Summary of Environmental Conditions

Environmental conditions for the week has predominately consisted of southerly, and south easterly winds, with the sea state altering between a slight sea state (no or few white caps), and a choppy sea (many white caps). The swell has varied between a low swell (< 2m) and a medium swell (2-4 m) with a Beaufort fore scale of ranging from 4 to 6 for the most part of the week. The visibility has been very poor for most of the week, and precipitation has ranged from no rain to moderate rain, making PAM the most practical tool for mitigation.

Appendix-A 5: *Ships station list*

Station	Time-stamp	Device	Action	Latitude	Longitude	Depth	Speed	Course	Wind Dir	Wind Velocity	Comment
[No.]	[UTC]					[m]	[kn]	[°]			
MSM67_7-2	20.09.2017 07:28	Seismic Source	alter course	76° 41,117' N	006° 49,093' E	2464.6	4,9	188,80	104	24,40	rwk 051–
MSM67_7-2	20.09.2017 06:46	Seismic Source	alter course	76° 44,555' N	006° 51,274' E	2305.7	5,1	166,90	105	20,40	rwk 190–
MSM67_7-2	20.09.2017 05:22	Seismic Source	alter course	76° 48,327' N	006° 54,453' E	2151.1	5,0	340,50	68	13,10	rwk 163–
MSM67_7-2	19.09.2017 22:52	Seismic Source	alter course	76° 22,485' N	007° 23,445' E	3006.5	4,7	195,50	54	17,20	rwK 339–
MSM67_7-2	19.09.2017 17:42	Seismic Source	alter course	76° 33,644' N	008° 10,580' E	1423.7	4,9	96,70	42	20,10	rwk 209–
MSM67_7-2	19.09.2017 11:04	Seismic Source	alter course	76° 33,057' N	006° 33,024' E	2580.3	5,2	225,00	356	12,40	rwK 098–
MSM67_7-2	19.09.2017 07:26	Seismic Source	alter course	76° 48,115' N	007° 15,607' E	3218.0	5,6	231,00	347	13,80	rwk 213–
MSM67_7-2	19.09.2017 07:12	Seismic Source	profile start	76° 48,835' N	007° 19,455' E	3272.7	5,0	232,20	355	13,20	v=5kn rwk 231–
MSM67_7-2	19.09.2017 07:12	Seismic Source	information	76° 48,835' N	007° 19,455' E	3272.7	5,7	232,20	355	13,20	End "Soft-Start"
MSM67_7-2	19.09.2017 06:49	Seismic Source	information	76° 50,042' N	007° 25,921' E	3196.1	4,9	234,30	348	12,80	Beginn "Soft-Start"
MSM67_7-2	19.09.2017 05:59	Seismic Source	Airgun in water	76° 52,633' N	007° 39,924' E	2844.8	5,0	234,40	335	16,40	40 m Bb. Array with 8G-Guns
MSM67_7-2	19.09.2017 05:42	Seismic Source	Airgun in water	76° 53,440' N	007° 44,124' E	2698.5	4,7	227,50	335	15,50	40m Stb. Array with 8G-Guns
MSM67_7-1	19.09.2017 05:26	Seismic Towed Receiver	PAM in water	76° 54,231' N	007° 48,573' E	2419.3	4,4	238,90	337	14,50	200m length
MSM67_0_ Underway-6	18.09.2017 12:51	Deep-sea Multibeam Echosounder	profile start	77° 57,409' N	012° 24,672' E	239.5	8,8	252,10	175	36,60	
MSM67_0_ Underway-7	18.09.2017 12:51	Thermosalino-graph	profile start	77° 57,409' N	012° 24,672' E	239.5	8,8	252,10	175	36,60	
MSM67_6-2	16.09.2017 10:15	Seismic Source	Airgun on deck	74° 53,115' N	014° 17,920' W	181.7	4,2	156,20	358	26,20	STB Array
MSM67_6-2	16.09.2017 09:46	Seismic Source	Airgun on deck	74° 54,891' N	014° 20,543' W	170.9	4,4	152,20	336	20,20	BB Array
MSM67_6-2	16.09.2017 09:25	Seismic Source	profile end	74° 56,321' N	014° 22,608' W	172.0	5,6	158,80	334	15,50	Profil 208
MSM67_6-2	16.09.2017 08:47	Seismic Source	profile start	74° 59,582' N	014° 24,097' W	153.7	5,8	214,00	321	12,20	Profil 209; v= 5,4 kn; rwk 159–
MSM67_6-2	16.09.2017 08:43	Seismic Source	profile end	74° 59,902' N	014° 23,506' W	155.1	4,9	201,50	324	12,20	Profil 208
MSM67_6-2	16.09.2017 01:26	Seismic Source	profile start	75° 13,698' N	012° 03,571' W	688.6	5,0	287,50	157	21,90	Profil 208; v= 5,4 kn; rwk 250–
MSM67_6-2	16.09.2017 01:21	Seismic Source	profile end	75° 13,562' N	012° 02,030' W	741.4	5,2	290,20	156	20,20	Profil 207

MSM67_6-2	15.09.2017 21:47	Seismic Source	profile start	74° 58,085' N	011° 22,841' W	2448.8	5,7	11,10	165	22,90	Profil 207; v= 5,4 kn; rwk 329–
MSM67_6-2	15.09.2017 21:43	Seismic Source	profile end	74° 57,760' N	011° 22,822' W	2466.7	5,6	359,10	167	20,90	Profil 206
MSM67_6-2	15.09.2017 14:38	Seismic Source	profile start	74° 30,801' N	012° 56,103' W	2433.9	5,3	333,60	158	14,40	Profil 206; v= 5,4 kn; rwk 046–
MSM67_6-2	15.09.2017 13:40	Seismic Source	profile end	74° 29,928' N	012° 39,584' W	2566.6	4,9	233,40	153	14,20	Profil 205
MSM67_6-2	15.09.2017 01:41	Seismic Source	profile start	75° 29,832' N	013° 18,052' W	188.5	5,7	181,60	155	14,70	Profil 205; v= 5,4 kn, rwk 169–
MSM67_6-2	15.09.2017 01:41	Seismic Source	information	75° 29,863' N	013° 18,050' W	191.2	5,6	174,70	159	14,40	End "Soft-Start"
MSM67_6-2	15.09.2017 01:20	Seismic Source	information	75° 31,521' N	013° 15,635' W	190.3	5,3	222,00	162	11,40	Beginn "Soft-Start"
MSM67_6-2	15.09.2017 00:59	Seismic Source	Airgun in water	75° 32,429' N	013° 09,511' W	194.1	4,5	259,40	168	12,80	Bb. Array with 8 G-Guns
MSM67_6-2	15.09.2017 00:37	Seismic Source	Airgun in water	75° 32,466' N	013° 03,061' W	192.8	4,3	265,30	162	11,90	Stb. Array with 8 G-Guns
MSM67_6-1	16.09.2017 13:22	Seismic Towed Receiver	Streamer on deck	74° 40,017' N	014° 11,700' W	179.2	4,2	184,80	358	13,10	
MSM67_6-1	16.09.2017 11:14	Seismic Towed Receiver	Magnetometer on deck	74° 49,460' N	014° 12,648' W	180.9	3,9	167,60	344	23,20	
MSM67_6-1	16.09.2017 11:14	Seismic Towed Receiver	PAM on deck	74° 49,510' N	014° 12,689' W	180.9	3,9	167,60	345	22,50	
MSM67_6-1	14.09.2017 23:58	Seismic Towed Receiver	PAM in water	75° 32,433' N	012° 51,438' W	199.7	4,4	273,20	166	11,10	250m streamer length
MSM67_6-1	14.09.2017 23:52	Seismic Towed Receiver	Magnetometer in water	75° 32,422' N	012° 49,526' W	201.1	2,2	270,60	166	13,20	700m streamer length
MSM67_6-1	14.09.2017 18:51	Seismic Towed Receiver	Streamer in water	75° 31,943' N	011° 10,119' W	1117.8	4,4	270,20	111	5,90	4700m streamer length
MSM67_5-2	14.09.2017 07:13	Seismic Source	Airgun on deck	75° 17,267' N	014° 19,155' W	166.7	5,7	78,20	67	9,30	Bb.-Array
MSM67_5-2	14.09.2017 06:49	Seismic Source	Airgun on deck	75° 16,897' N	014° 27,343' W	196.8	5,2	85,50	4	13,50	Stb.- Array
MSM67_5-2	14.09.2017 06:10	Seismic Source	information	75° 17,114' N	014° 40,742' W	210.7	6,2	94,50	357	13,50	Lost tail buoy
MSM67_5-2	14.09.2017 05:01	Seismic Source	profile end	75° 13,643' N	014° 44,630' W	203.3	4,9	287,80	1	18,70	Cancellation due to ice conditions
MSM67_5-2	13.09.2017 17:53	Seismic Source	profile start	74° 40,283' N	011° 40,639' W	2755.3	4,7	285,00	16	18,80	Profil 204 v=5,4kn rwk 308–
MSM67_5-2	13.09.2017 17:50	Seismic Source	information	74° 40,169' N	011° 39,728' W	2773.0	5,5	292,10	18	19,20	End "Soft-Start"
MSM67_5-2	13.09.2017 17:30	Seismic Source	information	74° 39,764' N	011° 33,400' W	2846.7	4,7	266,70	14	19,70	Beginn "Soft-Start"
MSM67_5-2	13.09.2017 17:14	Seismic Source	Airgun in water	74° 40,253' N	011° 28,877' W	2870.7	5,0	235,90	12	18,80	40m Stb. Array with 8 G-Guns
MSM67_5-2	13.09.2017 16:03	Seismic Source	Airgun in water	74° 45,376' N	011° 21,031' W	2855.5	6,0	184,50	13	17,80	40m Bb.-Array with 8 G-Guns
MSM67_5-2	13.09.2017 10:51	Seismic Source	Airgun on deck	74° 51,052' N	012° 03,953' W	2067.6	4,7	60,50	20	15,00	Stb Array for maintenance work on deck

MSM67_5-2	13.09.20 17 09:59	Seismic Source	Airgun on deck	74° 49,336' N	012° 16,66 0' W	1901.8	4,3	55,50	28	13,00	BB Array for maintenance work on deck
MSM67_5-2	13.09.20 17 09:52	Seismic Source	profile end	74° 49,094' N	012° 18,38 7' W	1877.4	5,3	64,40	31	12,50	
MSM67_5-2	12.09.20 17 18:13	Seismic Source	information	74° 09,264' N	016° 45,63 3' W	0.0	4,2	70,60	343	44,10	Continuation of Profiltrack
MSM67_5-2	12.09.20 17 16:41	Seismic Source	information	74° 05,396' N	017° 09,12 4' W	195.0	6,0	50,40	344	38,00	Deviation from profiltrack due to ice conditions
MSM67_5-2	12.09.20 17 16:33	Seismic Source	profile start	74° 04,960' N	017° 11,40 0' W	197.6	5,4	50,20	346	40,90	Beginn Profil 203
MSM67_5-2	12.09.20 17 16:30	Seismic Source	profile end	74° 04,809' N	017° 12,04 2' W	208.9	5,3	56,80	345	38,10	
MSM67_5-2	12.09.20 17 16:20	Seismic Source	alter course	74° 04,114' N	017° 13,94 9' W	207.0	5,3	36,80	345	35,90	rwk 058−
MSM67_5-2	12.09.20 17 13:03	Seismic Source	information	73° 49,074' N	017° 42,99 4' W	307.5	5,3	23,80	346	33,40	Continuation of planned Profiltrack after ice induced deviation
MSM67_5-2	12.09.20 17 12:14	Seismic Source	information	73° 45,301' N	017° 50,11 6' W	277.0	5,7	38,90	347	32,10	Deviation from Profiltrack due to ice condition
MSM67_5-2	11.09.20 17 16:00	Seismic Source	information	72° 08,644' N	020° 34,47 7' W	222.4	5,4	25,30	8	12,90	Continuation of planned Profiltrack after ice induced deviation
MSM67_5-2	11.09.20 17 15:30	Seismic Source	information	72° 06,255' N	020° 38,18 5' W	202.7	5,9	29,10	2	13,90	Deviation from Profiltrack due to ice condition
MSM67_5-2	11.09.20 17 12:10	Seismic Source	profile start	71° 49,915' N	021° 00,80 7' W	347.7	5,7	341,60	342	13,50	Beginn Profil 202; v= 5,4kn; rwk 025−
MSM67_5-2	11.09.20 17 12:04	Seismic Source	profile end	71° 49,414' N	021° 00,42 7' W	325.7	5,1	346,20	344	26,10	Profil 201
MSM67_5-2	11.09.20 17 10:02	Seismic Source	information	71° 43,233' N	020° 32,59 3' W	248.2	6,1	294,20	348	17,70	Continuation of planned Profiltrack after ice induced deviation
MSM67_5-2	11.09.20 17 08:31	Seismic Source	information	71° 39,333' N	020° 11,66 8' W	230.6	5,6	306,70	354	17,30	Deviation from Profiltrack due to ice condition
MSM67_5-2	10.09.20 17 18:53	Seismic Source	profile start	71° 00,343' N	016° 58,97 1' W	1484.1	5,4	279,80	1	23,00	Continuation of Profil 201; v=5,5kn; rwk 304−
MSM67_5-2	10.09.20 17 18:19	Seismic Source	profile end	71° 01,086' N	016° 50,77 4' W	1529.7	5,6	222,70	356	21,70	Profil 200
MSM67_5-2	10.09.20 17 18:06	Seismic Source	alter course	71° 02,098' N	016° 48,91 3' W	1449.8	5,5	196,00	353	21,70	rwk 304−
MSM67_5-2	10.09.20 17 16:03	Seismic Source	profile start	71° 12,699' N	016° 39,21 7' W	1560.2	2,8	196,60	356	24,40	Beginn Profil 200; v= 5,4kn; rwk 197−
MSM67_5-2	10.09.20 17 16:03	Seismic Source	information	71° 12,705' N	016° 39,21 2' W	1560.2	2,9	194,20	356	24,40	Ende "Soft-Start"
MSM67_5-2	10.09.20 17 15:42	Seismic Source	information	71° 14,608' N	016° 38,84 0' W	1521.5	1,0	162,80	0	23,60	Beginn "Soft-Start"
MSM67_5-2	10.09.20 17 11:07	Seismic Source	information	71° 01,452' N	017° 05,06 5' W	1510.1	3,0	304,80	358	27,80	Profil 201 interrupted due to technical problems
MSM67_5-2	10.09.20 17 08:46	Seismic Source	profile start	70° 54,274' N	016° 33,37 7' W	1315.9	3,7	326,30	353	26,60	Profil 201
MSM67_5-2	10.09.20 17 08:46	Seismic Source	information	70° 54,267' N	016° 33,36 2' W	1311.6	5,1	327,00	353	26,50	End "Soft - Start"

MSM67_5-2	10.09.2017 08:21	Seismic Source	information	70° 52,217' N	016° 31,894' W	1385.9	5,4	11,20	347	26,90	Beginn "Soft - Start"
MSM67_5-2	10.09.2017 07:36	Seismic Source	Airgun in water	70° 49,045' N	016° 33,761' W	1307.6	4,3	8,30	351	8,60	40m Bb. Array with 8 G-Guns
MSM67_5-2	10.09.2017 06:04	Seismic Source	Airgun in water	70° 44,918' N	016° 36,182' W	1303.8	4,4	10,90	357	26,90	40m Stb. Array with 8 G-Guns
MSM67_5-1	14.09.2017 12:39	Seismic Towed Receiver	information	75° 15,033' N	014° 56,893' W	835.2	4,9	295,20	130	10,50	Head buoy on deck
MSM67_5-1	14.09.2017 11:32	Seismic Towed Receiver	Streamer on deck	75° 15,620' N	014° 15,046' W	182.8	4,6	278,30	112	8,40	
MSM67_5-1	14.09.2017 07:29	Seismic Towed Receiver	Magnetometer on deck	75° 17,512' N	014° 15,111' W	178.8	3,8	71,80	93	5,90	
MSM67_5-1	14.09.2017 07:13	Seismic Towed Receiver	PAM on deck	75° 17,264' N	014° 19,211' W	161.7	4,5	77,70	68	8,60	
MSM67_5-1	13.09.2017 16:31	Seismic Towed Receiver	PAM in water	74° 43,138' N	011° 23,029' W	2875.3	4,4	195,30	11	18,00	200m streamer length
MSM67_5-1	13.09.2017 15:37	Seismic Towed Receiver	Magnetometer in water	74° 47,286' N	011° 19,327' W	2838.2	5,7	192,40	3	18,00	650 m streamer length
MSM67_5-1	13.09.2017 13:56	Seismic Towed Receiver	information	74° 54,599' N	011° 17,227' W	2633.1	5,8	147,30	18	16,80	Full streamer length (4700 m)
MSM67_5-1	13.09.2017 13:00	Seismic Towed Receiver	information	74° 55,479' N	011° 31,680' W	2392.8	6,0	65,40	20	17,70	Start of streamer resuspension
MSM67_5-1	13.09.2017 12:59	Seismic Towed Receiver	information	74° 55,461' N	011° 31,819' W	2391.9	3,0	63,70	20	17,80	800 m streamer retrieve
MSM67_5-1	13.09.2017 11:22	Seismic Towed Receiver	information	74° 52,142' N	011° 56,128' W	2168.2	3,3	64,80	25	14,20	Begin retrieve streamer
MSM67_5-1	13.09.2017 10:44	Seismic Towed Receiver	PAM on deck	74° 50,820' N	012° 05,591' W	2042.0	4,1	56,30	24	15,30	
MSM67_5-1	13.09.2017 10:26	Seismic Towed Receiver	Magnetometer on deck	74° 50,240' N	012° 09,998' W	1977.7	9,2	57,70	25	13,80	On Deck due to maintenance work
MSM67_5-1	10.09.2017 14:50	Seismic Towed Receiver	information	71° 17,125' N	016° 51,473' W	1299.5	11,0	93,60	357	28,00	Streamer used with full length
MSM67_5-1	10.09.2017 14:06	Seismic Towed Receiver	information	71° 14,774' N	017° 00,889' W	1436.4	12,1	19,70	349	27,90	Streamer auf 2000 m retrieve
MSM67_5-1	10.09.2017 12:10	Seismic Towed Receiver	information	71° 06,567' N	017° 07,280' W	1509.7	12,1	7,80	351	24,50	Begin retrieve streamer
MSM67_5-1	10.09.2017 06:58	Seismic Towed Receiver	Magnetometer in water	70° 47,272' N	016° 34,806' W	1265.8	0,9	12,10	349	29,50	650m streamer lenght
MSM67_5-1	10.09.2017 05:48	Seismic Towed Receiver	PAM in water	70° 44,149' N	016° 36,627' W	1339.7	0,8	7,30	354	27,50	200m streamer lenght
MSM67_5-1	10.09.2017 05:10	Seismic Towed Receiver	Streamer in water	70° 41,039' N	016° 38,436' W	1412.5	2,3	12,50	357	25,90	4700m streamer lenght
MSM67_0_Underway-4	18.09.2017 03:58	Thermosalinograph	profile end	77° 57,409' N	012° 24,672' E	0.0	0,9	49,80	166	33,80	
MSM67_0_Underway-5	18.09.2017 03:05	Deep-sea Multibeam Echosounder	profile end	77° 57,409' N	012° 24,672' E	0.0	2,9	78,10	166	33,80	
MSM67_0_Underway-5	08.09.2017 22:55	Deep-sea Multibeam Echosounder	profile start	69° 06,233' N	009° 30,064' W	0.0	1,4	48,40	46	15,20	Simultaneous usage of EM712 und Parasound with variating configurations

MSM67_0_ Underway-4	08.09.2017 22:55	Thermosalinograph	profile start	69° 06,233' N	009° 30,064' W	0.0	1,7	48,40	46	15,20	
MSM67_4-1	06.09.2017 14:37	Expandedable Sound Velocimeter	information	69° 39,231' N	005° 31,550' W	0.0	1,4	172,40	124	8,10	End of measurement
MSM67_4-1	06.09.2017 14:25	Expandedable Sound Velocimeter	in the water	69° 39,231' N	005° 31,550' W	0.0	2,7	193,00	121	7,60	
MSM67_3-1	04.09.2017 17:06	Expandedable Sound Velocimeter	information	69° 44,673' N	011° 52,445' W	1691.1	2,9	315,10	119	29,70	End of measurement
MSM67_3-1	04.09.2017 17:01	Expandedable Sound Velocimeter	in the water	69° 44,669' N	011° 52,447' W	1692.3	4,8	356,10	117	30,80	
MSM67_2-2	04.09.2017 13:42	Seismic Towed Receiver	PAM on deck	69° 41,046' N	012° 01,559' W	1812.1	5,0	147,60	125	29,30	
MSM67_2-2	04.09.2017 13:36	Seismic Towed Receiver	Magnetometer on deck	69° 41,186' N	012° 01,952' W	1814.8	5,4	119,10	127	27,70	
MSM67_2-2	02.09.2017 23:57	Seismic Towed Receiver	Magnetometer in water	69° 42,662' N	005° 05,990' W	3149.3	5,9	204,30	207	24,20	652m streamer length
MSM67_2-2	02.09.2017 23:50	Seismic Towed Receiver	PAM in water	69° 42,848' N	005° 05,686' W	3146.6	1,6	206,50	208	25,20	200m streamer length
MSM67_2-1	04.09.2017 17 14:14	Seismic Source	Airgun on deck	69° 40,280' N	011° 59,393' W	1854.8	1,5	141,80	123	29,40	Stb. Array
MSM67_2-1	04.09.2017 13:16	Seismic Source	Airgun on deck	69° 41,661' N	012° 03,296' W	1822.0	0,6	146,70	128	26,90	Bb. Array
MSM67_2-1	04.09.2017 12:01	Seismic Source	profile end	69° 44,072' N	012° 03,004' W	2857.7	3,2	258,60	131	27,00	
MSM67_2-1	03.09.2017 02:57	Seismic Source	profile start	69° 38,617' N	005° 14,928' W	3014.9	2,4	262,80	198	29,40	v= 4,5 kn; rwK 275–
MSM67_2-1	03.09.2017 02:16	Seismic Source	information	69° 39,791' N	005° 14,581' W	3035.5	4,2	79,70	205	24,60	End "Soft-Start"
MSM67_2-1	03.09.2017 01:47	Seismic Source	information	69° 38,878' N	005° 12,286' W	3026.5	1,6	238,40	206	26,30	Beginn "Soft-Start"
MSM67_2-1	03.09.2017 00:28	Seismic Source	Airgun in water	69° 41,763' N	005° 07,446' W	3148.6	2,4	211,60	205	28,00	40m Bb. Array with 8 G-Guns
MSM67_2-1	02.09.2017 23:10	Seismic Source	Airgun in water	69° 44,003' N	005° 03,811' W	3171.1	3,9	213,30	214	24,40	40m Stb. Array with 8 G-Guns
MSM67_1-30	06.09.2017 14:24	Seismic Ocean Bottom Receiver	on deck	69° 39,230' N	005° 31,555' W	0.0	0,9	180,60	129	8,40	
MSM67_1-30	06.09.2017 14:14	Seismic Ocean Bottom Receiver	at surface	69° 39,706' N	005° 31,740' W	0.0	0,9	155,90	129	8,70	
MSM67_1-30	06.09.2017 13:41	Seismic Ocean Bottom Receiver	Hydrophon on deck	69° 39,743' N	005° 45,169' W	0.0	1,0	303,20	142	7,90	
MSM67_1-30	06.09.2017 13:35	Seismic Ocean Bottom Receiver	released	69° 39,719' N	005° 45,022' W	0.0	2,6	262,50	144	7,70	
MSM67_1-30	06.09.2017 13:33	Seismic Ocean Bottom Receiver	Hydrophon in water	69° 39,718' N	005° 44,978' W	0.0	3,3	185,30	130	8,00	
MSM67_1-30	02.09.2017 21:42	Seismic Ocean Bottom Receiver	OBS deployed	69° 39,124' N	005° 31,269' W	2991.6	6,2	17,00	214	21,40	Geomar 98
MSM67_1-29	06.09.2017 13:32	Seismic Ocean Bottom Receiver	on deck	69° 39,729' N	005° 44,971' W	0.0	0,2	160,90	131	7,90	
MSM67_1-29	06.09.2017 13:26	Seismic Ocean Bottom Receiver	at surface	69° 39,923' N	005° 45,175' W	0.0	0,7	165,90	130	9,30	

MSM67_1-29	06.09.2017 12:54	Seismic Ocean Bottom Receiver	Hydrophon on deck	69° 39,809' N	005° 58,247' W	0.0	0,2	246,80	129	7,30	
MSM67_1-29	06.09.2017 12:50	Seismic Ocean Bottom Receiver	released	69° 39,814' N	005° 58,184' W	0.0	1,2	246,10	114	7,90	
MSM67_1-29	06.09.2017 12:47	Seismic Ocean Bottom Receiver	Hydrophon in water	69° 39,817' N	005° 58,144' W	0.0	1,1	344,40	109	7,80	
MSM67_1-29	02.09.2017 21:11	Seismic Ocean Bottom Receiver	OBS deployed	69° 39,562' N	005° 44,636' W	2958.3	2,4	42944,00	196	19,00	Geomar 98
MSM67_1-28	06.09.2017 12:47	Seismic Ocean Bottom Receiver	on deck	69° 39,817' N	005° 58,138' W	0.0	1,4	267,10	115	7,60	
MSM67_1-28	06.09.2017 12:34	Seismic Ocean Bottom Receiver	at surface	69° 40,511' N	005° 58,515' W	0.0	1,9	159,10	89	6,00	
MSM67_1-28	06.09.2017 12:06	Seismic Ocean Bottom Receiver	Hydrophon on deck	69° 40,146' N	006° 11,529' W	0.0	0,9	165,80	119	7,30	
MSM67_1-28	06.09.2017 12:02	Seismic Ocean Bottom Receiver	released	69° 40,179' N	006° 11,488' W	0.0	0,3	193,40	118	6,60	
MSM67_1-28	06.09.2017 12:00	Seismic Ocean Bottom Receiver	Hydrophon in water	69° 40,181' N	006° 11,449' W	0.0	1,2	230,40	115	6,10	
MSM67_1-28	02.09.2017 20:37	Seismic Ocean Bottom Receiver	OBS deployed	69° 39,945' N	005° 58,039' W	2898.1	1,6	320,00	192	20,10	Geomar 99
MSM67_1-27	06.09.2017 12:00	Seismic Ocean Bottom Receiver	on deck	69° 40,178' N	006° 11,427' W	0.0	2,1	329,50	118	6,40	
MSM67_1-27	06.09.2017 11:44	Seismic Ocean Bottom Receiver	at surface	69° 40,544' N	006° 11,572' W	0.0	1,0	149,00	108	12,20	
MSM67_1-27	06.09.2017 11:13	Seismic Ocean Bottom Receiver	Hydrophon on deck	69° 40,596' N	006° 24,187' W	0.0	0,1	179,40	154	6,80	
MSM67_1-27	06.09.2017 11:03	Seismic Ocean Bottom Receiver	released	69° 40,669' N	006° 24,277' W	2656.5	1,2	347,90	145	10,20	
MSM67_1-27	06.09.2017 11:03	Seismic Ocean Bottom Receiver	Hydrophon in water	69° 40,665' N	006° 24,269' W	2659.8	1,9	12,50	139	9,90	
MSM67_1-27	02.09.2017 20:04	Seismic Ocean Bottom Receiver	OBS deployed	69° 40,304' N	006° 11,328' W	2813.9	1,4	268,80	198	18,30	Geomar 100
MSM67_1-26	06.09.2017 11:02	Seismic Ocean Bottom Receiver	on deck	69° 40,655' N	006° 24,235' W	2660.1	1,7	290,50	127	10,00	
MSM67_1-26	06.09.2017 10:42	Seismic Ocean Bottom Receiver	at surface	69° 41,040' N	006° 25,409' W	2645.2	1,8	1,30	117	10,10	
MSM67_1-26	06.09.2017 10:28	Seismic Ocean Bottom Receiver	released	69° 41,038' N	006° 25,413' W	2647.5	2,1	354,10	96	11,00	
MSM67_1-26	06.09.2017 10:16	Seismic Ocean Bottom Receiver	Hydrophon in water	69° 41,039' N	006° 25,410' W	2704.3	1,9	175,40	94	9,80	
MSM67_1-26	06.09.2017 09:49	Seismic Ocean Bottom Receiver	Hydrophon on deck	69° 41,273' N	006° 37,166' W	2634.3	1,2	141,90	100	10,10	
MSM67_1-26	06.09.2017 09:48	Seismic Ocean Bottom Receiver	released	69° 41,273' N	006° 37,167' W	2634.3	0,5	83,20	101	10,10	
MSM67_1-26	06.09.2017 09:44	Seismic Ocean Bottom Receiver	Hydrophon in water	69° 41,279' N	006° 37,187' W	2637.3	1,0	19,10	85	9,90	
MSM67_1-26	02.09.2017 19:31	Seismic Ocean Bottom Receiver	OBS deployed	69° 40,669' N	006° 24,669' W	2715.2	1,4	244,30	197	16,30	DanSeis 101
MSM67_1-25	06.09.2017 06:12	Seismic Ocean Bottom Receiver	on deck	69° 41,141' N	006° 37,690' W	2579.0	1,3	355,60	87	3,50	

MSM67_1-25	06.09.2017 05:58	Seismic Ocean Bottom Receiver	Hydrophon on deck	69° 41,288' N	006° 38,561' W	2572.5	0,3	193,70	123	4,90	
MSM67_1-25	06.09.2017 05:58	Seismic Ocean Bottom Receiver	at surface	69° 41,288' N	006° 38,561' W	2571.5	0,8	58,80	123	4,90	
MSM67_1-25	06.09.2017 05:51	Seismic Ocean Bottom Receiver	released	69° 41,286' N	006° 38,573' W	2571.1	0,9	19,10	124	4,40	
MSM67_1-25	06.09.2017 05:41	Seismic Ocean Bottom Receiver	Hydrophon in water	69° 41,278' N	006° 38,593' W	2572.4	0,8	300,50	116	4,40	
MSM67_1-25	06.09.2017 05:09	Seismic Ocean Bottom Receiver	Hydrophon on deck	69° 41,475' N	006° 51,516' W	2506.6	0,7	284,70	123	4,40	
MSM67_1-25	06.09.2017 05:09	Seismic Ocean Bottom Receiver	released	69° 41,473' N	006° 51,508' W	2506.5	0,1	278,70	121	4,20	
MSM67_1-25	06.09.2017 05:04	Seismic Ocean Bottom Receiver	Hydrophon in water	69° 41,450' N	006° 51,386' W	2505.5	0,7	305,50	118	4,40	
MSM67_1-25	02.09.2017 18:55	Seismic Ocean Bottom Receiver	OBS deployed	69° 41,004' N	006° 38,067' W	2634.3	0,4	297,50	200	18,90	DanSeis 102
MSM67_1-24	06.09.2017 05:03	Seismic Ocean Bottom Receiver	on deck	69° 41,451' N	006° 51,375' W	2506.2	1,2	280,20	122	4,30	
MSM67_1-24	06.09.2017 04:54	Seismic Ocean Bottom Receiver	Hydrophon on deck	69° 41,573' N	006° 52,008' W	2505.0	0,7	142,30	124	4,80	
MSM67_1-24	06.09.2017 04:54	Seismic Ocean Bottom Receiver	at surface	69° 41,573' N	006° 52,008' W	2502.8	1,5	143,20	126	5,10	
MSM67_1-24	06.09.2017 04:19	Seismic Ocean Bottom Receiver	released	69° 41,572' N	006° 52,006' W	2505.9	1,7	266,80	112	4,60	
MSM67_1-24	06.09.2017 04:03	Seismic Ocean Bottom Receiver	released	69° 41,574' N	006° 52,010' W	2505.8	1,7	92,50	130	5,80	
MSM67_1-24	06.09.2017 04:02	Seismic Ocean Bottom Receiver	Hydrophon in water	69° 41,573' N	006° 52,006' W	2503.8	2,0	133,30	128	5,80	
MSM67_1-24	06.09.2017 03:29	Seismic Ocean Bottom Receiver	Hydrophon on deck	69° 41,533' N	007° 05,698' W	2445.7	3,1	135,90	121	7,70	
MSM67_1-24	06.09.2017 03:28	Seismic Ocean Bottom Receiver	released	69° 41,542' N	007° 05,689' W	2443.3	1,6	192,90	134	7,00	
MSM67_1-24	06.09.2017 03:24	Seismic Ocean Bottom Receiver	Hydrophon in water	69° 41,532' N	007° 05,569' W	2448.7	3,2	308,30	113	6,10	
MSM67_1-24	02.09.2017 18:20	Seismic Ocean Bottom Receiver	OBS deployed	69° 41,381' N	006° 51,395' W	2556.8	0,5	306,50	201	17,30	DanSeis 103
MSM67_1-23	06.09.2017 03:21	Seismic Ocean Bottom Receiver	on deck	69° 41,529' N	007° 05,448' W	2444.5	0,9	233,60	121	9,50	
MSM67_1-23	06.09.2017 02:57	Seismic Ocean Bottom Receiver	at surface	69° 41,918' N	007° 05,636' W	2447.9	0,1	307,80	114	9,50	
MSM67_1-23	06.09.2017 02:57	Seismic Ocean Bottom Receiver	released	69° 41,917' N	007° 05,634' W	2449.5	0,2	319,10	112	9,70	
MSM67_1-23	06.09.2017 02:56	Seismic Ocean Bottom Receiver	Hydrophon in water	69° 41,914' N	007° 05,625' W	2447.6	0,2	302,80	111	9,80	
MSM67_1-23	06.09.2017 02:12	Seismic Ocean Bottom Receiver	Hydrophon on deck	69° 41,756' N	007° 19,754' W	2308.4	0,2	228,70	101	9,50	
MSM67_1-23	06.09.2017 02:10	Seismic Ocean Bottom Receiver	released	69° 41,764' N	007° 19,702' W	2305.7	0,2	224,90	95	10,40	
MSM67_1-23	06.09.2017 02:03	Seismic Ocean Bottom Receiver	Hydrophon in water	69° 41,776' N	007° 19,371' W	2308.8	0,5	280,40	104	9,20	

MSM67_1-23	02.09.2017 17:46	Seismic Ocean Bottom Receiver	OBS deployed	69° 41,630' N	007° 04,772' W	2495.9	0,2	268,90	200	13,60	DanSeis 104
MSM67_1-22	06.09.2017 01:45	Seismic Ocean Bottom Receiver	on deck	69° 42,248' N	007° 19,055' W	2319.1	0,6	212,90	121	12,40	
MSM67_1-22	06.09.2017 01:45	Seismic Ocean Bottom Receiver	Hydrophon on deck	69° 42,248' N	007° 19,057' W	2312.2	0,3	152,50	125	11,50	
MSM67_1-22	06.09.2017 01:43	Seismic Ocean Bottom Receiver	at surface	69° 42,245' N	007° 19,060' W	2319.5	0,1	60,10	128	11,40	
MSM67_1-22	06.09.2017 01:08	Seismic Ocean Bottom Receiver	released	69° 42,246' N	007° 19,064' W	2318.7	0,5	357,00	119	12,20	
MSM67_1-22	06.09.2017 01:04	Seismic Ocean Bottom Receiver	Hydrophon in water	69° 42,248' N	007° 19,060' W	2319.3	0,1	303,00	117	12,30	
MSM67_1-22	02.09.2017 17:12	Seismic Ocean Bottom Receiver	OBS deployed	69° 41,922' N	007° 18,205' W	2517.4	0,6	290,90	183	11,10	DanSeis 105
MSM67_1-21	09.09.2017 07:48	Seismic Ocean Bottom Receiver	information	69° 42,191' N	007° 31,612' W	1963.5	0,3	76,20	32	15,70	Device did not emerge. Station was ended.
MSM67_1-21	09.09.2017 07:18	Seismic Ocean Bottom Receiver	Hydrophon on deck	69° 42,024' N	007° 32,185' W	1917.0	1,1	170,70	42	16,60	
MSM67_1-21	09.09.2017 06:03	Seismic Ocean Bottom Receiver	information	69° 41,927' N	007° 32,520' W	1909.2	3,8	0,30	49	19,40	Waited for time release, OBS not to be seen after repeated releasing
MSM67_1-21	09.09.2017 06:03	Seismic Ocean Bottom Receiver	released	69° 41,927' N	007° 32,520' W	1909.2	0,4	310,20	49	19,30	
MSM67_1-21	09.09.2017 06:01	Seismic Ocean Bottom Receiver	Hydrophon in water	69° 41,927' N	007° 32,521' W	1908.7	1,0	122,70	51	16,90	
MSM67_1-21	09.09.2017 05:44	Seismic Ocean Bottom Receiver	Hydrophon on deck	69° 41,950' N	007° 30,588' W	1985.5	1,0	226,40	51	16,00	
MSM67_1-21	09.09.2017 05:43	Seismic Ocean Bottom Receiver	released	69° 41,956' N	007° 30,577' W	1985.2	3,0	214,20	53	17,30	
MSM67_1-21	09.09.2017 05:36	Seismic Ocean Bottom Receiver	Hydrophon in water	69° 41,976' N	007° 30,522' W	1983.3	3,4	50,70	50	17,30	
MSM67_1-21	09.09.2017 05:25	Seismic Ocean Bottom Receiver	Hydrophon on deck	69° 42,487' N	007° 32,628' W	1889.1	1,4	343,60	51	19,10	
MSM67_1-21	09.09.2017 05:24	Seismic Ocean Bottom Receiver	released	69° 42,486' N	007° 32,626' W	1889.4	0,6	288,00	50	15,80	
MSM67_1-21	09.09.2017 05:16	Seismic Ocean Bottom Receiver	Hydrophon in water	69° 42,486' N	007° 32,629' W	1889.5	2,3	334,40	42	16,50	
MSM67_1-21	09.09.2017 05:06	Seismic Ocean Bottom Receiver	Hydrophon on deck	69° 41,878' N	007° 32,641' W	1907.9	0,9	306,60	56	18,00	
MSM67_1-21	09.09.2017 05:00	Seismic Ocean Bottom Receiver	released	69° 41,877' N	007° 32,646' W	1908.0	0,6	123,10	50	18,40	
MSM67_1-21	09.09.2017 04:59	Seismic Ocean Bottom Receiver	Hydrophon in water	69° 41,877' N	007° 32,648' W	1907.9	1,3	166,60	49	17,30	
MSM67_1-21	06.09.2017 01:11	Seismic Ocean Bottom Receiver	information	69° 42,248' N	007° 19,062' W	2318.0	1,7	192,90	124	12,20	OBS did not emerge, waited for time release!
MSM67_1-21	05.09.2017 23:01	Seismic Ocean Bottom Receiver	released	69° 41,710' N	007° 30,231' W	2012.3	1,8	321,90	124	9,40	
MSM67_1-21	05.09.2017 22:13	Seismic Ocean Bottom Receiver	Hydrophon on deck	69° 42,535' N	007° 32,358' W	1900.7	1,8	349,20	133	11,90	
MSM67_1-21	05.09.2017 21:45	Seismic Ocean Bottom Receiver	released	69° 42,535' N	007° 32,355' W	1899.9	0,2	340,10	139	11,70	

MSM67_1-21	05.09.2017 21:44	Seismic Ocean Bottom Receiver	Hydrophon in water	69° 42,534' N	007° 32,357' W	1900.8	0,9	140,60	127	12,20	
MSM67_1-21	05.09.2017 21:15	Seismic Ocean Bottom Receiver	Hydrophon on deck	69° 42,419' N	007° 45,142' W	1510.8	0,1	138,00	139	14,70	
MSM67_1-21	05.09.2017 21:14	Seismic Ocean Bottom Receiver	released	69° 42,435' N	007° 45,186' W	1502.6	1,0	145,30	137	14,40	
MSM67_1-21	05.09.2017 21:07	Seismic Ocean Bottom Receiver	Hydrophon in water	69° 42,452' N	007° 45,258' W	1500.8	1,8	295,30	142	14,60	
MSM67_1-21	02.09.2017 16:40	Seismic Ocean Bottom Receiver	OBS deployed	69° 42,200' N	007° 31,601' W	1964.9	1,7	334,20	192	11,90	DanSeis 106
MSM67_1-20	05.09.2017 21:07	Seismic Ocean Bottom Receiver	on deck	69° 42,449' N	007° 45,241' W	1501.5	2,5	319,80	146	15,10	
MSM67_1-20	05.09.2017 20:52	Seismic Ocean Bottom Receiver	Hydrophon on deck	69° 42,798' N	007° 45,760' W	1426.9	1,0	142,50	136	15,90	
MSM67_1-20	05.09.2017 20:50	Seismic Ocean Bottom Receiver	at surface	69° 42,800' N	007° 45,767' W	1423.5	1,4	196,80	137	16,60	
MSM67_1-20	05.09.2017 20:15	Seismic Ocean Bottom Receiver	released	69° 42,802' N	007° 45,771' W	1426.4	1,9	251,90	127	17,30	
MSM67_1-20	05.09.2017 20:13	Seismic Ocean Bottom Receiver	Hydrophon in water	69° 42,801' N	007° 45,767' W	1426.8	0,5	164,00	127	16,80	
MSM67_1-20	05.09.2017 19:44	Seismic Ocean Bottom Receiver	Hydrophon on deck	69° 42,676' N	007° 58,552' W	1010.5	0,6	138,80	127	16,70	
MSM67_1-20	05.09.2017 19:44	Seismic Ocean Bottom Receiver	released	69° 42,677' N	007° 58,555' W	1010.7	1,1	129,90	128	16,60	
MSM67_1-20	05.09.2017 19:38	Seismic Ocean Bottom Receiver	Hydrophon in water	69° 42,696' N	007° 58,447' W	1012.3	1,2	268,70	118	17,70	
MSM67_1-20	02.09.2017 16:05	Seismic Ocean Bottom Receiver	OBS deployed	69° 42,460' N	007° 45,008' W	2934.7	1,4	9,70	181	9,20	DanSeis 107
MSM67_1-19	05.09.2017 19:37	Seismic Ocean Bottom Receiver	on deck	69° 42,698' N	007° 58,444' W	1013.2	0,4	233,70	119	17,70	
MSM67_1-19	05.09.2017 19:28	Seismic Ocean Bottom Receiver	Hydrophon on deck	69° 42,910' N	007° 59,210' W	992.4	1,2	123,50	131	16,90	
MSM67_1-19	05.09.2017 19:28	Seismic Ocean Bottom Receiver	at surface	69° 42,910' N	007° 59,212' W	991.2	2,2	142,50	131	16,90	
MSM67_1-19	05.09.2017 19:01	Seismic Ocean Bottom Receiver	released	69° 42,867' N	007° 59,083' W	995.9	2,6	134,60	126	18,00	
MSM67_1-19	05.09.2017 18:58	Seismic Ocean Bottom Receiver	Hydrophon in water	69° 42,864' N	007° 59,073' W	825.3	0,8	125,10	133	18,50	
MSM67_1-19	05.09.2017 18:25	Seismic Ocean Bottom Receiver	Hydrophon on deck	69° 43,028' N	008° 12,018' W	908.5	0,7	310,00	129	19,10	
MSM67_1-19	05.09.2017 18:25	Seismic Ocean Bottom Receiver	released	69° 43,026' N	008° 12,015' W	908.1	1,9	310,20	130	19,70	
MSM67_1-19	05.09.2017 18:21	Seismic Ocean Bottom Receiver	Hydrophon in water	69° 43,001' N	008° 11,993' W	908.2	1,8	153,80	128	20,60	
MSM67_1-19	02.09.2017 15:28	Seismic Ocean Bottom Receiver	OBS deployed	69° 42,702' N	007° 58,366' W	1024.7	0,7	329,60	187	6,90	DanSeis 108
MSM67_1-18	05.09.2017 18:20	Seismic Ocean Bottom Receiver	on deck	69° 43,005' N	008° 11,982' W	908.6	1,0	203,40	123	20,60	
MSM67_1-18	05.09.2017 18:12	Seismic Ocean Bottom Receiver	Hydrophon on deck	69° 43,155' N	008° 12,705' W	900.8	2,0	113,70	126	20,70	

MSM67_1-18	05.09.2017 18:11	Seismic Ocean Bottom Receiver	at surface	69° 43,156' N	008° 12,706' W	900.9	1,1	345,00	130	21,00	
MSM67_1-18	05.09.2017 17:58	Seismic Ocean Bottom Receiver	released	69° 43,155' N	008° 12,705' W	900.5	2,0	12,10	127	22,00	
MSM67_1-18	05.09.2017 17:54	Seismic Ocean Bottom Receiver	Hydrophon in water	69° 43,157' N	008° 12,703' W	900.8	0,7	169,50	126	21,80	
MSM67_1-18	05.09.2017 17:22	Seismic Ocean Bottom Receiver	Hydrophon on deck	69° 43,192' N	008° 25,701' W	870.6	2,9	106,30	120	23,00	
MSM67_1-18	05.09.2017 17:22	Seismic Ocean Bottom Receiver	released	69° 43,192' N	008° 25,708' W	869.1	10,9	104,70	120	22,80	
MSM67_1-18	05.09.2017 17:17	Seismic Ocean Bottom Receiver	Hydrophon in water	69° 43,180' N	008° 25,548' W	862.2	1,9	219,50	112	23,20	
MSM67_1-18	02.09.2017 14:51	Seismic Ocean Bottom Receiver	OBS deployed	69° 42,929' N	008° 11,776' W	1137.6	2,1	1,50	199	8,40	DanSeis 109
MSM67_1-17	05.09.2017 17:16	Seismic Ocean Bottom Receiver	on deck	69° 43,183' N	008° 25,529' W	863.0	2,4	216,80	111	22,80	
MSM67_1-17	05.09.2017 17:10	Seismic Ocean Bottom Receiver	Hydrophon on deck	69° 43,334' N	008° 26,069' W	832.7	0,2	328,00	113	24,00	
MSM67_1-17	05.09.2017 17:10	Seismic Ocean Bottom Receiver	at surface	69° 43,333' N	008° 26,068' W	832.5	1,1	281,20	112	24,30	
MSM67_1-17	05.09.2017 16:45	Seismic Ocean Bottom Receiver	released	69° 43,333' N	008° 26,066' W	832.9	6,5	118,60	113	22,00	
MSM67_1-17	05.09.2017 16:41	Seismic Ocean Bottom Receiver	Hydrophon in water	69° 43,333' N	008° 26,066' W	831.2	1,1	349,90	107	23,50	
MSM67_1-17	05.09.2017 16:07	Seismic Ocean Bottom Receiver	Hydrophon on deck	69° 43,482' N	008° 39,673' W	1175.5	1,1	250,90	103	22,60	
MSM67_1-17	05.09.2017 16:06	Seismic Ocean Bottom Receiver	released	69° 43,484' N	008° 39,614' W	1174.2	1,0	208,70	105	23,10	
MSM67_1-17	05.09.2017 16:01	Seismic Ocean Bottom Receiver	Hydrophon in water	69° 43,484' N	008° 39,338' W	1177.8	0,5	271,50	101	24,00	
MSM67_1-17	02.09.2017 14:14	Seismic Ocean Bottom Receiver	OBS deployed	69° 43,137' N	008° 25,199' W	847.0	0,7	310,50	177	7,10	DanSeis 110
MSM67_1-16	05.09.2017 16:01	Seismic Ocean Bottom Receiver	on deck	69° 43,483' N	008° 39,324' W	1177.7	1,0	278,00	101	24,20	
MSM67_1-16	05.09.2017 15:42	Seismic Ocean Bottom Receiver	at surface	69° 43,601' N	008° 45,309' W	1276.1	11,2	77,10	111	23,50	
MSM67_1-16	05.09.2017 15:22	Seismic Ocean Bottom Receiver	Hydrophon on deck	69° 43,583' N	008° 53,090' W	1731.0	2,4	234,30	100	22,80	
MSM67_1-16	05.09.2017 15:17	Seismic Ocean Bottom Receiver	released	69° 43,566' N	008° 52,777' W	1728.6	2,4	302,70	104	22,00	
MSM67_1-16	05.09.2017 15:15	Seismic Ocean Bottom Receiver	Hydrophon in water	69° 43,554' N	008° 52,659' W	1730.9	0,8	282,20	101	22,40	
MSM67_1-16	02.09.2017 13:38	Seismic Ocean Bottom Receiver	OBS deployed	69° 43,315' N	008° 38,587' W	1212.4	1,3	348,00	189	7,70	Geomar 111
MSM67_1-15	05.09.2017 15:15	Seismic Ocean Bottom Receiver	on deck	69° 43,552' N	008° 52,644' W	1731.2	6,9	317,30	102	22,10	
MSM67_1-15	05.09.2017 15:06	Seismic Ocean Bottom Receiver	at surface	69° 44,155' N	008° 53,286' W	1639.1	0,9	147,40	104	23,90	
MSM67_1-15	05.09.2017 14:32	Seismic Ocean Bottom Receiver	Hydrophon on deck	69° 43,754' N	009° 06,253' W	1994.3	0,2	230,50	111	22,50	

MSM67_1-15	05.09.2017 14:30	Seismic Ocean Bottom Receiver	released	69° 43,741' N	009° 06,160' W	1996.0	0,3	272,10	103	23,20	
MSM67_1-15	05.09.2017 14:27	Seismic Ocean Bottom Receiver	Hydrophon in water	69° 43,701' N	009° 05,905' W	1990.9	0,9	317,50	106	23,10	
MSM67_1-15	02.09.2017 13:01	Seismic Ocean Bottom Receiver	OBS deployed	69° 43,483' N	008° 52,031' W	1730.5	0,7	304,70	186	14,60	Geomar 112
MSM67_1-14	05.09.2017 14:26	Seismic Ocean Bottom Receiver	on deck	69° 43,698' N	009° 05,848' W	1990.7	9,6	312,10	103	22,30	
MSM67_1-14	05.09.2017 14:07	Seismic Ocean Bottom Receiver	at surface	69° 43,902' N	009° 11,725' W	2017.8	2,2	69,90	111	22,90	
MSM67_1-14	05.09.2017 13:40	Seismic Ocean Bottom Receiver	released	69° 43,795' N	009° 19,222' W	2079.5	0,9	296,00	98	21,00	
MSM67_1-14	05.09.2017 13:39	Seismic Ocean Bottom Receiver	Hydrophon in water	69° 43,788' N	009° 19,120' W	2080.9	1,3	266,30	98	20,40	
MSM67_1-14	02.09.2017 12:25	Seismic Ocean Bottom Receiver	OBS deployed	69° 43,655' N	009° 05,415' W	2012.7	0,7	336,10	176	17,30	Geomar 113
MSM67_1-13	05.09.2017 13:38	Seismic Ocean Bottom Receiver	on deck	69° 43,787' N	009° 19,095' W	2079.8	0,6	310,60	98	20,30	
MSM67_1-13	05.09.2017 13:28	Seismic Ocean Bottom Receiver	at surface	69° 44,313' N	009° 20,167' W	2068.9	7,5	141,50	100	22,30	
MSM67_1-13	05.09.2017 12:57	Seismic Ocean Bottom Receiver	Hydrophon on deck	69° 43,976' N	009° 32,641' W	2085.0	7,1	125,30	99	21,50	
MSM67_1-13	05.09.2017 12:53	Seismic Ocean Bottom Receiver	released	69° 43,974' N	009° 32,526' W	2091.1	1,0	340,90	103	21,10	
MSM67_1-13	05.09.2017 12:50	Seismic Ocean Bottom Receiver	Hydrophon in water	69° 43,966' N	009° 32,510' W	2089.5	1,8	351,90	100	21,30	
MSM67_1-13	02.09.2017 11:53	Seismic Ocean Bottom Receiver	OBS deployed	69° 43,790' N	009° 18,821' W	2534.4	0,6	287,90	182	13,90	Geomar 114
MSM67_1-12	05.09.2017 12:50	Seismic Ocean Bottom Receiver	on deck	69° 43,968' N	009° 32,513' W	2090.3	0,7	200,00	101	20,40	
MSM67_1-12	05.09.2017 12:41	Seismic Ocean Bottom Receiver	at surface	69° 44,443' N	009° 33,636' W	2089.9	1,3	107,70	106	21,10	
MSM67_1-12	05.09.2017 12:14	Seismic Ocean Bottom Receiver	Hydrophon on deck	69° 44,144' N	009° 46,459' W	1919.3	0,9	272,50	100	19,00	
MSM67_1-12	05.09.2017 12:10	Seismic Ocean Bottom Receiver	released	69° 44,102' N	009° 46,239' W	1930.7	0,1	308,80	110	17,90	
MSM67_1-12	05.09.2017 12:07	Seismic Ocean Bottom Receiver	Hydrophon in water	69° 44,091' N	009° 46,228' W	1929.4	1,5	203,00	102	19,00	
MSM67_1-12	02.09.2017 11:20	Seismic Ocean Bottom Receiver	OBS deployed	69° 43,915' N	009° 32,300' W	2134.5	0,6	320,50	188	15,80	Geomar 115
MSM67_1-11	05.09.2017 12:06	Seismic Ocean Bottom Receiver	on deck	69° 44,093' N	009° 46,219' W	1930.0	2,1	236,70	101	18,70	
MSM67_1-11	05.09.2017 11:57	Seismic Ocean Bottom Receiver	at surface	69° 44,422' N	009° 46,895' W	1908.4	0,5	92,70	116	18,70	
MSM67_1-11	05.09.2017 11:56	Seismic Ocean Bottom Receiver	at surface	69° 44,417' N	009° 47,621' W	1921.2	0,9	88,20	112	19,90	
MSM67_1-11	05.09.2017 11:22	Seismic Ocean Bottom Receiver	Hydrophon on deck	69° 44,049' N	009° 59,437' W	2145.7	0,6	163,00	115	17,30	
MSM67_1-11	05.09.2017 11:21	Seismic Ocean Bottom Receiver	released	69° 44,050' N	009° 59,435' W	2141.3	2,1	154,10	116	16,50	

MSM67_1-11	05.09.2017 11:19	Seismic Ocean Bottom Receiver	Hydrophon in water	69° 44,052' N	009° 59,42 2' W	2144.5	2,2	288,10	117	17,60	
MSM67_1-11	02.09.2017 10:46	Seismic Ocean Bottom Receiver	OBS deployed	69° 44,032' N	009° 45,66 6' W	1968.0	2,5	38,00	195	17,40	Geomar 116
MSM67_1-10	05.09.2017 11:19	Seismic Ocean Bottom Receiver	on deck	69° 44,054' N	009° 59,41 6' W	2144.3	1,4	181,80	117	17,90	
MSM67_1-10	05.09.2017 11:11	Seismic Ocean Bottom Receiver	Hydrophon on deck	69° 44,362' N	009° 59,81 5' W	2145.2	2,4	42803,00	120	16,20	
MSM67_1-10	05.09.2017 11:11	Seismic Ocean Bottom Receiver	at surface	69° 44,362' N	009° 59,81 5' W	2144.7	0,5	181,60	121	15,80	
MSM67_1-10	05.09.2017 10:30	Seismic Ocean Bottom Receiver	released	69° 44,361' N	009° 59,81 9' W	2141.3	0,2	140,20	133	19,20	
MSM67_1-10	05.09.2017 10:26	Seismic Ocean Bottom Receiver	Hydrophon in water	69° 44,361' N	009° 59,81 9' W	2143.5	0,9	168,10	131	18,80	
MSM67_1-10	05.09.2017 09:52	Seismic Ocean Bottom Receiver	Hydrophon on deck	69° 44,076' N	010° 13,29 1' W	2144.2	1,0	332,50	119	16,90	
MSM67_1-10	05.09.2017 09:51	Seismic Ocean Bottom Receiver	released	69° 44,077' N	010° 13,29 4' W	2146.3	0,2	38,70	124	16,60	
MSM67_1-10	05.09.2017 09:47	Seismic Ocean Bottom Receiver	Hydrophon in water	69° 44,092' N	010° 13,27 4' W	2147.4	0,4	178,00	125	16,80	
MSM67_1-10	02.09.2017 10:13	Seismic Ocean Bottom Receiver	OBS deployed	69° 44,090' N	009° 59,12 1' W	2343.6	0,1	40,80	195	15,60	DanSeis 117
MSM67_1-9	05.09.2017 09:46	Seismic Ocean Bottom Receiver	on deck	69° 44,084' N	010° 13,15 6' W	2145.9	2,8	295,40	132	15,00	
MSM67_1-9	05.09.2017 09:35	Seismic Ocean Bottom Receiver	Hydrophon on deck	69° 44,505' N	010° 13,46 0' W	2145.4	0,7	151,80	126	15,90	
MSM67_1-9	05.09.2017 09:25	Seismic Ocean Bottom Receiver	released	69° 44,512' N	010° 13,47 3' W	2140.2	2,6	355,90	127	17,40	
MSM67_1-9	05.09.2017 08:46	Seismic Ocean Bottom Receiver	released	69° 44,510' N	010° 13,47 2' W	2140.6	1,8	246,30	133	20,30	
MSM67_1-9	05.09.2017 08:42	Seismic Ocean Bottom Receiver	Hydrophon in water	69° 44,511' N	010° 13,47 4' W	2143.7	1,0	61,00	136	20,20	
MSM67_1-9	05.09.2017 08:08	Seismic Ocean Bottom Receiver	Hydrophon on deck	69° 44,168' N	010° 26,35 1' W	1762.9	1,4	295,40	144	22,10	
MSM67_1-9	05.09.2017 08:07	Seismic Ocean Bottom Receiver	released	69° 44,166' N	010° 26,35 2' W	1763.0	0,7	176,20	143	20,60	
MSM67_1-9	05.09.2017 08:00	Seismic Ocean Bottom Receiver	Hydrophon in water	69° 44,174' N	010° 26,33 1' W	1762.5	2,0	196,50	140	20,90	
MSM67_1-9	02.09.2017 09:40	Seismic Ocean Bottom Receiver	OBS deployed	69° 44,172' N	010° 12,58 7' W	2181.6	1,4	13,20	189	17,30	DanSeis 118
MSM67_1-8	05.09.2017 08:00	Seismic Ocean Bottom Receiver	on deck	69° 44,175' N	010° 26,32 8' W	1759.6	1,3	277,90	142	20,70	
MSM67_1-8	05.09.2017 07:51	Seismic Ocean Bottom Receiver	Hydrophon on deck	69° 44,523' N	010° 26,78 0' W	1741.5	0,3	252,40	143	21,00	
MSM67_1-8	05.09.2017 07:50	Seismic Ocean Bottom Receiver	at surface	69° 44,523' N	010° 26,77 9' W	1741.7	2,2	304,90	143	21,50	
MSM67_1-8	05.09.2017 07:23	Seismic Ocean Bottom Receiver	released	69° 44,522' N	010° 26,78 0' W	1738.8	2,8	288,60	148	20,80	
MSM67_1-8	05.09.2017 07:19	Seismic Ocean Bottom Receiver	released	69° 44,523' N	010° 26,77 8' W	1739.4	0,7	125,30	146	20,80	

MSM67_1-8	05.09.20 17 07:12	Seismic Ocean Bottom Receiver	Hydrophon in water	69° 44,511' N	010° 26,68 4' W	1746.3	2,6	118,20	136	19,30	
MSM67_1-8	05.09.20 17 06:42	Seismic Ocean Bottom Receiver	Hydrophon on deck	69° 44,348' N	010° 39,74 8' W	1550.8	1,8	158,40	140	19,00	
MSM67_1-8	05.09.20 17 06:40	Seismic Ocean Bottom Receiver	released	69° 44,349' N	010° 39,72 7' W	1550.9	1,0	310,70	141	19,20	
MSM67_1-8	05.09.20 17 06:35	Seismic Ocean Bottom Receiver	Hydrophon in water	69° 44,334' N	010° 39,66 4' W	1552.8	1,4	344,00	144	20,10	
MSM67_1-8	02.09.20 17 09:06	Seismic Ocean Bottom Receiver	OBS deployed	69° 44,220' N	010° 26,01 4' W	1812.7	0,7	3,40	193	14,80	DanSeis 119
MSM67_1-7	05.09.20 17 06:34	Seismic Ocean Bottom Receiver	on deck	69° 44,333' N	010° 39,66 2' W	1552.7	2,0	195,20	144	19,90	
MSM67_1-7	05.09.20 17 06:26	Seismic Ocean Bottom Receiver	Hydrophon on deck	69° 44,601' N	010° 40,19 2' W	1543.5	1,4	145,20	147	19,60	
MSM67_1-7	05.09.20 17 06:26	Seismic Ocean Bottom Receiver	at surface	69° 44,603' N	010° 40,19 6' W	1543.6	1,3	189,60	148	19,40	
MSM67_1-7	05.09.20 17 06:19	Seismic Ocean Bottom Receiver	released	69° 44,602' N	010° 40,19 4' W	1541.1	0,3	154,80	144	21,40	
MSM67_1-7	05.09.20 17 05:50	Seismic Ocean Bottom Receiver	released	69° 44,604' N	010° 40,19 5' W	1542.9	2,2	37,80	148	23,90	
MSM67_1-7	05.09.20 17 05:46	Seismic Ocean Bottom Receiver	Hydrophon in water	69° 44,603' N	010° 40,19 8' W	1542.6	1,1	330,30	151	22,20	
MSM67_1-7	05.09.20 17 05:14	Seismic Ocean Bottom Receiver	Hydrophon on deck	69° 44,476' N	010° 53,16 0' W	1700.3	1,7	121,50	144	21,90	
MSM67_1-7	05.09.20 17 05:11	Seismic Ocean Bottom Receiver	released	69° 44,479' N	010° 53,17 4' W	1700.6	1,2	345,60	141	21,70	
MSM67_1-7	05.09.20 17 05:09	Seismic Ocean Bottom Receiver	Hydrophon in water	69° 44,478' N	010° 53,16 8' W	1696.5	1,5	344,80	139	21,60	
MSM67_1-7	02.09.20 17 08:30	Seismic Ocean Bottom Receiver	OBS deployed	69° 44,256' N	010° 39,40 5' W	1581.1	0,8	11,90	208	14,70	DanSeis 120
MSM67_1-6	05.09.20 17 05:06	Seismic Ocean Bottom Receiver	on deck	69° 44,476' N	010° 53,14 3' W	1700.8	1,1	302,40	138	21,60	
MSM67_1-6	05.09.20 17 04:49	Seismic Ocean Bottom Receiver	at surface	69° 44,775' N	010° 53,81 4' W	1708.4	1,3	132,20	144	20,80	
MSM67_1-6	05.09.20 17 04:41	Seismic Ocean Bottom Receiver	Hydrophon on deck	69° 44,776' N	010° 53,82 2' W	1706.8	1,2	349,20	142	21,50	
MSM67_1-6	05.09.20 17 04:15	Seismic Ocean Bottom Receiver	released	69° 44,776' N	010° 53,81 6' W	1708.2	1,8	330,30	132	22,70	
MSM67_1-6	05.09.20 17 04:11	Seismic Ocean Bottom Receiver	Hydrophon in water	69° 44,777' N	010° 53,82 6' W	1732.8	1,8	317,60	135	22,70	
MSM67_1-6	02.09.20 17 07:53	Seismic Ocean Bottom Receiver	OBS deployed	69° 44,266' N	010° 52,85 7' W	1719.4	0,5	308,20	213	18,10	DanSeis 121
MSM67_1-5	04.09.20 17 22:29	Seismic Ocean Bottom Receiver	on deck	69° 44,488' N	011° 07,23 3' W	796.6	1,0	273,70	102	35,80	
MSM67_1-5	04.09.20 17 22:08	Seismic Ocean Bottom Receiver	at surface	69° 44,872' N	011° 06,98 8' W	1743.3	0,9	100,30	107	35,30	
MSM67_1-5	04.09.20 17 21:40	Seismic Ocean Bottom Receiver	released	69° 44,875' N	011° 06,99 0' W	1831.8	1,1	211,20	111	32,50	
MSM67_1-5	04.09.20 17 21:36	Seismic Ocean Bottom Receiver	Hydrophon in water	69° 44,873' N	011° 06,99 0' W	1833.6	1,9	341,30	109	33,10	

MSM67_1-5	04.09.20 17 20:57	Seismic Ocean Bottom Receiver	Hydrophon on deck	69° 44,330' N	011° 20,84 5' W	1864.7	2,2	160,60	106	34,50	
MSM67_1-5	04.09.20 17 20:56	Seismic Ocean Bottom Receiver	released	69° 44,345' N	011° 20,85 7' W	1865.1	2,4	165,90	106	32,40	
MSM67_1-5	04.09.20 17 20:50	Seismic Ocean Bottom Receiver	Hydrophon in water	69° 44,436' N	011° 20,68 5' W	1859.6	1,6	222,50	108	33,00	
MSM67_1-5	02.09.20 17 07:17	Seismic Ocean Bottom Receiver	OBS deployed	69° 44,266' N	011° 06,28 3' W	2443.5	0,5	283,40	204	17,30	DanSeis 122
MSM67_1-4	04.09.20 17 20:48	Seismic Ocean Bottom Receiver	on deck	69° 44,441' N	011° 20,50 6' W	1838.3	6,9	310,70	108	33,90	
MSM67_1-4	04.09.20 17 20:33	Seismic Ocean Bottom Receiver	at surface	69° 44,560' N	011° 21,24 6' W	1859.6	2,2	124,40	108	34,50	
MSM67_1-4	04.09.20 17 20:14	Seismic Ocean Bottom Receiver	released	69° 44,560' N	011° 21,24 5' W	1863.5	1,3	145,10	107	32,40	
MSM67_1-4	04.09.20 17 20:10	Seismic Ocean Bottom Receiver	Hydrophon in water	69° 44,558' N	011° 21,24 4' W	1862.2	4,1	156,30	108	33,80	
MSM67_1-4	04.09.20 17 19:59	Seismic Ocean Bottom Receiver	Hydrophon on deck	69° 44,559' N	011° 21,24 5' W	1852.1	3,6	268,30	107	32,90	
MSM67_1-4	04.09.20 17 19:56	Seismic Ocean Bottom Receiver	released	69° 44,559' N	011° 21,24 5' W	1863.6	1,7	332,90	106	33,10	
MSM67_1-4	04.09.20 17 19:51	Seismic Ocean Bottom Receiver	Hydrophon in water	69° 44,555' N	011° 21,23 2' W	1855.8	3,4	343,10	108	32,00	
MSM67_1-4	04.09.20 17 19:16	Seismic Ocean Bottom Receiver	Hydrophon on deck	69° 44,316' N	011° 33,91 7' W	1850.1	3,3	97,30	107	32,20	
MSM67_1-4	04.09.20 17 19:14	Seismic Ocean Bottom Receiver	released	69° 44,341' N	011° 34,02 4' W	1843.8	1,3	150,70	107	32,10	
MSM67_1-4	04.09.20 17 19:10	Seismic Ocean Bottom Receiver	Hydrophon in water	69° 44,334' N	011° 33,87 8' W	1796.9	3,6	331,20	111	30,90	
MSM67_1-4	02.09.20 17 06:42	Seismic Ocean Bottom Receiver	OBS deployed	69° 44,252' N	011° 19,73 0' W	1883.3	0,9	330,30	211	15,30	DanSeis 123
MSM67_1-3	04.09.20 17 19:08	Seismic Ocean Bottom Receiver	on deck	69° 44,350' N	011° 33,82 6' W	1852.3	1,6	201,90	108	31,00	
MSM67_1-3	04.09.20 17 18:53	Seismic Ocean Bottom Receiver	at surface	69° 44,765' N	011° 34,46 8' W	1867.0	1,0	333,00	112	32,40	
MSM67_1-3	04.09.20 17 18:29	Seismic Ocean Bottom Receiver	Hydrophon on deck	69° 44,764' N	011° 34,47 0' W	1865.7	2,7	306,10	116	31,20	
MSM67_1-3	04.09.20 17 18:23	Seismic Ocean Bottom Receiver	released	69° 44,767' N	011° 34,46 9' W	1869.8	1,0	12,50	116	31,00	
MSM67_1-3	04.09.20 17 18:21	Seismic Ocean Bottom Receiver	Hydrophon in water	69° 44,767' N	011° 34,46 5' W	1870.7	0,4	178,00	113	31,20	
MSM67_1-3	04.09.20 17 17:43	Seismic Ocean Bottom Receiver	Hydrophon on deck	69° 44,392' N	011° 47,61 2' W	1772.7	4,5	122,80	114	32,40	
MSM67_1-3	04.09.20 17 17:41	Seismic Ocean Bottom Receiver	released	69° 44,408' N	011° 47,70 8' W	1637.5	6,0	91,50	113	32,90	
MSM67_1-3	04.09.20 17 17:37	Seismic Ocean Bottom Receiver	Hydrophon in water	69° 44,418' N	011° 47,73 5' W	1769.4	0,5	151,10	114	32,40	DanSeis 124
MSM67_1-3	02.09.20 17 06:05	Seismic Ocean Bottom Receiver	OBS deployed	69° 44,214' N	011° 33,16 0' W	1894.4	0,4	113,80	202	15,70	
MSM67_1-2	04.09.20 17 17:37	Seismic Ocean Bottom Receiver	on deck	69° 44,422' N	011° 47,73 8' W	1768.1	2,5	176,10	114	33,40	

MSM67_1-2	04.09.2017 17:04	Seismic Ocean Bottom Receiver	at surface	69° 44,676' N	011° 52,44 4' W	1694.3	0,8	124,10	119	31,00	
MSM67_1-2	04.09.2017 17:01	Seismic Ocean Bottom Receiver	Hydrophon on deck	69° 44,668' N	011° 52,44 2' W	1694.3	1,4	289,00	117	30,40	
MSM67_1-2	04.09.2017 17:00	Seismic Ocean Bottom Receiver	released	69° 44,667' N	011° 52,44 0' W	1693.0	2,6	43,40	116	31,00	
MSM67_1-2	04.09.2017 16:56	Seismic Ocean Bottom Receiver	Hydrophon in water	69° 44,666' N	011° 52,43 4' W	1692.9	1,3	320,50	115	29,90	
MSM67_1-2	04.09.2017 16:30	Seismic Ocean Bottom Receiver	Hydrophon on deck	69° 44,261' N	012° 00,98 1' W	1731.3	4,9	131,20	119	30,20	
MSM67_1-2	04.09.2017 16:28	Seismic Ocean Bottom Receiver	released	69° 44,329' N	012° 01,19 1' W	1731.9	0,8	327,00	118	30,60	
MSM67_1-2	04.09.2017 16:23	Seismic Ocean Bottom Receiver	Hydrophon in water	69° 44,293' N	012° 01,08 3' W	1731.8	1,0	297,50	118	30,60	
MSM67_1-2	02.09.2017 05:30	Seismic Ocean Bottom Receiver	OBS deployed	69° 44,204' N	011° 46,58 7' W	1871.6	0,7	342,90	211	17,30	DanSeis 125
MSM67_1-1	04.09.2017 16:16	Seismic Ocean Bottom Receiver	on deck	69° 44,276' N	012° 00,79 7' W	1727.9	1,7	253,30	114	31,50	
MSM67_1-1	04.09.2017 16:01	Seismic Ocean Bottom Receiver	Hydrophon on deck	69° 44,512' N	012° 01,50 2' W	1732.3	2,4	142,70	120	32,20	
MSM67_1-1	04.09.2017 15:57	Seismic Ocean Bottom Receiver	at surface	69° 44,520' N	012° 01,52 3' W	1730.9	0,7	123,70	120	32,50	
MSM67_1-1	04.09.2017 15:26	Seismic Ocean Bottom Receiver	released	69° 44,519' N	012° 01,51 9' W	1731.4	0,6	304,90	125	32,50	
MSM67_1-1	04.09.2017 15:23	Seismic Ocean Bottom Receiver	Hydrophon in water	69° 44,519' N	012° 01,52 1' W	1728.1	1,7	150,60	123	29,30	
MSM67_1-1	04.09.2017 14:33	Seismic Ocean Bottom Receiver	Hydrophon on deck	69° 40,139' N	011° 59,01 0' W	1819.4	1,3	287,70	126	30,70	
MSM67_1-1	04.09.2017 14:32	Seismic Ocean Bottom Receiver	released	69° 40,125' N	011° 58,96 4' W	1822.5	1,0	339,80	123	30,00	
MSM67_1-1	04.09.2017 14:27	Seismic Ocean Bottom Receiver	Hydrophon in water	69° 40,118' N	011° 58,94 2' W	1819.7	1,0	146,70	123	28,70	
MSM67_1-1	02.09.2017 04:54	Seismic Ocean Bottom Receiver	OBS deployed	69° 44,094' N	012° 00,05 8' W	1751.7	0,4	329,10	208	16,50	DanSeis 126
MSM67_0_ Underway-3	06.09.2017 21:14	Thermosalinograph	profile end	68° 51,338' N	008° 42,98 0' W	909.9	12,9	235,80	8	12,10	
MSM67_0_ Underway-3	02.09.2017 03:55	Thermosalinograph	profile start	69° 35,223' N	012° 19,70 4' W	1832.4	13,1	53,50	214	18,70	
MSM67_0_ Underway-2	06.09.2017 21:14	Deep-sea Multibeam Echosounder	profile end	68° 51,338' N	008° 42,98 0' W	909.9	12,9	235,80	8	12,10	
MSM67_0_ Underway-2	02.09.2017 03:55	Deep-sea Multibeam Echosounder	profile start	69° 35,184' N	012° 19,86 2' W	1828.3	13,0	53,70	214	19,00	Simultaneous usage of EM712 and Parasound in variating configurations
MSM67_0_ Underway-1	28.08.2017 09:42	Weatherstation	station start	62° 41,139' N	033° 03,55 6' W	2891.9	0,1	93,10	305	14,50	